DEVELOPMENT OF A DAMAGE BASED DESIGN CRITERION FOR FIBER REINFORCED VESSELS

by

Paul Henry Ziehl, B.S., M.S.

Dissertation

Presented to the Faculty of the Graduate School
of The University of Texas at Austin
in Partial Fulfillment
of the Requirements
for the Degree of

Doctor of Philosophy

The University of Texas at Austin
December 2000

Dedication

To my Grandmother

DEVELOPMENT OF A DAMAGE BASED DESIGN CRITERION FOR FIBER REINFORCED VESSELS

Approved by

Dissertation Committee:

_____

_____

_____

_____

_____

Acknowledgements

It is very difficult to express the full extent of my thanks to all those who made this an enjoyable and worthwhile experience. There are many people who have provided me with support and friendship when I was in dire need of both.

First, I wish to express my sincere thanks to Professor Timothy Fowler. Dr. Fowler's technical expertise is only surpassed by his ability to see the most unusual and important angle to a given problem. This angle often makes little sense to others at first but seems to grow in validity over time. Dr. Fowler's contributions to the field of acoustic emission in fiber reinforced composites are enormous and I have borrowed from them freely. I owe a great debt to him and to the effect that is named after his daughter. I have enjoyed every conversation I have had with Dr. Fowler over the years. I have always left with a different perspective than the one I had coming in. I also thank his gracious and charming wife Marie.

I wish to express special thanks to Dr. Engelhardt and Dr. Kreger. Dr. Engelhardt and Dr. Kreger both provided much needed funding and emotional support at critical times in the research effort. It is unlikely that this would have been written without their help. I thank Dr. Breen for his insight and support along the way. I also thank Dr. Wheat for her help and encouragement.

I thank Ershigs, Inc. for financial support and the donation of the test vessel. I thank Bob Davis for his patience and technical assistance.

I thank Frank Mayfield of Fibergrate and Juan Bustillos of Dow Chemical for their technical support.

I owe a very large debt to Dan Sturm. Dan donated at least six days of his life to accomplish the modifications to the test vessel. Without him this research could not have been accomplished.

To Professor Guillermo Ramirez, who always fought the good fight. I am extremely happy to see you have made it. I can rest well at night knowing the future of composite materials and nondestructive testing rests in your capable hands. Thank

you for all the help you gave and the inspirational example you set. I know I thanked you for this once before, but thank you for being one of my closest friends.

Fernando Ulloa, who showed me what it meant to work hard and to believe. Thank you for all your help, both in the lab and classroom and especially outside of those two places.

Professor Charles Barnes, who was always helpful in good times and bad. Thank you for all the laughs and valuable insights. Don't forget the definitions.

Bob Bocchieri, who always keeps things in perspective. Thank you for contributing in a meaningful way to the field of composites and for showing me how I am supposed to ski.

Yajai, who did extremely good work and was always willing to brighten my day.

Nat, who is always helpful and cheerful. Good luck with everything.

Edgar, who was always friendly and full of insight. I am sure you are still smiling.

All my other friends at Ferguson Lab. I have been around so long that the list is too long to mention everyone. All I can say is I have never met a better group of people than the students at the Lab.

All the technicians at the lab – Blake Stassney, Wayne Fontenot, Mike Bell, Ray Madonna, Wayne Little and Pat Ball. Your help through the many years is greatly appreciated.

My very special thanks to Michele Young. Your smile and energy are beacons in a sometimes murky world. I appreciate all your support and encouragement and help. Thank you for your friendship. I pray that I continue to have it long into the future.

To my Grandmother Reppe, who is much too smart for me. Thank you for your support.

To my parents. I have always been able to count on you and for that I am eternally grateful.

Paul Ziehl

December 2000

DEVELOPMENT OF A DAMAGE BASED DESIGN CRITERION FOR FIBER REINFORCED VESSELS

Publication No._____

Paul Henry Ziehl, Ph.D.
The University of Texas at Austin, 2000

Co-Supervisor: Timothy J. Fowler
Co-Supervisor: Michael D. Engelhardt

The objective of this investigation was to develop a damage based criterion for the design of fiber reinforced vessels.

The investigation involved the use of acoustic emission to determine the onset of damage in coupon specimens. The variables investigated were fiber architecture and resin type. Damage was determined with the well-established Felicity effect.

The data gathered from the acoustic emission testing was used to develop a damage based design criterion. The damage based criterion addresses the onset of damage as opposed to the ultimate stress approach that is used in the governing codes and standards. The damage based approach provides additional insight into the behavior of the composite.

Laminas made with flexible and brittle resins are compared. Laminas made with flexible resins were found to sustain higher levels of stress prior to damage than laminas made with more brittle resins for matrix dominated behavior. Little difference was observed between laminas made with brittle resins and those made with flexible resins for fiber dominated behavior.

The damage criterion was used in conjunction with finite element analysis to design modifications to a 21’-6” tall by 7’-0” diameter filament wound pressure

vessel. The modifications made were a 24”diameter manway and an 8” diameter nozzle.

The modifications to the vessel were implemented. The vessel was tested to a superposed pressure of 23.0 psi. Acoustic emission monitoring was performed during re-loadings and no signs of significant distress were found.

Chapter 1: *Introduction*

1.1 General Background

Fiber reinforced structures have been used in many industries since before the 1950's. Some of the most notable applications have been the Chevrolet corvette, the Stealth bomber and the Big Bertha driver. Composites are well known for their high strength/weight ratio and resistance to corrosion. The resistance to corrosion is particularly important in the tank and pressure vessel industries. In these industries, hazardous and oftentimes highly corrosive materials must be stored for extended periods of time. Composite structures with corrosion resistant resins are ideally suited to this purpose. The cost of composites is high when compared to mild steel, but competitive with corrosion resistant alloys and stainless steel.

1.1.1 Design of composite vessels

Fiber reinforced tanks and vessels are currently designed based on an ultimate strength (or in some cases maximum strain) approach. These approaches do not take into account the onset of damage. Rather, safety factors are imposed on the ultimate values. Several variables affect the onset of damage in composites. These include fiber type, fiber geometry, volume percentage of fibers, fiber-matrix interface, fiber packing geometry and resin type. Of these, resin type is easily changed and is of particular importance[1.1]. It has been shown that although the ultimate strength of composite specimens made with differing resins is similar, significant differences are apparent in the onset of damage. Investigators have found that for a particular glass type and geometry, composites made with more flexible resins typically undergo higher levels of strain prior to the onset of damage than companion specimens made with more brittle resins. As expected, this is more true for matrix-dominated behavior (such as loading perpendicular to the fibers or in-plane shear) than for fiber-dominated behavior (such as loading parallel to the fibers).

The general design method for tanks and vessels specified in the American Society of Mechanical Engineers standard[1.2, 1.3] is based on the Quadratic Interaction Criterion. This criterion is based on the ultimate strength of individual laminas in tension, compression and shear. These strength values are obtained experimentally. Due to the lower modulus a lamina made with a flexible resin will often have lower ultimate strength values than a lamina made with a more brittle resin. For loading perpendicular to the fibers use of a flexible resin will generally result in higher failure strains than a brittle resin. These ultimate values overlook the more important issue of the onset of damage in the lamina. For matrix dominated behavior the onset of damage will occur at much higher strains for laminas with flexible resins. Unfortunately, the current design procedures discourage designers from using the flexible resins even though their use can lead to safer designs and better vessel and tank performance. The research reported in this dissertation is directed at developing a design method that will take advantage of the benefits offered by flexible resins.

The current state of practice regarding even the ultimate strength of composite specimens is not well developed. A large amount of scatter is present in experimentally derived ultimate strength values and predictions derived from micromechanics rarely correspond to experimental results[1.4]. Time consuming and costly testing of small-scale laminates is required to get ultimate strength values. Predicting the onset of damage is even less well understood and not directly addressed by today's codes. In the vessel industry, onset of damage is of great importance. This is due to the fact that cracking will allow the corrosive contents to penetrate to the fibers and failure will ensue. Onset of damage is also important from a purely structural standpoint in the sense that significant damage will alter the properties of the composite (lower the modulus) and reduce the fatigue life[1.5].

The lack of understanding regarding the onset of damage and inability to predict ultimate strengths with accuracy has led to large safety factors imposed by the governing codes. For the code governing the design of tanks not in critical service, a safety factor of between 8 and 10 is imposed on the inner corrosion resistant layer and a safety factor

of 1.6 is imposed on the structural layers[1.2] (this factor of 1.6 is actually quite low, refer to Chapter 2). For the code governing pressure vessels, a safety factor of 6 is imposed on all layers[1.3]. These safety factors are in all cases against ultimate strength. It should be remembered that there is some justification for a conservative approach, since composites experience damage very early in the loading process. However, a more rational approach would be to place a safety factor on the onset of damage, as opposed to ultimate strength.

The coupon testing presented in Chapter 4 addresses the issue of identifying the onset of damage in composites. The primary variable investigated was resin type. Composites made with flexible and brittle resins were tested. Different fiber geometries and types were also investigated. Some qualitative conclusions were drawn regarding the effects of using the different resins. In general, the composites made with the more flexible resins were found to undergo higher strain (and stress) prior to the onset of damage. In addition to the qualitative analysis, the results of the coupon testing were used to develop a damage based criterion. This criterion was then used in the analysis of finite element models developed for the vessel.

1.1.2 Modified design of discontinuity regions

In addition to the basic lack of understanding of composite material behavior, there is also a lack of understanding of more global design issues. Fiber reinforced vessels tend to have complicated geometries and a high degree of anisotropy. This greatly complicates the design of discontinuity regions, such as nozzles, manways, shell-to-head and shell-to-base attachments.

In an ideal situation, the stresses imposed by the discontinuity regions should be in the same range as the stresses in the vessel wall away from any discontinuities. For the case of a manway design, it can be shown through finite element analysis that the design procedures specified in the governing design standards cause elevated stresses in the wall of the vessel (Chapter 7). Other discontinuity regions are similarly affected. Therefore, the vessel would be apt to fail at an area of discontinuity. This has generally been

observed to be the case. These failures at discontinuity regions are another reason for the large safety factors imposed by the governing codes. If these discontinuity regions could be better understood and designed, then failures would be equally likely to occur in the vessel wall and more reasonable safety factors might result for the design of the entire vessel. This would lead to better economies in the construction of these vessels.

A secondary opportunity for better understanding and design of discontinuity regions presents itself with the use of knitted fabrics. Current practice makes use of woven roving reinforcements in discontinuity regions. Woven roving has several disadvantages. First, the fibers in the warp (longitudinal) direction are woven above and below the fibers in the weft (transverse) direction. This interweaving causes a loss of stiffness in the warp direction, as the fibers must straighten under load[1.6]. The strength in this direction is also adversely affected. A second drawback of using woven roving is that the strength is essentially the same in the 0 and 90 degree directions. This is a drawback unless the stress is essentially balanced biaxially. This is rarely the case and therefore it is preferable to have fibers that can be oriented in a more desirable way. A third drawback is that the geometric nature of woven roving tends to make it difficult to get good resin penetration throughout the layer. This leads to numerous entrapped voids between the woven and non-woven fiber bundles. These voids cause acoustic emission, an early indication of damage, very early in the loading process and woven roving laminates tend to be acoustically “noisy”. Subsequent loadings are better, but still tend to be noisy. This is not simply a problem with the acoustic emission test. Rather, it points to the fact that woven roving laminates undergo significantly more damage for a given level of stress than their knitted fabric counterparts. This suggests that the long-term strength of woven roving laminates will be inferior to knitted fabric laminates made from similar materials.

The design of modified discontinuity regions and knitted fabrics is discussed in Chapter 8. The analysis was carried out with a commercially available finite element program. The damage criterion developed in Chapter 5 was used as opposed to an ultimate strength criterion. A 24” diameter manway and an 8” diameter nozzle were

modeled. The stress ratios throughout the discontinuity region were kept in the same range as those in the shell of the vessel. Therefore, the resulting attachments should be capable of sustaining the same internal pressure as the vessel wall. Significantly different fiber orientations and reinforcement geometries were used than are required by the current design methods. More fiber and resin is required in the discontinuity region to accomplish this than would be required if the standard design methods were followed. As was mentioned earlier, the hope is that by obtaining a better understanding of the onset of damage and the design of the discontinuity regions, the safety factors imposed on the entire vessel can be reduced.

1.2 Acoustic Emission Monitoring of Tanks and Vessels

Prior to the 1970's, fiber reinforced tanks and vessels (hereafter referred to as vessels) had a poor performance record[1.7]. This poor performance can be attributed to improper design, abuse in service, and a lack of well-established testing methods. During the late 1970's, a testing program was begun[1.8] with the intent of developing acceptance/rejection criteria for both new and in-service vessels. This program focused on acoustic emission as the test method. Acoustic emission is a non-destructive test method that can be used to economically monitor an entire large-scale vessel. Other test methods are less satisfactory either due to quality of results, expense, or a lack of global monitoring ability.

Acoustic emission monitoring makes use of piezoelectric sensors placed on the surface of a structure. Either resonant or wide band sensors may be used. When the amount or damage occurring in a structure increases, such as when a stress concentration is relieved through crack tip growth, body waves are produced in the structure. The resulting surface displacements disturb the pressure sensitive sensor and these disturbances are converted into electrical signals that can then be interpreted. When resonant sensors are used, the waveform is distorted. Resonant sensors have the advantages of higher sensitivity in the resonant frequency range and reduced cost.

Experience has shown that 150 kHz resonant sensors are particularly useful for monitoring fiber reinforced vessels[1.9].

When vessels or other structures are loaded the amount of damage in the structure will increase. For fiber reinforced structures (as opposed to steel structures), damage begins very early in the loading process and continues until failure. At some point the damage will begin to increase dramatically. This increase is associated with "critical" damage. Acoustic emission monitoring, therefore, tends to focus on locating this point of critical damage. There rarely exists one single point of critical damage and some interpretation of the data is required. Data interpretation focuses on general trends as opposed to absolute values of specific emissions[1.9].

Due to the success of the acoustic emission testing that was carried out in the late 1970's and early 1980's by Fowler and others, acceptance/rejection criteria for fiber reinforced equipment were developed. These criteria were outlined in the Recommended Practice for Acoustic Emission Testing of Fiber reinforced Tanks/Vessels[1.9]. This document is important for both the tank (vessels designed to operate below 15 psi) and pressure vessel industries (vessels designed to operate above 15 psi). It is important in the tank industry in the sense that the governing standard permits lower safety factors to be used if an acoustic emission test is performed. It is also important in this industry to assess the structural integrity of in-service vessels. The document is even more important in the pressure vessel industry. Prior to the advent of this document, all pressure vessels were required to undergo very time-consuming cyclic tests and then pass a proof test of six times the design pressure. This type of testing relied on the destruction of prototype vessels. Therefore, the manufacture of one-of-a-kind vessels was very costly. Acoustic emission testing provided a way of testing one-of-a-kind vessels without a prototype and did away with the need for time-consuming cyclic testing. In-service vessels could also be tested with acoustic emission. Aside from the obvious advantages to industry, acoustic emission testing also provides an insight into the damage mechanisms that take place in fiber reinforced structures.

1.3 Experimental Program

The experimental program consists of three parts: acoustic emission and strain gage testing of small scale coupons, acoustic emission and strain gage testing of the standard vessel and acoustic emission and strain gage testing of the modified vessel.

1.3.1 Small scale coupon testing

More than fifty small-scale coupon specimens (1" x 3/8" x 7") were tested in four-point bending. The primary variable investigated in this testing was resin type. Of particular interest were the effects of brittle versus flexible resins. Several different fiber geometries and orientations were tested. These included oriented fibers at 0, 45 and 90 degrees and woven roving. An acoustic emission procedure was developed to determine the onset of damage. The acoustic emission procedure made use of the well-known Felicity effect[1.8, 1.9]. Results from this procedure were compared with the departure from linear behavior in the specimens and were found to correlate well. The general conclusion from this testing was that flexible resins did provide advantages over brittle resins for matrix dominated behavior. For fiber dominated behavior, however, the flexible resins showed no advantage. The results of this testing were used to develop a damage based criterion. This criterion was later used in the design of the modified discontinuity regions of the vessel.

1.3.2 Tests of original vessel

The original vessel was filled with water and superposed pressure was applied on several different occasions. On the third occasion, the superposed head was taken to 22.0 psi (substantially above the design superposed pressure of 15 psi). At that point, significant damage occurred. The damage occurred at the gusset-to-shell connection of the 4" gusseted nozzle. The acoustic emission data gave notice of this impending failure. The failure occurred on the exterior of the shell and no leakage was observed.

1.3.3 Tests of modified vessel

The damaged 4” gusseted nozzle was removed and replaced with a newly designed 8” nozzle. A newly designed manway was also installed opposite the original manway. The modified vessel was then filled with water and superposed pressure was applied. An audible noise was heard as the superposed pressure reached 22.0 psi. The cause of this noise was not determined. There was some concern regarding the adequacy of the hold-down system for this level of load. Loading was discontinued to avoid failing the hold-down system or the vessel. The vessel was then re-loaded several times. The modified vessel was acoustically quiet during the re-loadings. This led to the conclusion that little structural damage had been done to the vessel.

1.4 Definitions of Terminology

1.4.1 Acoustic emission terms

Acoustic emission data was collected continuously during loading of all coupon specimens. The well-established AE parameters cumulative signal strength, Felicity ratio and historic index were used to aid in interpretation of the AE data. To aid in visualization of the AE data, an idealized diagram of a typical AE hit is shown in Figure 1.1. An idealized diagram of the rectified signal envelope is shown in Figure 1.2. This is similar to Fowler, Blessing and Conlisk, 1989[1.7].

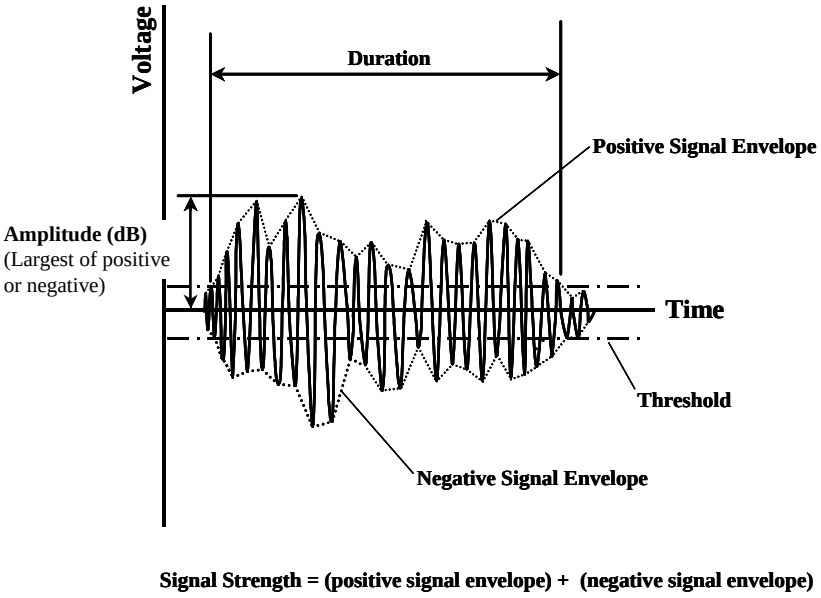

Figure 1.1 – Idealized acoustic emission hit

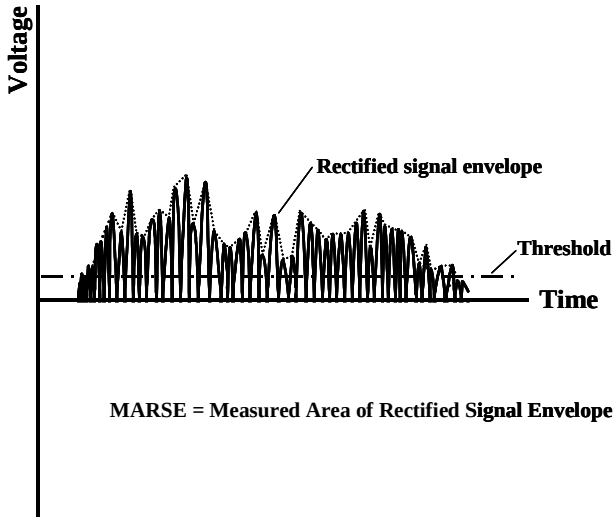

Figure 1.2 – Schematic of rectified acoustic emission signal

Acoustic emission channel[1.9] – An assembly of sensor(s), preamplifier, filters, secondary amplifier, connecting cables, detector, processor and/or other instrumentation as needed (ASTM E 1316)[1.10].

Acoustic Emission Signal Amplitude[1.9] – The peak voltage (measured in decibels) of the largest excursion attained by the signal waveform from an emission event (ASTM E 1316)[1.10].

Acoustic Emission Event[1.9] (event, emission event) – A local material change giving rise to acoustic emission (ASTM E 1316)[1.10].

Acoustic Emission Source[1.9] – The position of one or more AE events.

Felicity Effect[1.9] – The presence of detectable acoustic emission at a fixed predetermined sensitivity level at stress levels below those previously applied (ASTM E 1316)[1.10]. The fixed sensitivity level will be the same as was used for the previous loading or test.

Felicity Ratio[1.9] – The ratio of the stress at which the Felicity effect occurs to the previously applied maximum stress (ASTM E 1316)[1.10].

For the CARP Recommended Practice[1.9], the Felicity ratio is determined from the ratio of the load at the onset of significant emission to the previously applied maximum load. The Felicity ratio is further discussed in Section 12.7 "Significance of Criteria." The following is an excerpt:

'……..The onset of "significant" emission for determining the Felicity ratio is matter of operator experience. The following are offered as guidelines for determining onset of significant emission on an individual channel:

- More than 5 bursts of emission during a 10% increase in load. One or more hits constitute a burst, and all hits for the five seconds following the initial hit are considered part of the same burst.

- More than $N_D/20$ duration (counts) during a 10% increase in load, where N_D is the duration criterion defined in Section B2.1.

- Emission continues at a load hold. Continuing emission is defined as a rate of more than 3 hits per minute for each minute of a load hold. For purposes of this guideline, a short (one minute or less) load hold can be inserted in the procedure.'

Historic Index[1.9] – A measure of the change in signal strength throughout a test. It is defined by the formula:

$$H(t) = \frac{N}{N-K} \frac{\sum_{i=K+1}^{i=N} S_{Oi}}{\sum_{i=1}^{i=N} S_{Oi}}$$

Where:

N = Number of hits (ordered by time) up to and including time t

S_{0i} = Signal strength of i^{th} hit

K is an empirically derived factor that varies with the number of hits. Values of K are given in table 2.1:

Table 2.1 – K factor for historic index

Number of Hits, N	***K***
Less than 20	Not applicable
20 to 100	0
101 to 500	0.8 N
> 500	N – 100

Hit duration[1.9] (duration) – The time from the first threshold crossing to the last threshold crossing of the signal or envelope of the linear voltage time signal. Hit durations does not include the hit definition time at the end of a hit.

Kaiser effect[1.10] – the absence of detectable acoustic emission at a fixed sensitivity level, until previously applied stress levels are exceeded.

Knee in the Cumulative Signal Strength Curve - When cumulative signal strength is plotted versus time, the cumulative signal strength will generally increase sharply at a certain time. This is typically referred to as the knee in the cumulative curve. This change in slope of the cumulative signal strength curve is often correlated to damage.

MARSE[1.9] – Measured area of the rectified signal envelope. A measurement of the area under the envelope of the rectified linear voltage time signal from the sensor (ASME Code Section V, Article 12)[1.11].

Sensor Hit[1.9] - One AE hit is defined as the signal that occurs between an initial and final threshold crossing.

Severity[1.9] **–** Severity is defined as the average signal strength for the J hits having the largest numerical value of signal strength:

$$S_r = \frac{1}{J} \sum_{m=1}^{m=J} S_{0_m}$$

Where:

S_{Om} is the signal strength of the mth hit. m is ordered on the magnitude of the signal strength with m=1 being the hit having the largest signal strength.

J is an empirically derived constant that depends on the material of construction. Values of J are given in Table 4.2.

Table 4.2 – *J* factor for severity

Total Number of Hits	***J***
Less than 20	Not applicable
More than 20	20

Signal Strength[1.9] – The area under the envelope of the linear voltage time signal from the sensor. The signal strength will normally include the absolute area of both the positive and negative envelopes.

For purposes of this dissertation, MARSE was used as an approximation of signal strength. MARSE appears to have a value of approximately one-half the signal strength. This is not the case due to Section B7 of "Mandatory Appendix B – Instrument Calibration" of the CARP Recommended Practice[1.9].

Voltage Threshold (Threshold)[1.9] – A voltage on an electronic comparator such that signals with absolute amplitude larger than this level will be recognized.

1.4.2 Fiber reinforced polymer terms

Fiber reinforced composites are generally fabricated from several layers of resin and glass. One layer is referred to as a lamina. More than one lamina is referred to as a laminate. Each lamina is denoted by a letter or group of letters describing the lamina. The laminas are divided by a slash. An example follows:

M / M / WR / M / M

This indicates a laminate with five laminas. The laminas are as follows:

M = Random mat (1.5 oz./sq. foot)

WR = Woven roving (24 oz./sq. yard)

The types of laminas are described in greater detail in Chapters 6 and 8. Reinforcement is typically expressed in weight per unit area. The convention in the industry is to express random mat and other light reinforcement in oz./sq. foot and to express woven roving and other heavy reinforcement in oz./sq. yard. To convert these weights per unit area to a weight per unit volume it is necessary to assume a thickness of the lamina.

Lamina thicknesses are approximate and vary depending on the construction process. Trilam[1.12] is a computer program that is tailored to the tank and pressure vessel industry. This program was used to establish lamina stiffness properties. When using Trilam, the user is prompted to input fiber reinforcement in weight per unit area and then a typical thickness is assigned. The thicknesses assigned for laminas of random mat and woven roving are as follows:

M = Random mat = 0.043” thick

WR = Woven roving = 0.038” thick

Trilam does not address knitted fabrics. The thickness of the knitted fabric laminas was assumed to be the same as the thickness of the woven roving laminas. The weight per unit area of the knitted fabrics used was also 24 oz./sq. yard.

When discussing percentage of fiber, industry representatives commonly refer to percent weight. However, stiffness and strength calculations are performed with percent volume.

Chapter 2: *Literature Review*

This chapter is a review of selected literature. Acoustic emission monitoring of small FRP specimens and the differences between flexible and brittle resins are addressed in the reviews of Cortez, et. al. and Lorenzo and Hahn. The development of acoustic emission testing of FRP equipment is addressed in the review of Fowler and Gray. Principles for the design of FRP storage tanks are addressed in the review of Isham. Advantages of knitted fabrics are addressed in the review of Garcia. The current design codes for FRP vessels and tanks are addressed in the review of ASME Section X and RTP-1. The current design code for acoustic emission testing of FRP vessels is addressed in the review of the CARP Recommended Practice.

2.1 *Use of Acoustic Emission to Characterize Resin Performance in Laminates,* Cortez, Enos, Francis and Heck, 1983[2.1]

This work is the most applicable to the coupon testing discussed in this dissertation. Cortez et. al. discuss the differences between different resins and the correlation between high failure strain of a resin and what they describe as "toughness". The general implication is that composites constructed with more flexible resins undergo higher levels of strain prior to the onset of damage, even though composites constructed of different resins have similar ultimate strengths. The authors address the fact that codes do not account for this difference in resins and suggest that acoustic emission be used to quantify the toughness of composites constructed with different resins.

The primary experimental program consisted of tensile testing 1/4" thick x 1" wide x 12" long dogbones with similar glass construction (V/M/M/Wr/M/Wr/M) but different resins. The total glass content was between 38 and 39%. The code for the glass sequence was:

V = chemical glass veil

M = chopped strand mat, 1.5 oz./sq. ft.

Wr = woven roving, 24 oz./sq. yd.

Of secondary interest was tensile testing of bis A (epoxy based) vinyl ester specimens with different glass orientations. The tensile tests were in accordance with ASTM D-638. The resin types were Dow vinyl ester bis A (epoxy based), modified vinyl ester bis A (fumarate based), vinyl ester bis A fumarate and corrosion resistant polyester isophthalic grade. The number of specimens tested and the ultimate strain of the resins were not stated.

Two Dunegan/Endevco S-9224 (resonant at 72 kHz) sensors were placed on each specimen. Events below 70 dB were not considered. The main AE parameter utilized was counts. Counts were plotted with stress versus strain data, and a significant increase in the number of counts was assumed to indicate damage. Plots of this data are only given for the specimens with similar glass construction and different resin types. If 10 events greater than 70 dB were recorded during the test, the strain at which this occurred was noted. Results (based on counts) are summarized in Tables 2.1 and 2.2:

Table 2.1 – Specimens with similar glass construction (V/MM/Wr/M/Wr/M), (Cortez, et. al., 1983)

Resin Type	***Micro-strain at Increase in counts***	***Stress (psi) at Increase in counts***
Vinyl ester bis A (epoxy based)	14,200	19,400
Modified vinyl ester bis A (fumarate based)	13,000	19,800
Corrosion resistant isophthalic	5,500	5,500
Bis A fumarate	3,600	5,600

Table 2.2 - Specimens with similar resin type (Bis A epoxy based vinyl ester), (Cortez, et. al., 1983)

Laminate Construction	*Micro-strain at Increase in counts*	*Stress (psi) at Increase in counts*
V/MM/Wr/M/Wr/M	14,200	19,400
Unidirectional 0 degrees	12,400	48,000
Unidirectional 90 degrees	8,200	6,700

The conclusions drawn were as follows:

1. The resin type significantly influences the critical strain/strength properties of laminates. In this case critical strain is synonymous with strain at onset of significant AE.
2. AE can be used to determine resin "toughness".
3. Although resins are similar in ultimate strength, they vary significantly in critical strength.
4. The influence of resin type may be a bigger factor in critical strength/strain than glass construction.

This paper was a summary of work in progress. For future testing, the Felicity and Kaiser effects were to be investigated.

This paper is directly applicable to the work presented in this dissertation. The concept of resin "toughness" and the focus on the onset of damage as opposed to ultimate stress or strain is important. Current design codes and procedures are based either on an ultimate strength or maximum strain approach. These approaches do not address the fact that damage occurs at different levels for composites made with different resins. In later chapters, a damage-based criterion is developed to account for the use of different resins. This criterion is based on acoustic emission testing and makes use of the Felicity effect as opposed to AE counts.

2.2 *Static and Fatigue Monitoring in Unidirectional Composites by Acoustic Emission,* Lorenzo and Hahn, 1986[2.2]

This work involves acoustic emission monitoring of glass and graphite fibers embedded in brittle and ductile resins. Only longitudinal fiber orientations were investigated. The weight percent of the fibers is not stated. Fiber bundles and bundle sizes are mentioned. It is clear that only a single layer of fibers was used. Both static and cyclic tests were discussed. Optical microscopy was used to monitor the fracture processes during testing. All specimens were tested in tension. Epon 815/Versamid 140 was used for the ductile resin and Epon 828/Epon Z was used as the brittle resin. These are epoxies manufactured by Shell. The brittle resin was reported to be stiffer than the more ductile one and had a tensile strength twice that of the more ductile resin.

Acoustic emissions were monitored with an AET Model 5000. The transducers were AET AC375L resonant at 375 kHz. The specimens were also monitored in-situ with optical microscopy.

Stress strain information is given up to failure for statically loaded specimens. Failure modes are listed at intermediate strain levels. Resin micro-cracks were detected at 12,000 micro-strain for glass fibers specimens and 8,000 micro-strain for graphite fiber specimens. This behavior was independent of resin type. The difference in strain level at resin micro-cracking was attributed to a larger mismatch in longitudinal modulus between the graphite fibers and resin.

The micro-cracks were normal to the applied load and originated in regions of densely packed fibers. The cracks were smaller in graphite specimens and this was attributed to the smaller diameter of the graphite fibers. It was noted that crack size depends on crack opening displacement, and therefore the stiffer graphite specimens exhibited smaller micro-cracks.

Initial fiber breaks were isolated at low and moderate strain levels. At higher strains the fiber breaks propagated and eventually led to failure of the specimen.

Interfacial failure was particularly noted in the ductile resin specimens with glass fibers. Cracking tended to propagate along the fiber. This was not as pronounced for the glass specimens with the more brittle resin. No interfacial damage was noticed in the graphite specimens, regardless of resin type.

Specimens were cyclically tested at varying levels of strain. The maximum strain was plotted against number of cycles to failure (Figure 2.1). Specimens with more ductile resin were found to have more fiber breaks than the brittle resin counterparts. Failure of glass fibers was followed by extensive interfacial yielding. Brittle resin specimens with glass fibers exhibited interfacial debonding after fiber failure. Transverse micro-cracks were observed in glass fiber specimens at all strain levels. Micro-cracking was more extensive in the high-cycle region. Some micro-cracks were observed to turn and grow along the fibers.

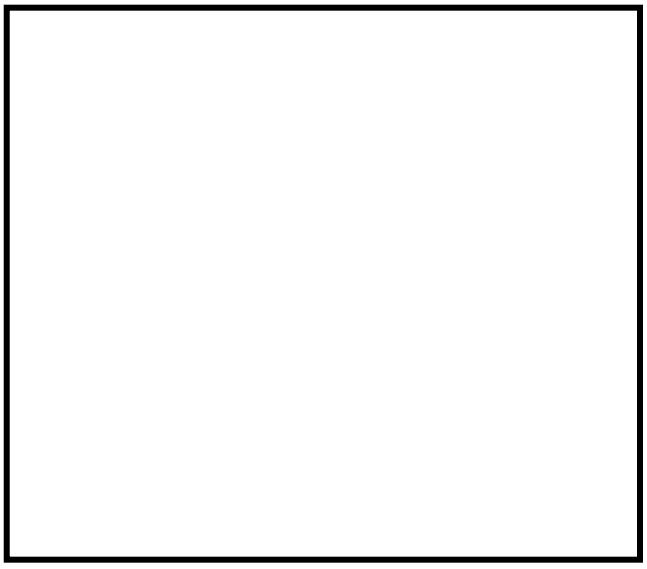

Figure 2.1 – Maximum Strain vs. Log of Cycles to Failure (Lorenzo and Hahn, 1987)

Graphite fibers in the ductile resins also showed more fiber breaks than their brittle resin counterparts. Brittle resin specimens showed only isolated fiber breaks. Interfacial failure was not detected in the graphite specimens.

It was observed that the amount of damage suffered by the fibers depended on the applied strain. Brittle resin specimens showed fewer fiber breaks. In brittle resins, glass fibers showed less interfacial damage. Graphite fiber specimens showed no matrix cracking in the fiber bundles.

It was observed that crack tip blunting in ductile resin specimens may redistribute stress over a large area. When this is coupled with interfacial failure, the stress on neighboring fibers is increased greatly and may lead to failure.

Acoustic emission activity was found to occur earlier in ductile resin specimens regardless of reinforcement type. Less total acoustic activity was recorded in brittle resin specimens. Failure strains were fairly close and therefore less damage was thought to occur in specimens with brittle resins prior to failure. It was concluded that the more ductile resins were more capable of relieving stress and were therefore more “tough”.

Peak amplitudes were lower for glass fiber specimens, but independent of resin type for graphite specimens. The authors postulated that the fiber failures accompanied by debonding may have produced lower amplitudes than fiber breakage only. In graphite specimens, no interfacial failure occurred and therefore the peak amplitudes were similar.

Stronger AE activity in ductile resin specimens was attributed to larger zones of fiber breakage and more extensive matrix damage from zones of fiber break accumulation. The ductile resin was thought to allow more damage accumulation prior to final fracture.

Glass fiber specimens with both ductile and brittle resins showed a large increase in emissions just prior to failure (final 10% of loading life). This was not the case for graphite fiber specimens. Higher amplitude events increased as failure approached.

Conclusions were as follows:

- Emissions from fiber failures were identified, but matrix micro-cracking could not be distinguished.
- Interfacial related activity was not distinguishable, but rather seemed to affect the peak amplitude of the fiber breaks.
- Ductile resin specimens generally showed more acoustic activity than specimens with brittle resins.

2.3 *Development of an Acoustic Emission Test for FRP Equipment,* Fowler and Gray, 1979[2.3]

This paper deals with the development of a generalized acoustic emission test procedure to assess the structural integrity of FRP equipment. Both small coupons and large scale test specimens are discussed. The experimental work consisted of tensile and flexural tests of small coupons, pipe tests and the large scale test of an FRP tank. The results of the flexural tests were similar to those of the tensile tests and therefore will not be discussed.

This was one of the earliest and most comprehensive investigations in the use of acoustic emission as a means of assessing damage in FRP equipment. The findings reported in this paper were later used as one of the data sets to develop the Recommended Practice for Acoustic Emission Testing of Fiberglass Reinforced Plastic Resin (RP) Tanks/Vessels (CARP, 1982). The Recommended Practice (also known as the CARP procedure) is discussed later in this chapter.

Tensile tests of small coupons: Dow Derakane press molding resin and Owens/Corning Fiberglass E-980 resin were used. Glass configurations were varied and included random glass, continuous axial and cross-ply fibers and varying combinations of random and continuous fibers. Constructions were typical of those in use at the time for construction of fiber reinforced plastic tanks. The glass was Owens/Corning Fiberglas

433. The specimens were 0.10”-0.20” thick x 0.50” wide. The tests were conducted in accordance with ASTM D-638. Acoustic emissions were monitored with Dunegan/Endevco 3000 series equipment. Single D50 (50 kHz resonant) and D140 (140 kHz resonant) transducers were attached at opposite ends of each specimen. Aluminum plates were bonded to the ends of the test specimens to eliminate grip noise. Load was applied in a step-wise fashion with periodic unloadings. Acoustic emission counts were plotted continuously.

The test results focus on the emissions of a 65% (by weight) random glass/Derakane specimen. The Kaiser and Felicity effects were observed in the test results. Log AE counts were plotted against load. A locus of reemission (also referred to as a Felicity locus) was established by drawing a line through the points of onset of emission (Figure 2.2). Felicity ratio was also plotted against percent of ultimate load (Figure 2.3). The Felicity ratio was found to drop below 1.0 somewhere between 40 and 60 percent of ultimate load for 50 % and 65% random mat specimens. The loading pattern was found to have some effect on the Felicity ratio. It was noted that random glass will tend to emit sooner than continuous straight fibers (either longitudinal or transverse). It was also noted that combinations of different types of constructions (e.g. random and longitudinal) and woven roving, will emit sooner than only random fibers. The type of resin was noted to affect the onset of emission.

Figure 2.2 – Log AE counts vs. Load (Fowler and Gray, 1979)

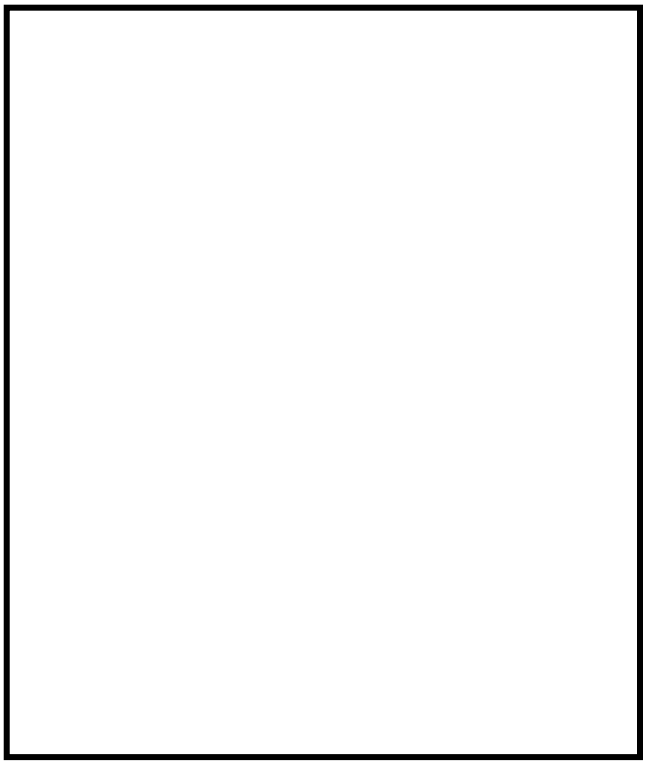

Figure 2.3 – Felicity Ratio vs. Percentage of Ultimate Load (Fowler and Gray, 1979)

Continuing emissions during load hold were noted and attributed to creep. Continuing emissions during load hold were later attributed to accumulating damage (which can be viewed as a form of creep) in the CARP criteria. High amplitude events were noticed to increase as the specimen approached failure. Amplitudes of 70 dB or higher were attributed to fiber breakage. It was noted that this value is dependent on the sensitivity of the sensor and the proximity of the source. Later in the CARP criteria, high amplitude events were attributed to major structural damage (in addition to fiber breakage). To minimize the effect of differences in monitoring equipment, an empirical method for determining "high amplitude" events was later developed for the CARP criteria.

Four acceptance/rejection criteria were discussed:

a. A specific number of counts. Total counts were believed to be an indication of the amount of cracking. It was pointed out that in corrosive environments, cracks can be as important as strength.

b. Felicity effect. A Felicity ratio of less than 0.95 was believed to be an indication of damage.

c. High amplitude events. Events of greater than 70 dB were believed to be indicative of fiber breakage. Therefore, a limit of the number of events greater than 70 dB was suggested.

d. Continuous emission during a load hold. Emission during a load hold was thought to be indicative of creep. It was pointed out that creep is a common cause of FRP equipment failure. Therefore, a limit on emissions during load hold was suggested. As mentioned previously, the term creep was later replaced with accumulating damage in the CARP criteria.

It was noted that general qualitative trends were discernable, but considerable quantitative scatter was present.

Pipe tests: Several pipe specimens were tested in an attempt to relate the acoustic emission behavior of the small specimens to larger components. The pipes were 30” long x 2.23” internal diameter x 0.095” thick. The resin was Dow epoxy 331 with a Jeffamine AP 22 catalyst. The glass was filament wound at 55 degrees. The glass content was experimentally determined to be 70% (by weight). The pipe specimens were plugged at the ends and loaded by internal pressure. The load was applied in a stepwise fashion with load holds and unload/reload cycles. Leakage always occurred before catastrophic failure and some AE was attributed to this leakage.

The general pattern of the acoustic emission was found to be similar to that of the small coupon specimens. A plot of counts versus internal pressure clearly shows the Felicity ratio decreasing with increasing damage to the specimen.

The primary conclusion of the pipe tests was that AE criteria could be applied to larger components.

Tank test: To further relate the work to full scale equipment, a large FRP tank was tested to failure. The tank was constructed with a flat bottom and domed head. The internal diameter was 7'-7". The height of the straight wall was 8'-8-15/16". The wall construction was as follows:

0.01" – 0.02" veil (10% glass by weight)

0.08" – 0.10" chopped strand liner (24% glass by weight)

0.08" Filament wound (90 degree orientation, 68% glass by weight)

The tank was manufactured in March of 1977 by Owens Corning Fiberglas and tested in July of that year. A standpipe was used to pressurize the tank. The total water depth at "failure" was 36'-3".

D140 transducers were used in regions of high stress and close to nozzles and hold-down lugs. Two D50 transducers were used at mid-height of the wall (front and back).

A plot of counts versus depth of water was constructed and damage mechanisms were identified on the plot. Significant emissions were found to occur at water depths of 16' to 18'. This became more apparent when the scale of the plot was changed. The changing of scales on AE plots is often necessary to find the area where a change in slope of the emissions first occurs. It was noted that minor emissions occur very early in the loading process, but these did not become significant until the 16'-18' level was reached.

The onset of damage (as determined by the change in slope of the AE data) was found to occur at 44-49% of the ultimate failure load (ultimate water height). This result

was in agreement with the tensile and flexural tests. It was noted that at the onset of emission, the equipment had a safety factor in the range of 2 to 2-1/2.

The number of counts was discussed as a possible acceptance/rejection criterion. The exact cutoff number was not thought to be important. From the data, a number in the range of 2,000 to 10,000 was thought to be acceptable and 5,000 counts was determined to be an appropriate number. It was mentioned that this number should be adjusted as necessary for different numbers of sensors. To account for differences in monitoring equipment, an empirical method for determining the appropriate number of counts was later developed for the CARP criteria.

Emissions during load holds were noted and tabulated. At water depths between 13’ and 18’ emissions during load holds occurred but died out after 1 minute. At a water depth of 19’, emissions continued for 3 minutes. For depths of 20’ and above, emission continued throughout load holds. The load holds varied between 1 and 12 minutes.

The emissions during holds were again attributed to creep. Emission during load holds was recommended as a second acceptance/rejection criteria. A time limit of 2 minutes was recommended.

The Felicity ratio was recommended as a third acceptance/rejection criterion. It was noted that during the 19’-14’-19’ unload/reload cycle, reemission occurred at 16’-9”. This resulted in a Felicity ratio of 0.88, which was unacceptable. It was noted that the Felicity effect is indicative of previous damage.

High amplitude events were recommended as a fourth acceptance/rejection criterion. Between 18’ and 19’, twenty events greater than 70 dB were recorded. These high amplitude events were attributed to fiber breakage. It was recommended that no more than 10 events greater than 70 dB be allowed.

Visible damage in the form of a 5” long crack occurred at a depth of 19’. The crack grew and an audible pop was heard at a depth of 21’. As loading progressed, the anchor bolts began to pull out of the concrete. Visible cracks occurred in the lower

knuckle at 30'. At 36'-3" the hold-down bolts threatened to break free of the concrete floor and the test was stopped. Some leakage occurred at the top and bottom knuckles.

Conclusions were as follows:

Acoustic emission showed considerable promise as a non-destructive test for FRP equipment. It was noted that additional development work was required, but the following acceptance/rejection criteria were proposed:

1. Total counts in excess of 5,000 on either of the two counters.
2. More than 10 events of greater than 70 dB amplitude.
3. During a load hold, emissions continue beyond 2 minutes.
4. A Felicity ratio of less than 0.95. The Felicity ratio was defined as the load at onset of emission, divided by the maximum load previously attained.

It was noted that the criteria above applied to specific Dunegan/Endevco equipment and that some modification would be necessary for different equipment. The first criterion was attributed to cracking, the second to fiber breakage, the third to creep instability and the fourth to a measure of previous damage.

The criteria were thought to provide a safety factor of 1.5 to 3.0, and were therefore less conservative than normal FRP design factors (generally in the range of 6.0, depending on the code). This was stated to be a desirable aspect of an acceptance/rejection criterion.

Future work was to be carried out on field specimens.

2.4 *Design of Fiberglass Reinforced Plastic Chemical Storage Tanks,* Isham, A. B., 1966[2.4]

This study focuses on the long term durability of fiber reinforced vessels constructed with the filament winding procedure. Cyclic tests were conducted to get a measure of the expected durability. An "optimization" scheme was developed for the

construction of the vessel wall. This scheme consisted of cyclic tensile testing of pipe specimens to determine a long-term design strain and then apply this, in conjunction with some safety factors, to the design of the vessel wall. The author points out that the design of FRP chemical storage tanks is rarely concerned with ultimate strength, but rather with performance and durability over many years. Failure is defined as cracking of the two inside layers. This could allow the internal fluid to penetrate to the filament wound layers. The thickness of the interior corrosion barrier and exterior veil were assumed and then the thickness of the filament winding layer was calculated. Tensile strain, buckling stress and impact damage were all addressed. Only tensile strain will be discussed here.

The construction of the typical tank wall at the time the paper was written consisted of four layers. The inside surface is resin reinforced with a ply of fiberglass surfacing mat. The next surface is a layer of chopped strand reinforced resin with low glass content (less than 30% by weight). These two interior layers are referred to as the corrosion barrier. The low glass content is important for chemical resistance. It leads to fewer air voids and therefore the corrosion barrier is more impervious to passage of fluids. The third layer is the filament winding. The outside layer is resin reinforced with surfacing mat to provide resistance against weathering and chemical spillage. This type of construction is similar to the vessel specimen tested as part of the research reported in this dissertation.

For the determination of design strain, 9-1/4" inside diameter tubes were tested under internal pressure. Floating end connections were used to eliminate axial stress in the pipe wall. Each pipe had a molded-in leak detector that provided notice if the inner layer was breached. The leak detector was a narrow strip of fine mesh bronze screen placed at the interface of the chopped strand and filament wound layers. A change in resistance of the pipe wall was taken as an indication that a leak had occurred. "Failure" was defined as the number of cycles required to crack the inner surface and allow fluid to penetrate to the leak detector. Internal pressures of between 400 and 1000 psi were used for the tests. Specimens were cycled at the rate of 700 and 900 times per hour.

A one cycle static test was first conducted to establish the "strain to crack". This inner layer was breached at 4,000 micro-strain. Eight specimens were tested at various strain levels and number of cycles until failure occurred. This figure is reproduced as Figure 2.4.

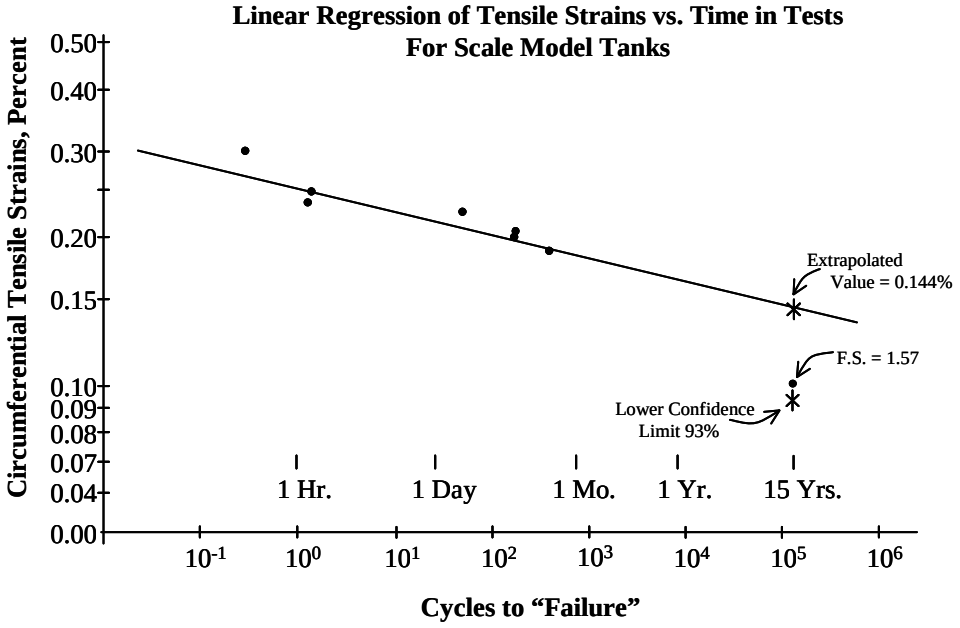

Figure 2.4 – Circumferential tensile strain versus cycles to "failure" (reproduced from Isham, 1966)

The design life was defined as 15 years (131,500 hours). After applying a safety factor of 1.57 to the extrapolated design strain level, the final value for design strain was 930 micro-strain. The value of the safety factor and reason for its use are not clearly explained. Reference is made to environmental aging effects and their effect on modulus. A reduction in modulus would seem to indicate an increase in strain. It is important to note that the long-term design strain is less than 25% of the design strain if it was based on only one cycle.

2.5 *Material Selection, Design and Tooling for Structural Plastics*, Garcia, E., 1984[2.5]

This paper deals with the use of oriented knitted fabrics as opposed to woven fabrics. Woven fabrics are commonly used throughout the tank and pressure vessel industry. This is primarily due to their low cost and ease of fabrication. The author provides test data to support the superiority in both modulus and ultimate strength of knitted fabrics.

The experimental work consisted testing five test specimens of differing fiber orientations and types. The five constructions were uniaxial fibers, woven roving with 1.5 oz./sq. ft. mat, 0 / 90 degree knitted fabric with 1.5 oz. / sq. ft. mat, and two sets of specimens with different weights per unit area of knitted fabric. Specimens were tested in the 0, 45 and 90 degree directions. A computer program was developed to obtain properties at each 10 degrees. Five different tests were run for each specimen type.

1. ASTM D638-80 – Tensile Properties of Plastics
2. ASTM D695-80 – Compressive Properties of Rigid Plastics
3. ASTM D2344-76 – Apparent Interlaminar Shear Strength of Parallel Fiber Composites by Short-beam Method
4. ASTM D3846-79 – In-plane Shear Strength of Reinforced Plastics
5. ASTM D790-80 – Flexural Properties of Plastics and Electrical Insulating Materials

Only the tensile tests and the in-plane shear tests are of interest for this research program. The test results indicate lower standard deviations for knitted as opposed to woven materials. The authors attribute this to the 12% elongation factor that occurs prior to woven fibers loading in true tension. Knitted fibers are essentially straight to begin with, and therefore load in tension immediately. This phenomenon also effects modulus and ultimate strength, Luger 1982[2.6].

For unidirectional specimens, when loaded in tension in the direction of the fibers an ultimate stress of 73,700 psi and modulus of 3,510,000 psi were obtained. When loaded in tension in the direction transverse to the fibers, an ultimate stress of 2,400 psi and modulus of 110,000 psi were obtained. This indicates the extreme difference in properties due to fiber orientation.

Specimens of 24 oz./sq. yard woven roving and 1.5 oz./sq. ft. mat are comparable with specimens of 24 oz./sq. yard 0/90 knit fabric and 1.5 oz./sq. ft. mat. One conclusion is that the weft (90 degree) fibers of the woven specimen are more efficient than the woven warp (0 degree) fibers. The author explains that the warp fibers have an initially straight geometry and the weft fibers are woven around these straight warp fibers. The knitted specimen was significantly stronger and stiffer than the woven specimen in the 0 degree direction. This was attributed to the initially straight fibers in this direction for the knitted specimen. Another interesting result was a significant increase in the in-plane shear strength and stiffness values for the knitted specimen. The knitted fabric was less stiff than the woven in the 90-degree direction. The author does not address this point. The significant values (all in psi) for both specimens are given in Table 2.3:

Table 2.3 – Material Properties of Woven Roving and Knitted Fabric

	0/90 knitted fabric with 1.5 oz. mat	*Woven roving with 1.5 oz. mat*
Tensile modulus at 90 degrees:	1,270,000	1,620,000
Tensile modulus at 0 degrees:	1,870,000	1,750,000
Ultimate tensile stress at 90 degrees:	26,300	27,500
Ultimate tensile stress at 0 degrees:	41,500	32,800
Shear modulus at 90 degrees:	3,200,000	2,080,000
Shear modulus at 0 degrees:	4,000,000	2,720,000
Ultimate shear stress at 90 degrees:	4,300	2,880
Ultimate shear stress at 0 degrees:	4,700	2,720

The remainder of the tests were concerned with different weights per area of knitted fabric. The results are not relevant for the purposes of this dissertation.

Conclusions were as follows:

1. Fabrics can be engineered to meet specific strengths and modulus.
2. Knitted fabrics containing straight reinforcement fibers are more efficient than woven fabrics.
3. Each fabric style must be tested to establish its characteristic values.

2.6 *Section X: Fiber-Reinforced Plastic Pressure Vessels*, ASME Boiler and Pressure Vessel Committee, Subcommittee on Fiber-Reinforced Plastic Pressure Vessels, 1998 Edition with 1999 Addenda and 2000 Addenda[2.7]

This code is the primary standard governing the design of fiber reinforced pressure vessels. It is an international code. Failure of fiber reinforced pressure vessels is often catastrophic and can result in loss of life. Furthermore, the design of fiber reinforced structures does not lend itself to a simple straightforward analysis. Therefore, the code tends to be conservative, lengthy and involved. Only the basic points of the code will be summarized here.

A background in the various failure theories for composites is necessary to understand and apply certain provisions of the code. The main failure theories for composites are described in Chapter 5.

The design of vessels is broken into two main parts:

a) Class I Design – qualification of a vessel design through pressure testing of a prototype.

b) Class II Design – mandatory design rules and acceptance testing by nondestructive methods.

The two methods may not be intermixed.

Class I design is intended for manufactured vessels with multiple vessels that are identical. Class I designs require that fatigue testing be performed on a prototype vessel. The prototype must be cycled 100,000 times over a pressure range of atmospheric to the design pressure. The prototype is then hydrostatically tested. The minimum strength of the prototype vessel must be at least six times the design pressure. An exception is vessels constructed with uncut filaments. In that case, the minimum strength of the prototype vessel must be only 5 times the minimum design pressure and only 33,000 cycles are required. Class I designs are limited to 1,500 psi for filament-wound vessels and 3,000 psi for filament wound vessels with polar boss openings.

Class II design is intended for a one-of-a-kind vessel. Class II designs are governed by Article RD-11 and Article RD-6. The maximum design pressure depends on the diameter of the vessel and whether Design Rules or Discontinuity Analysis is used. In no case can the design pressure exceed 200 psi. No cyclic testing is required for vessels designed as Class II. Destructive pressure testing is also not required. Rather, the vessel is pressured to 1.10 times the design load and evaluated with non-destructive techniques. These techniques include visual inspection, leak testing and acoustic emission. If the vessel passes the non-destructive evaluation it can then be placed into service.

Allowable fabrication methods for Class I and Class II vessels are described in Article RG-4. Material requirements for fibers and resins are described in Part RM.

Part RD describes design requirements. This portion of the code addresses load combinations, acceptance testing, degradation and other factors to be considered in the design.

Article RD-4 addresses secondary bonding. Class I vessels are allowed to use either adhesive bonding or laminate overlay. Class II vessels are restricted to laminate overlay only. Secondary bonded joints must employ overlays calculated in accordance with Articles RD-11 and RD-12 and pass the Acceptance Test criteria of Article RT-6.

Article RD-5 addresses the reinforcement of openings. Class I openings may be designed by any method. Class II vessels must have openings designed in accordance with Articles RD-11 (mandatory design rules for Class II vessels) and RD-12.

Article RD-6 addresses the design of nozzles and other connections. This article is similar to that regarding reinforcement of openings. Schematics of several nozzle installation types are shown. For Class II vessels, the nozzle opening reinforcement is required to be designed by RD-1174.2. The reinforcement may be evenly divided between the inside and outside of the vessel (figures RD-620.5 and RD-620.6.). Flange thicknesses for various pressures are given in Table RD-620.1.

Design of Class II vessels:

Article RD-11 describes the "Mandatory Design Rules for Class II Vessels". As mentioned previously, Class II vessels are designed by rules and then acceptance tested by visual inspection and acoustic emission individually. Two different design methods may be followed when designing a Class II vessel:

a) Method A - Design Rules: RD-1170

b) Method B – Discontinuity Analysis: RD-1180

The maximum strain theory of failure is used for Method A and the quadratic interaction criterion is used for Method B.

A registered engineer must certify the design of Class II vessels. The engineer must be knowledgeable in the design of reinforced plastics.

The design of Class II vessels is limited as follows:

a) Vessels designed in accordance with Method A are limited to 75 psi internal pressure and 96 inch inside diameter.

b) Vessels designed in accordance with Method B are limited as follows:

   1) the algebraic product of the internal pressure (psi) and the inside diameter (inches) shall not exceed 7200.

   2) the maximum internal pressure shall not exceed 200 psi

   3) the maximum inside diameter shall not exceed 144 inches

c) Vessels may be designed using a combination of Methods A and B. For such vessels the maximum design pressure is limited to 75 psi and the maximum inside diameter is limited to 96 inches.

Vessels designed by either method are limited to 15 psi external pressure. A schematic of these limitations is given in Figure RD-1120.1 of the code and is reproduced here (Figure 2.5) for convenience.

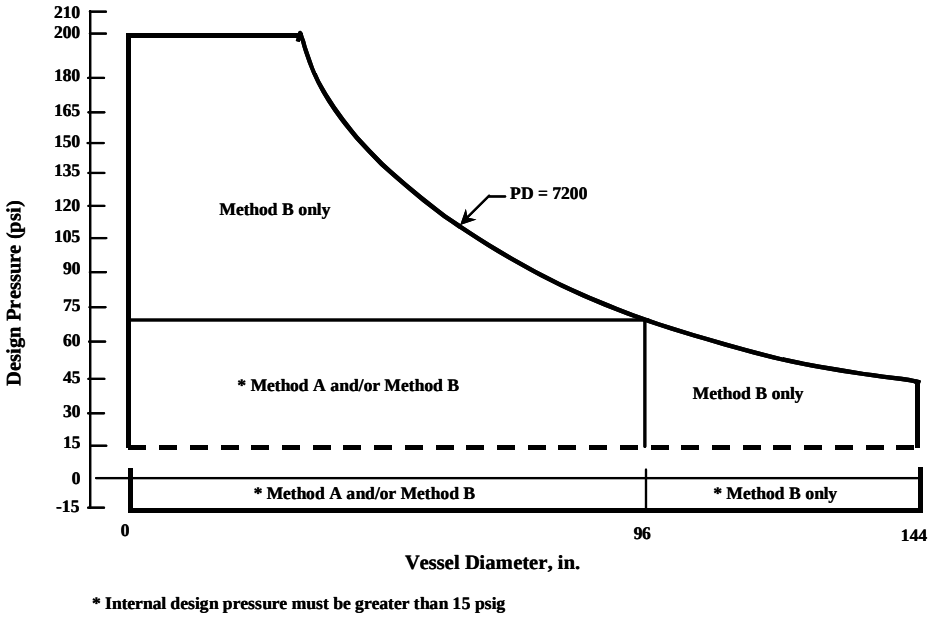

Figure 2.5 – Limitations for Design of Class II Vessels – (Reproduced from Section X of ASME Code, 1998)

Physical testing of laminas is required and covered in Article RT-7 "Determination of Mechanical Properties of Lamina for Use with Class II Vessels". This article requires that four elastic constants (E_x, E_y, E_s, ν_x) and five strength constants (X, X_c, Y, Y_c, S) be determined for each lamina, where;

E_x = modulus along the fiber direction

E_y = modulus transverse to the fiber direction

E_s = in-plane longitudinal shear modulus

ν_x = major Poisson ratio (the negative of the strain transverse to the fiber direction divided by the strain along the fiber direction when a uniaxial stress is applied along the fiber direction)

X = tensile strength along the fiber direction

X_c = compressive strength along the fiber direction

Y = tensile strength transverse to the fiber direction

Y_c = compressive strength transverse to the fiber direction

S = in-plane shear strength

Classical lamination theory is then used to determine the characteristics of laminates.

Design calculations are required for (but not limited to) the following:

a) vessel shell

b) vessel heads

c) openings and their reinforcement

d) secondary bonds joining two or more vessel parts

e) internal and external attachments

This section is divided into two parts: design by Method A and design by Method B.

Article RD-1170 Design Rules – Method A (revised by Addenda 2000)

As mentioned previously, design by Method A is governed by maximum strain theory. The absolute value of membrane strain in any direction is not allowed to exceed 1,000 micro-strain. Semi-empirical formulas are given for different portions of the vessel. The main sections are listed below. For formulas, the reader is directed to the original document.

RD-1171 Thickness of Shells

RD-1172 Vessel Shells Under External Pressure

RD-1173 Thickness of Heads

RD-1174 Openings in Shells and Heads

RD 1175 Joining Vessel Parts

RD-1176 Design of Flanges

Article RD-1180 Discontinuity Analysis – Method B (no revisions)

Design of Class II vessels by discontinuity analysis requires detailed stress analysis and evaluation of the results against the quadratic stress interaction criteria. Primary and secondary stresses must be investigated at gross structural discontinuities. Gross structural discontinuities are defined as relatively large portions of the structure that have a significant effect on the overall stress or strain pattern or on the structure as a whole. Examples are head-to-shell and flange-to-shell junctions, nozzles, and junctions between shells of different diameters or thicknesses. Linear elastic stress analysis is allowed. A procedure for basic discontinuity analysis is outlined and a few simple examples are given. However, it is mentioned that for vessels with openings, complex geometries or anisotropic materials hand calculations are very difficult and computer programs are normally used. Essentially, all portions of the structure must be modeled (generally by using a commercially available finite element or finite difference program) and the stresses compared with the quadratic interaction criteria. Fortunately, many finite element programs are equipped with the interaction criteria employed by the code.

The design is considered to be acceptable if:

a) the design is such that the stress at any point in the vessel does not exceed the limits stated in RD-1189 (this is essentially the quadratic interaction criteria with a stress ratio of 6)

b) for configurations where compressive stress occurs, the design must meet the requirements of RD-1183

c) the average shear stress between the vessel and overlays must not exceed 200 psi

d) interlaminar shear between shell lamina need not be considered

Examples of calculating lamina stresses and strains are given. Section RD-1188.5 gives the quadratic interaction criterion to be used:

$$R^2(F_{xx}\sigma_x^2 + 2F_{xy}\sigma_x\sigma_y + F_{yy}\sigma_y^2 + F_{ss}\sigma_s^2) + R\,(F_x\sigma_x + F_y\sigma_y) - 1 = 0 \qquad \text{(Eqn. 2.1)}$$

where:

$F_{xx} = 1/XX_c$

$F_{yy} = 1/YY_c$

$F_{ss} = 1/S^2$

$F_x = 1/X - 1/X_c$

$F_y = 1/Y - 1/Y_c$

$F_{xy} = F_{xy}^*[F_{xx}F_{yy}]^{1/2}$, with F_{xy}^* taken to be –1/2

where:

X = ultimate tensile strength of a lamina in the x (strong) direction

X_c = ultimate compressive strength of a lamina in the x direction

Y = ultimate tensile strength of a lamina in the y (weak) direction

Y_c = ultimate compressive strength of a lamina in the y direction

S = ultimate shear strength with respect to shear stress in the x-y plane

This is the Tsai-Wu interaction criterion with an R factor included. The R term is referred to as a "stress ratio" as opposed to a "safety factor" to distinguish the orthotropic laminate from an isotropic layer. A value of greater than 6.0 is required for this stress ratio.

2.7 *Reinforced Thermoset Plastic Corrosion Resistant Equipment, ASME RTP-1*, American Society of Mechanical Engineers, 1995 Edition (Revision of ASME RTP-1 – 1992 Edition), with Addendums ASME RTP 1a-1995, ASME RTP-1b-1997, ASME RTP 1c-1998, ASME RTP-1d, 1998 and ASME RTP –1e, 1999[2.8]

This code is the American standard governing the design of fiber reinforced vessels that have design pressures of less than 15 psi. Low pressure vessels are often referred to as tanks. These tanks often contain toxic products. Failure of tanks can also result in loss of life. This code is similar to Section X and is also conservative, lengthy and involved. RTP-1 goes into more detail about fabrication details and construction techniques. Acoustic emission testing is not required, but a reduced stress ratio can be used if acoustic emission testing is conducted. Only the basic points of the code will be summarized here.

Proof testing of the constituent laminates is required for pressures in excess of 2 psi. Destructive testing of the as-constructed vessel is not required.

As in Section X, the code is divided into two parts: Subpart 3A – Design by Rules and Subpart 3B – Design by Stress Analysis. These methods may be intermixed.

Subpart 3A – Design by Rules (revised RTP-1a, 1995, RTP-1b, 1997, RTP-1c, 1998, RTP-1d, 1998 and RTP-1e, 1999)

The design by rules is governed by semi-empirical equations and maximum stress or strain theory. The maximum strain is again 1,000 micro-strain. Maximum stresses are determined from proof testing of laminates and the application of a design

factor. A design factor of 10 is generally required. The basic sections are listed below. Formulas and nomenclature can be found in the original document.

3A-200 Design for Internal Pressure

3A-210 Calculation of Minimum Thickness of Cylindrical Shells

3A-220 Minimum Thickness of Torispherical Heads

3A-250 Minimum Thickness of Flat Bottom Heads

3A-300 Design for External Pressure

3A-310 Cylindrical Shells

3A-320 Torispherical Heads

3A-330 Stiffening Rings

3A-340 Top Head Loads

3A-700 Reinforcement of Circular Openings

3A-710 Reinforcement in Shells and Heads

3A-720 Opening Reinforcement Diameter

3A-730 Opening Reinforcement Thickness

3A-800 Secondary Bond Shear Stress

Subpart 3B – Design by Stress Analysis (revised RTP-1b, 1997, RTP-1c, 1998 and RTP-1d, 1998)

As with Section X, the "Design by Stress Analysis" (referred to as "Discontinuity Analysis" in Section X) is governed by the quadratic interaction criteria. However, a series of "strength ratios" are given as opposed to the single stress ratio of 6.0 given in Section X. Also, the analysis of the internal corrosion layers is considered separately from the filament winding and other structural layers. The minimum strength ratio in the inner surface and interior layer must be as follows:

a) for vessels using combinations of Subparts 3A and 3B, the minimum strength ratio must be 10

b) for vessels designed entirely by Subpart 3B, the minimum strength ratio must be 9

c) for vessels designed entirely by Subpart 3B and for which an acoustic emission examination by Appendix M-10 is performed, the minimum strength ratio must be 8

d) for vessels in critical service, the minimum strength ratios in a) through c) must be multiplied by 1.25

The strength ratios in the rest of the laminate are surprisingly non-conservative. For vessels not in critical service, the strength ratio must be at least 1.6 for these layers. For vessels in critical service, the strength ratio must be at least 2.0 for these layers. This is far below the strength ratio of 6.0 required by Section X when Discontinuity Analysis is performed.

The values given in a), b) and c) may be divided by 1.2 for wind or seismic loading. If the strength ratio is less than 1.6 in any lamina, the designer must account for the possibility of reduced mechanical properties in the laminate.

When computing strength ratios for Design by Stress Analysis, each individual lamina is considered. This differs from the Design by Rules, where the entire laminate is considered. Temporary oblation is also considered.

e) for loadings due to temporary oblation, the design factor must be greater than or equal to 3.0, and the criterion for the strength ratios of the laminate layers are as follows:

    1) interior mat layers shall be greater than or equal to 3.0

    2) the strength ratio of C-veil inner layers shall be greater than or equal to 3.0

3) the strength ratio of synthetic veil inner layers shall be greater than or equal to 2.0 when the veil is in tension, and greater than or equal to 3.0 when the veil is in compression.

4) The strength ratio of the structural layers shall be greater than or equal to 1.5 with the exception of axially oriented fiber layers, which may be less than 1.0. Microcracking shall be permitted only in axially oriented fiber layers.

Mandatory Appendix M-10: Acoustic Emission Examination (revised RTP-1a, 1995)

This appendix is rather brief. The CARP criteria are referenced as a further source of information. Calibration procedures for the acoustic emission test are given. Four acceptance/rejection criteria are given:

1. Emissions during load hold. For the first and subsequent fillings, none beyond 2 minutes are allowed.

2. Felicity ratio. A Felicity ratio of less than 0.95 is not allowed.

3. Total counts. For the first filling, counts above N_c are not allowed. For subsequent fillings, none above $N_c/2$ are allowed. Counts are reliant on the equipment being used to monitor the emissions and the acoustic properties of the vessel being monitored. Therefore, N_c is determined by an empirical method involving pencil lead breaks on the vessel. Breaks are conducted both above and below the water line.

4. Number of events greater than the reference amplitude threshold. For the first filling and subsequent fillings, no more than 10 such events are allowed. The reference amplitude threshold also depends on the equipment being used to monitor the emissions and the acoustic properties of the tank itself. Therefore, the reference amplitude threshold

is determined empirically as well. Pencil lead breaks are conducted on a mild steel bar at a distance of 7 feet from the sensor.

2.8 *Recommended Practice for Acoustic Emission Testing of Fiberglass Reinforced Plastic Resin Tanks/Vessels,* The Society of the Plastics Industry, Inc., Committee on Acoustic Emission from Reinforced Plastics (CARP) of the Composites Institute, 1987[2.9]

This recommended practice addresses the structural evaluation of fiber reinforced plastic vessels with acoustic emission monitoring. The practice is limited to 65 psi internal pressure and 9 psi vacuum. The practice recommends that flaws located by acoustic emission be more closely examined with other non-destructive methods, repaired and then re-tested with acoustic emission.

The practice covers basic AE definitions, instrumentation, pre-test preparation, sensors, and test procedure. Both high and low frequency sensors are required. Loading algorithms are given for atmospheric vessels (vessels that operate with less than 15 psi head) and pressure vessels. For new vessels, initial loadings are monitored, but in the event that the vessel does not pass the acoustic emission test, re-loadings are permitted. The vessel is required to be conditioned between loadings. A conditioning period is outlined in Table 1 of the recommended practice and is reproduced in Table 2.4 for convenience. In-service vessels are also covered by the recommended practice.

Table 2.4 – Conditioning requirements (CARP, 1987)

Percent of Operating Pressure and/or Load	*Time at Reduced Level*
10 or less	12 hours
20	18 hours
30	30 hours
40	2 days
50	4 days
60	7 days

The acceptance criteria for vessels with less than 14.7 psig head are shown in Table 2.5. Underlined criteria carry the greatest weight.

Table 2.5 – Acceptance criteria – vessels below 14.7 psi (CARP, 1987)

	First filling	***Subsequent fillings***
Emissions during hold	No events having an amplitude greater than A_m beyond 2 minutes	None beyond 2 minutes
Felicity Ratio	Not applicable	Greater than 0.95
Total counts	Less than N_c	Less than $N_c/2$
Number of events greater than reference amplitude threshold	Less than 10	Less than 5

The count criterion N_c is determined experimentally with pencil lead breaks on the vessel wall. The reference amplitude threshold A_m is determined experimentally with pencil lead breaks on a mild steel bar. These procedures are described in the appendix of the recommended practice.

The acceptance criteria for pressure vessels (superposed head greater than 14.7 psi and less than 65 psi) are reproduced in Table 2.6.

Table 2.6 – Acceptance criteria – vessels between 14.7 and 65 psi (CARP, 1987)

	First filling	***Subsequent fillings***
Emissions during hold	Less than 5 events per minute having an amplitude greater than A_m beyond 2 minutes	None beyond 2 minutes
Felicity Ratio	Not applicable	Greater than 0.95
Total counts	Not excessive	Less than $N_c/2$
Number of events greater than reference amplitude threshold	Less than 10	Less than 5

For the total counts criteria, excessive counts are defined as a significant increase in the rate of emission as a function of load. On a plot of counts versus load, this shows as a departure from linearity.

The stated significance of the criteria is as follows:

Emission during hold – This criteria is thought to be particularly significant. Continuing emissions during a hold are indicative of continuing and permanent damage. Permanent damage is stated to include: microcracking, debonding and fiber pull-out.

Felicity ratio – This is a measure of previously induced damage and is particularly useful for in-service vessels. The onset of "significant" emission for determining this ratio is dependent on the interpretation of the operator. Guidelines offered are:

- more than 5 bursts of emission during a 10% increase in load
- more than $N_c/20$ counts during a 10% increase in load
- emission continuing during a load hold. A short (less than 1 minute) non-programmed load hold is allowed for determination of this ratio

High amplitude events – This criterion is important for new vessels. High amplitude events are often associated with fiber breakage and major structural damage. Emissions during load hold and Felicity ratio are more likely to govern for in-service vessels.

Total counts – the practice recommends looking at trends in count data as opposed to total counts for most applications. However, excessive counts (as defined above) are noted to be a sign of impending failure.

As background information, it is noted that approximately 5,000 field tests had been carried out and 15 new and used vessels had been taken to failure. 243 small laboratory samples with different fiber constructions and resin types had also been tested. The resins had elongations to failure of 2% to 6% (20,000 to 60,000 micro-strain). The evaluation criteria were stated to be applicable for vessels designed for a maximum

allowable strain of up to 0.3% (3,000 micro-strain). This strain limit is 3 times as high as that allowed when designing by Method A (Design Rules) of Section X.

2.9 *Recommended Practice for Acoustic Emission Evaluation of Fiber Reinforced Plastic (FRP) Tanks and Pressure Vessels*, The Committee on Acoustic Emission from Reinforced Plastics (CARP), a Division of the Technical Council of The American Society for Nondestructive Testing, Inc., Draft I, October 1999[2.10]

This draft is similar to the 1987 Recommended Practice. Only the aspects in which it differs significantly will be addressed here.

The following instrument displays are required by section7.6:

1. Bar chart by channel of cumulative signal strength
2. Amplitude per hit versus time
3. Duration per hit versus time
4. Log duration (or counts) per hit versus amplitude per hit
5. Cumulative signal strength per channel versus time
6. Cumulative amplitude distribution or a tabular listing by channel number of total hits equal to and greater than defined amplitude values.

Intensity analysis is added to the Draft copy of the Recommended Practice in Section 12.10. Intensity analysis is intended to provide guidance about repair options to the owner or operator of the vessel. It is conducted on a per channel basis. The method uses two factors based on signal strength. This first is historic index, which compares the signal strength of the most recent hits to the signal strength of all hits. The second is severity, which is the average of the largest signal strength hits striking a sensor. Historic index and severity are defined in Chapter 1.

A plot of log historic index versus log severity is referred to as an “intensity chart”. The intensity chart is divided into zones labeled “insignificant”, “minor”,

"intermediate", "follow-up" and "major". The intensity chart is shown in Figure 12.10.3 of Draft I of the Recommended Practice and is reproduced in Figure 2.6.

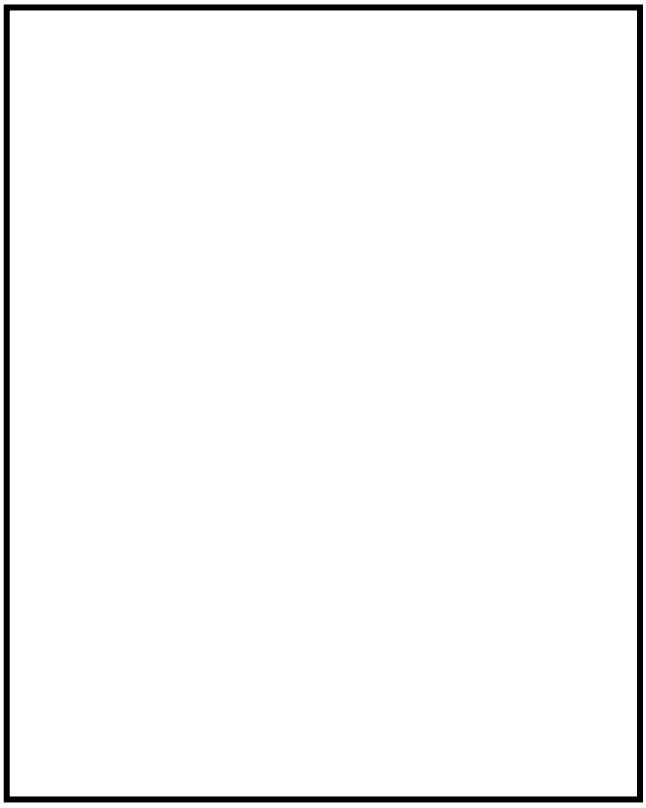

Figure 2.6 – Intensity Chart for FRP Vessels (Draft I, CARP 1999)

Recommended actions are listed in Table 12.10.4 of Draft I and are reproduced in Table 2.7.

Table 2.7 Minimum Recommended Follow-Up Action (Draft I, CARP 1999)

Intensity Category	*Recommended Action*
INSIGNIFICANT	Emission source is structurally insignificant
MINOR	Minor emission. Note for future reference. Visually inspect accessible areas.
INTERMEDIATE	Defect requiring follow-up evaluation. Evaluation may be based on further data analysis, retest, or complementary nondestructive examination. Visually inspect accessible areas.
FOLLOW-UP	Significant structural defect. Requires immediate inspection using complementary nondestructive examination methods.
MAJOR	Major structural defect. Immediate shutdown and nondestructive examination.

Chapter 3: *Overview of the Coupon Experimental Program*

This chapter addresses the testing of small coupon specimens. The geometry of the specimens, the loading frame, loading procedure and acoustic emission monitoring equipment are described. The mechanical properties of the resins and fibers and the nomenclature to differentiate between specimens are established.

3.1 Description of Coupon Specimens

Coupons were cut from larger plates of glass reinforced vinyl ester and polyester. The plates were laid up by hand at the Ershigs plant in Gatesville, Texas. Three types of coupons were tested. The first type had oriented fibers near the top and bottom of the specimen. These specimens were nominally 1" wide by 7" long by 3/8" thick. This type of specimen is shown in Figure 3.1. All dimensions are nominal.

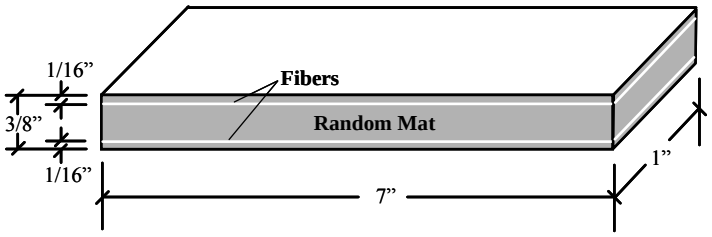

Figure 3.1 – Oriented fiber specimen

The second type of specimen had layers of woven roving distributed throughout the thickness. These specimens were nominally 1" wide by 6" long by 1/4" thick. This specimen type is shown in Figure 3.2.

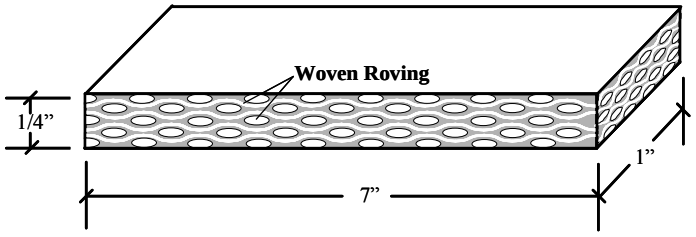

Figure 3.2 – Woven roving specimen

The third type of specimen was similar to the oriented fibers specimens, but the portion containing the oriented fibers was trimmed off. This left only the remaining random mat layer. These specimens were nominally 1" wide by 6" long by1/4" thick. This specimen type is shown in Figure 3.3.

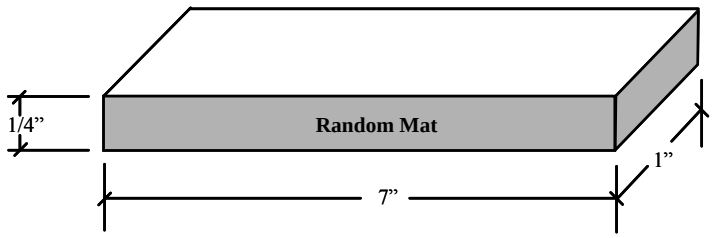

Figure 3.3 – Random mat specimen

For the purposes of this dissertation, global X, Y and Z axes are used to refer to the coupon specimen geometry. The X direction is along the length of the coupon, the Y direction is in the width direction and the Z direction is in the thickness direction. The convention for orientation of the fibers is shown in Figure 3.4 and is as follows:

Fiber direction = 1-axis

Direction transverse to fibers in X-Y plane = 2-axis

Direction transverse to fibers in X-Z plane = 3-axis

These conventions are shown in Figure 3.4.

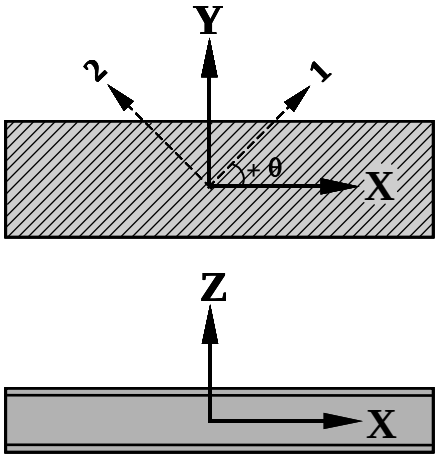

Figure 3.4 – Conventions used for global and material axes

Fiber architecture and resin type were investigated to determine the effect on the acoustic emission data.

Fiber orientations investigated were:

Fibers oriented parallel to the X-axis

Fibers oriented perpendicular to the Y-axis

Fibers oriented at + 45-degrees to the X-axis

For all cases involving woven roving the warp direction was oriented parallel to the X-axis. The warp direction is the long direction when the fabric is unrolled. The weft direction is the short direction when the fabric is unrolled.

Five resins were investigated. These are listed in Table 3.1. Available published properties are also given in Table 3.1[3.1]. The ISO listed in table 3.1 is manufactured by Ashland. The manufacturer of the ISO used for testing is not known with certainty.

When performing laminate calculations it is convenient to use a readily available commercial computer program. One such program is Trilam.[3.2]. When mechanical

properties were not available from the manufacturer this program was used to calculate the missing properties. The available calculated values from this program are given in Table 3.2. When values are available from both the manufacturer and the computer database, these values do not always coincide exactly. However, they are generally within good agreement with the exception of tensile strength. Tensile strength values provided by the manufacturer were used for calculations.

E-glass fibers were used for all specimens. Representatives of the company that constructed the specimens (Ershigs, Inc.) indicated that the fibers were most likely manufactured by Certainteed. The fibers were grouped into discrete bundles.

Published properties of E-glass fiber are as follows[3.3]:

Number of fibers per end = 204

Fiber diameter = 0.00036 inches

Density = 0.090 lb./cu. inch

Longitudinal modulus = 10,600 psi

Transverse modulus = 10,600 psi

Longitudinal shear modulus = 4,370 psi

Longitudinal Poisson ratio = 0.22

Transverse Poisson ratio = 0.22

Longitudinal tensile strength = 400,000 psi

Burnout tests (ASTM D2584-94) were performed by Fibergrate to determine the fiber content[3.4]. Fibergrate was provided with 1" by 1" samples of the coupons. Both total thickness specimens and specimens with the outer reinforcing layers removed were provided. The tests indicated that the fiber content of the random mat portion of the oriented fiber specimens was approximately 40% by weight. The fiber content of the entire thickness specimens was also determined to be approximately 40% by weight. The design fiber content of the woven roving specimens was 24 oz. / sq. yard, which is equivalent to a fiber content of approximately 50% by weight. Burnout tests of the woven roving specimens also indicated the fiber content was approximately 40% by weight.

Table 3.3 summarizes the number of specimens tested of each "fiber architecture" and resin type. Fiber architecture is a term that encompasses type, content, placement and orientation of the fibers.

Table 3.3 – Number of Specimens Tested of Different Fiber Architecture and Resin Type

	0-degree	90-degree	45-degree	woven roving	random mat
Derakane 470	2	7	-	-	-
Derakane 411	3	6	2	1	1
Derakane 8084	3	8	2	3	1
Ashland 197	3	3	2	3	1
General ISO	3	3	-	-	-

Nomenclature was developed to differentiate between coupon specimens. The nomenclature used is as follows:

Resin type – fiber architecture – specimen number

In accordance with industry practice, shorthand was used for the resin types because several of the resin names are lengthy. The resins were abbreviated as follows:

Derakane 470-300 = 470
Derakane 411-350 = 411
Derakane 8084 = 8084
Hetron 197-3 = 197
Aropol 7241T-15 = ISO

Fiber architecture was abbreviated as follows:

WR = Woven roving specimen

RM = Random mat specimen

90 = Oriented fiber specimen with fibers oriented at 90-degrees

0 = Oriented fiber specimen with fibers oriented at 0-degrees

45 = Oriented fiber specimen with fibers oriented at 45-degrees

Example: 411-90-1

411 = Resin type

90 = Orientation of fibers with respect to the X-axis

1 = Specimen number (of the 411-90 type)

Example: 8084–WR–3

8084 = Resin type

WR = Woven roving

3 = Specimen number (of the 8084–WR type)

The actual thickness of each specimen varied considerably. The measured dimensions of all 90-degree, 0-degree, 45-degree, woven roving and random mat specimens prepared are shown in the Tables 3.4, 3.5, 3.6, 3.7 and 3.8 respectively.

3.2 Loading Frame and Loading Procedure

The coupons were loaded in four-point bending to obtain a region of constant moment and zero shear. Load was applied with a hydraulic ram. For the first group of specimens (approximately 10) load was read from a pressure gage. For the remaining specimens, load was read with a load cell (Sensotec model number 53/0239-04, 5,000-pound maximum, certificate of calibration Oct. 3, 1995). A schematic of the applied loading geometry and resulting shear and moment diagrams is shown in Figure 3.5. A photograph of the loading frame is shown in Figure 3.6.

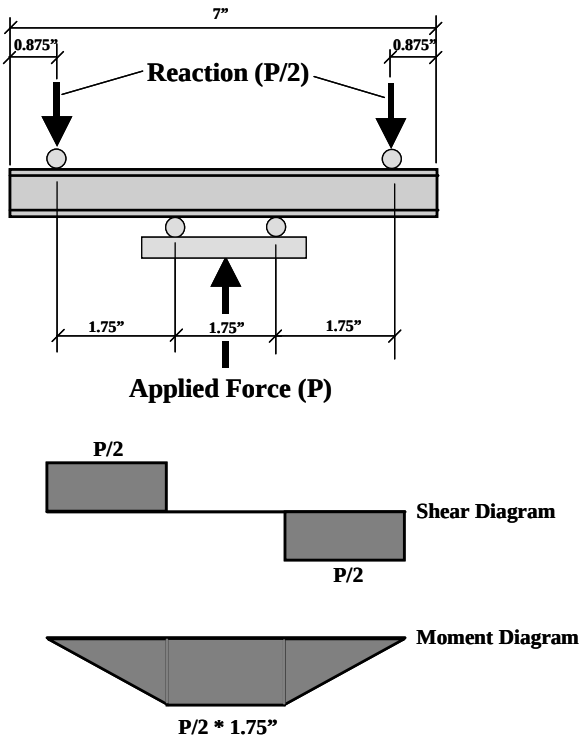

Figure 3.5 – Loading Geometry and Resulting Shear and Moment Diagrams

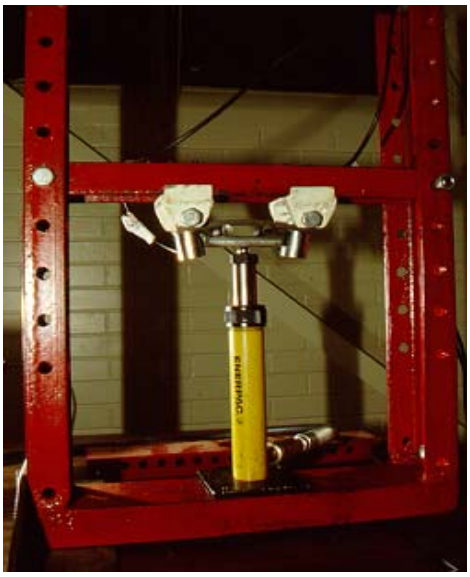

Figure 3.6 – Photograph of Loading Frame

The loading increment depended on the specimen being tested. In most cases, the load was applied in increments of approximately 5% of the estimated ultimate load of the specimen. Load was applied in a stepwise fashion with load holds of two minutes. A schematic of the loading sequence is shown in Figure 3.7.

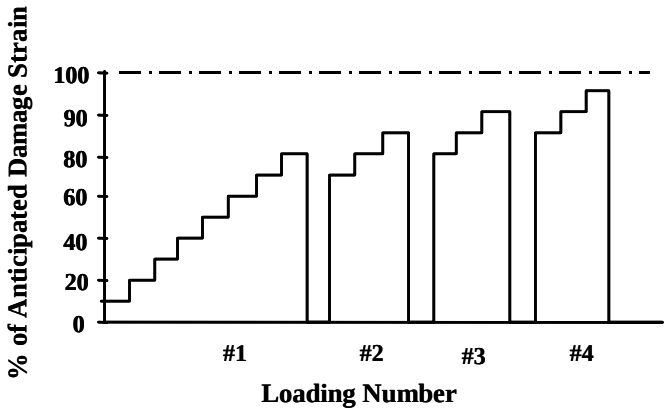

Figure 3.7 – Idealized Loading Sequence

3.3 Strain Gage Monitoring

For specimens with transverse and longitudinal fiber orientations, one strain gage was affixed to the top and bottom of each specimen. The same was true for woven roving specimens. These gages were oriented parallel to the global X-axis. For specimens with fibers oriented at an angle to the applied stress, three strain gages were affixed to the tensile side of the specimen and one gage was affixed to the compressive side. On the tensile side, two gages were oriented parallel to the 1 and 2-axes and the third was aligned parallel to the X-axis. On the compressive side, the single gage was oriented parallel to the X-axis. These gage locations are shown schematically in Figure 3.8.

It is important to use relatively large area strain gages when monitoring composites due to significant local variations in strain. These come about due to the non-

homogeneous nature of the laminate. Depending on the specimen geometry it is sometimes advantageous to use very large strain gages. This is not advantageous for areas with large strain gradients or for small specimens.

Most resins have low thermal conductivity and it is possible to overheat the strain gages. This is particularly true in the case of stacked rosettes. For this reason and for greater accuracy in the readings, it is generally recommended that 350- Ω gages be used for composites. However, expense and availability are also issues to be considered. For the coupon testing, 120- Ω (Micro-measurements model no. CEA-06-250UW-120) and 350- Ω (Micro-measurements model no. CEA-06-250UW-350) gages were used interchangeably. For the first group of specimens (approximately 10), the strains were read with a switch and balance box. For the remaining specimens, the strain data was collected electronically with a Hewlett Packard data acquisition system.

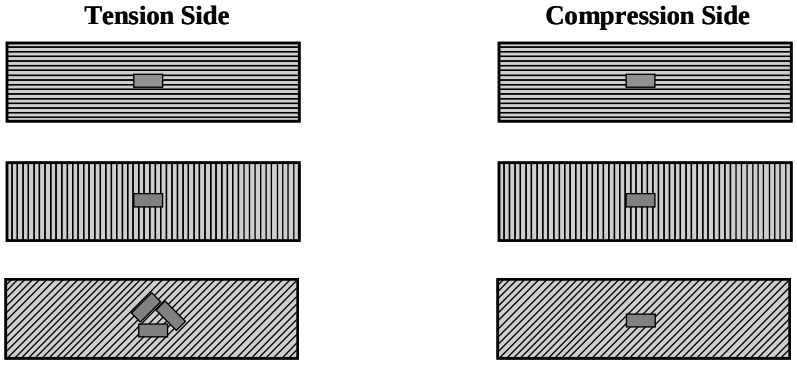

Figure 3.8 – Strain Gage Locations for Oriented Fiber Specimens

3.4 Acoustic Emission Monitoring

All acoustic emission (AE) equipment was as manufactured by Physical Acoustics Corporation (PAC). In most cases, the acoustic emission of the coupon specimens was monitored with one R15I sensor. A Transportation Instrument was used to collect AE data from the R15I sensor. In some cases, one wideband sensor (No. S9208) was also used to monitor emission. When a wideband sensor was used, the AE

data was collected with a Mistras 2000. A sketch of typical AE sensor locations is shown in Figure 3.9.

In most cases, the sensors were attached with hot melt glue. The sensors were applied while the glue was fresh from the glue gun and pressure was applied by hand for approximately two minutes. In some cases, the sensors were attached with a thin layer of vacuum grease. In this case, duct tape was wrapped around both the sensor and the coupon specimen to provide constant pressure. The method involving vacuum grease proved to be the more sensitive of the two and was less time consuming.

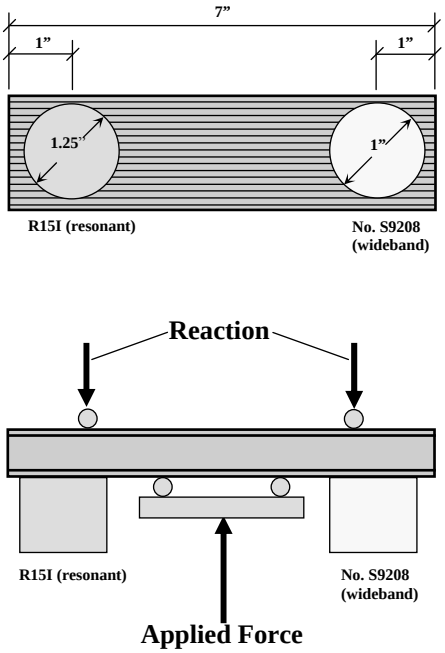

Figure 3.9 – Acoustic Emission Sensor Locations

Prior to testing, the sensors were calibrated by using 0.3 mm 2H pencil lead breaks. In accordance with Section 9 of the CARP criteria, the lead was extended approximately 2.5 mm from a mechanical pencil and broken at an angle of approximately 30-degrees to the X-Y plane. Three lead breaks were conducted for each sensor on each specimen. The recorded amplitudes were required to be within 3 dB of each other prior to testing. In most cases, the sensors were also calibrated after the test to insure that no loss of sensitivity had occurred during the testing. If a loss of sensitivity of more than 3 dB was noticed the test results were not used.

Chapter 4: *Determination of Damage in Coupon Specimens*

4.1 Introduction

Designing with composites is generally accomplished with destructive testing of sample laminas or a maximum strain criterion that is based on previous experience. When destructive testing of sample laminas is conducted, the results are used in conjunction with a biaxial stress criterion and a stress ratio is assigned. Both the biaxial stress and maximum strain criteria ignore the damage mechanisms that lead to failure of laminas. Only the ultimate stress or strain is considered.

The onset of damage is of primary interest in designing with fiber reinforced polymers. If the onset of damage can be determined experimentally design codes can address this issue directly. This appears to be particularly significant for flexible as opposed to more conventional resins. As described in the paper by Cortez, et. al., 1983[4.1], composites made with flexible resins can undergo higher strain and stress prior to the onset of damage. This is true even though the ultimate failure stress for composites constructed with flexible and more conventional resins is similar.

In the paper by Cortez, et. al., AE counts were used as a measure of damage in coupon specimens during a single loading to failure. In this chapter, an AE test procedure is described that determines the onset of significant AE in a large variety of coupon specimens. The test procedure involves a loading and reloading procedure and makes use of the Felicity effect. The primary variable investigated in the testing was resin type. Specimens with fibers oriented at 0 degrees, 90 degrees, 45 degrees and woven roving specimens were investigated.

4.2 Acoustic Emission Parameters Used to Determine Damage

Acoustic emission is produced from fiber reinforced polymers as stress concentrations are relieved. Many different sources can create acoustic emission in FRP specimens. Some of the most commonly listed are:

- Fiber breakage
- Fiber pullout
- Fiber-matrix debonding
- Matrix cracking (both macro and micro)
- Delamination

These mechanisms can occur individually or in combination with one another. Several attempts have been made (by others) to differentiate between these mechanisms with AE. This field of AE is commonly referred to as signature analysis. At present, a well-established criterion to determine which mechanism has caused a particular AE hit or series of hits does not exist. Several methods have been proposed. Some of these methods are based on amplitude and duration and others are based on frequency content. Methods based on frequency content are difficult to apply for field testing where resonant sensors are typically used. Combinations of the two are also possible. Another possible method for signature analysis is the examination of the patterns of AE hits. This area of AE analysis is the subject of the dissertation in progress at the University of Texas by Charles Barnes[4.2].

Due to the geometry of the coupon specimens that were tested, the possible AE source mechanisms can be surmised without rigorous analysis of the AE data. For oriented fiber specimens loaded transverse to the fibers, the source mechanisms are primarily fiber-matrix debonding and matrix cracking. For specimens loaded parallel to the fibers, the source mechanisms are more varied. The mechanisms include fiber-matrix debonding, fiber pullout, fiber breakage and matrix cracking. All five source mechanisms listed above are possible for woven roving specimens. These mechanisms can occur simultaneously for all coupon specimens.

The focus of the coupon testing discussed here is not to determine which mechanisms occurred, but rather to determine at what levels of strain or stress significant damage occurred. Significant damage is determined by examining the basic trends in the AE data. When examining the data in this way the characteristics of individual hits are basically ignored. This is frequently referred to as trend analysis. Instead, the general AE activity over the course of a test is examined. This is consistent with established field test practice where thousands of hits are obtained and it can be misleading to focus on an individual hit. The AE parameter that best lends itself to this type of trend analysis is cumulative signal strength. Signal strength takes into account both the duration and amplitude of each AE hit. Cumulative signal strength gives a basic measure of the AE activity over time. When the slope of the cumulative signal strength versus time curve increases, this indicates that AE activity is also increasing. This increase in activity has historically been associated with damage in the specimen[4.3]. The specific type of damage is not determined from the AE data.

Damage to the specimen as determined by AE can be cross-correlated to the change in slope of the stress or load vs. strain curve (departure from linearity). This is somewhat complicated by the fact that the resin behaves visco-elastically. This is more of a complication for behavior that is matrix dominated (such as loading transverse to the fibers). Several specimens were loaded to failure as part of the testing procedure. These cases are presented at the end of this chapter along with the onset of damage as determined by AE.

During the initial loading of a specimen, the AE activity can be quite sporadic. This is believed to be due to the activation of several structurally non-significant sources. Some structurally non-significant sources include the breakage of weak fibers, cracking adjacent to entrapped air and cracking of strain gage adhesive. Fiber reinforced polymers are highly redundant structures with a very large number of possible load paths. On the first loading, several of the weaker loading paths are activated (causing AE) and the load paths will redistribute. This behavior is expected and is not a cause for concern. The activation of these non-significant sources leads to a cumulative signal strength versus

time curve with no well-defined change in slope (or knee). Rather, several ill-defined knees will appear. This behavior occurs regardless of resin type, but is more pronounced for more brittle resins. Figure 4.1 is a plot of cumulative signal strength and historic index versus time for the initial loading of a woven roving coupon specimen with Derakane 411 resin. This specimen was loaded to failure. Note the several different knees in the cumulative signal strength versus time curve and the several spikes in the historic index versus time plot.

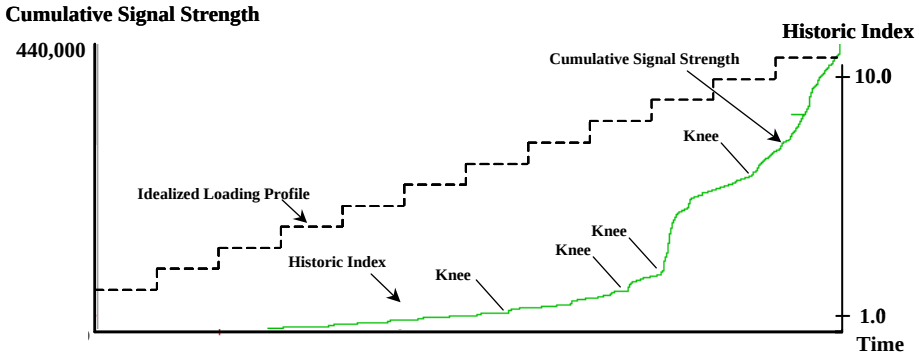

Figure 4.1 – 411-WR Specimen (Loaded to Failure)

One way to determine damage in FRP specimens is to use the Felicity ratio. The Felicity ratio requires that loading, unloading and reloading be performed. When an FRP specimen is reloaded, very little AE activity will be generated until it has reached the previous strain level. This is known as the Kaiser effect. This is true unless the specimen has been previously damaged.

If the specimen has been significantly damaged during a previous loading, emission will begin prior to the previous strain level. This is known as the Felicity effect.

When specimens are re-loaded, the knee in the cumulative signal strength curve is more easily determined. Figure 4.2 is a plot of cumulative signal strength versus time for a woven roving specimen that has been repeatedly reloaded (sixth loading). Note the very clear knee in the cumulative signal strength versus time curve and the very quiet

historic index prior to the knee. The initial spike in the historic index does not correspond to the initial knee in the cumulative signal strength versus time plot. This was a general trend in the data and it was concluded that historic index was not sensitive enough to determine the onset of significant AE in these small coupon specimens, although it did correlate fairly well with the onset of significant AE. For this reason, the onset of AE was determined by inspection of the data for each specimen, with the historic index used only as a general guide. For the purposes of the testing described here, the most sensitive indication of damage was desired. Therefore, the first knee as determined by direct inspection was used to establish the onset of significant AE. It is possible to use historic index or another method if the purpose is to detect the onset of more significant damage.

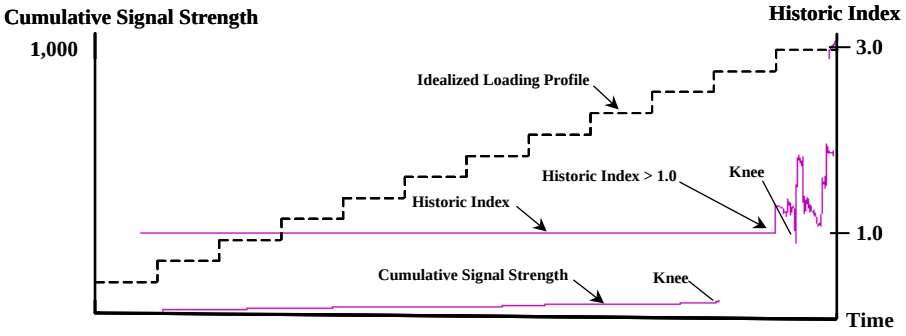

Figure 4.2 – 411-WR Specimen (Sixth Loading)

Both the mechanical and acoustic emission properties of FRP specimens are load history dependent. This is due to the visco-elastic nature of the resin. Upon loading, the FRP specimen will creep. After unloading, the specimen will recover over time. The mechanical implications of this are well known, but the implications for acoustic emission data are often overlooked. If a specimen is reloaded immediately after unloading, little or no AE activity will be detected. If, however, the specimen is allowed to recover for a period of 24 hours, the AE data upon reloading may be quite significant.

The process of allowing a specimen to recover between unloading and reloading is known as "conditioning." Conditioning is addressed in the CARP Recommended Practice.[4.4] The conditioning period for all coupon specimens tested was a minimum of 24 hours. This time period exceeds that required by the CARP Recommend Practice. Additional conditioning had little effect on the AE data.

Another indication of significant damage in an FRP specimen is continuing emission during a load hold. Emission during a load hold indicates that damage is continuing in the absence of increasing stress (self-propagating damage). To monitor emission during load holds, holds of two minutes were used between load steps.

Felicity ratios of less than 1.0 have been correlated to damage in FRP specimens[4.3, 4.4]. The strain at the onset of significant AE can be elevated on subsequent loadings, but the Felicity ratio will continue to decrease. Lower Felicity ratios are consistent with higher levels of damage in FRP specimens. Figure 4.3 shows idealized behavior of a typical specimen.

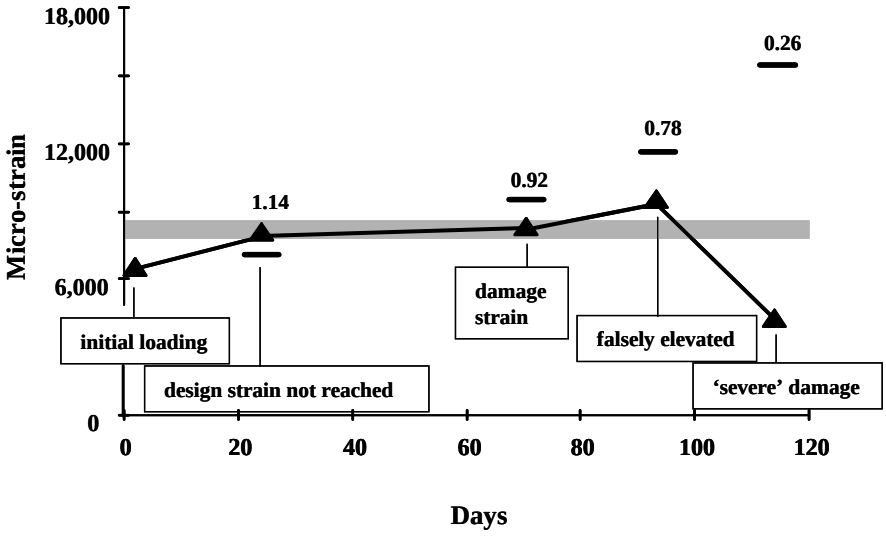

Figure 4.3 – Typical AE behavior of coupon specimens showing strain at onset of significant acoustic emission

The symbols used are as follows:

— = Previous strain to which the specimen was loaded

▲ = Strain at onset of significant AE

1.14 = Felicity ratio

▬ = Damage strain

Initial Loading: The first loading of the specimen. No conclusions about damage can be reached from an initial loading.

Damage strain not reached: The Felicity ratio is greater than 1.0 and therefore more loadings to higher strain are necessary to create significant damage.

Damage strain: At this level of strain, the Felicity ratio has dropped below 1.0. Felicity ratios below 1.0 have been correlated with damage.

Falsely elevated: The Felicity ratio remains below 1.0 and has decreased to 0.78. Even though the strain at onset of AE is higher than on the previous loading, this result is inadmissible.

'Severe' Damage: The Felicity ratio has dropped below 1.0 and has decreased to 0.26. The level of damage in the specimen increases with decreasing Felicity ratio.

A description of each loading follows.

Day 0:

The specimen for this idealized case was initially loaded (first loading) to 7,000 micro-strain. This is indicated from the bar indicating "previous strain" on day 23. The specimen was then fully unloaded. The onset of significant emission for this initial loading occurred at 6,100 micro-strain. It is not possible to determine the Felicity ratio from an initial loading since there is no previous loading information.

Day 23:

From day zero to day 23 the specimen was allowed to recover. It was then loaded (second loading) to 9,800 micro-strain on day 23. This is indicated from the bar indicating previous strain on day 72. The specimen was then fully unloaded. The onset of significant emission for this loading occurred at 7,800 micro-strain. This value is greater than 7,000 micro-strain which is the previous strain to which the specimen was loaded. The resulting Felicity ratio is:

$$\text{Felicity ratio} = \frac{7{,}800}{7{,}000} = 1.14$$

This value is greater than unity and therefore it is concluded that the damage strain has not been reached and additional loadings are required.

Day 70:

From day 23 to day 70 the specimen was allowed to recover. It was then loaded to 12,000 micro-strain on day 70. This is indicated from the bar indicating previous strain on day 92. The specimen was then fully unloaded. The onset of significant emission for this third loading occurred at 9,016 micro-strain. This value is less than 9,800 micro-strain which is strain to which the specimen was previously loaded. The resulting Felicity ratio is:

$$\text{Felicity ratio} = \frac{9{,}016}{9{,}800} = 0.94$$

This value is less than unity and greater than 0.90. Felicity ratios that are close to unity without exceeding unity are desirable. As the Felicity ratio decreases, the damage strain can become falsely elevated. Due to lack of control over the application of load, Felicity ratios as low as 0.80 were accepted as a determination of damage strain. The Felicity ratio for this loading is 0.94 and so it is concluded that the damage strain is reached. For this specimen, the damage strain bar is scaled to accommodate a 10 % error in the results and the middle of the bar is placed at the strain at which the onset of

significant AE is recorded. This gives an approximate idea of where damage occurs in this specimen.

Day 94:

From day 72 to day 94 the specimen was allowed to recover. It was then loaded (fourth loading) to 16,000 micro-strain on day 94. This is indicated from the bar indicating previous strain on day 115. The specimen was then fully unloaded. The onset of significant emission for this loading occurred at 9,360 micro-strain. This value is less than 12,000 micro-strain which is the previous strain to which the specimen was loaded. The resulting Felicity ratio is:

$$\text{Felicity ratio} = \frac{9{,}360}{12{,}000} = 0.78$$

This value is less than unity and therefore it is concluded that the damage strain has been reached. Note that the strain at onset of AE is higher than the strain at onset of AE for the previous loading. As was mentioned in the description for day 70, this specimen has already reached the damage strain. Therefore it is concluded that the strain at onset of AE is falsely elevated.

Day 115:

From day 94 to day 115 the specimen was allowed to recover. It was then loaded above 16,000 micro-strain on day 115. The specimen was then fully unloaded. The actual strain to which the specimen was loaded on day 115 is not important and is not shown on this plot. The onset of significant emission for this fifth loading occurred at 4,160 micro-strain. This value is much less than the previous strain to which the specimen was loaded. The resulting Felicity ratio is:

$$\text{Felicity ratio} = \frac{4{,}160}{16{,}000} = 0.26$$

This value is much less than unity and therefore it is concluded that the damage strain has been reached. This value is also much less than 0.80. Note that the strain at

onset of significant AE is much lower than the strain at onset of significant AE from the previous loading. Therefore it is concluded that the specimen has been severely damaged. In general, Felicity ratios less than 0.50 are correlated with severe damage.

Figures 4.4 through 4.10 show test data that was gathered early in the test program. The conventions for previous strain and strain at onset of significant AE are as discussed above. The schematic in the upper right hand portion of the figures indicates the direction of the loading in reference to the direction of the fiber orientation.

This preliminary program was conducted to get a general understanding of the acoustic emission response of selected specimens. The specimens were loaded somewhat haphazardly to get a general idea of the effect this would have on the AE response. Historic index was used to determine the onset of AE for these early specimens. An estimate of the damage strain as determined by the Felicity ratio is indicated with a light gray bar. The damage strain was defined as the strain when the Felicity ratio was between 0.80 and 1.0 for these specimens. The large range of 0.80 to 1.0 was necessary due to the haphazard nature of the loading program.

The damage strain bar is centered on the damage strain as determined by the Felicity ratio. The width of the damage strain bar is 10 % of the damage strain. In several instances, the damage strain bars for two different specimens overlap. This is true for many of the 90-degree specimens. More scatter is present in the results for the 0-degree specimens than is present in the results for the 90-degree specimens. When the damage strain bars for two different specimens are separated due to this scatter, the area between the two bars is filled in. This results in a wider damage strain bar for the 0-degree specimens.

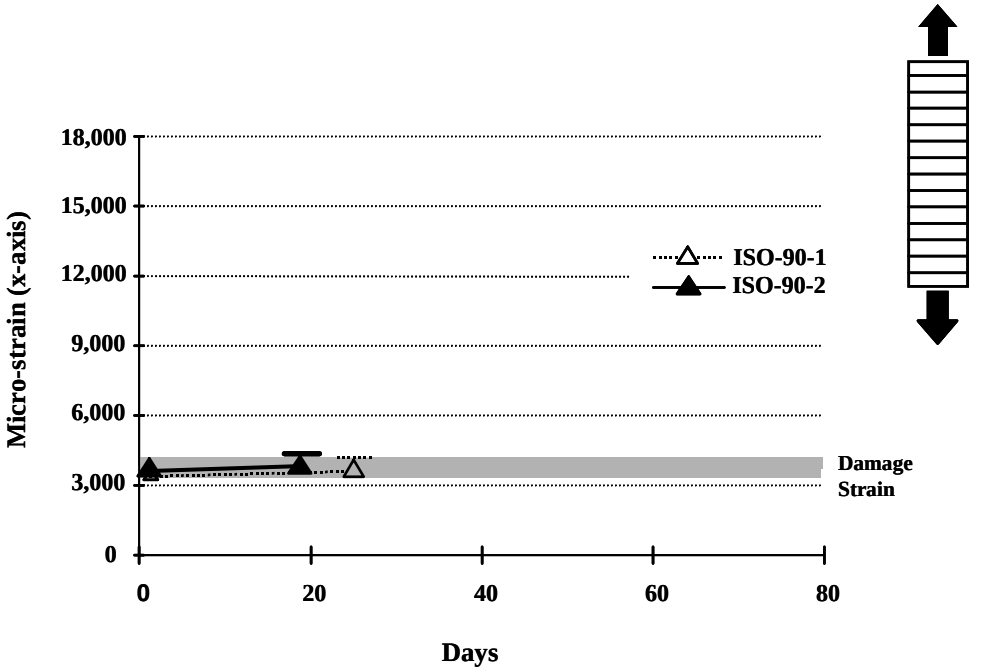

Figure 4.4 – Preliminary results for specimen type ISO-90

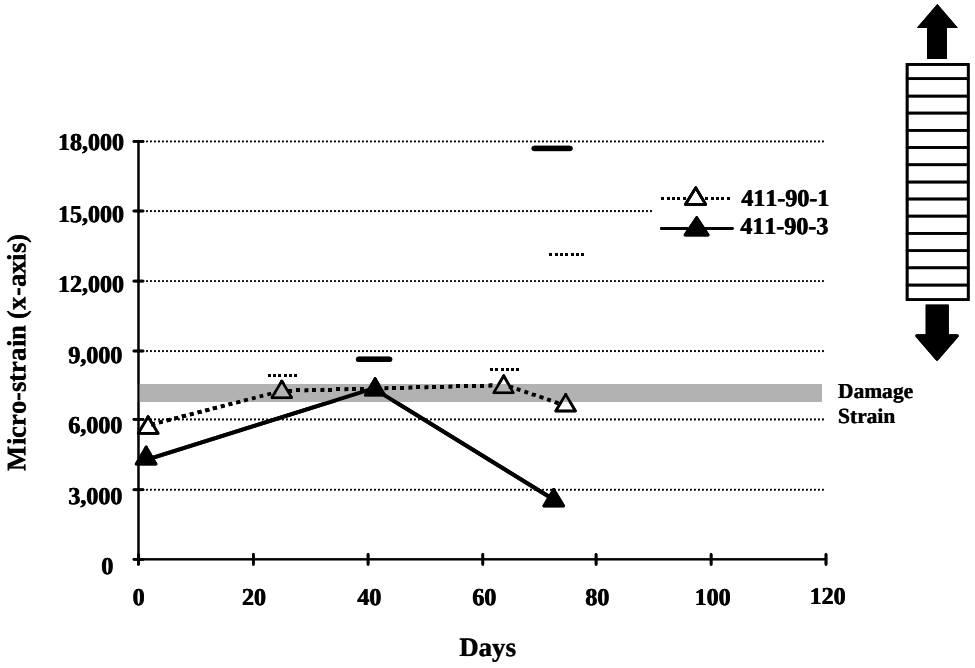

Figure 4. 5 – Preliminary results for specimen type 411-90

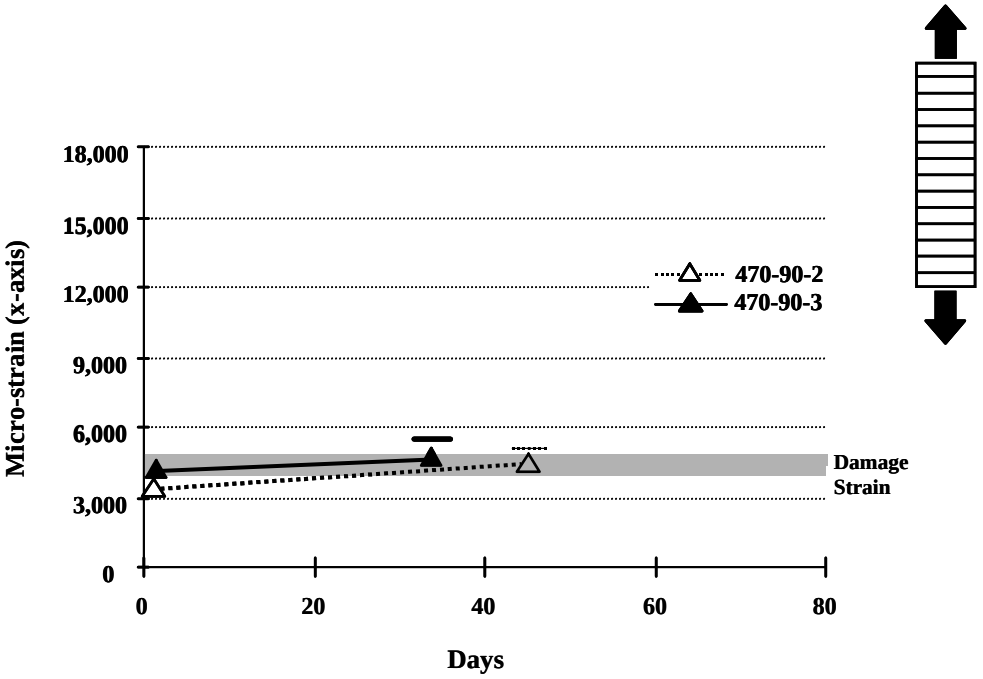

Figure 4.6 – Preliminary results for specimen type 470-90

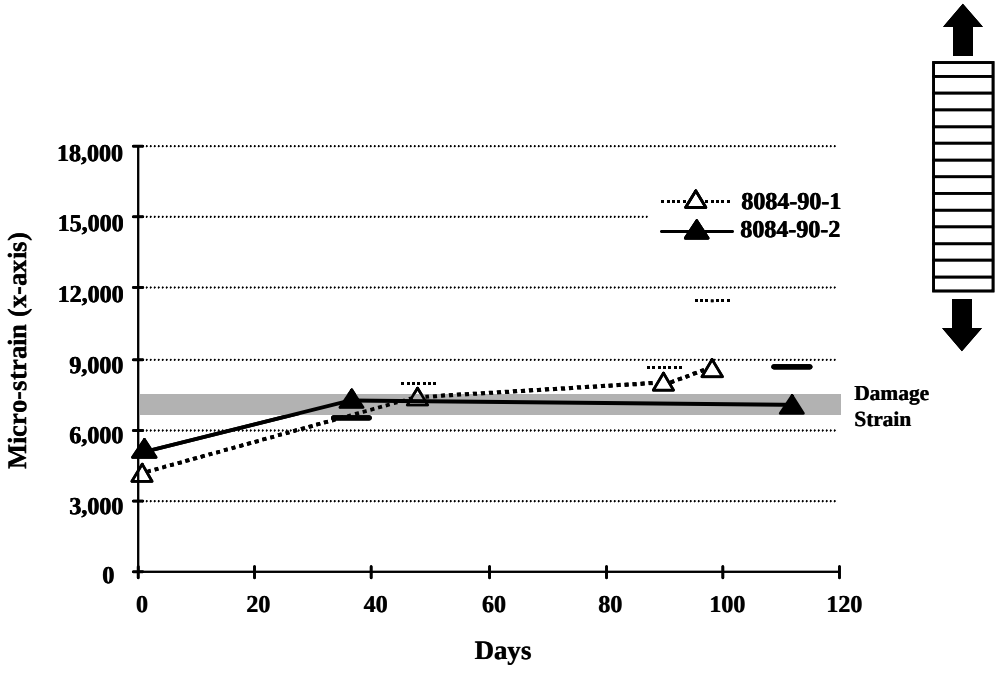

Figure 4.7 – Preliminary results for specimen type 8084-90

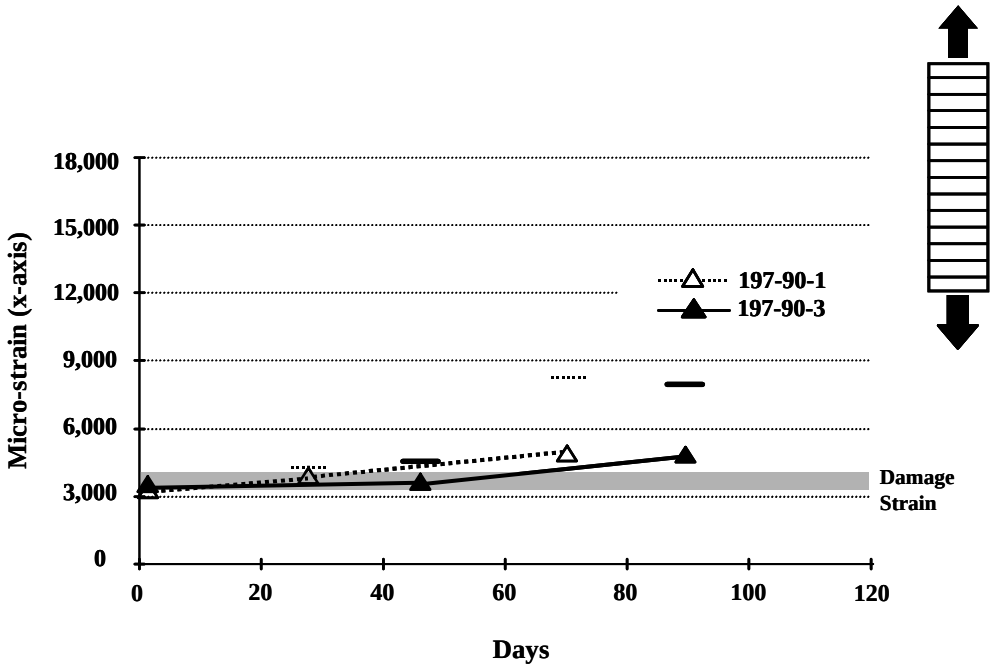

Figure 4.8 – Preliminary results for specimen type 197-90

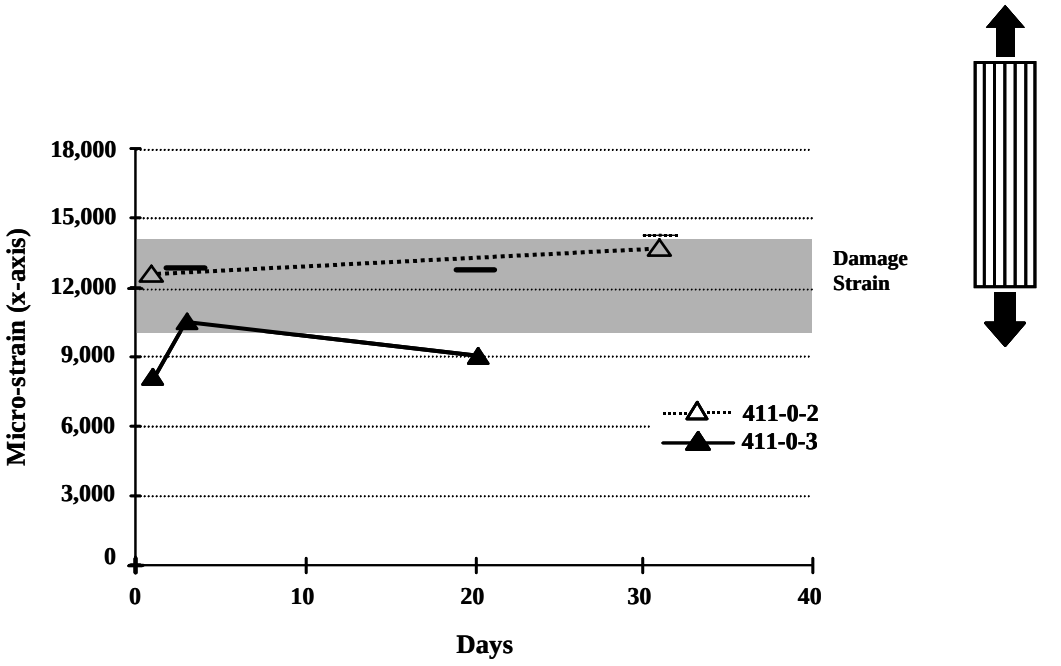

Figure 4.9 – Preliminary results for specimen type 411-0

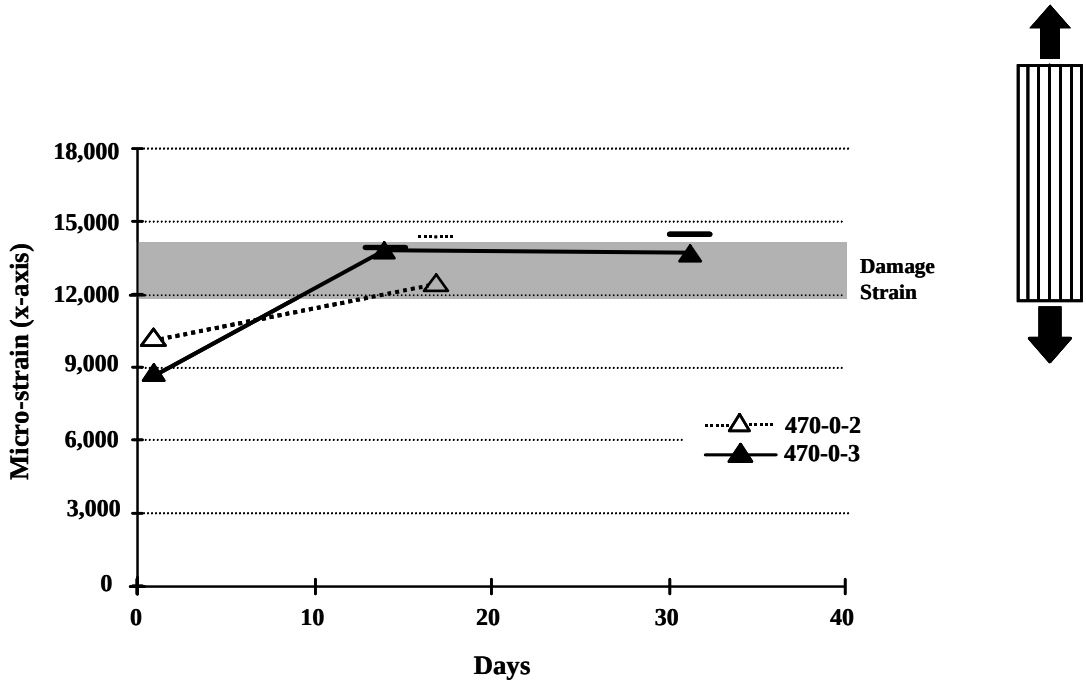

Figure 4.10 – Preliminary results for specimen type 470-0

As mentioned previously, there is a good deal of scatter present in these early results. Nonetheless, certain aspects of AE behavior became apparent due to this testing. Some of the conclusions are as follows:

- The strain at onset of significant AE may be falsely elevated if the Felicity ratio is less than 0.90.
- High levels of damage are associated with a Felicity ratio of less than 0.50.
- Acoustic emission behavior of fiber reinforced polymers is strongly load history dependent
- A range on the Felicity ratio of 0.90 to 1.0 is preferred to determine the onset of significant emission
- The historic index can be used as a means to determine the onset of significant AE. However, this parameter is not as sensitive as direct interpretation of the test data.
- More scatter is present in the 0-degree specimens when compared to the 90-degree specimens.
- For the 90-degree specimens the 8084 and 411 resins experience higher strain prior to the onset of significant AE.
- For the 0-degree specimens the onset of AE appeared to be independent of resin type

This preliminary test program led to the development of a more rigorous loading procedure. This loading procedure was designed to obtain a Felicity ratio of between 0.90 and 1.00. This loading method was applied to all the specimens following this initial program of 10 specimens. An idealized plot of the loading procedure is shown in Figure 4.11.

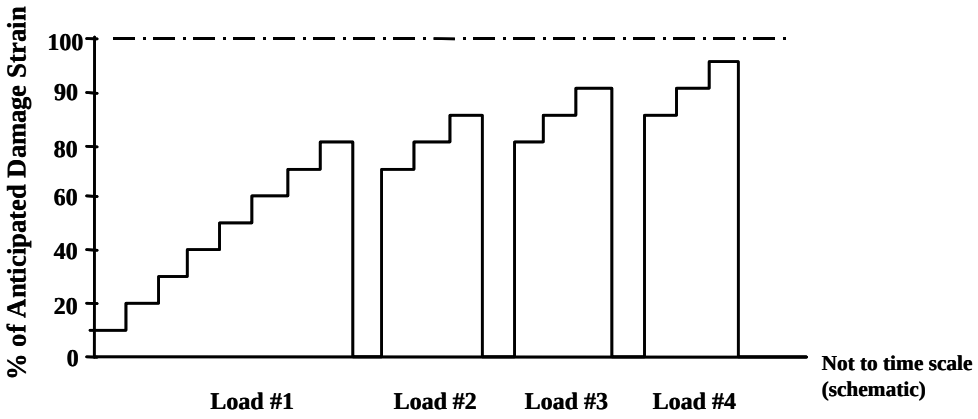

Figure 4.11 – Idealized Loading Sequence

When this loading procedure is followed, it is possible to determine when the Felicity ratio becomes less than 1.0. A conditioning period of at least 24 hours is required between each loading. The onset of damage generally occurs near the end of the linear range of mechanical behavior. If the specimen is in the linear range stress, strain or load can be used to calculate the Felicity ratio. Due to the visco-elastic nature of the resin, strain was used for comparison of the coupon specimens.

The Felicity ratio was observed to stay above 1.0 prior to a certain strain and then drop off. This type of behavior is shown in Figure 4.12. This figure is a compilation of test records of several different specimens.

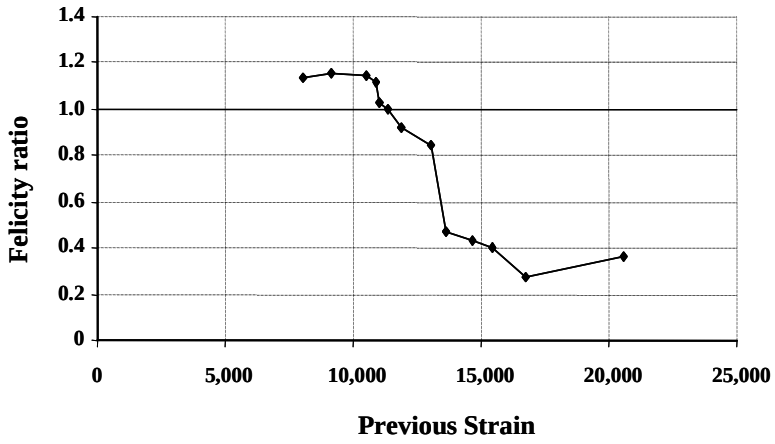

Figure 4.12 – Typical Felicity ratio behavior of coupon specimens

4.3 Results for All Specimens Tested

After the loading procedure shown in Figure 4.4 was developed, coupon specimens of varying fiber orientation, fiber construction and resin type were tested in general agreement with this loading procedure. Each specimen was repeatedly loaded until a Felicity ratio of less than 1.0 was determined.

As discussed previously, the Historic index was found to be less sensitive than direct inspection of the data as a means of determining the onset of significant AE. Therefore, direct inspection of the data was used to develop the results presented here.

Due to the loading apparatus, load was applied rapidly between load steps. Therefore, when the onset of significant AE occurred at a particular strain, this was actually an upper bound for strain at onset of significant AE. The lower bound was the strain that the specimen had experienced prior to this load step. The lower and upper bound values for strain at onset of significant AE are plotted along with the strain that the specimen experienced on the previous loading. The results for 0 degree, 90 degree, 45 degree and woven roving specimens are shown in Figures 4.12, 4.13, 4.14 and 4.15 respectively. The results are plotted only for the loading when the Felicity ratio first drops below 1.0.

Not all of the specimens shown in Figures 4.12 to 4.15 were acceptable for use in the final results. The specimens that were used are enclosed in a box and the Felicity ratio is labeled above the results for that specimen. The selection of specimens for final results is discussed in the following section.

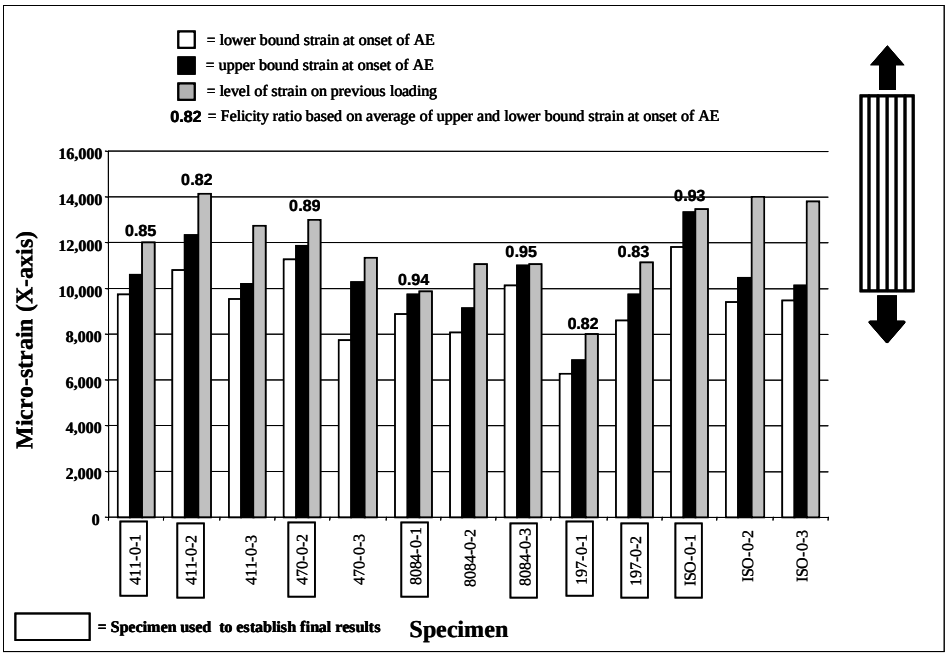

Figure 4.13 – Strain at onset of significant AE - 0 degree specimens

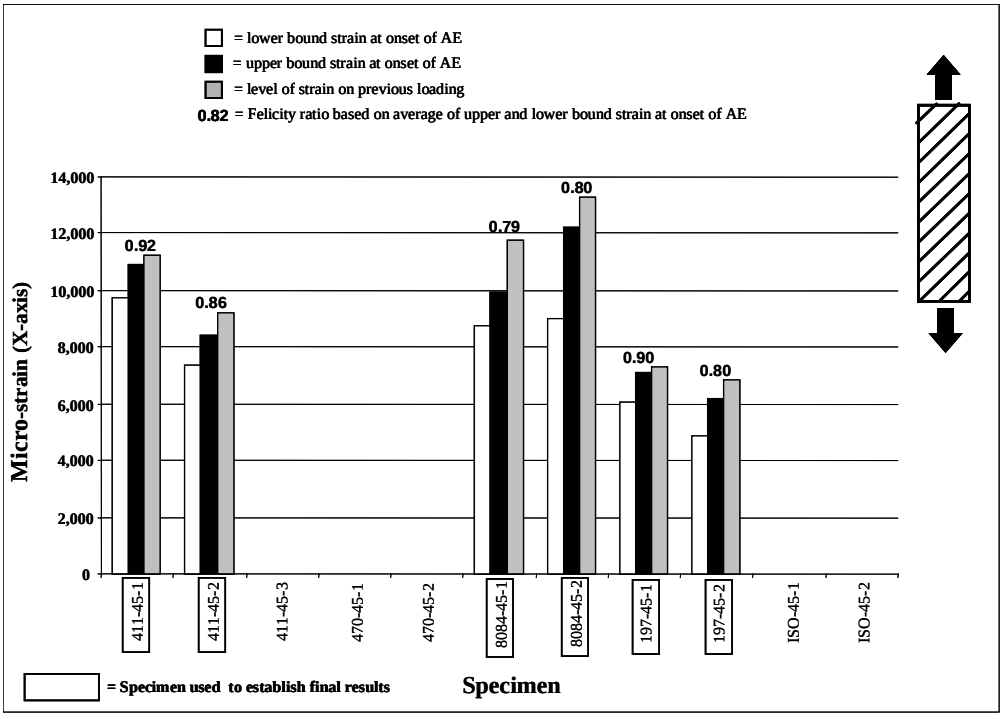

Figure 4.15 – Strain at onset of significant AE - 45 degree specimens

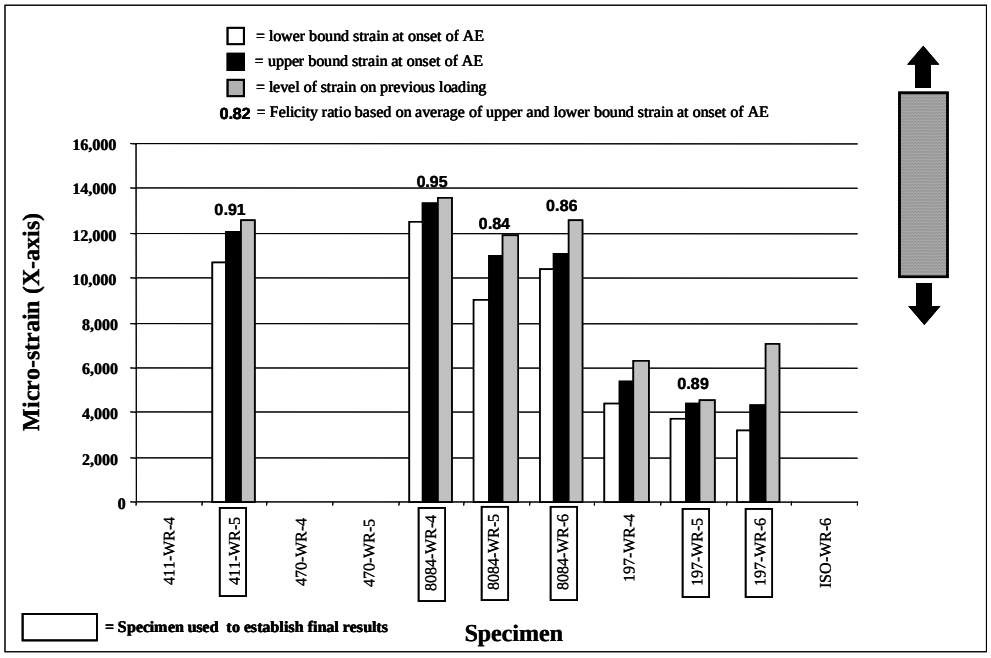

Figure 4.16 – Strain at onset of significant AE - woven roving specimens

4.4 Final Acoustic Emission Results

The AE data as presented in Figures 4.12 through 4.15 is somewhat confusing. This is because the lower bound strain for onset of significant AE, upper bound strain for onset of significant AE and level of strain from the previous loading are all plotted together. Not all of the AE data presented above is of interest.

Selected specimens were used for the development of the final results. As mentioned above, due to the step loading procedure the exact strain at the onset of significant AE was not known. Therefore, the upper bound and lower bound values for strain at onset of significant AE were averaged to obtain a reasonable approximation. The Felicity ratio thus determined was lower than if only the upper bound value had been used. For this reason, the range of acceptable Felicity ratios was broadened to accept values between 0.79 and 1.0. The name of each specimen that achieved this range is enclosed with a box and the Felicity ratio is labeled above the bar chart. The results for specimens of a particular type (such as 411-N) were then averaged. If only one specimen of a certain type remained after discarding the questionable specimens, that specimen was used for the final results.

The final results for 0 degree, 90 degree, 45 degree and woven roving specimens are shown in Figures 4.16, 4.17, 4.18 and 4.19 respectively. The variable investigated for a given fiber architecture is resin type. These results are used to develop the AE based damage criterion described in subsequent chapters.

4.4.1 Specimens with fibers at 0 degrees

The results for specimens with fibers oriented parallel to the applied stress are shown in Figure 4.16.

The specimens with the more flexible resins (411 and 8084) underwent approximately the same (or in some cases less) strain prior to damage as the specimens

with the less flexible resins. This is to be expected since the damage mechanism for this fiber orientation is primarily fiber dominated.

4.4.2 Specimens with fibers at 90 degrees

The results for specimens with fibers oriented perpendicular to the applied stress are shown in Figure 4.17.

The specimens with the more flexible resins underwent significantly higher strain prior to damage than the specimens with the less flexible resins. This is also to be expected since the damage mechanisms for this fiber orientation are matrix dominated.

There is very little difference between the results for 8084 and 411 even though 8084 has a much higher elongation strain to failure (see Chapter 3, Table 3.1). This suggests that beyond a certain limit the elongation to failure of the resin is not important.

4.4.3 Specimens with fibers at 45 degrees

The results for specimens with fibers oriented at 45 degrees to the applied stress are shown in Figure 4.18.

The specimens with the more flexible resins underwent higher strain prior to damage than the specimens with the less flexible resins. It appears that the behavior of the resin contributes significantly for this fiber orientation. Shear stresses are coupled with biaxial stresses for this fiber orientation. Shear and transverse tension behavior are both matrix dominated.

4.4.4 Specimens with woven roving

The results for the woven roving specimens are shown in Figure 4.19. For all woven roving specimens, the warp direction was oriented parallel to the applied stress. The variable investigated for these specimens was resin type.

The specimens with the more flexible resins underwent significantly higher strain prior to damage than the specimens with the less flexible resins. This is to be expected

since the early damage mechanisms for woven roving are matrix dominated. The final failure mechanism for woven roving is thought to be fiber dominated.

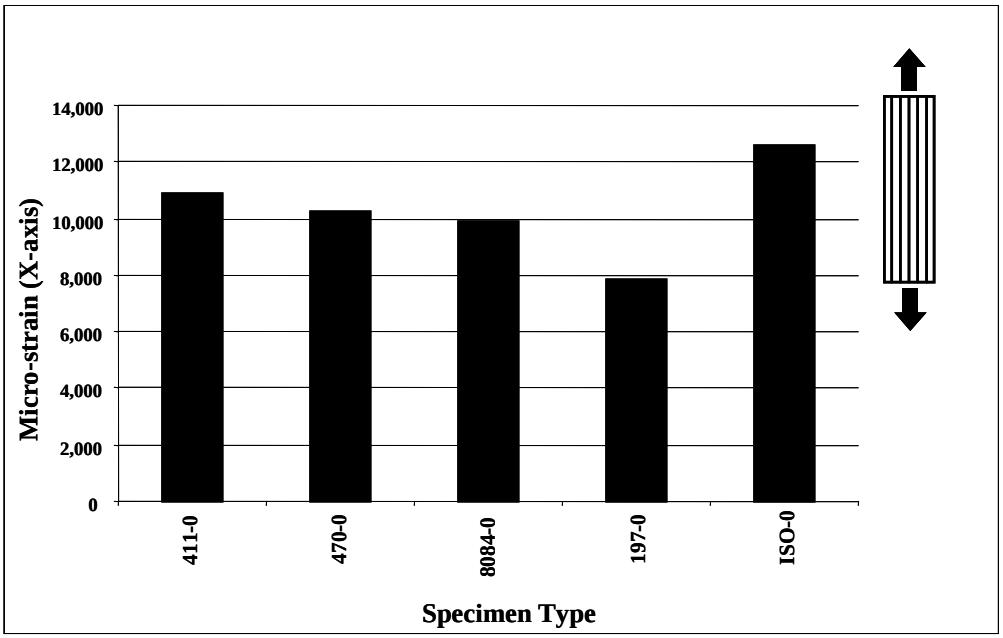

Figure 4.17 – Strain at significant AE – average of selected 0 degree specimens

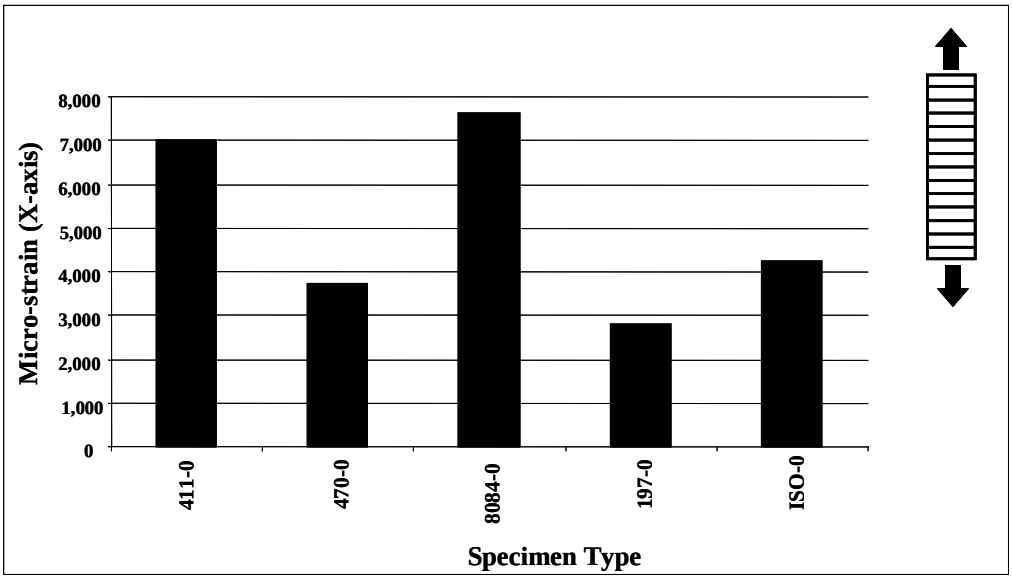

Figure 4.18 – Strain at significant AE – average of selected 90 degree specimens

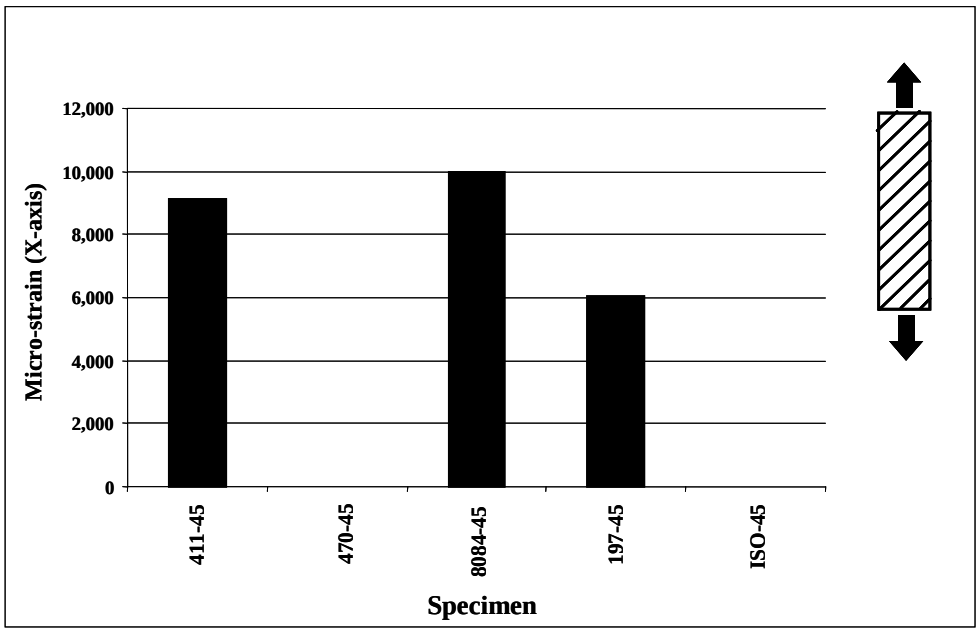

Figure 4.19 – Strain at significant AE – average of selected 45 degree specimens

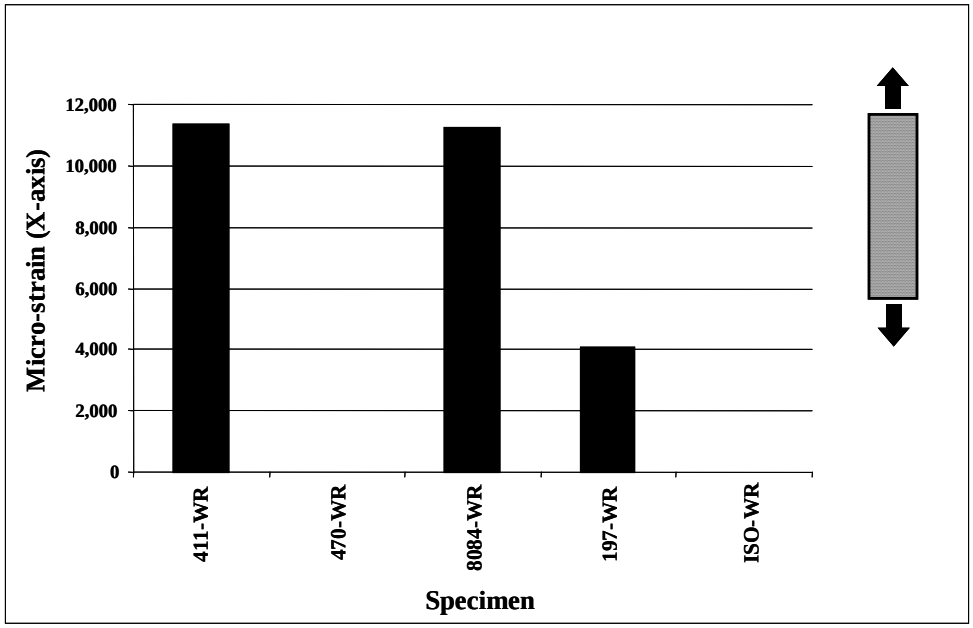

Figure 4.20 – Strain at significant AE – average of selected woven roving specimens

4.5 Correlation of Mechanical Behavior and Acoustic Emission

As discussed in Section 4.2, the onset of acoustic emission has generally been observed to occur prior to the departure from linearity on a load (or stress) versus strain curve. This was the case for the specimens tested here. The results from Section 4.5 were used to develop the strain at onset of AE for different specimens. Specimens of a certain type were then loaded to failure and the damage strain as predicted by AE was plotted for these companion specimens. These results are presented for 0 degree, 90 degree and woven roving specimens in Figures 4.20 through 4.32. This behavior indicates that the AE procedure is detecting damage within a reasonable range.

Nonlinearity in the load versus strain curve has at least two causes. These are nonlinear behavior of the resin and the accumulation of damage in the specimen. The nonlinearity of the resin is more pronounced for matrix dominated behavior, such as loading transverse to the fiber direction. This type of nonlinearity is apparent in the results. Fibers contribute significantly to the stiffness of laminas loaded in the transverse direction. When the fiber-matrix bond is broken, this will lead to a loss of stiffness. Matrix cracking will also lead to a loss of stiffness. All of these mechanisms occur together and it is difficult to separate the affects of one from the others. It is possible to separate creep from damage through close inspection of creep and recovery data. This is due to the fact that non-recoverable creep can be attributed to damage only. Close inspection of the creep and recovery data was not done for these specimens. However, a sharp decrease in the load versus strain curve is more likely to be associated with damage mechanisms than with only nonlinearity of the resin.

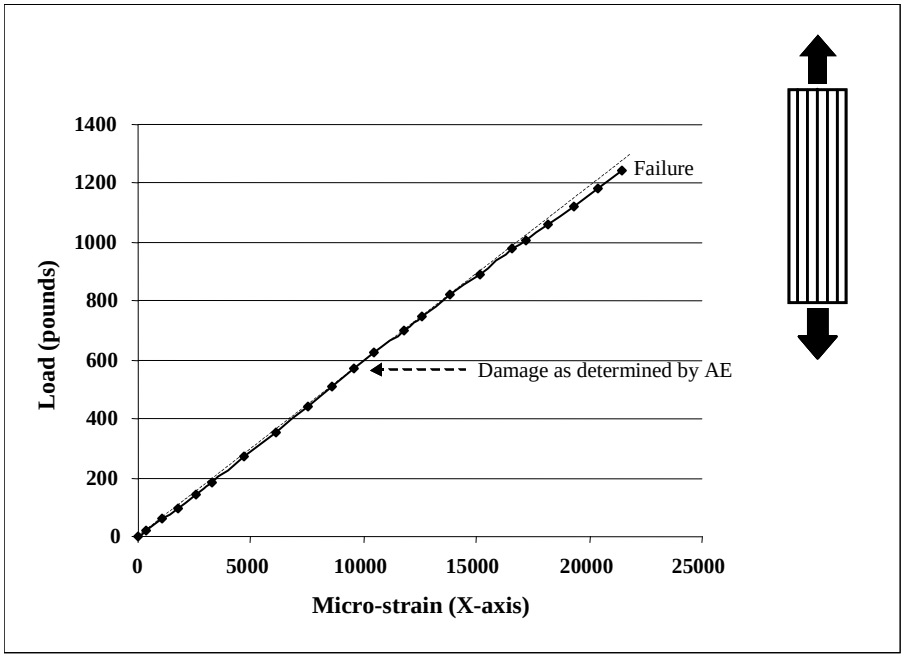

Figure 4.21 – Damage as determined by AE – specimen type 411-0

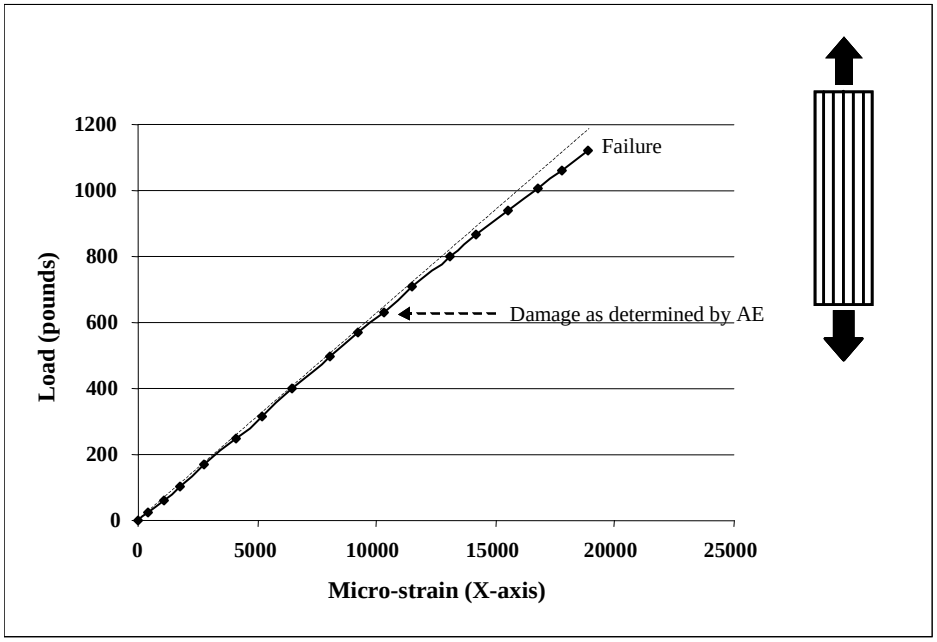

Figure 4.22 – Damage as determined by AE – specimen type 470-0

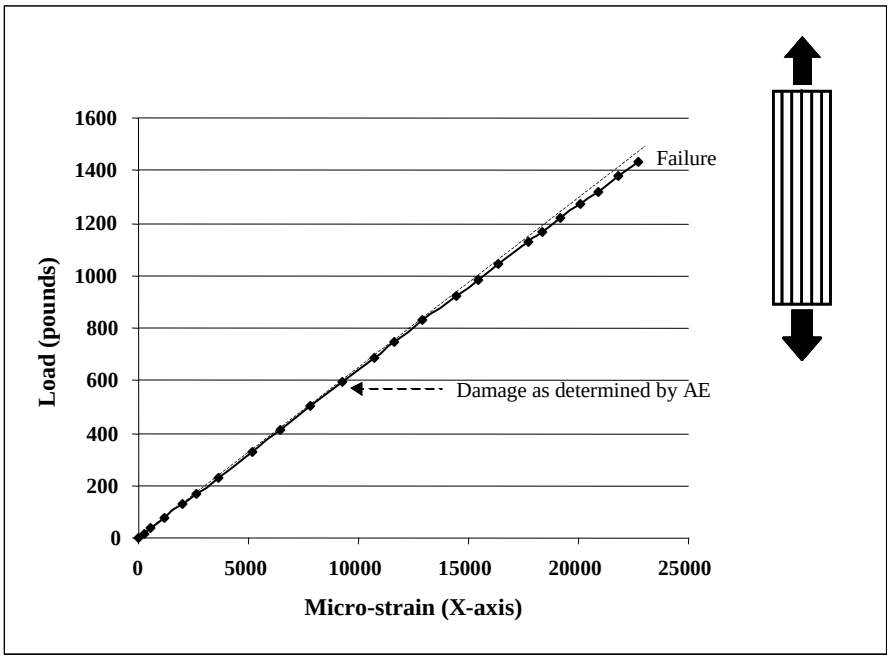

Figure 4.23 – Damage as determined by AE – specimen type 8084-0

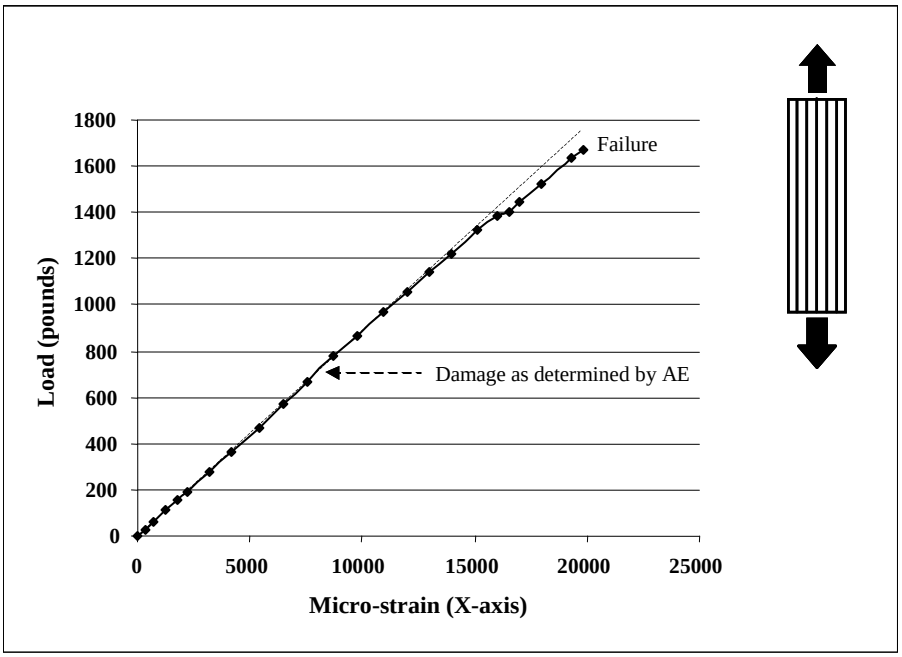

Figure 4.24 – Damage as determined by AE – specimen type 197-0

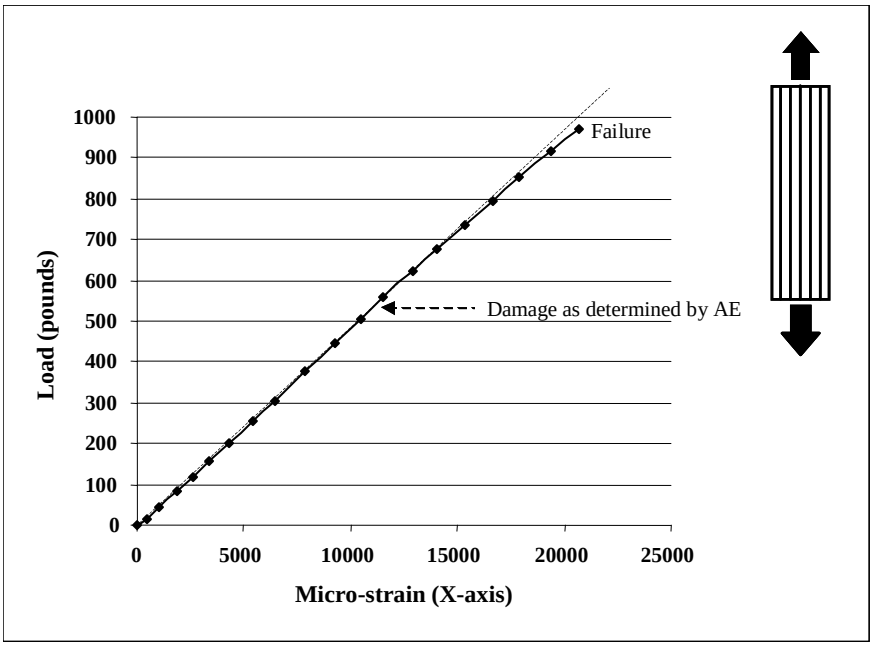

Figure 4.25 – Damage as determined by AE – specimen type ISO-0

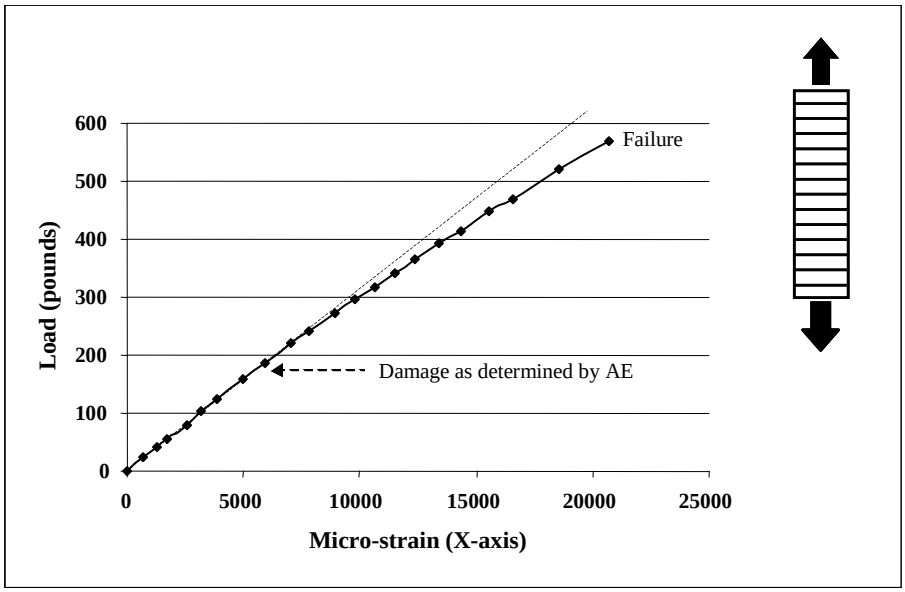

Figure 4.26 – Damage as determined by AE – specimen type 411-90

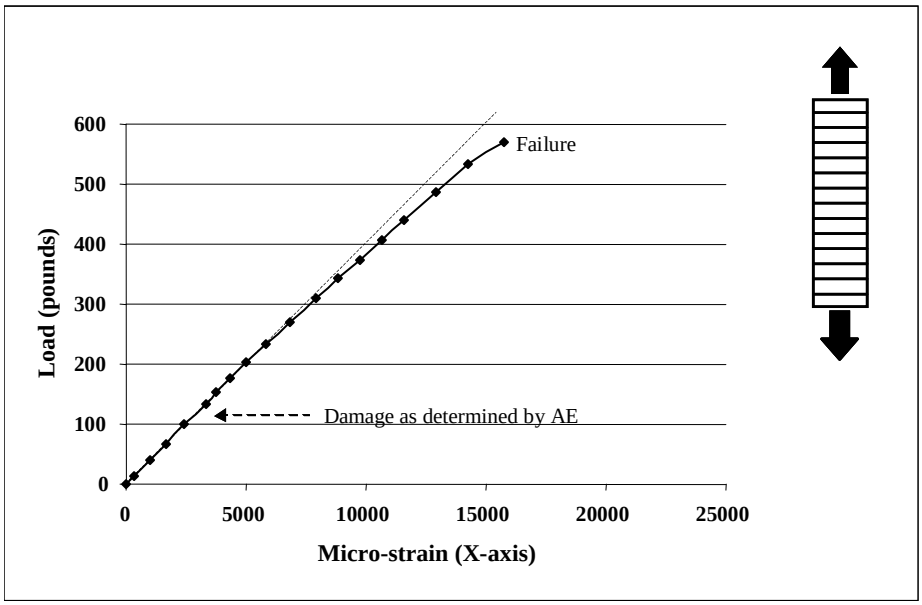

Figure 4.27 – Damage as determined by AE – specimen type 470-90

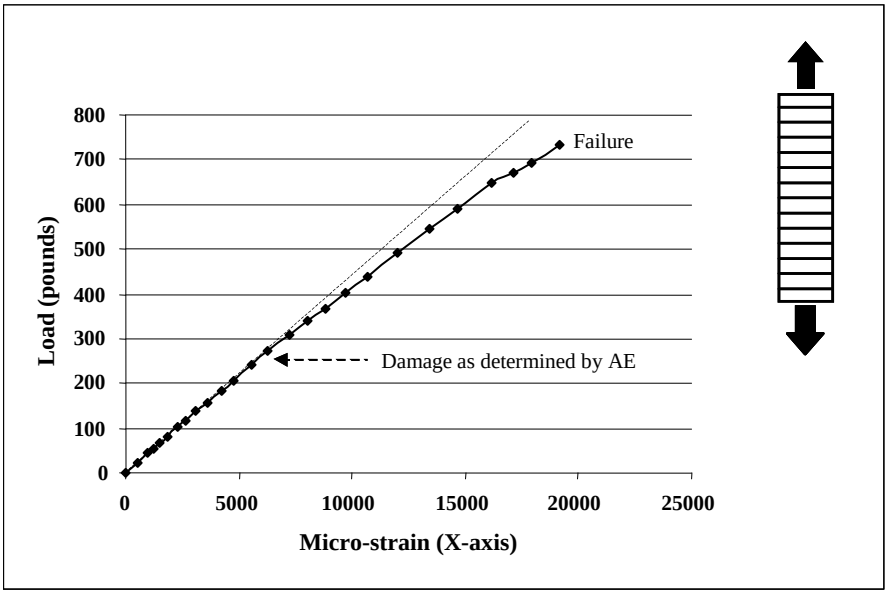

Figure 4.28 – Damage as determined by AE – specimen type 8084-90

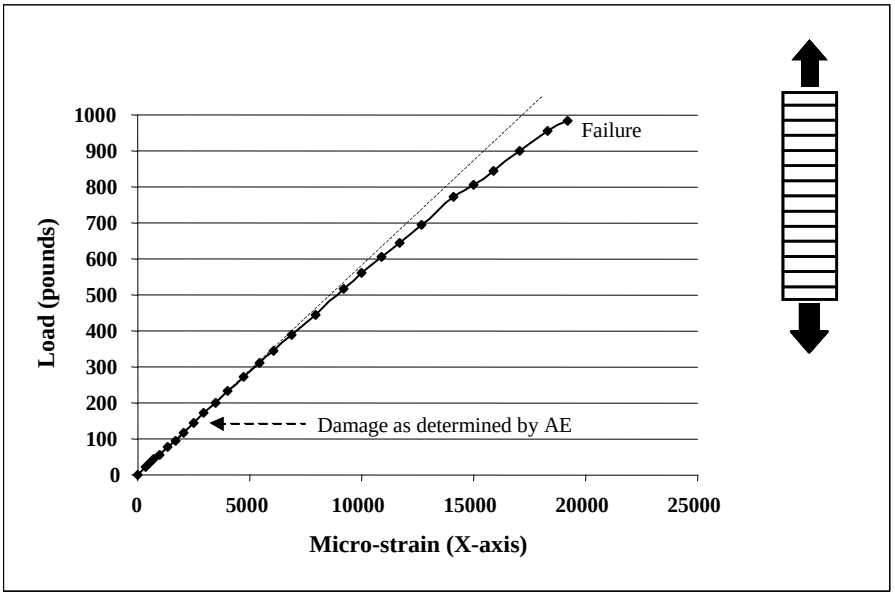

Figure 4.29 – Damage as determined by AE – specimen type 197-90

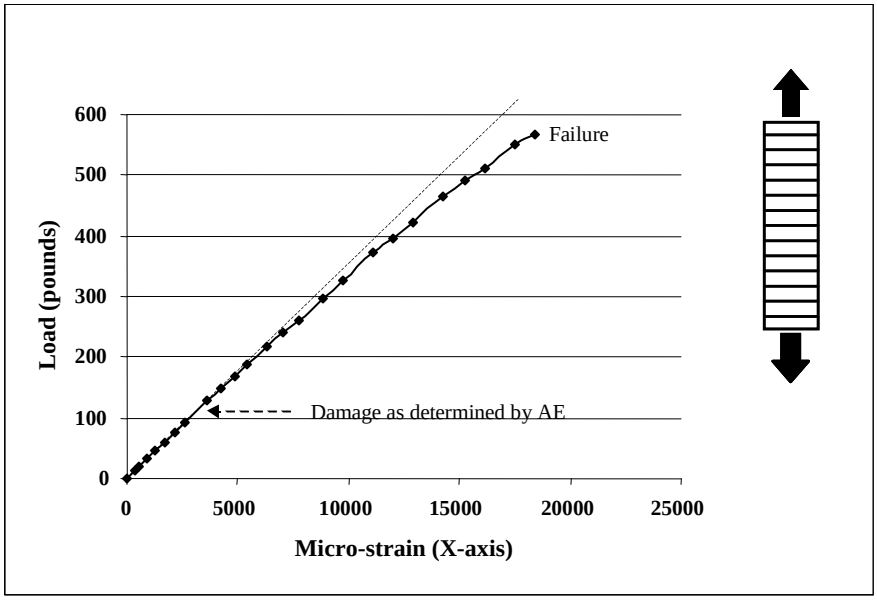

Figure 4.30 – Damage as determined by AE – specimen type ISO-90

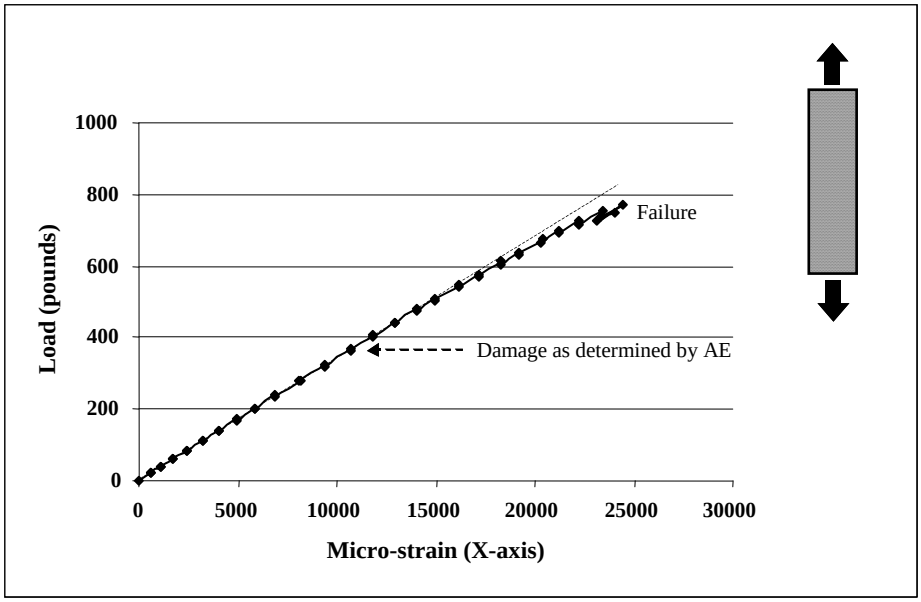

Figure 4.31 – Damage as determined by AE – specimen type 411-WR

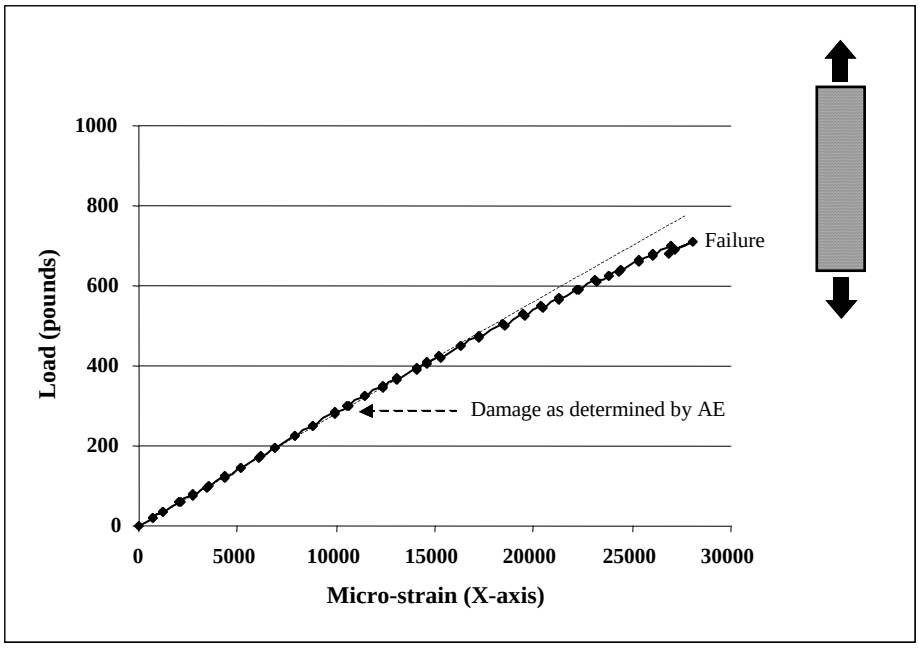

Figure 4.32 – Damage as determined by AE – specimen type 8084-WR

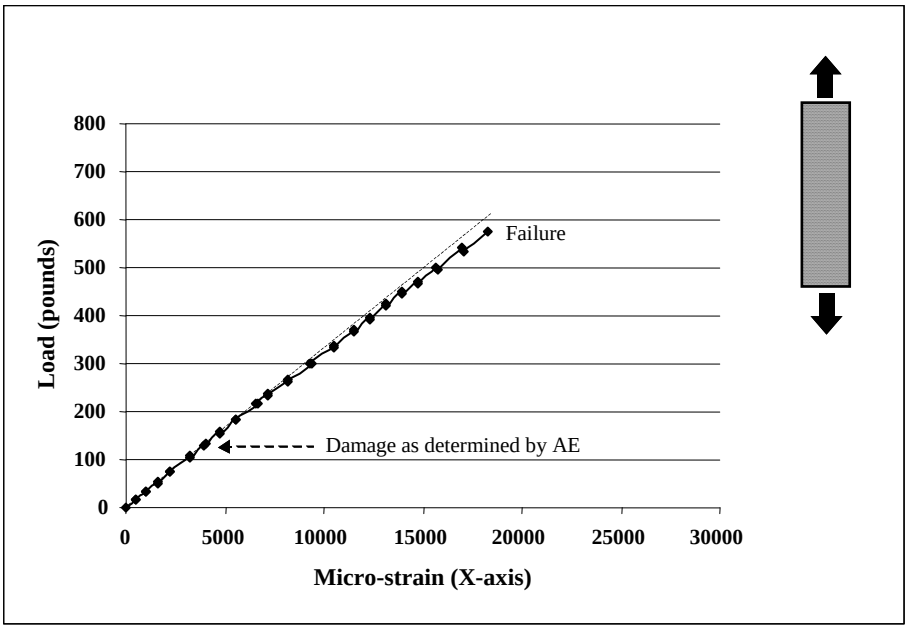

Figure 4.33 – Damage as determined by AE – specimen type 197-WR

4.6 Conclusions

An acoustic emission test procedure was developed to determine the onset of damage in small coupon specimens. The test procedure involves loading and reloading of specimens until a Felicity ratio of less than 1.0 is obtained. Felicity ratios of less then 1.0 have been correlated with damage in composites[4.3, 4.4]. Historic index was used as a guide for determining the onset of significant acoustic emission. However, determination with the historic index was found to trail the onset of significant acoustic emission in most cases. Therefore, the onset of significant acoustic emission was determined by direct inspection of the data.

For specimens with fibers oriented at 45 and 90 degrees to the applied stress, composites made with more flexible resins underwent higher levels of strain prior to damage. The same was true for woven roving specimens made with flexible resins. For specimens with fibers oriented at 0 degrees to the applied stress, there was little difference between specimens made with different resins.

With the exception of specimens with fibers oriented at 0 degrees to the applied stress, the specimens made with the more flexible resins experienced damage at a higher percentage of ultimate load.

The results of this chapter were used as the basis for the damage based design criterion described in Chapter 5.

Chapter 5: *Development of Acoustic Emission Based Damage Criterion*

5.1 Introduction

In this chapter, the two dimensional stress-strain relationships for composite laminas are given. Existing two dimensional failure criteria are then described. In the absence of experimental testing micromechanics models are often used. Commonly used micromechanics models for the prediction of strength are summarized.

Results of the acoustic emission testing discussed in Chapter 4 are used to compare data based on damage to results based on existing failure criteria. The results based on damage are plotted for laminas made with each of the five different resins. These results are also compared to those predicted by micromechanics models.

Prior to discussing the failure criteria, the stress-strain relationships for a lamina in a state of two dimensional stress are summarized. This development is taken directly from Gibson[5.1]. Linear elastic behavior is assumed.

5.2 Stress-Strain Relationships for the Two Dimensional Specially Orthotropic Lamina

A specially orthotropic lamina is a lamina in which the global axes and material axes coincide. Setting $\sigma_3 = \tau_{23} = \tau_{31} = 0$, the following stress-strain relationships are obtained:

$$\begin{Bmatrix} \varepsilon_1 \\ \varepsilon_2 \\ \varepsilon_3 \end{Bmatrix} = \begin{bmatrix} S_{11} & S_{12} & 0 \\ -S_{21} & S_{22} & 0 \\ 0 & 0 & S_{66} \end{bmatrix} \begin{Bmatrix} \sigma_1 \\ \sigma_2 \\ \tau_{12} \end{Bmatrix} \qquad \text{(Eqns. 5.1)}$$

where:

σ_i = stress in the *'i'* direction

τ_{ij} = shear stress in the *'ij'* direction

ε_i = strain in the *'i'* direction

S_{ij} = compliance in the *'ij'* direction

The compliances S_{ij} and the engineering constants are related by the equations:

$$S_{11} = \frac{1}{E_1}$$

$$S_{22} = \frac{1}{E_2} \qquad \text{(Eqns. 5.2)}$$

$$S_{12} = S_{21} = - \frac{\nu_{21}}{E_2} = \frac{\nu_{12}}{E_1}$$

$$S_{66} = \frac{1}{G_{12}}$$

where:

E_i = modulus of the lamina in the *'i'* direction

G_{ij} = shear modulus of the lamina in the *'ij'* direction

v_{ij} = Poisson ratio of the lamina in the *'ij'* direction

There are five non-zero compliances and only four independent compliances for the specially orthotropic lamina. The lamina stresses in terms of tensor strains are as follows:

$$\begin{Bmatrix} \sigma_1 \\ \sigma_2 \\ \tau_{12} \end{Bmatrix} = \begin{bmatrix} Q_{11} & Q_{12} & 0 \\ Q_{21} & Q_{22} & 0 \\ 0 & 0 & 2Q_{66} \end{bmatrix} \begin{Bmatrix} \varepsilon_1 \\ \varepsilon_2 \\ \gamma_{12} / 2 \end{Bmatrix} \qquad \text{(Eqns. 5.3)}$$

where the Q_{ij} are the components of the lamina stiffness matrix, which are related to the compliances and the engineering constants by:

$$Q_{11} = \frac{S_{22}}{S_{11}S_{22} - S_{12}^2} = \frac{E_1}{1 - \nu_{12}\nu_{21}}$$

$$Q_{12} = Q_{21} = \frac{S_{12}}{S_{11}S_{22} - S_{12}^2} = \frac{\nu_{12}E_2}{1 - \nu_{12}\nu_{21}} \qquad \text{(Eqns. 5.4)}$$

$$Q_{22} = \frac{S_{11}}{S_{11}S_{22} - S_{12}^2} = \frac{E_2}{1 - \nu_{12}\nu_{21}}$$

$$Q_{66} = \frac{1}{S_{66}} = G_{12}$$

The factor of 2 is introduced in the Q_{66} term of equation 5.3 to compensate for the use of tensor shear strain. The experimental characterization of the specially orthotropic lamina involves the measurement of four independent engineering constants such as E_1, E_2, G_{12}, and ν_{12}.

5.3 Stress-Strain Relationships for the Two Dimensional Generally Orthotropic Lamina

It is necessary to know the stress-strain relationships of a lamina with principal material axes that are not coincident with the global axes. This is referred to as a generally orthotropic lamina. The following is also taken directly from Gibson[5.1].

The stresses in the material axes are related to the global axes through the following equations:

$$\begin{Bmatrix} \sigma_1 \\ \sigma_2 \\ \tau_{12} \end{Bmatrix} = [T] \begin{Bmatrix} \sigma_x \\ \sigma_y \\ \tau_{xy} \end{Bmatrix} \qquad \text{(Eqns. 5.5)}$$

where [T] is the transformation matrix:

$$[T] = \begin{bmatrix} c^2 & s^2 & 2cs \\ s^2 & c^2 & -2cs \\ -cs & cs & (c^2 - s^2) \end{bmatrix} \qquad \text{(Eqns. 5.6)}$$

where:

$c = \cos\theta$

$s = \sin\theta$

Similarly, the strains in the local material axes are related to the global axes through the following equations:

$$\begin{Bmatrix} \varepsilon_1 \\ \varepsilon_2 \\ \gamma_{12}/2 \end{Bmatrix} = [T] \begin{Bmatrix} \varepsilon_x \\ \varepsilon_y \\ \gamma_{xy}/2 \end{Bmatrix} \qquad \text{(Eqns. 5.7)}$$

where:

ε_x = strain in the '*x*' direction

ε_y = strain in the '*y*' direction

γ_{xy} = shear strain in the '*xy*' direction

The global stresses are related to the global strains through the following equations:

$$\begin{Bmatrix} \sigma_x \\ \sigma_y \\ \tau_{xy} \end{Bmatrix} = \begin{bmatrix} \overline{Q}_{11} & \overline{Q}_{12} & \overline{Q}_{16} \\ \overline{Q}_{21} & \overline{Q}_{22} & \overline{Q}_{26} \\ \overline{Q}_{16} & \overline{Q}_{26} & \overline{Q}_{66} \end{bmatrix} \begin{Bmatrix} \varepsilon_x \\ \varepsilon_y \\ \gamma_{xy}/2 \end{Bmatrix} \qquad \text{(Eqns. 5.8)}$$

where:

σ_x = stress in the '*x*' direction

σ_y = stress in the '*y*' direction

τ_{xy} = shear stress in the '*xy*' direction

$$\overline{Q}_{11} = Q_{11}c^4 + Q_{22}s^4 + 2(Q_{12} + 2Q_{66})s^2c^2$$

$$\overline{Q}_{12} = (Q_{11} + Q_{22} - 4Q_{66})s^2c^2 + Q_{12}(c^4 + s^4)$$

$$\overline{Q}_{22} = Q_{11}s^4 + Q_{22}c^4 + 2(Q_{12} + 2Q_{66})s^2c^2 \qquad \text{(Eqns. 5.9)}$$

$$\overline{Q}_{16} = (Q_{11} - Q_{12} - 2Q_{66})c^3s - (Q_{22} - Q_{12} - 2Q_{66})cs^3$$

$$\overline{Q}_{26} = (Q_{11} - Q_{12} - 2Q_{66})cs^3 - (Q_{22} - Q_{12} - 2Q_{66})c^3s$$

$$\overline{Q}_{66} = (Q_{11} + Q_{22} - 2Q_{12} - 2Q_{66})s^2c^2 + Q_{66}(s^4 + c^4)$$

With equations 5.1 through 5.9 established, the stress-strain relationships for the generally orthotropic lamina are well defined.

5.4 Existing Two Dimensional Failure Criteria for Fiber Reinforced Polymers

The following discussion of failure criteria is also taken directly from Gibson[5.1]. The relationships below are used to develop the stress criteria.

$$s_L^{(+)} = E_1 e_L^{(+)}$$

$$s_T^{(+)} = E_2 e_T^{(+)}$$

$$s_{LT} = G_{12} e_{LT} \qquad \text{(Eqns. 5.5)}$$

$$s_L^{(-)} = E_1 e_L^{(-)}$$

$$s_T^{(-)} = E_2 e_T^{(-)}$$

where:

$s_L^{(+)}$ = tensile failure stress of the lamina in the longitudinal direction

$s_T^{(+)}$ = tensile failure stress of the lamina in the transverse direction

s_{LT} = shear failure stress of the lamina in the longitudinal-transverse direction

$s_L^{(-)}$ = compressive failure stress of the lamina in the longitudinal direction

$s_T^{(-)}$ = compressive failure stress of the lamina in the transverse direction

$e_L^{(+)}$ = tensile failure strain of the lamina in the longitudinal direction

$e_T^{(+)}$ = tensile failure strain of the lamina in the transverse direction

e_{LT} = shear failure strain of the lamina in the longitudinal-transverse direction

$e_L^{(-)}$ = compressive failure strain of the lamina in the longitudinal direction

$e_T^{(-)}$ = compressive failure strain of the lamina in the transverse direction

Failure tests are assumed to be conducted on specially orthotropic laminas. The subscript '*L*' is used to denote a longitudinal test with the fibers oriented at 0 degrees to the axis of applied stress. The subscript '*T*' is used to denote a transverse test with the fibers oriented at 90 degrees to the axis of applied stress. The superscripts '*(+)*' and '*(-)*' are used to denote tensile and compressive tests, respectively.

5.4.1 Maximum stress criterion

The maximum stress criterion for orthotropic laminas was first suggested by Jenkins[5.2] in 1920. It is an extension of Rankine's theory for isotropic materials. Failure is predicted when any principal material axis stress component exceeds the strength of this component. The criterion implies that in order to avoid failure the following inequalities must be satisfied:

$$-s_L^{(-)} < \sigma_1 < s_L^{(+)}$$

$$-s_T^{(-)} < \sigma_2 < s_T^{(+)} \qquad \text{(Eqns. 5.6)}$$

$$|\tau_{12}| < s_{LT}$$

The failure surface in $\sigma_1 - \sigma_2$ space is a rectangle (see Figure 5.1). This failure criterion is independent of the shear stress τ_{12} in $\sigma_1 - \sigma_2$ space. An independent check on the shear stress is made in the third equation of Equations 5.6. The sign of the shear stress is neglected for this check. This criterion does not account for interaction between the stress components. Since the interaction is not accounted for, agreement between experimental data and predicted failure values for biaxial loading is not good.

5.4.2 Maximum strain criterion

The maximum strain criterion for orthotropic laminas was first suggested by Waddoups[5.3] in 1967. It is an extension of St. Venant's theory for isotropic materials. Failure is predicted when any principal material axis strain component exceeds the ultimate strain of this component. The criterion implies that in order to avoid failure the following inequalities must be satisfied:

$$-e_L^{(-)} < \varepsilon_1 < -e_L^{(+)}$$

$$-e_T^{(-)} < \varepsilon_2 < e_T^{(+)} \qquad \text{(Eqns. 5.7)}$$

$$|\gamma_{12}| < e_{LT}$$

The failure surface in $\varepsilon_1 - \varepsilon_2$ space is a rectangle. In $\sigma_1 - \sigma_2$ space, however, the shape of the failure surface is a skewed parallelogram (Figure 5.1). The shape of the parallelogram is generated by combining the lamina stress-strain relationships given in Equations 5.1 with the relationships given in Equations 5.5. The intercepts of the maximum strain criterion parallelogram need not coincide with the intercepts of the maximum stress rectangle in $\sigma_1 - \sigma_2$ space. As with the maximum stress criterion, the maximum strain criterion does not account for interaction between the stress components.

As expected, there is poor agreement between experimental data and predicted failure values for biaxial loading.

Even though they do not give good results, the maximum stress and the maximum strain criteria are used extensively. This is because the equations are relatively simple.

5.4.3 Tsai-Hill biaxial stress criterion

In 1948, Hill[5.4] suggested that the von Mises criterion for metals could be modified to include the effects induced by anisotropic behavior. The failure (or yield) surface for the Hill criterion in $\sigma_1 - \sigma_2 - \sigma_3$ space is described by the equation:

$$A(\sigma_2 - \sigma_3)^2 + B(\sigma_3 - \sigma_1)^2 + C(\sigma_1 - \sigma_2)^2 + 2D\tau_{23}^2 + 2E\,\tau_{31}^2 + 2F\tau_{12}^2 = 1.0$$

(Eqn. 5.8)

Where A, B, C, D, E, and F are determined from the yield strength in uniaxial or shear loading. Failure is predicted if the left hand side of this equation is greater than 1.0.

Azzi and Tsai[5.5] and later Tsai[5.6] formulated the extension of this criterion to the prediction of failure in an orthotropic, transversely isotropic lamina. This criterion is generally referred to as the Tsai-Hill criterion. The equation is generated by assuming a state of plane stress and replacing the yield strengths of the Hill criterion with the effective lamina strengths. The failure surface is described by the equation:

$$\frac{\sigma_1^2}{s_L^2} - \frac{\sigma_1\sigma_2}{s_L^2} + \frac{\sigma_2^2}{s_T^2} + \frac{\tau_{12}^2}{s_{LT}^2} = 1 \qquad \text{(Eqn. 5.9)}$$

If equal failure strengths are assumed in tension and compression the failure surface will be a symmetrical ellipse. The equation can be used when tensile and compressive strengths are different by substituting the appropriate values for each quadrant of stress space. This procedure is inconsistent with the assumptions used in

formulating the original Hill criterion, but it has been used successfully for some composites.

Another shortcoming of the Tsai-Hill criterion stems from the fact that it is based on principal stress differences and the corresponding shear stresses and strains that drive slip and dislocation movement in metallic crystals. For example, the Tsai-Hill criterion predicts that failure will never occur under a state of hydrostatic stress. Due to shear coupling, a hydrostatic state of stress will lead to failure in an anisotropic material.

5.4.4 Tsai-Wu biaxial stress criterion

The Tsai-Wu criterion was first proposed by Tsai and Wu[5.7] in 1971. It is an improved and simplified version of a failure theory for anisotropic materials that was first proposed by Gol'denblat and Kopnov[5.8] in 1965. It is the most general of the quadratic interaction criteria. The failure surface in three dimensional stress space is described by the following equation:

$$F_i\sigma_i + F_{ij}\sigma_i\sigma_j = 1.0 \qquad \text{(Eqn. 5.10)}$$

where $i, j = 1, 2, 3, 4, 5, 6$

This equation can be simplified for the case of plane stress with $\sigma_3 = \sigma_{33} = 0$, $\sigma_4 = \tau_{23} = 0$, $\sigma_5 = \tau_{13} = 0$. Equation 5.10 then reduces to:

$$F_{11}\sigma_1^2 + F_{22}\sigma_2^2 + F_{66}\sigma_6^2 + F_1\sigma_1 + F_2\sigma_2 + 2F_{12}\sigma_1\sigma_2 = 1.0 \qquad \text{(Eqn. 5.11)}$$

The linear terms in the shear stress $\sigma_6 = \tau_{12}$ are dropped because the shear strength along the material axes is not affected by the sign of the shear stress. The linear terms in the normal stresses remain because they take into account the different strengths in tension and compression. The term $2F_{12}\sigma_1\sigma_2$ accounts for interaction between the normal stresses.

With the exception of F_{12}, all of the constants (F_i and F_{ij}) in equation 5.11 can be found by setting the appropriate stress terms equal to the appropriate uniaxial and shear

strengths and solving the resulting simultaneous equations. This approach leads to the following values for the F_i and F_{ij} terms:

$$F_{11} = \frac{1}{s_L^{(+)} s_L^{(-)}}$$

$$F_1 = \frac{1}{s_L^{(+)}} - \frac{1}{s_L^{(-)}}$$

$$F_{22} = \frac{1}{s_T^{(+)} s_T^{(-)}} \qquad \text{(Eqns. 5.12)}$$

$$F_2 = \frac{1}{s_T^{(+)}} - \frac{1}{s_T^{(-)}}$$

$$F_{66} = \frac{1}{s_{LT}^{2}}$$

To experimentally determine the interaction parameter F_{12} a biaxial test must be conducted. The correct ratio of σ_1 to σ_2 is a matter of controversy. Wu[5.9] has suggested that the ratio must be optimized to account for the sensitivity of F_{12} to experimental scatter in the applied stresses. Tsai and Hahn[5.10] have proposed the following equation for the interaction parameter:

$$F_{12} = -\frac{(F_{11}F_{22})^{1/2}}{2} \qquad \text{(Eqn. 5.13)}$$

This causes the Tsai-Wu equation to take on the form of the Von Mises criterion. This modification is not endorsed by Schapery[5.11]. If no experimental data is available, Schapery recommends that a value of zero be used for the interaction parameter F_{12}.

The Tsai-Wu criterion will reduce to the Tsai-Hill criterion if the tensile and compressive strengths are assumed to be equal and the following value is used for the interaction parameter:

$$F_{12} = -\frac{1}{2s_L^{\,2}} \qquad \text{(Eqn. 5.14)}$$

5.4.5 General summary of existing two-dimensional failure criteria

For purposes of comparison, a plot of the failure criteria described above is shown in Figure 5.1. All four criteria are plotted in stress space. A value of zero was assumed for the F_{12} parameter in the Tsai-Wu criterion. The values represented are based on calculated values for a lamina of similar construction to the wall of the experimental vessel discussed in Chapter 6. The fiber weight fraction used for calculations was 61.3%. The resin used for calculations was Hetron 922. Values for the resin properties were obtained from Trilam[5.12]. As discussed in Section 5.4.1, the actual failure values for longitudinal tension would be expected to be less than those predicted from the micromechanics equations.

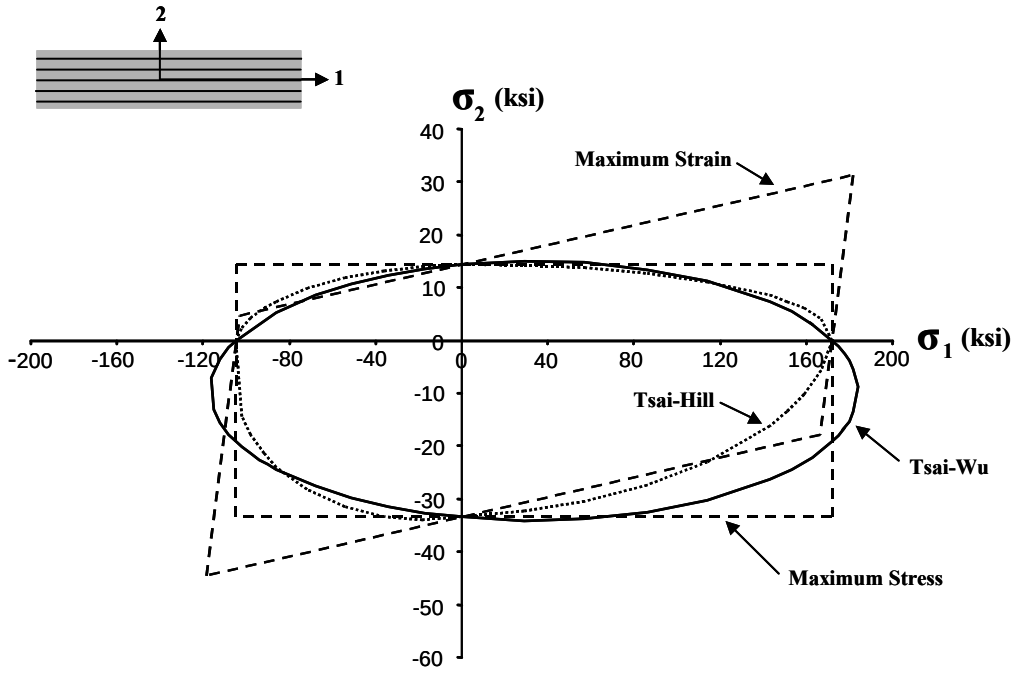

Figure 5.1 – Commonly used 2-D failure criteria

The issue of multi-axial strength criteria for composites is far from resolved. Several improved theories have been suggested. Some of these include theories by Hashin[5.13] and Tennyson[5.14]. Experimental verification of the theories for a wide range of fiber and matrix combinations and varying states of stress is a time consuming task. All theories presented above are based on macromechanical behavior of the lamina.

5.5 Micromechanics Models for Lamina Strength

In the absence of experimental testing, micromechanics models are often used to predict the failure stresses and strains of laminas. Micromechanics models for the prediction of strength are generally not as accurate as those for the prediction of stiffness (the prediction of stiffness is addressed in Chapter 7). This is because material and geometric non-homogeneity can have a significant effect on local variations in stress and strain. Also, different failure modes exist for different loading directions and these can vary with different fiber-matrix combinations. The following micromechanics models are also taken directly from Gibson[5.1].

5.5.1 Longitudinal tensile strength

Longitudinal tensile strength can be developed from the rule of mixtures for longitudinal stress. For glass-reinforced polymers, the matrix generally has a higher failure strain than the fiber. The lamina is assumed to fail at a strain equal to the fiber tensile strain. Theoretically and under some loading conditions, the lamina can reach the matrix failure strain before failure. For practical purposes, fiber failure is assumed to equal failure of the lamina. The equation for this case is given as:

$$s_L^{(+)} = s_{f1}^{(+)} V_f + s_{mf1} V_m \qquad \text{(Eqn. 5.15)}$$

where:

$s_{f1}^{(+)}$ = fiber failure stress in the longitudinal direction

s_{mf1} = matrix stress corresponding to fiber failure strain in the longitudinal direction

V_f = volume fraction of the fibers

V_m = volume fraction of the matrix

This equation is only meaningful if the fiber volume fraction is sufficiently large. If the fiber volume fraction is too low, the composite strength will be less than the matrix

strength. For practical purposes, however, the critical fiber volume fraction is less than 5 percent. For the composites discussed in this dissertation, the fraction is sufficiently large for the equation to be meaningful.

While this equation is simple, it does not generally predict the failure stress of the composite with good accuracy. One reason for this is that fiber strength varies widely from fiber to fiber. Also, the strength of the fibers is dependent on length since more imperfections exist in longer fibers.

This equation assumes linear elastic behavior up to failure. While this assumption is incorrect for the matrix, the error introduced is small due to the small contribution of the matrix to the strength of the lamina.

If the matrix failure strain is less than that of the fibers, all of the load will be carried by the fibers and equation 5.16 will govern. As with equation 5.15, this applies to composites with fiber volumes that are sufficiently large.

$$s_L^{(+)} = s_{fl}^{(+)} V_f \qquad \text{(Eqn. 5.16)}$$

5.5.2 Longitudinal compressive strength

Predictive equations of longitudinal compressive strength are complicated by several factors. First, several different failure mechanisms are possible. Second, the failure mechanisms are often dependent on the test setup. There appear to be three basic failure mechanisms:

1. Micro-buckling of fibers in either the shear or the extensional mode
2. Transverse tensile rupture due to Poisson strains
3. Shear failure of fibers without buckling

Variations and combinations of these mechanisms also exist.

The transverse tensile rupture model due to Poisson strains has been observed to show good agreement for fiberglass/epoxy composites. The resulting predictive equation is:

$$s_L(-) = \frac{E_1 e_T^{(+)}}{\nu_{12}} \qquad \text{(Eqn. 5.17)}$$

5.5.3 Transverse tensile strength

The transverse tensile strength is generally the weakest of the composite strengths. The failure of a laminate is often controlled by the transverse tensile failure of the weakest ply. This is referred to as "first ply failure". This low value of strength is due to strain concentrations around the fibers. Higher fiber volume (or weight) fractions therefore result in lower transverse tensile strength. The predictive equation for transverse tensile strain is given by:

$$e_T^{(+)} = \frac{e_m^{(+)}}{F} \qquad \text{(Eqn. 5.18)}$$

where F = strain concentration factor (> 1.0)

The strain concentration factor is more appropriate than stress due to the typically non-linear nature of the matrix and the resulting nonlinear nature of the composite in transverse tensile loading. The value for F is given by:

$$F = \frac{1}{\frac{d}{s}\left[\frac{E_m}{E_{f2}} - 1\right] + 1} \qquad \text{(Eqn. 5.19)}$$

where:

E_m = modulus of resin

E_{f2} = modulus of fiber in the transverse direction

d = fiber diameter

s = fiber spacing

If a triangular array for fiber packing is assumed and the volume fraction of the fibers is known, the ratio of fiber diameter to fiber spacing can be calculated from the relationship:

$$V_f = \frac{\pi}{2\sqrt{3}} \left(\frac{d}{s}\right)^2 \qquad \text{(Eqn. 5.20)}$$

If linear behavior is assumed, the relationships in Equations 5.5 can be used to calculate the transverse tensile strength.

5.5.4 Transverse compressive strength

The transverse compressive failure strain can be predicted with Equation 5.18 and substitution of the appropriate compressive strains. If linear behavior is assumed, the relationships in Equations 5.5 can be used to calculate the transverse compressive strength.

As a simplified approach, an upper bound on the compressive strength can be set as the matrix compressive strength. However, the actual strength will be lower due to strain concentrations, fiber/matrix interfacial bond failure, voids and/or longitudinal fiber splitting.

5.5.5 In-plane shear strength

The form of the predictive equation for in-plane shear failure strain is identical to that for transverse tensile strain. The shear modulus for fibers and matrix is substituted for tensile modulus. The strain concentration is analogous as well. The equations are as follows:

$$e_{LT}^{(+)} = \frac{e_m^{(+)}}{F_s} \qquad \text{(Eqn. 5.21)}$$

where:

F_s = shear strain concentration factor (> 1.0)

$$F_s = \frac{1}{\frac{d}{s}\left[\frac{G_{m12}}{G_{f12}} - 1\right] + 1} \qquad \text{(Eqn. 5.22)}$$

where:

G_{m12} = in-plane shear modulus of matrix

G_{f12} = in-plane shear modulus of fiber

If linear behavior is assumed, the relationships in Equations 5.5 can be used to calculate the in-plane shear strength.

In a manner similar to the transverse compressive strength, the matrix shear strength can be set as an upper bound. However, the actual strength will be lower due to the reasons listed above for transverse compressive strength.

5.6 Comparison of Damage Based Results with Existing Failure Criteria

As noted above, the existing criteria for the prediction of strength of composites are known to be inaccurate. Tsai-Wu theory is the most general and is considered to do the best job of predicting strength. However, it is also the most complicated and therefore is not widely used. The maximum strain theory is perhaps the simplest of the formulas (in strain space) and therefore is widely used. It can be argued that the maximum strain criterion does the worst job of predicting strength.

All of the existing criteria have the shortcoming of requiring destructive tests in several different orientations. Differing fiber volumes adds further complications. This type of testing is time-consuming and a large amount of scatter is to be expected. These shortcomings are significant. However, the most significant drawback of the existing criteria is that they are all based on the ultimate failure load of the lamina. Generally, when these criteria are incorporated into a code, a large stress ratio is imposed on failure. In the case of pressure vessels designed by Section X of the ASME code, this stress ratio is six (refer to Chapter 2). This is partially due to the poor agreement between the failure criteria and experimental data. However, it is largely due to the fact that laminas experience damage prior to the failure of the entire lamina. The safety factor is an attempt to keep the lamina in the relatively undamaged state in service. It should be noted that laminas experience some damage at extremely low stress levels and keeping the lamina in the completely undamaged state would be impractical.

For these reasons a test method that directly addresses the onset of significant damage, as opposed to ultimate strength, could be beneficial. If such a method were available the safety factors placed on the initiation of significant damage could be more reasonable.

As mentioned in Chapter 4, several AE methods have been developed for the detection of damage in composites. A well established AE parameter is the Felicity ratio. This parameter was used extensively to determine the onset of damage in the composite

coupon specimens. The AE test results for coupons with different resins and fiber architectures are given in Chapter 4.

The final AE results as presented in Section 4.4 were used to develop plots of damage and failure of the coupon specimens in stress and strain space. Micromechanics equations do a good job of predicting stiffness, but a relatively poor job of predicting strength. Since the fiber content of the laminas was known, the stiffness could be calculated. Therefore, it was possible to convert the strain data to stress based on the stiffness of the laminas.

As described in Section 4.5, the behavior of the 90-degree specimens was highly nonlinear at failure. This nonlinearity was considered when converting from strain to stress. Nonlinearity was also considered for the corresponding micromechanics predictions in the 90-degree direction. Nonlinearity was not considered for the 0-degree specimens. Strain gages were mounted on the surface of the specimen. The reinforcing fibers were located very near the surface. The distance from the surface to the fibers was measured. Based on this information, a reduction of 10 percent was used to account for a decrease in strain from the surface to the depth of the fibers.

The experimentally determined stress and strain results for damage, failure as determined by experiment and damage as predicted by micromechanics are shown in Figures 5.2a through 5.6b. Results from laminas made with all five different resin types are presented. The figures are ordered by resin type with the results for the most flexible resin type presented first.

Tensile and compressive stresses were applied to the coupon specimens through bending. The applied tensile stress was of primary interest. Due to Poisson effects, the tensile stresses created theoretical transverse compressive strains and compressive stresses. The compressive stress arises due to a Poisson mismatch between the fiber layers and the mat layer of the test specimens. For this reason, even in stress space the experimental test results are not strictly confined to the first quadrant ($+\sigma_1$ and $+\sigma_2$).

However, the results are very nearly confined to this quadrant, and this is the quadrant of interest for shell structures where tensile stresses dominate (such as pressure vessels).

Where strain space is plotted, only the maximum strain failure envelope is shown. Where stress space is plotted, only the Tsai-Wu failure envelope is shown. The calculated failure criteria are based on micromechanics failure calculations of the lamina (as described in this Chapter) as opposed to experimental testing of the lamina. These micromechanics calculations are based on resin properties provided by the resin manufacturers and fiber properties as described in Chapter 3. A fiber weight fraction of 40% was used for the calculations. This is the fiber fraction of the continuous fiber reinforced portion of the test coupons as determined by burnout testing.

On-axis tests (both longitudinal and transverse) were conducted to produce a state of predominantly uniaxial stress. For these on-axis tests, the surface strain measured was generally ε_x. Off-axis tests were conducted to produce a pronounced state of bi-axial stress. The surface strains measured were ε_1,, ε_2 *and* ε_x (refer to Chapter 3 for strain gage locations). The remaining strains were then solved by equation 5.7. Equations 5.8 and 5.5 were then used to obtain σ_1 and σ_2. Shear stresses are also generated as a consequence of the off-axis test.

Results plotted in stress space:

The results plotted in stress space indicate that the more flexible resins can sustain significantly higher levels of stress in the 90-degree direction prior to onset of AE. This is true even though the ultimate strength is similar for all five types of resin. When compared to 197 specimens, 411 specimens withstood nearly twice the stress prior to damage when loaded in the 90-degree direction. Similar observations are true for the specimens with the ISO and 470 resins to a lesser extent.

For loading in the 0-degree direction very little difference between the resin types is observed.

The results for damage do not follow the general elliptical shape of the Tsai-Wu interaction criterion. The damage stress envelope does fall well within the experimentally determined failure values.

The micromechanics equations do a poor job of predicting strength in both the 0-degree and 90-degree direction. The equations for transverse tensile strength are highly dependent on the failure strain of the resin. Failure stress is over-predicted for flexible resins and under-predicted for specimens with brittle resins in the 90-degree direction. The best correlation between micromechanics and experimental failure values in the 90-degree direction is found with the ISO specimens. The longitudinal tensile strength is over-predicted due to the issues regarding fiber strength mentioned previously in Section 5.4.1.

Results plotted in strain space:

The same observations that were made for the results in stress space also apply to strain space. The biaxial data points for damage follow the Tsai-Wu criterion more closely than the maximum strain criterion.

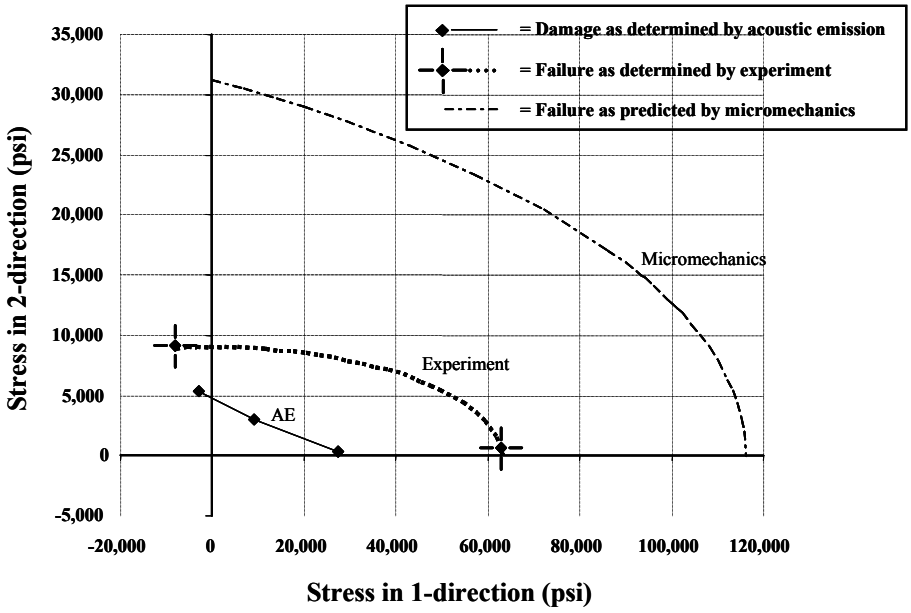

Figure 5.2a – Results for specimens with 8084 resin (stress space)

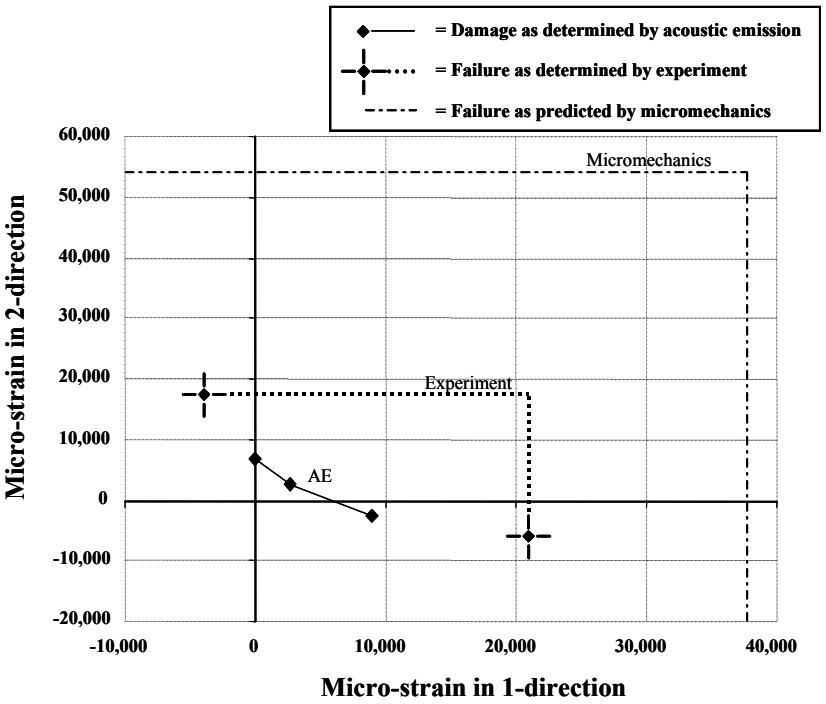

Figure 5.2b – Results for specimens with 8084 resin (strain space)

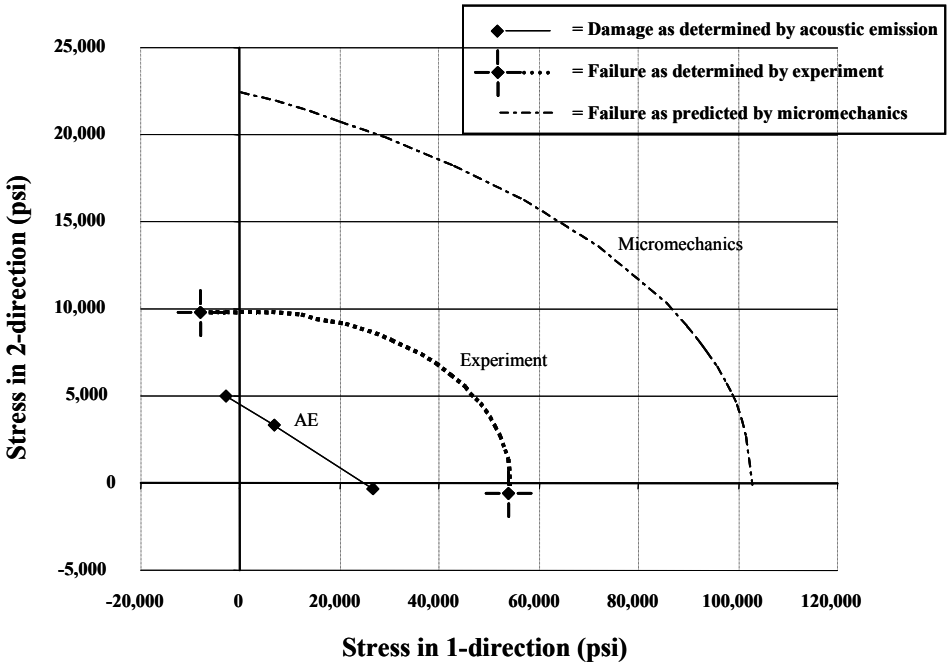

Figure 5.3a – Results for specimens with 411 resin (stress space)

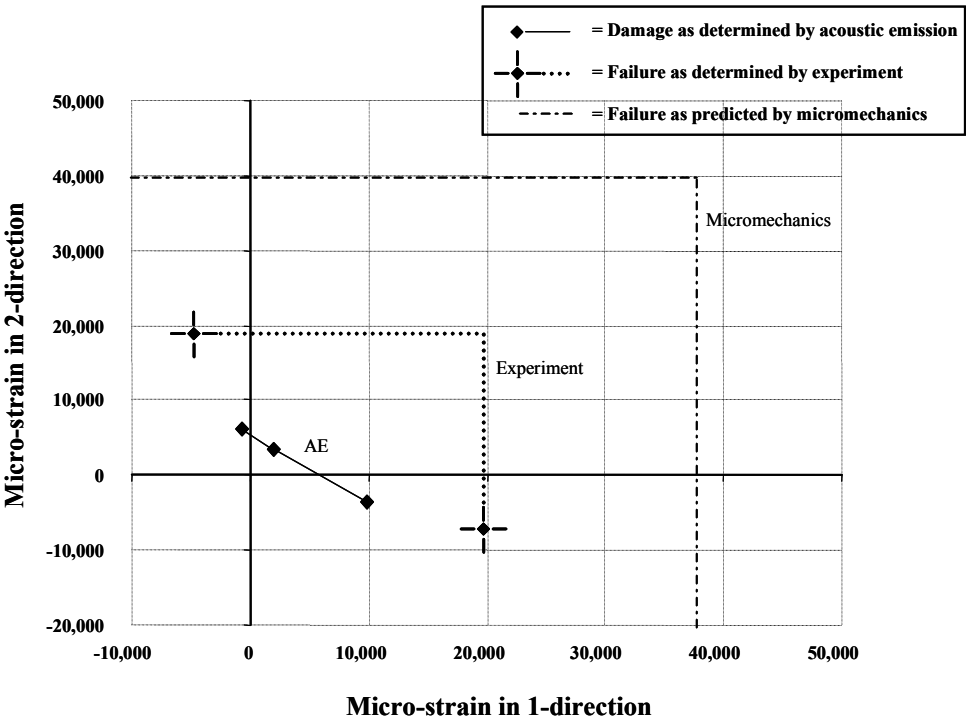

Figure 5.3b – Results for specimens with 411 resin (strain space)

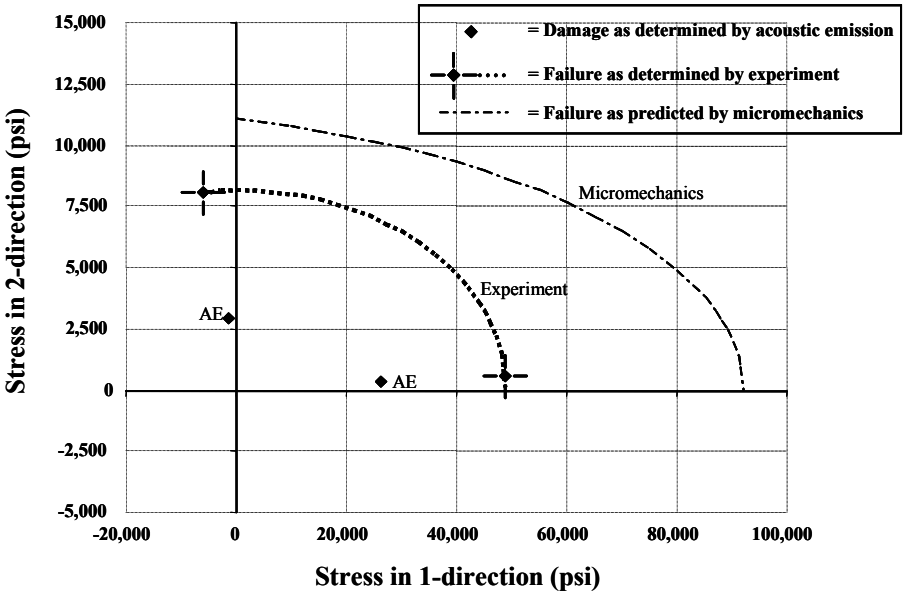

Figure 5.4a – Results for specimens with 470 resin (stress space)

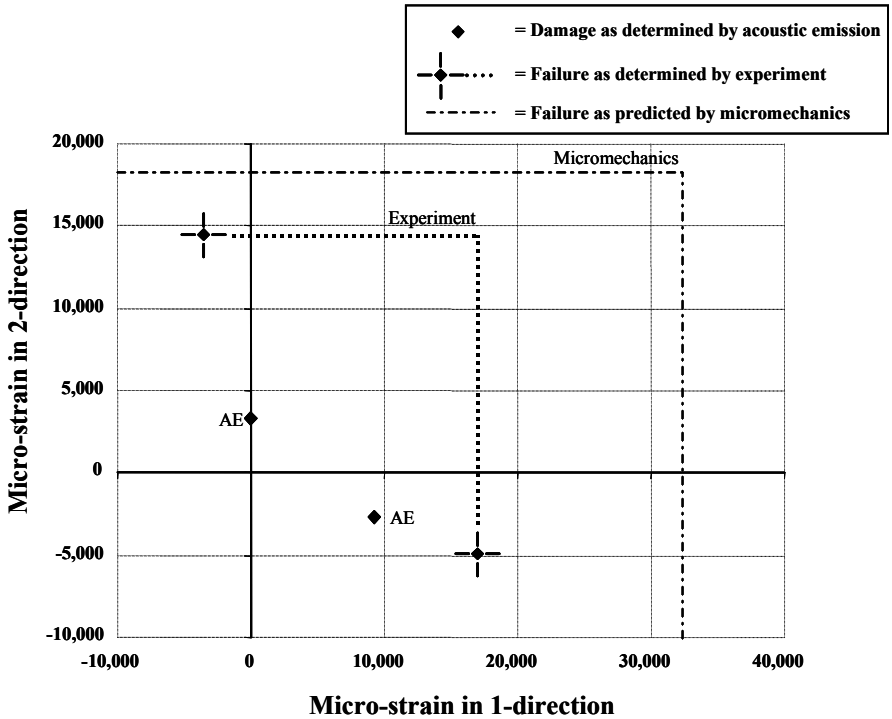

Figure 5.4b – Results for specimens with 470 resin (strain space)

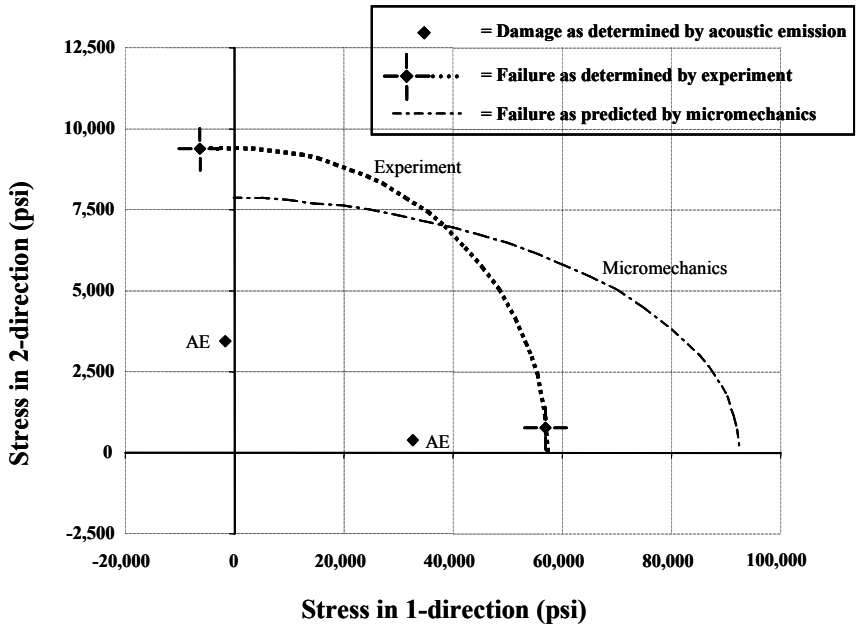

Figure 5.5a – Results for specimens with ISO resin (stress space)

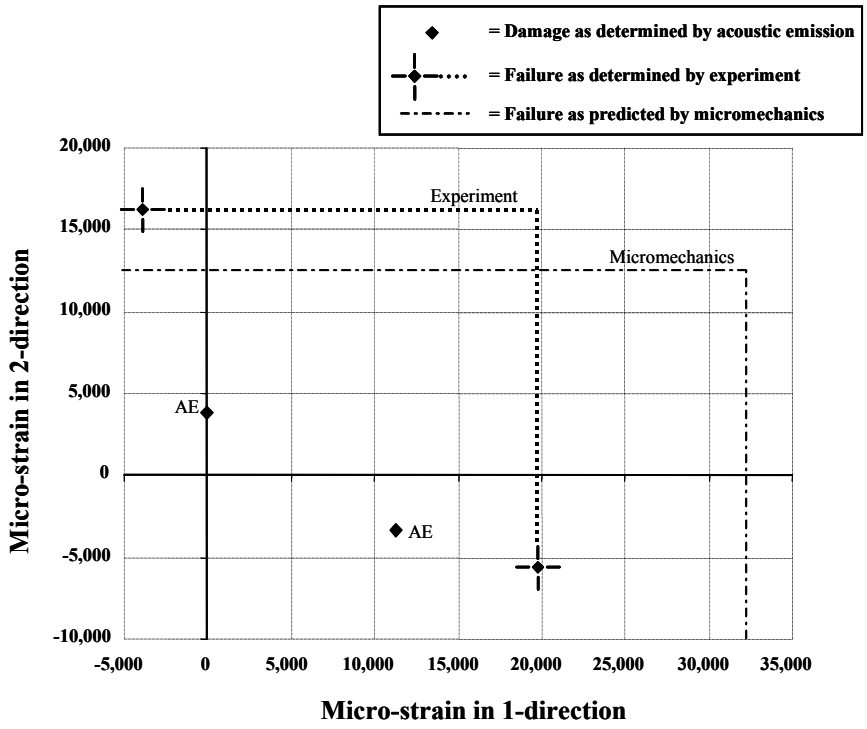

Figure 5.5b – Results for specimens with ISO resin (strain space)

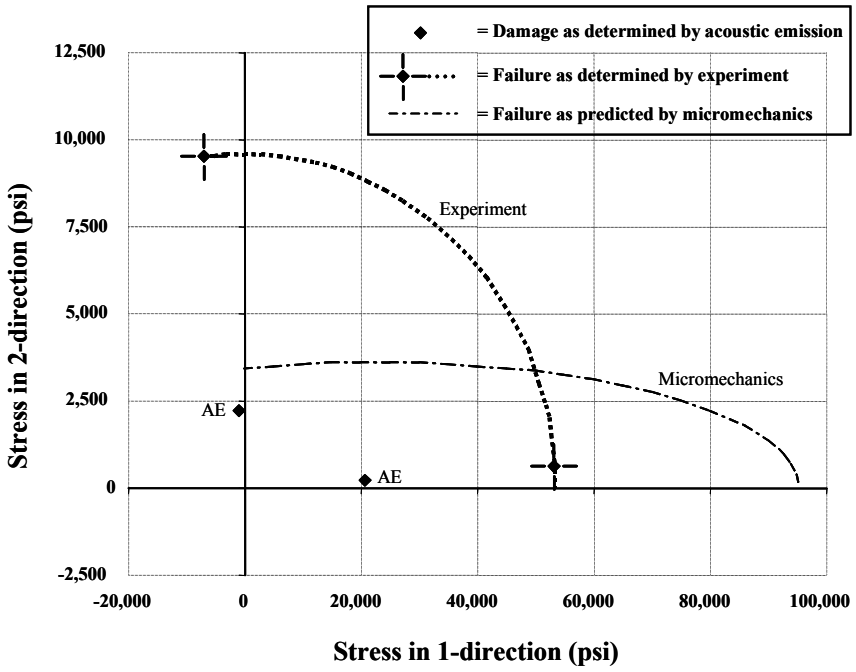

Figure 5.6a – Results for specimens with 197 resin (stress space)

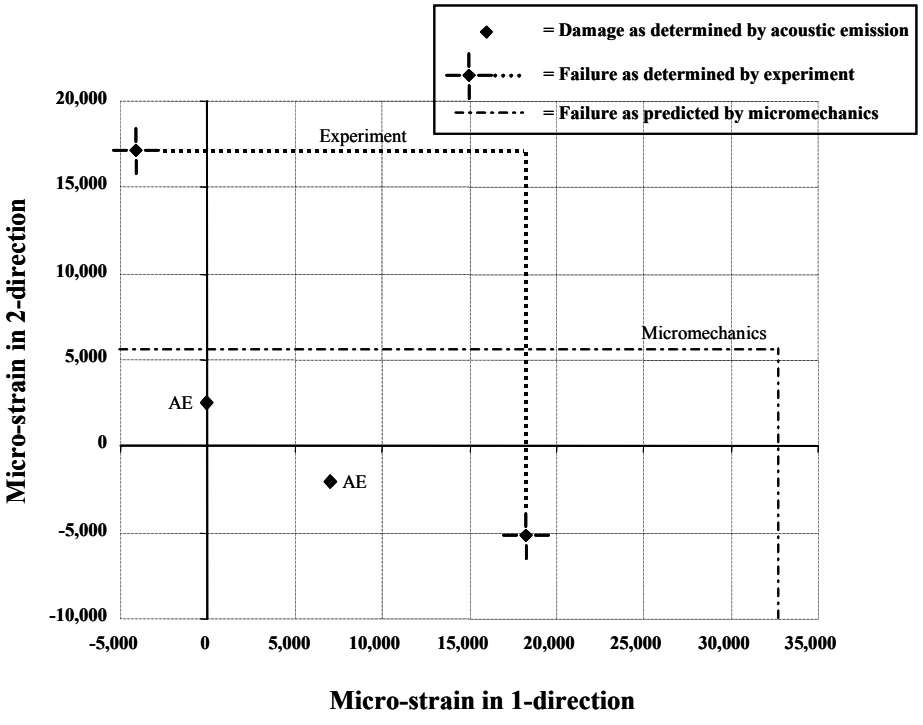

Figure 5.6b – Results for specimens with 197 resin (strain space)

5.7 Conclusions

The results obtained from the acoustic emission testing described in Chapter 4 were used to compare data based on damage to existing failure based criteria.

Unlike the failure based criteria, the data based on damage reflect the differences between the flexible and brittle resins. This is particularly true for the case of applied stress in the 90-degree direction. The general shape of the damage envelope will be substantially different for the damage criterion when compared to the failure criteria.

Considerable disagreement was found between commonly used micromechanics equations and failure as determined by experiment. This was particularly true for the case of applied stress in the 90-degree direction. For this case, failure for specimens made with the flexible resins was over-predicted and failure for the specimens made with brittle resins was under-predicted. Failure in the longitudinal direction was over-predicted for specimens made with both flexible and brittle resins.

Chapter 6: *Overview of the Vessel Experimental Program*

In this chapter the experimental testing of the original vessel is addressed. The vessel geometry, hold-down system, loading procedure, and strain gage monitoring are described. The acoustic emission monitoring is described briefly. A more thorough description of the acoustic emission monitoring is given in Chapter 10.

6.1 Vessel Geometry

The large scale research specimen is a 7'-0" diameter by 21'-6" tall filament wound vessel. The vessel was constructed at the Ershigs plant in Gatesville, Texas. This plant is no longer in operation. The vessel was designed for hydrostatic loading and 15 psi superposed pressure. For reference, an elevation and plan view are shown in Figure 6.1.

A hold-down system was fabricated to resist the uplift force at each of eight locations around the base of the vessel. The calculated hold-down force at each location for the 15 psi superposed pressure was 10,400 pounds. The hold-downs were fabricated from steel channels and W-shapes. A photograph of the hold-down system is shown in Figure 6.2.

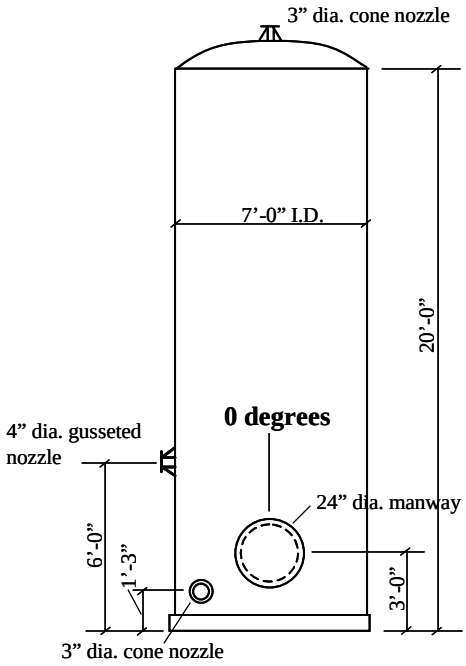

ELEVATION

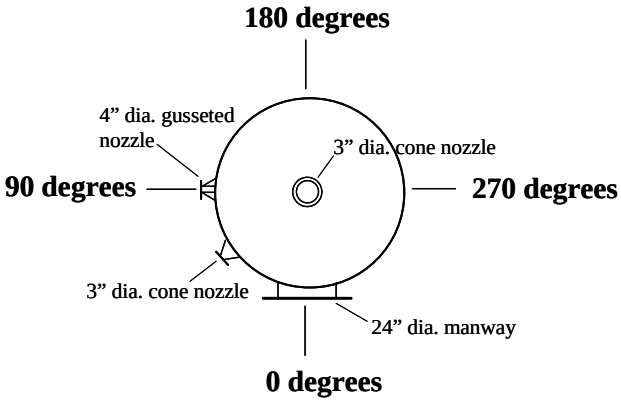

PLAN VIEW

Figure 6.1 – Elevation and plan view of original vessel

The nomenclature used for the lamination sequence of the vessel, manway and nozzles is as follows:

C = 1 layer C glass veil

M = 1 layer 1.5 oz./ sq. ft. chopped strand

R = 1 layer 24 oz./ sq. yd. woven roving

FW = 1 complete cycle of filament winding

A complete cycle of filament winding is a full layer of + and – degree fibers. The thickness of one cycle of filament winding is 0.052". The strand yield is 250 yards/pound and the strand density is 9 strands/inch.

The vessel wall is primarily filament wound. The total wall thickness is 0.20 inches. The layup sequence is C / M / FW / FW / FW. The winding angle is + - 15 degrees. The fibers are E-glass and the resin type is Hetron 922.

The vessel came equipped with one 24" diameter manway, a 4" diameter gusseted nozzle, a 3" diameter cone nozzle near the bottom of the vessel and a 3" diameter cone nozzle at the top of the vessel. The original manway, 4" gusseted cone nozzle and 3" cone nozzle at the base of the vessel are shown in Figures 6.3, 6.4 and 6.5 respectively. An additional 24" diameter manway was later installed opposite the original manway and the 4" gusseted nozzle was replaced with an 8" nozzle.

The reinforcing schemes for the original manway, the 4" gusseted nozzle and the 3" cone nozzle are shown in Figures 6.6 through 6.15.

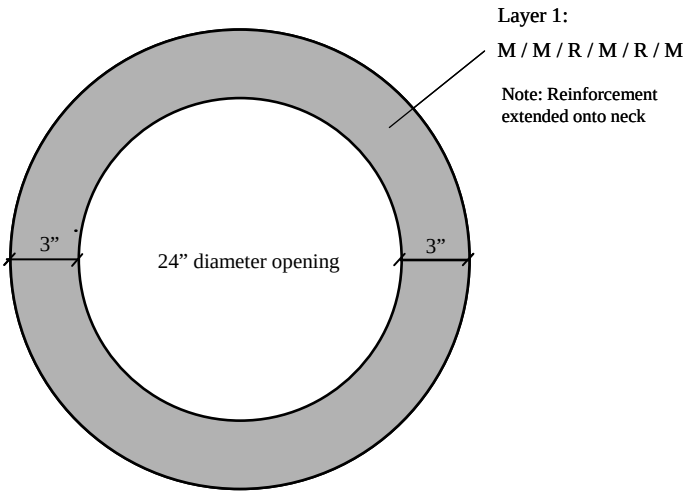

Figure 6.6 – Exterior reinforcement of standard manway - Layer 1

Figure 6.7 – Exterior reinforcement of original manway – Layer 2

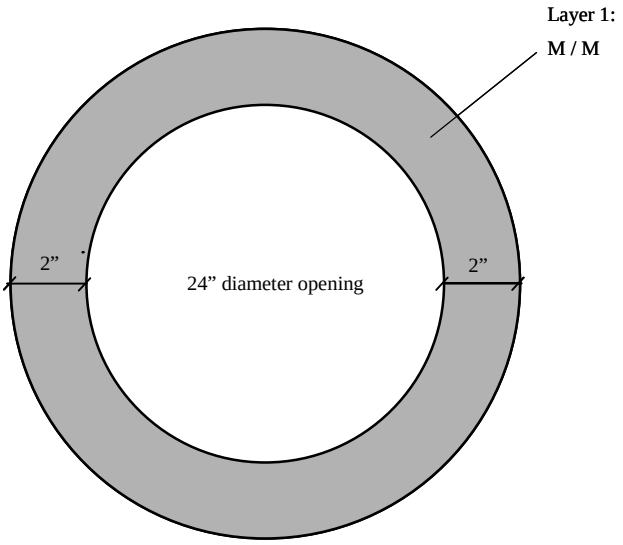

Figure 6.8 – Interior reinforcement of original manway – Layer 1

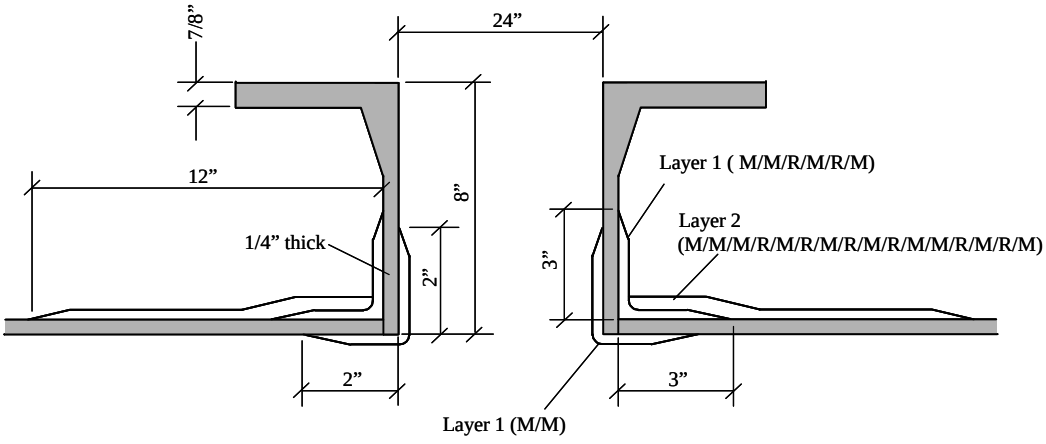

Figure 6.9 – Section view of original manway

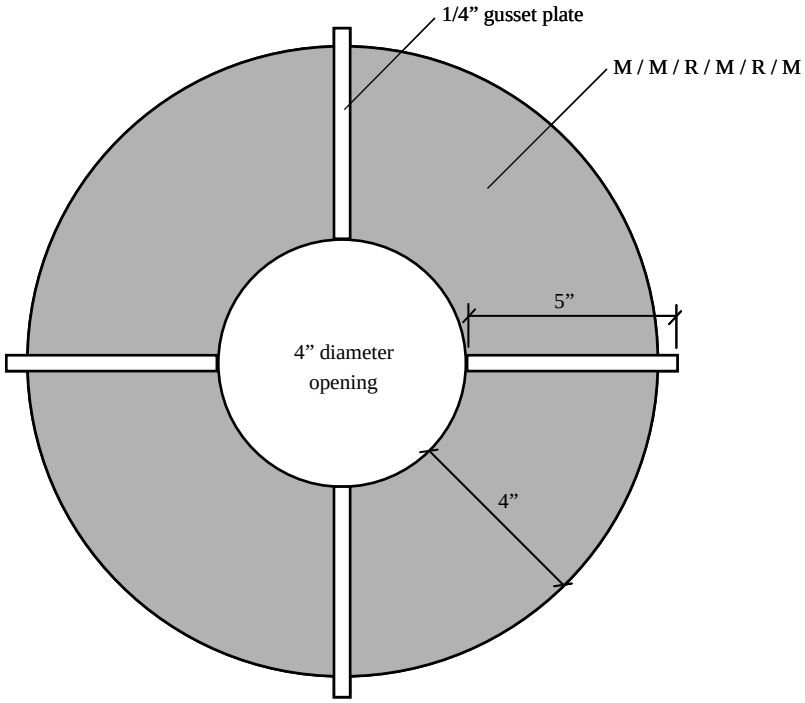

Figure 6.10 – Exterior reinforcement of 4” gusseted nozzle

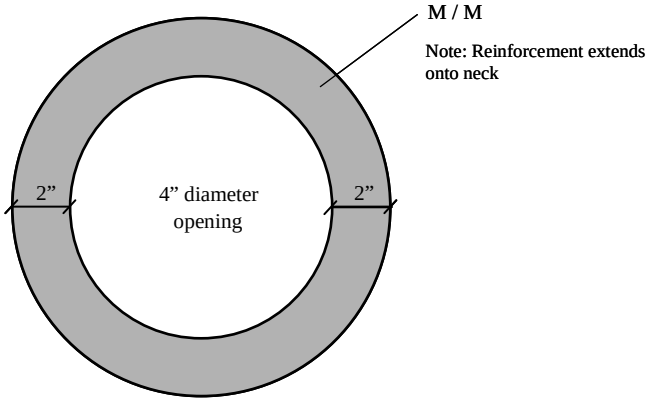

Figure 6.11 – Interior reinforcement of 4” gusseted nozzle

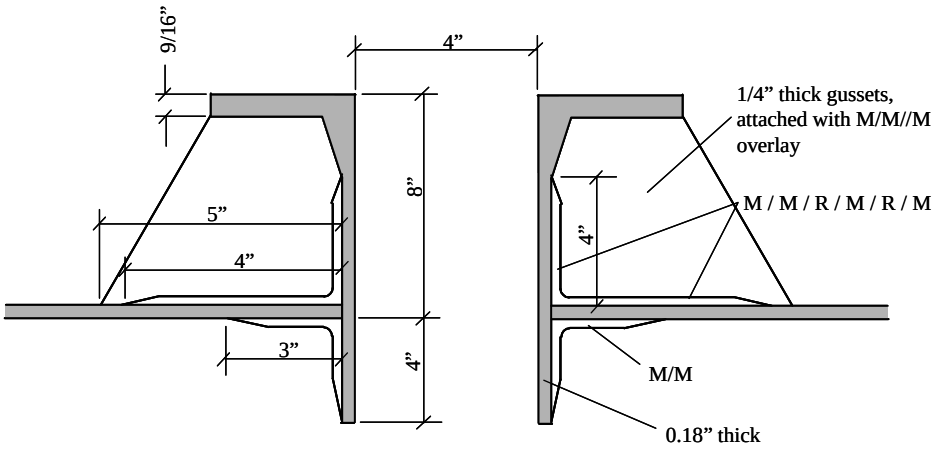

Figure 6.12 – Section view of 4” gusseted nozzle

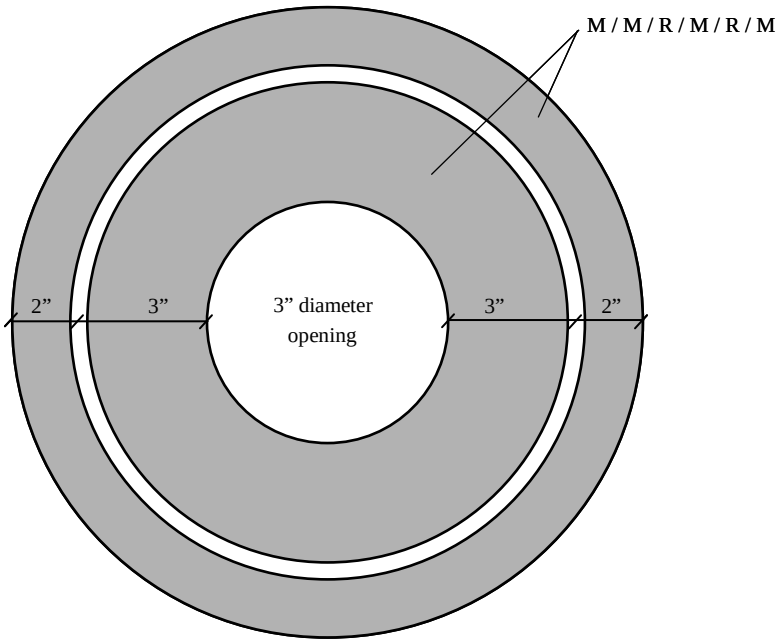

Figure 6.13 – Exterior reinforcement of 3” cone nozzle

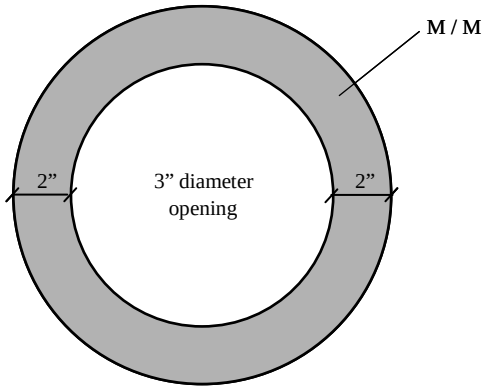

Figure 6.14 – Interior reinforcement of 3” cone nozzle

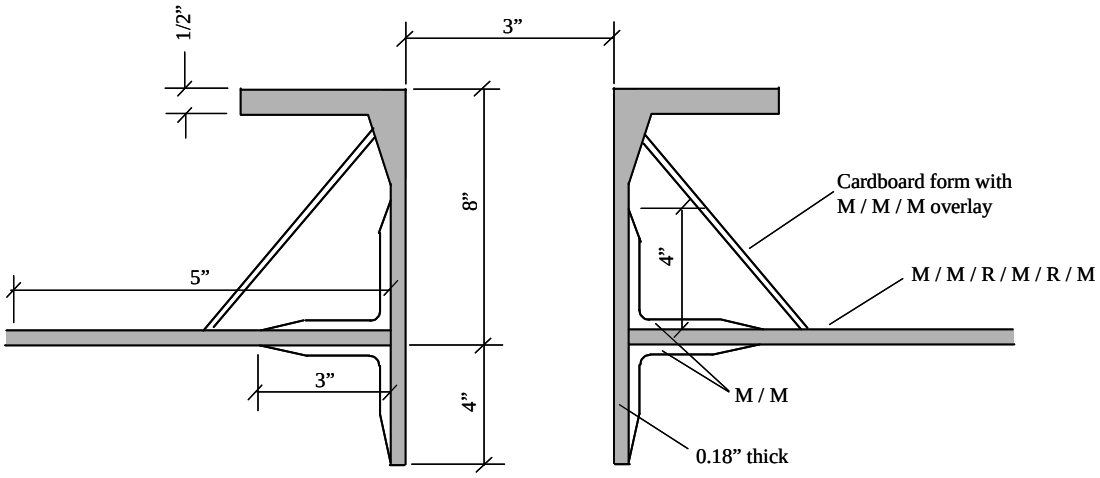

Figure 6.15 – Section view of standard 3” cone nozzle

6.2 Loading

The vessel was filled with water in increments of 2 feet 0 inches. When the vessel was full care was taken to make sure that all air was removed and the vessel was sealed. Additional pressure was applied with water. The vessel was filled and pressurized several times during the course of the testing. The maximum pressure that the vessel experienced was 23.0 psi.

Pressure was applied incrementally. An idealized loading profile is shown in Figure 6.16. Actual loading profiles are shown in Chapter 10.

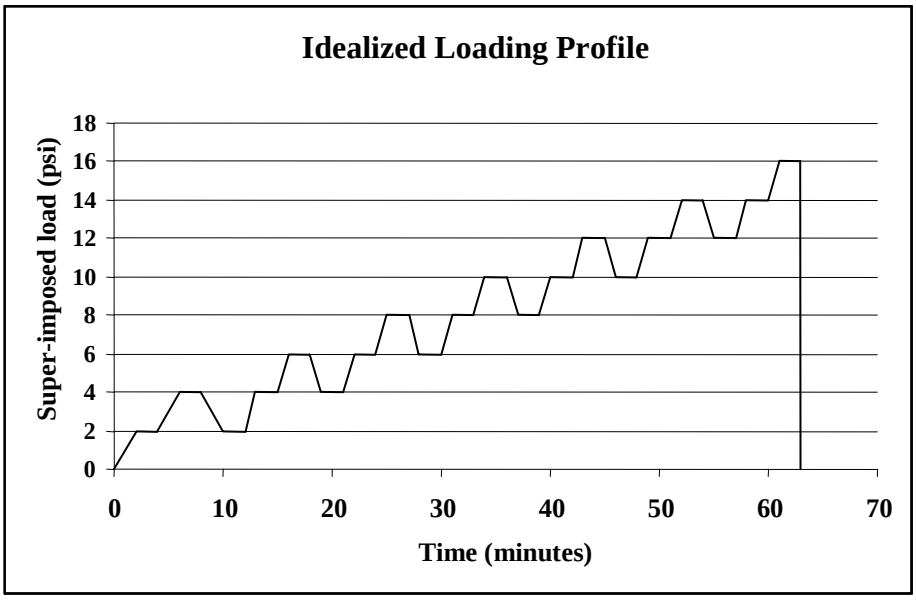

Figure 6.16 – Idealized loading profile

6.3 Strain Gage Monitoring

Strain gages were affixed at strategic locations around the vessel. Strain rosettes were located around the circumference of the vessel at 1'-6", 5'-6" and 11'-6" above floor level to obtain strain information away from the discontinuity areas. These rosettes were actually individual gages oriented by hand. A description of the use of strain gages

for composite materials is given in Chapter 3. This information was used to verify material properties. The locations of the rosettes are shown in Figure 6.17.

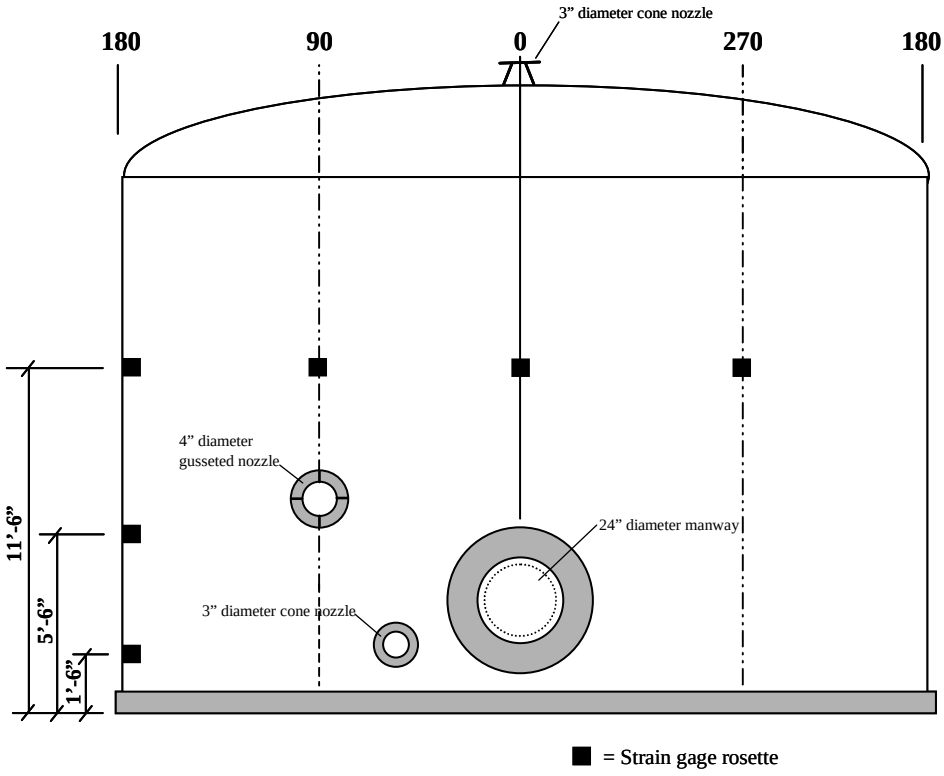

Figure 6.17 – Strain gage locations on vessel wall

Several strain gages were located around the manway and nozzles (Figures 6.18 through 6.20) to verify finite element models of the vessel. Strain gages were also located near the base of the vessel (Figure 6.21). Strain gage locations for the new manway and new 8" nozzle are described in Chapter 9.

The strain gages were not temperature compensated for plastics, but rather for steel. For plastics it is sometimes desirable to use gages with no temperature compensation, since the coefficient of thermal expansion varies for different orientations. The compensation for steel was used due to its availability and low cost. This

compensation was of little consequence since the testing was conducted at a fairly constant temperature (+ or – 5 degrees Fahrenheit range). When the water level in the vessel rose above the strain gage there was a noticeable discontinuity in the results. The data was adjusted to compensate for this localized effect.

When strain gages are used to monitor composites it is often difficult to obtain consistent results. This is due to a number of factors. The non-homogeneous nature of the composite leads to large local variations in strain. A large amount of the fabrication work is done by hand, and this can also lead to local variations in material properties. During the filament winding process, layers of fibers overlay one another as the subsequent band of reinforcing is placed over the previous. This leads to an overlapping pattern of reinforcement at about every 6 inches. This was initially a cause of poor strain gage results. The affected gages were removed and replaced with new gages in areas away from the overlap.

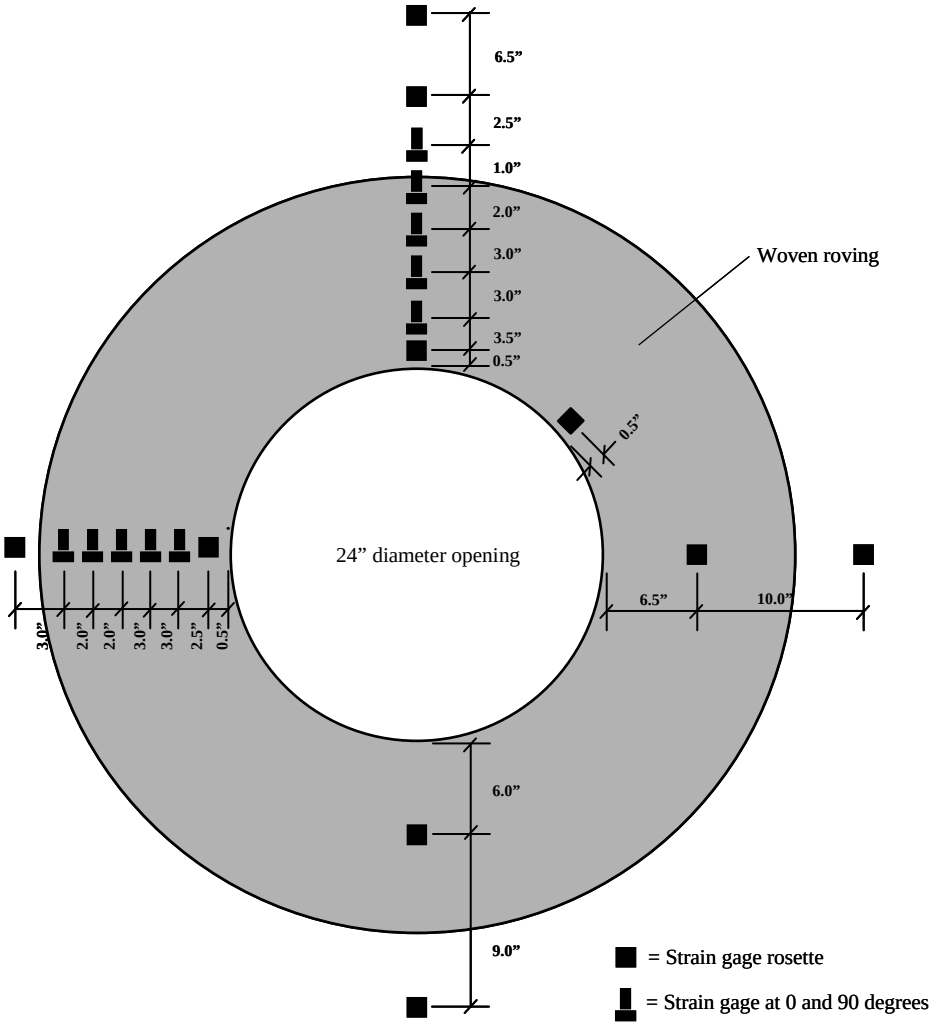

Figure 6.18 – Strain gage locations near original manway

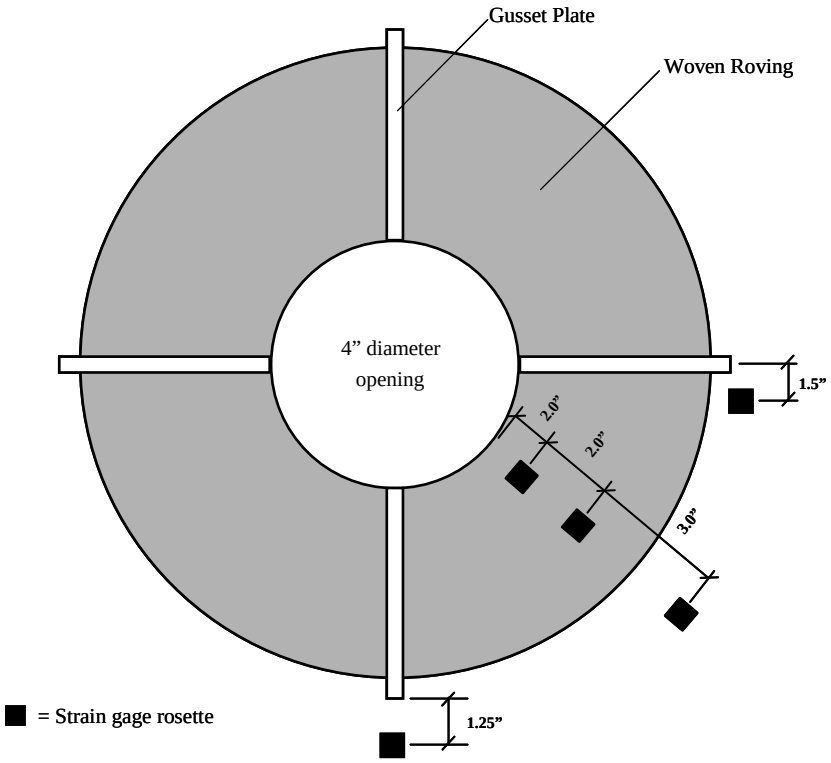

Figure 6.19 – Strain gage locations near 4” gusseted nozzle

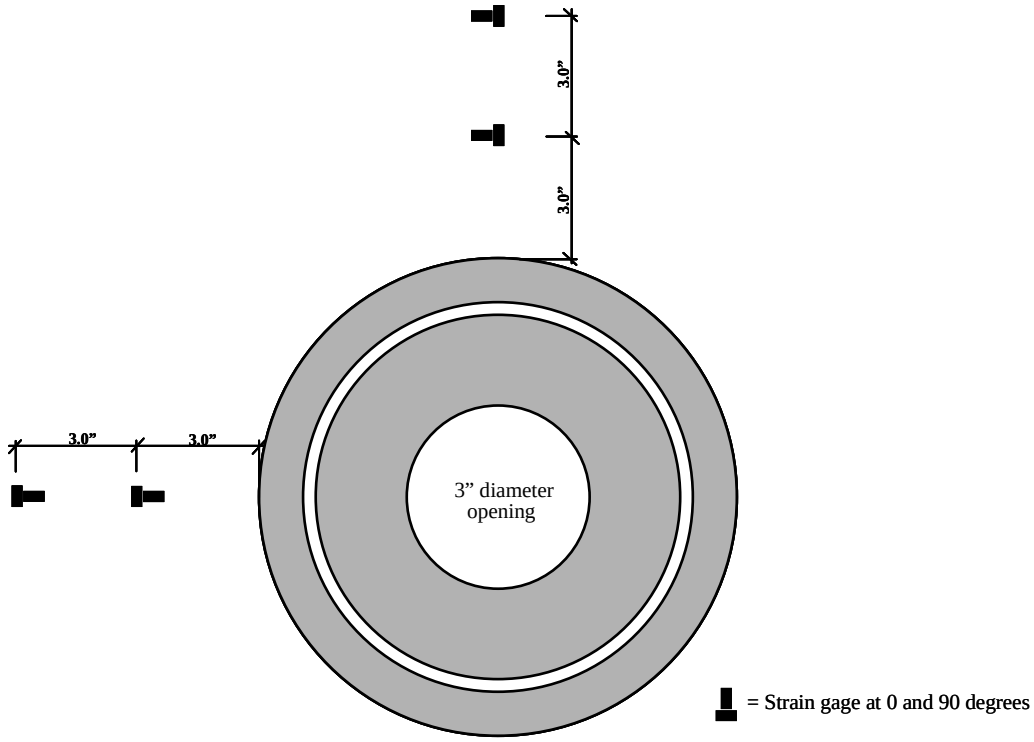

Figure 6.20 – Strain gage locations near 3” cone nozzle

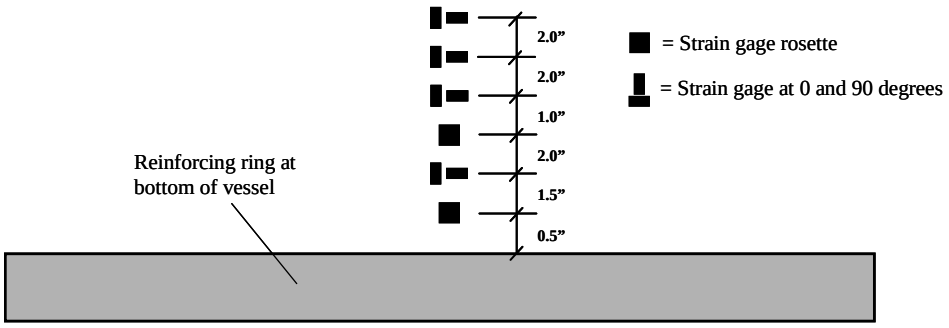

Figure 6.21 – Strain gage locations near reinforcing ring at bottom of vessel

6.4 Acoustic Emission Monitoring

Acoustic emission sensors were affixed to the vessel with hot melt glue. Sensors were clustered in areas of particular interest, such as the manway and the nozzles. The sensor locations and sensor (channel) numbers are shown in Chapter 10 for both the original and modified vessel.

Acoustic emission data for the R15I sensors was collected with the Transportation Instrument. When wide band sensors were used, the acoustic emission data was collected with the Mistras 2000.

Chapter 7*: Experimental Verification of Finite Element Models for the Original Vessel*

7.1 Introduction

This chapter addresses the development and verification of the finite element models for the original vessel. Micromechanics models for predicting lamina stiffness are given. Stiffness based on micromechanics was found to agree well with the stiffness as predicted with Trilam[7.1]. Trilam was used to predict the stiffness of the laminas. The calculated stiffness values are given for both the vessel wall and the hand layup portion of the original vessel. Finite element models were developed for the overall vessel and the discontinuity regions. The finite element models are described. The surface strains as predicted by the finite element models are compared to the experimentally measured strains.

7.2 Micromechanics Models for Predicting Stiffness

The micromechanics models for the prediction of stiffness are better developed than the models for predicting strength. However, a good deal of disagreement is still present between predicted and experimental results. This is particularly true for matrix dominated behavior, such as loading transverse to the fibers and in-plane shear.

Micromechanics equations for the prediction of stiffness can be found in Gibson[7.2]. For a specially orthotropic lamina with unidirectional continuous fibers equations used are as follows:

Longitudinal modulus:

$$E_{11} = V_f E_f + V_m E_m \qquad \text{(Eqn. 7.1)}$$

Transverse modulus[7.3]:

$$E_{22} = E_m \frac{(1 + \xi n_e V_f)}{(1 - n_e V_f)} \quad \text{(Eqn. 7.2)}$$

$$E_{33} = E_{22} \quad \text{(Eqn. 7.3)}$$

$$\text{where: } n_e = \frac{(E_f / E_m) - 1}{(E_f / E_m) + \xi} \quad \text{(Eqn. 7.4)}$$

E_f = fiber tensile modulus

E_m = resin tensile modulus

V_f = volume fraction of fibers

V_m = volume fraction of resin

ξ = 2

Shear modulus[7.3]:

$$G_{12} = G_m \frac{(1 + \xi n_g V_f)}{(1 - n_g V_f)} \quad \text{(Eqn. 7.5)}$$

$$G_{13} = G_{12} \quad \text{(Eqn. 7.6)}$$

$$G_{23} = \frac{E_{22}}{2(1 + \upsilon_{23})} \quad \text{(Eqn. 7.7)}$$

$$\text{where: } n_g = \frac{(G_f / G_m) - 1}{(G_f / G_m) + \xi} \quad \text{(Eqn. 7.8)}$$

G_f = fiber shear modulus

G_m = resin shear modulus

ξ = 1

Poisson ratio:

$$\nu_{12} = V_f \nu_f + V_m \nu_m \qquad \text{(Eqn. 7.9)}$$

$$\nu_{13} = \nu_{12} \qquad \text{(Eqn. 7.10)}$$

$$\nu_{21} = \nu_{12} \frac{E_{22}}{E_{11}} \qquad \text{(Eqn. 7.11)}$$

$$\nu_{32} = \nu_{23} \qquad \text{(Eqn. 7.12)}$$

$$\nu_{31} = \nu_{21} \qquad \text{(Eqn. 7.13)}$$

where: ν_f = fiber Poisson ratio

ν_m = resin Poisson ratio

The stiffness of a lamina with randomly oriented fibers is also covered in Gibson. Approximate expressions as developed by Tsai and Pagano[7.4] are as follows:

Modulus:

$$\tilde{E} = \frac{3}{8} E_{11} + \frac{5}{8} E_{22} \qquad \text{(Eqn. 7.14)}$$

Shear Modulus:

$$\tilde{G} = \frac{1}{8} E_{11} + \frac{1}{4} E_{22} \qquad \text{(Eqn. 7.15)}$$

The Trilam[7.1] results for stiffness are in general agreement with those found from the equations given above. Trilam is configured to calculate properties for layups that are generally found in practice, such as 24 oz./sq. yd. woven roving and 1.5 oz./sq. ft. random mat. Therefore, Trilam was used for the prediction of stiffness of all laminas. The finite element model results reported later in this chapter for the vessel shell were in good agreement with the strain gage results for both the hydrostatic and pressure tests.

Therefore, it can be concluded that Trilam did a good job of predicting the stiffness of the laminas and the resulting laminates.

7.3 Stiffness Properties of Existing Vessel Laminas

Hetron 922 was used as the input for the resin and E-glass was used as the input for the fiberglass reinforcing. The published properties for Hetron 922 and E-glass can be found in Chapter 3. The Trilam calculated stiffness properties used for the vessel wall and secondary layups were as follows:

C-Veil (0.11 oz./sq. ft., 10% fiber by weight)

E_{11} = 700,000 psi

E_{22} = 700,000 psi

ν_{12} = 0.362

G_{12} = 257,000 psi

Random Mat (1.5 oz./sq. ft., 31% fiber by weight)

E_{11} = 1,250,000 psi

E_{22} = 1,250,000 psi

ν_{12} = 0.394

G_{12} = 448,000 psi

Filament Wound Lamina (2.3 oz./sq. ft., 61.3% fiber by weight)

E_{11} = 4,466,000 psi

E_{22} = 1,343,000 psi

ν_{12} = 0.309

G_{12} = 413,000 psi

Woven Roving Lamina (24 oz./sq. ft., 50% fiber by weight)

E_{11} = 2,401,469 psi

E_{22} = 2,415,846 psi

ν_{12} = 0.15

G_{12} = 348,285 psi

7.4 Development of Finite Element Models

Several finite element (FE) models were developed for comparison with the strain gage results. Abaqus[7.5] was the finite element code used. The overall vessel was first modeled as a shell without the manway and nozzle regions. This model is referred to as the global model. Local models of the manway and nozzles were then developed.

The calculated displacements from the overall model were applied to the boundaries of the local models. The stress distributions for the local models were compared to those of the global model to assure correct modeling of the boundary conditions. The discontinuities of the local models were then developed. The resulting strain distributions were recorded and compared to the strain gage results.

As is typically the case for finite element models, approximations were made regarding geometry and boundary conditions. The cover was modeled as a continuous shell. The bolts and gasket were not modeled. No slip was accounted for between the cover and the flange of the manway. The same is true of the 8" nozzle model. For the global model, the hold-down system was modeled by restricting vertical movement at each node of the reinforcing ring. For the local models, the hold-down system was modeled by restricting movement in the vertical direction at discrete points around the reinforcing ring. No restraint was modeled for the hold-down system in the horizontal direction. The actual hold-down system displaces upward slightly during pressurization

and some restraint in the horizontal direction is present. Due to the mesh generating scheme used, all nodes in the model were mapped to a circular geometry. This resulted in a geometrical approximation for the manway and nozzle. The edges of the reinforcing layers are tapered on the actual vessel. The model does not take this into account. The head portion of the model is not curved to the same extent as that of the actual vessel.

Shell elements were used for both global and local finite element models. 9-noded shell elements (type S9R5) were used for the global model. 4-noded shell elements (type S4R5) were used for the local models to reduce computation time and conserve hard disk space. The *SHELL GENERAL SECTION command was used with the COMPOSITE variable enabled. With the COMPOSITE variable enabled, it is possible to input a large number of laminas with varying thicknesses and orientations. The OFFSET variable was also enabled for the local models. This variable allows the user to establish a reference plane for each element type. This is useful for asymmetric laminates such as those in the vicinity of the manway and nozzles. The *DLOAD command was used to model both hydrostatic and superposed pressure (HP and P variables).

For the local models, the mesh was developed in Patran[7.6] and the analysis was run in Abaqus. It was necessary to use Patran for the local models due to the complex geometries and relative fineness of the meshes developed. The *NMAP command was then inserted in the Abaqus code to create a curved geometry. The Abaqus input file was rewritten (with the exception of the node locations) to accommodate the composite material properties and geometry. In the manway region, one-fourth of the circumference was modeled and the vessel was discontinued at a height of 20 feet. This was adequate to reduce the effects of the discontinuity to an acceptable level near the edges of the manway models. The 4” diameter gusseted nozzle at 6 feet 0 inches above the floor level and the 3” diameter cone nozzle at the bottom of the vessel were also modeled. For the FE models of these nozzles one-eighth of the circumference of the vessel was modeled and the vessel was discontinued at a height of 12 feet. These dimensions were adequate

to reduce the effects of the discontinuity to an acceptable level near the edges of the local models.

The reinforcing used for the original manway is woven roving (24 oz./sq. yd.). This type of fabric has fibers oriented at 0 and 90 degrees. The fibers are interwoven with one another to allow for ease of handling. Visual inspection revealed that the fibers of the woven roving were oriented in the longitudinal and hoop directions of the vessel.

Each lamina of reinforcing fabric is sandwiched between at least one layer of 1.5 oz./sq. ft. of random mat. To conserve space in the code, each lamina is therefore modeled as a layer of woven roving reinforcement sandwiched between 0.75 oz./sq. ft of random mat. The resulting stiffness parameters of the combined laminate are as follows:

Woven Roving combined with 0.75 oz. Random Mat (top and bottom)

E_{11} = 1,730,000 psi

E_{22} = 1,730,000 psi

ν_{12} = 0.220

G_{12} = 381,000 psi

During layup of the manway reinforcement, the lay-up was discontinued and allowed to exotherm after three laminas of woven roving were placed. This results in two layers of random mat after every third layer of reinforcing fabric. This is accounted for in the code as a single lamina of random mat.

7.5 Continuity region strains – vessel body

7.5.1 Description of finite element models - vessel body

This model was developed to predict the strain response away from the discontinuity regions. One-fourth of the vessel was modeled. The typical element size is approximately 3 inches by 6 inches. The knuckle around the bottom of the vessel was modeled by thickening the shell elements in that region. The mesh is shown in Figure 7.1.

7.5.2 Comparison of strain gage results with finite element model results - vessel body

As described in Chapter 6, several strain gage rosettes were located on the main body of the vessel away from the discontinuity regions. These strain results were used to verify that reasonable material properties were assumed for the finite element model. The experimental strain results are plotted with the results predicted by the finite element model for hydrostatic loading in Figures 7.2, 7.3 and 7.4. The case of superposed pressure of 15 psi is shown in Figures 7.5, 7.6 and 7.7. The results are plotted for strains in the axial, hoop and 45-degree directions. The strains in the hoop, axial and 45-degree directions were measured directly. The predicted axial and hoop strains were read from the finite element model. Transformation equations were then used to calculate the predicted strain in the 45-degree direction. The axial strain for 15 psi loading was under-predicted by the finite element model. With this exception, reasonable agreement was found between the finite element model and the experimental results.

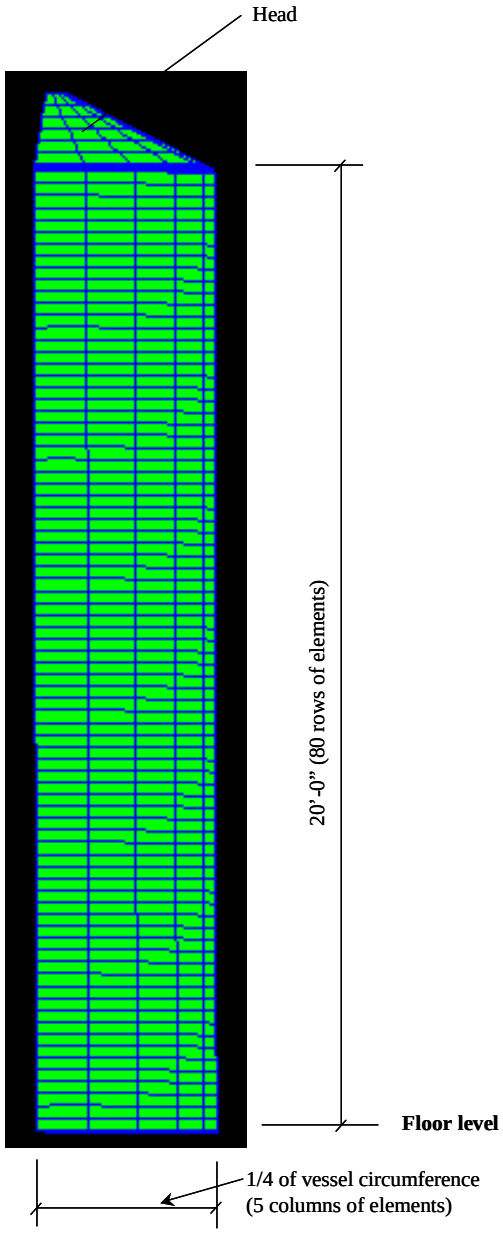

ELEVATION

Figure 7.1 – Finite element mesh of vessel body

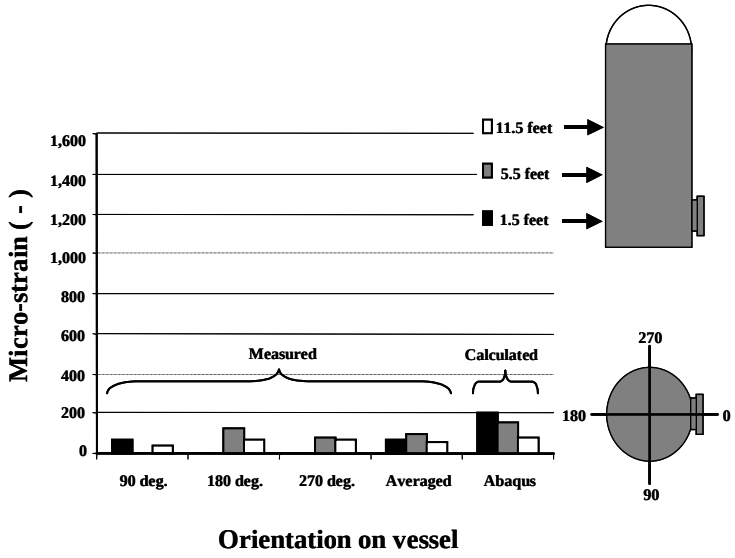

Figure 7.2 – Axial strain on vessel body (hydrostatic pressure)

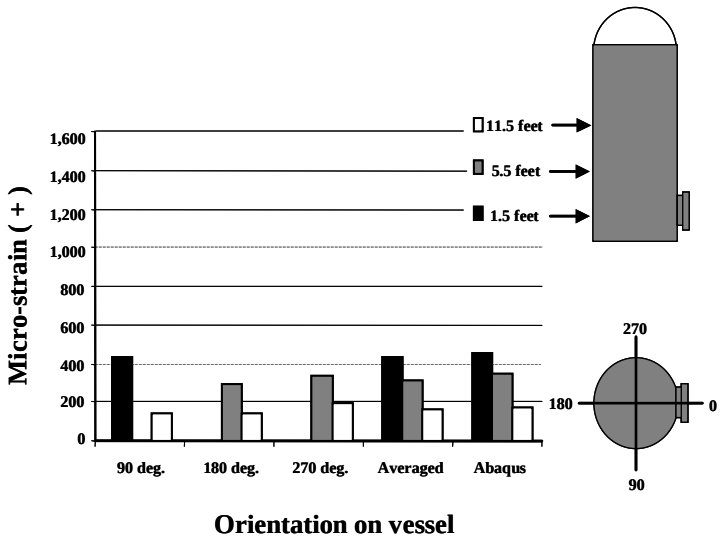

Figure 7.3 – Hoop strain on vessel body (hydrostatic pressure)

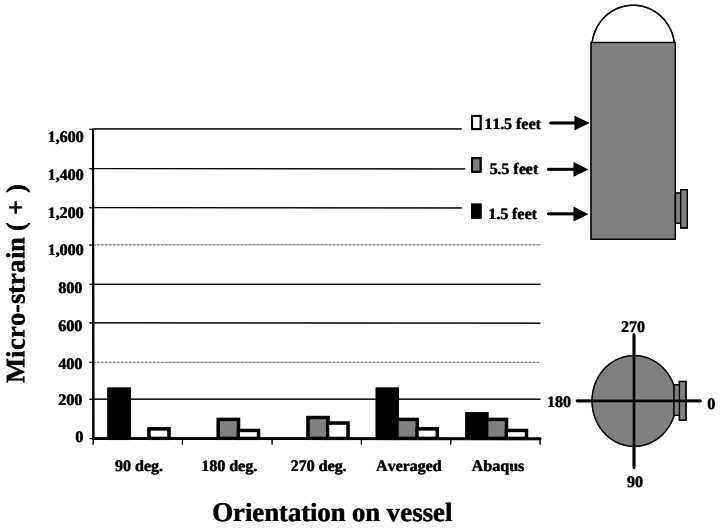

Figure 7.4 – Strain at 45-degrees on vessel body (hydrostatic pressure)

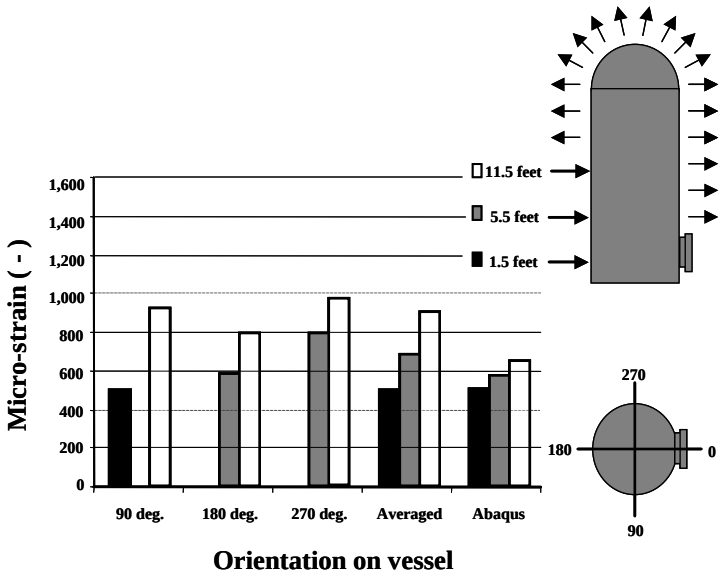

Figure 7.5 – Axial strain on vessel body (15 psi superposed pressure)

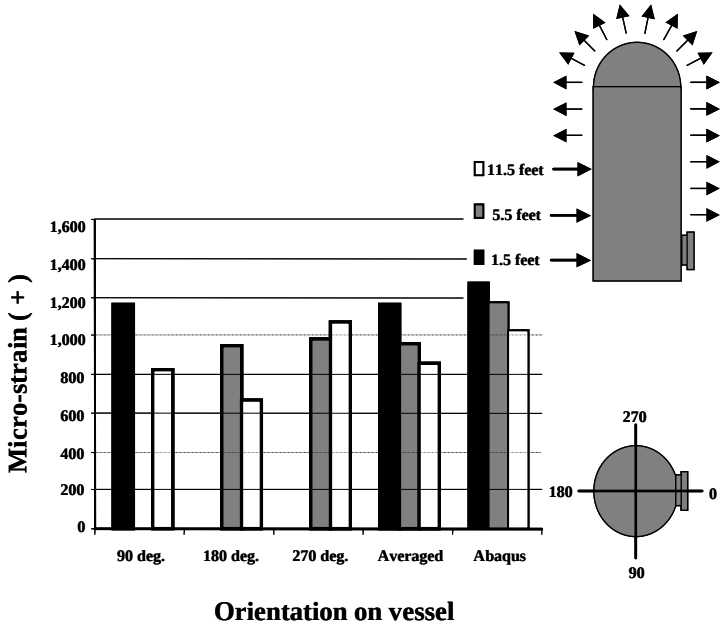

Figure 7.6 – Hoop strain on vessel body (15 psi superposed pressure)

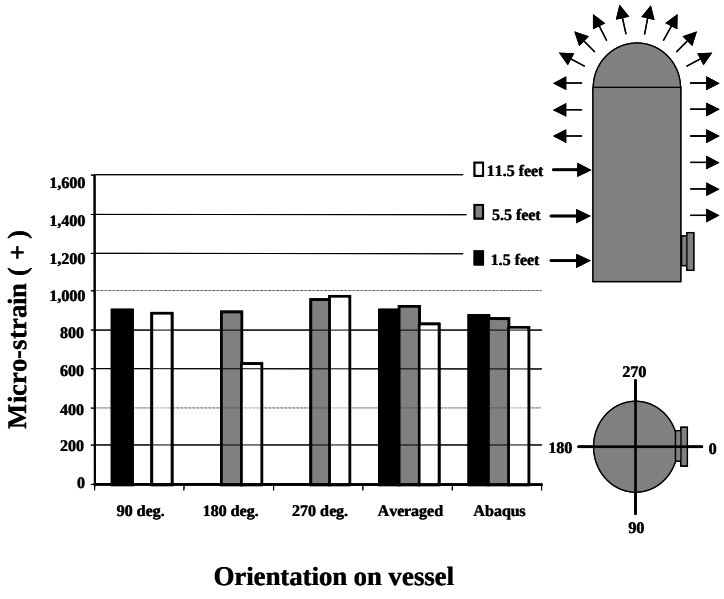

Figure 7.7 – Strain at 45-degrees on vessel body (15 psi superposed pressure)

7.6 Discontinuity region strains – near reinforcing ring

7.6.1 Description of finite element models - near reinforcing ring

The finite element model that was developed for the vessel body was also used to predict the strain response in the vicinity of the reinforcing ring. As mentioned previously, the reinforcing ring was modeled by thickening the shell elements in that region. The reinforcing ring is represented by the first two rows of elements.

7.6.2 Comparison of strain gage results with finite element model results - near reinforcing ring

As described in Chapter 6, several strain gage rosettes were located on the shell of the vessel in the vicinity of the vessel intersection with the reinforcing ring. The experimental strain results and the results predicted by the finite element model for 15 psi superposed loading are shown in Figures 7.8 and 7.9. Reasonable agreement was found between the finite element model and the experimental results. The strain gage results indicate slightly greater stiffness than the finite element models.

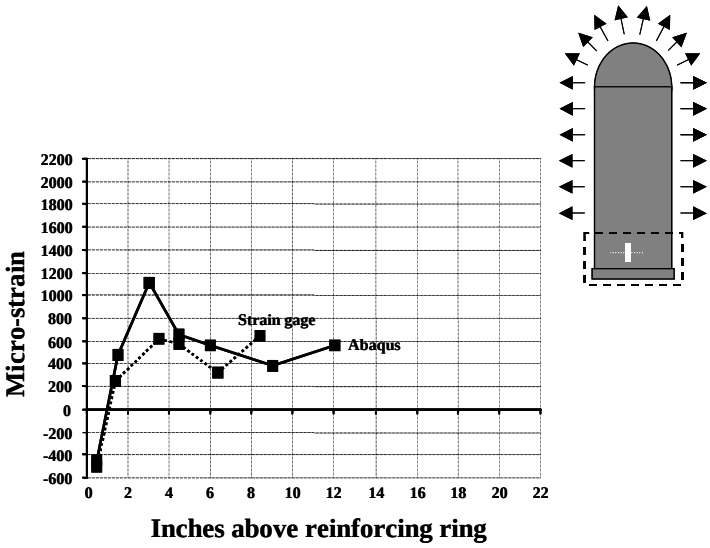

Figure 7.8 – Axial strain near reinforcing ring at bottom of vessel (15 psi superposed pressure)

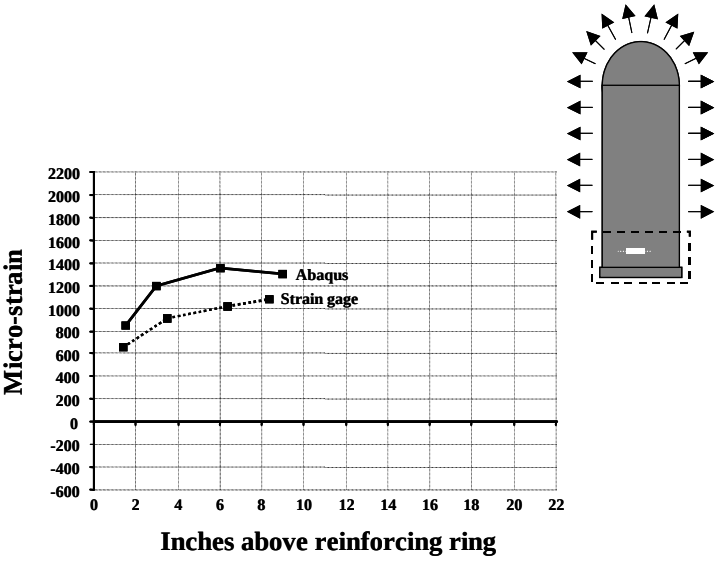

Figure 7.9 – Hoop strain near reinforcing ring at bottom of vessel (15 psi superposed pressure)

7.7 Discontinuity region strains – original manway

7.7.1 Description of finite element models - original manway

A finite element model of the original manway region was developed to predict the strain response in this area. The manway cover was modeled as an integral unit as opposed to modeling each of the bolted connections. The fineness of the mesh was increased near the connection of the flange to the vessel wall due to the large strain gradients in this area. The hold-down locations were taken into account in the model. Symmetry was used to reduce the sized of the model. An overall view of the mesh is shown in Figure 7.10 and a more detailed view is shown in Figure 7.11.

7.7.2 Comparison of strain gage results with finite element model results - original manway

As described in Chapter 6, several strain gages were located in the vicinity of the manway. The experimental strain results are plotted with the finite element model results for 15 psi superposed pressure in Figures 7.12 through 7.17. The measured hoop strain to the right of the manway was much higher than the predicted results (Figure 7.14). this is likely due to a problem with the gage since the gages on the opposite side are in agreement with each other and the finite element model results. The measured hoop strain at the bottom of the manway is much less than the predicted value. This may be due to the approximations made regarding the hold-down system discussed earlier. With these exceptions, reasonable agreement was found between the finite element model and the experimental results.

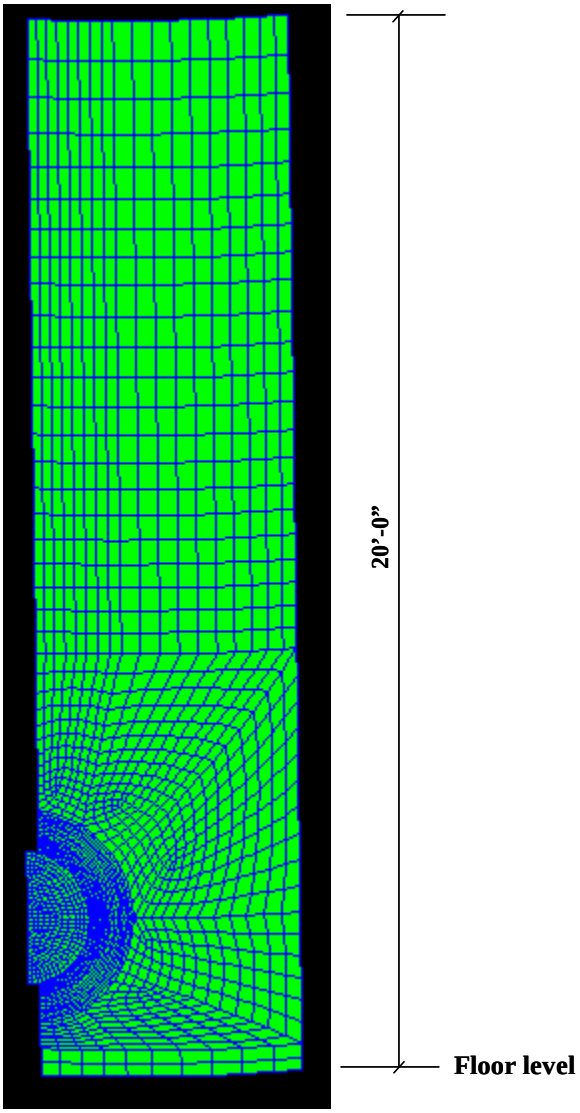

Figure 7.10 – Finite element mesh of original manway (overall view)

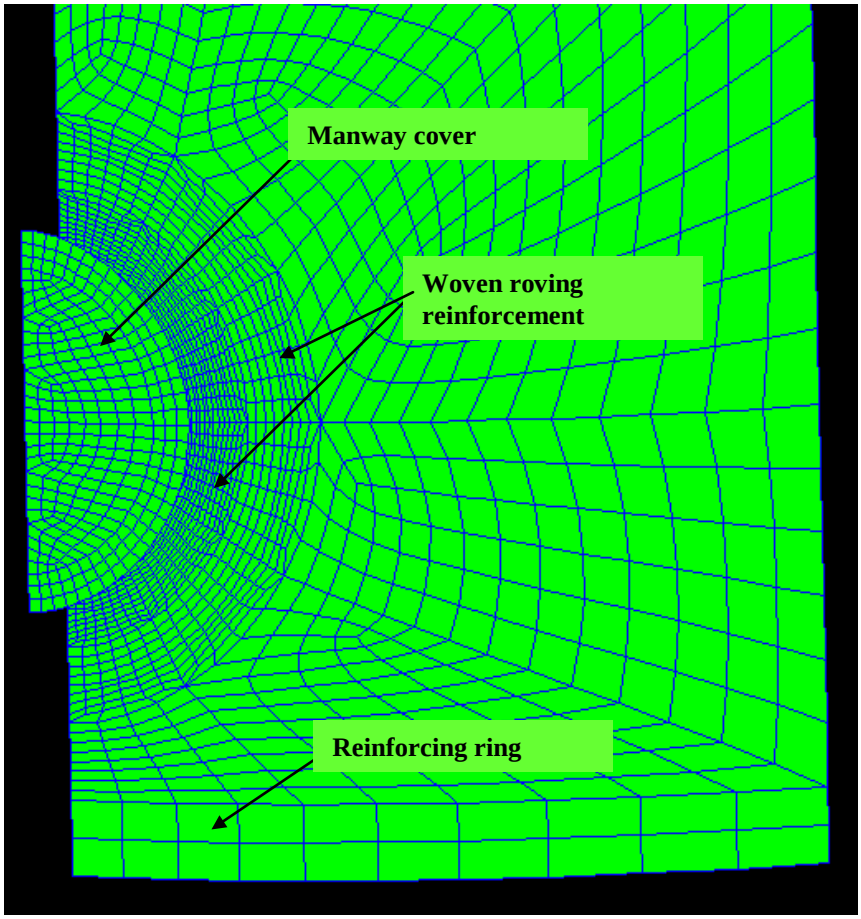

Figure 7.11 – Finite element mesh of original manway (detailed view)

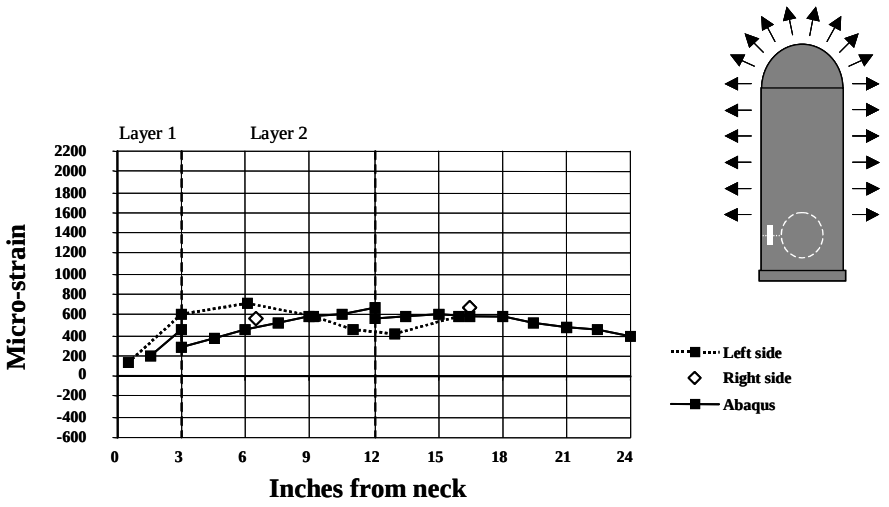

Figure 7.12 – Axial strain to side of original manway (15 psi superposed pressure)

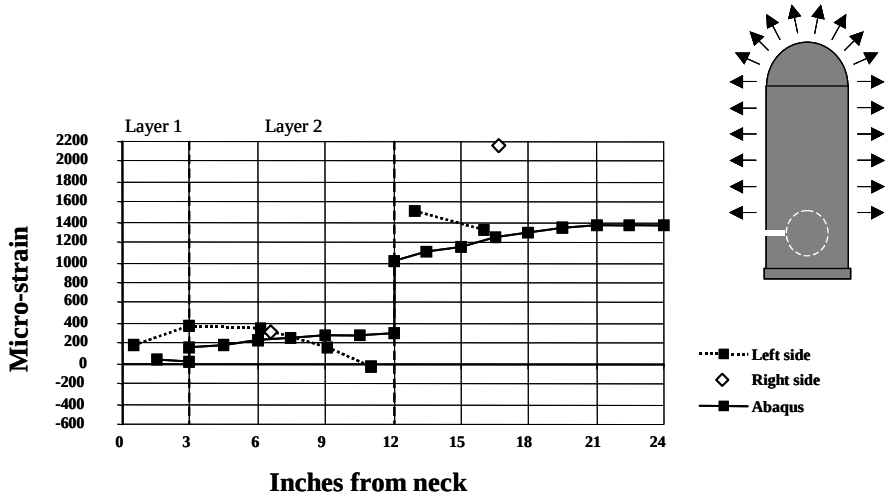

Figure 7.14 – Hoop strain to side of original manway (15 psi superposed pressure)

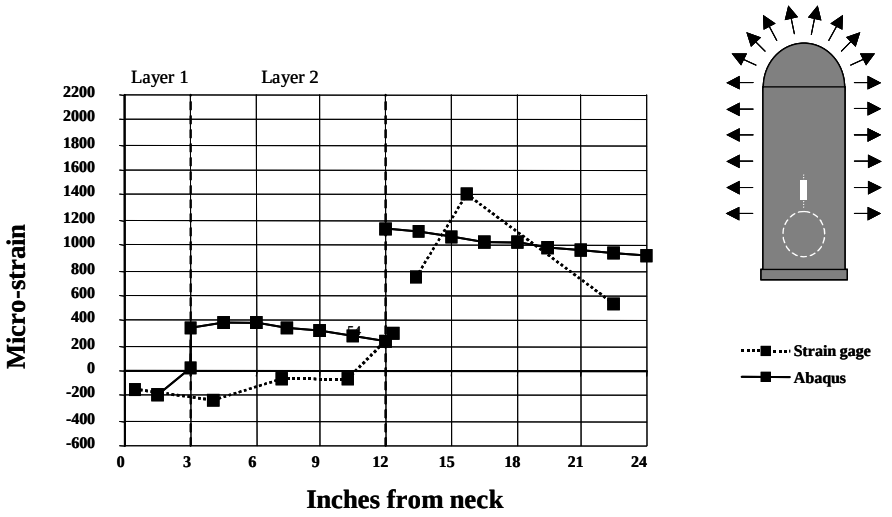

Figure 7.14 – Axial strain above original manway (15 psi superposed pressure)

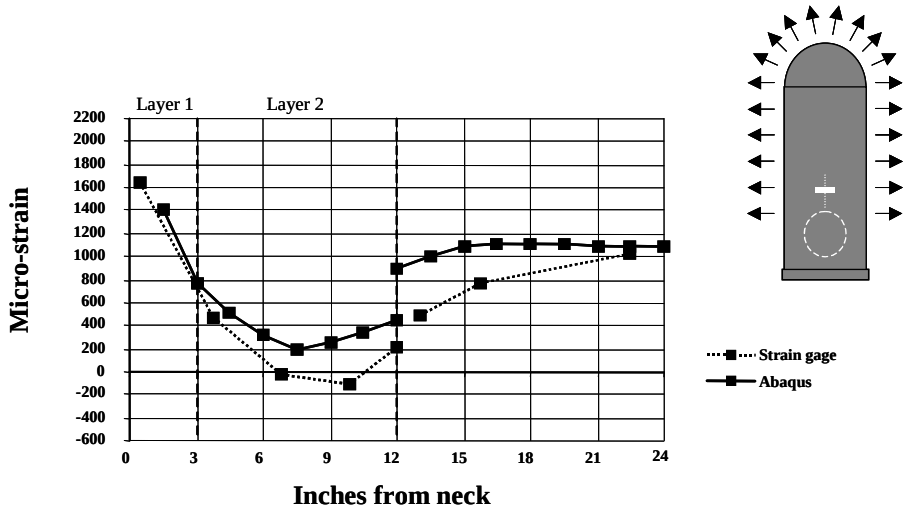

Figure 7.15 – Hoop strain above original manway (15 psi superposed pressure)

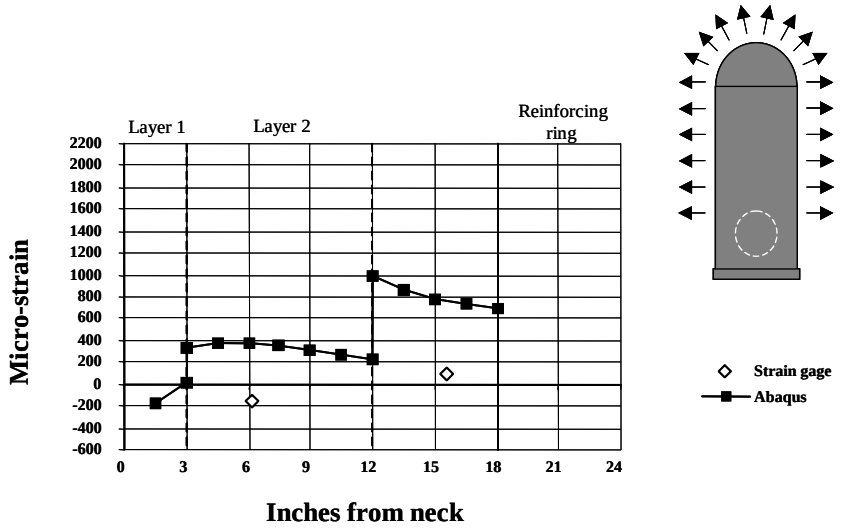

Figure 7.16 – Axial strain below original manway (15 psi superposed pressure)

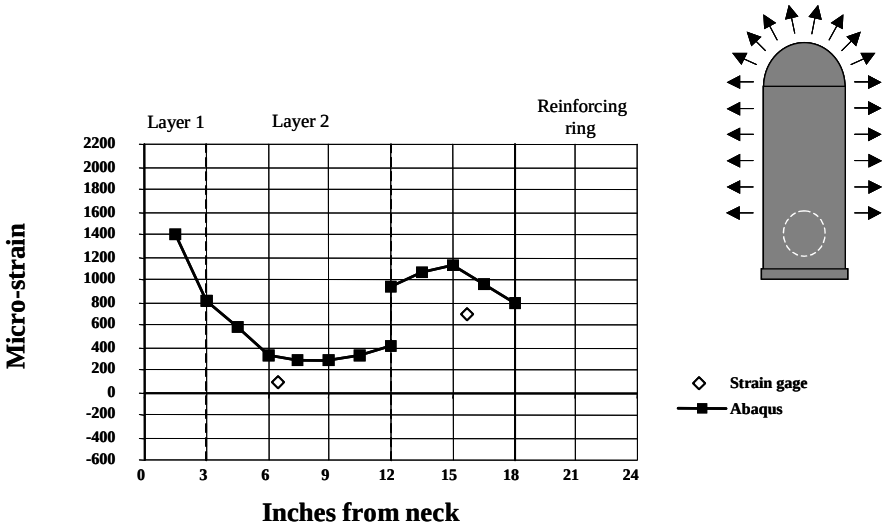

Figure 7.17 – Hoop strain below original manway (15 psi superposed pressure)

7.8 Discontinuity region strains – 3” cone nozzle

7.8.1 Description of finite element model - 3” cone nozzle

A finite element model of the cone nozzle near the bottom of the vessel was developed to predict the strain response in this area. The cover was modeled as an integral unit as opposed to modeling each of the bolted connections. The fineness of the mesh was increased near the connection of the flange to the vessel wall. Symmetry was again used. An overall view of the mesh is shown in Figure 7.18 and a more detailed view is shown in Figure 7.19.

7.8.2 Comparison of strain gage results with finite element model results - 3” cone nozzle

As described in Chapter 6, several strain gages were located in the vicinity of the cone nozzle. The experimental strain results are plotted with the finite element model results for 15 psi superposed pressure in Figures 7.20 through 7.23. The axial strain to the left of the nozzle is over-predicted by the finite element model. With this exception, reasonable agreement was found between the finite element model and the experimental results.

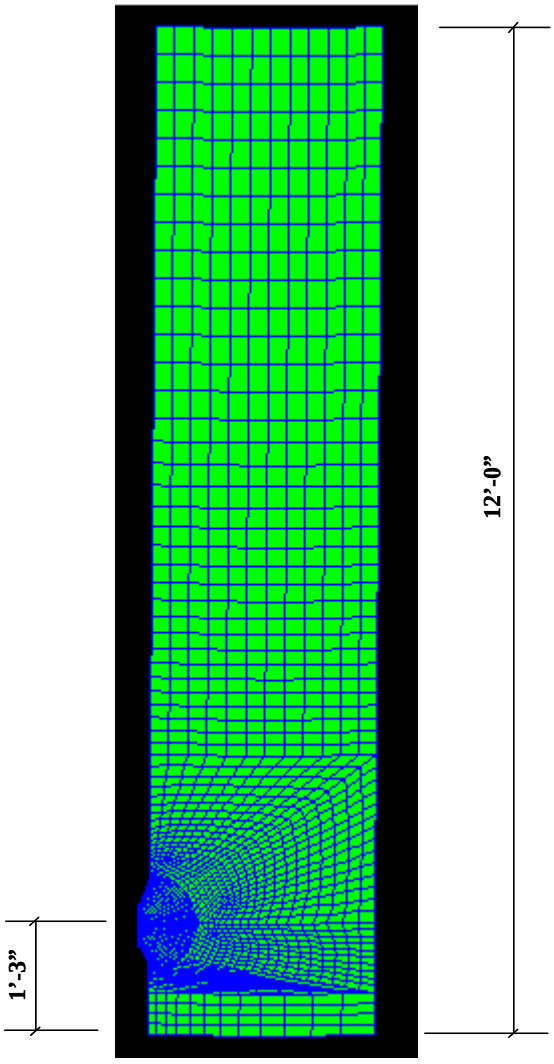

Figure 7.18 – Finite element mesh of 3" cone nozzle (overall view)

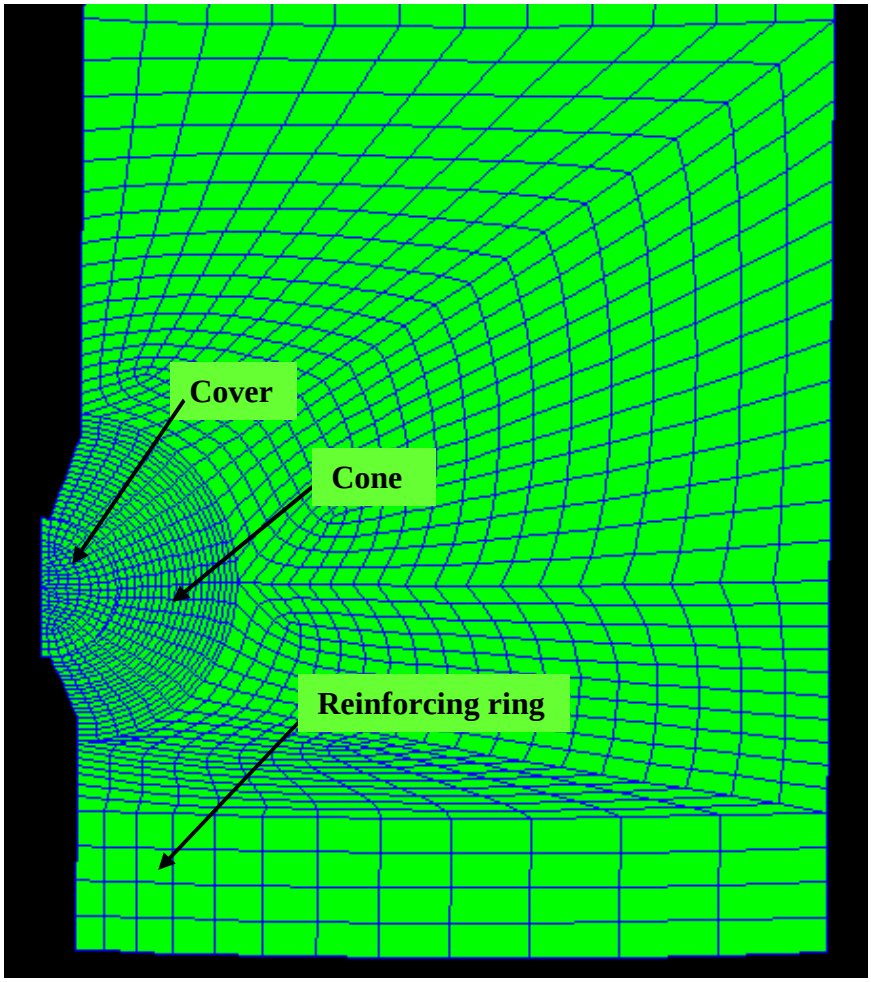

Figure 7.19 – Finite element mesh of 3” cone nozzle (detailed view)

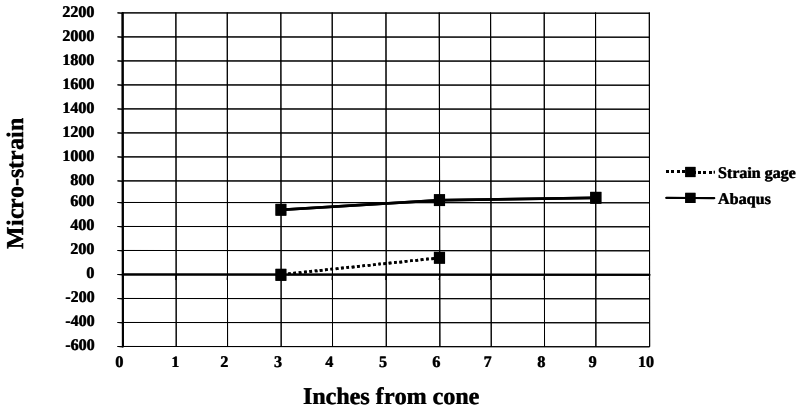

Figure 7.20 – Axial strain to left of 3” cone nozzle (15 psi superposed pressure)

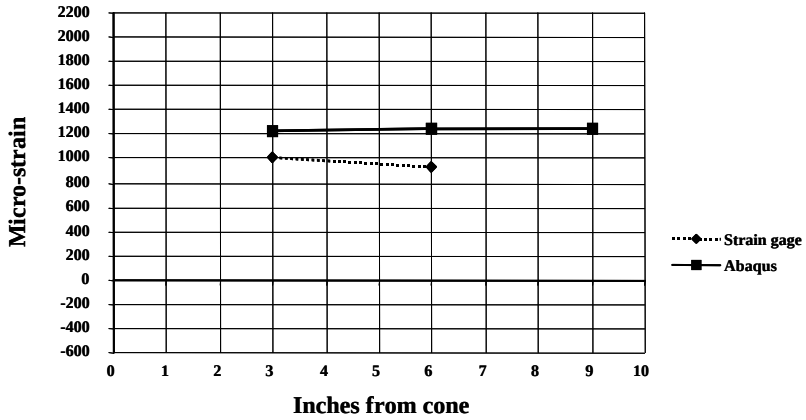

Figure 7.21 – Hoop strain to left of 3” cone nozzle (15 psi superposed pressure)

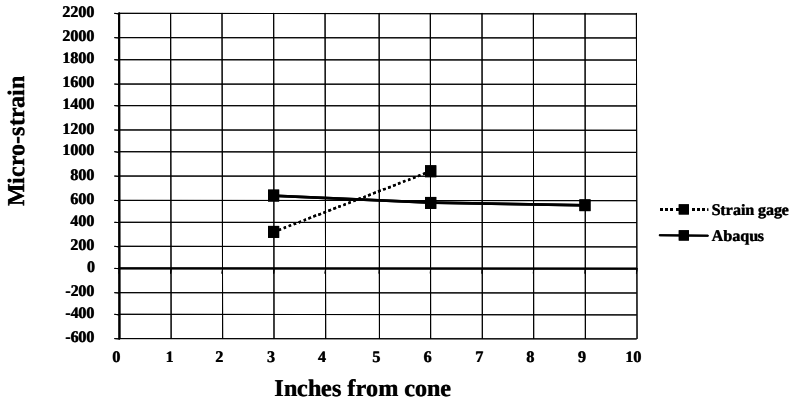

Figure 7.22 – Axial strain above 3” cone nozzle (15 psi superposed pressure)

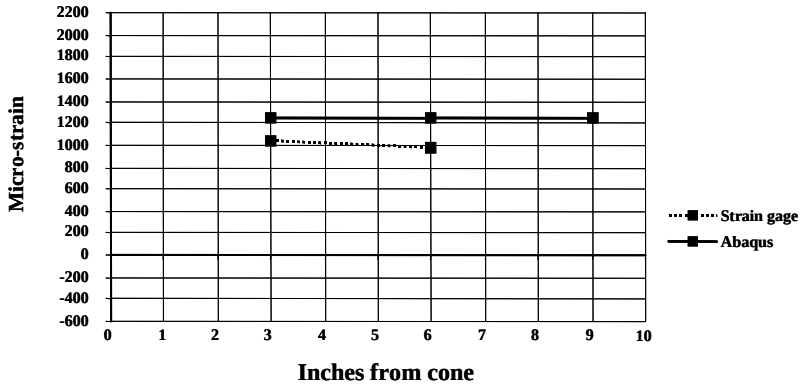

Figure 7.23 – Hoop strain above 3” cone nozzle (15 psi superposed pressure)

7.9 Discontinuity region strains – 4” gusseted nozzle

7.9.1 Description of finite element models - 4” gusseted nozzle

A finite element model of the 4” gusseted nozzle region was developed to predict the strain response in this area. The cover was modeled as an integral unit as opposed to modeling each of the bolted connections. The fineness of the mesh was increased near the connection of the flange to the vessel wall. Symmetry was again used. An overall view of the mesh is shown in Figure 7.24 and a more detailed view is shown in Figure 7.25.

7.9.2 Comparison of strain gage results with finite element model results - 4” gusseted nozzle

As described in Chapter 6, several strain gage rosettes were located on the 4” gusseted nozzle. The strain gages were not located in the area where damage occurred. The strain gages were of the stacked rosette variety and the results were of little use.

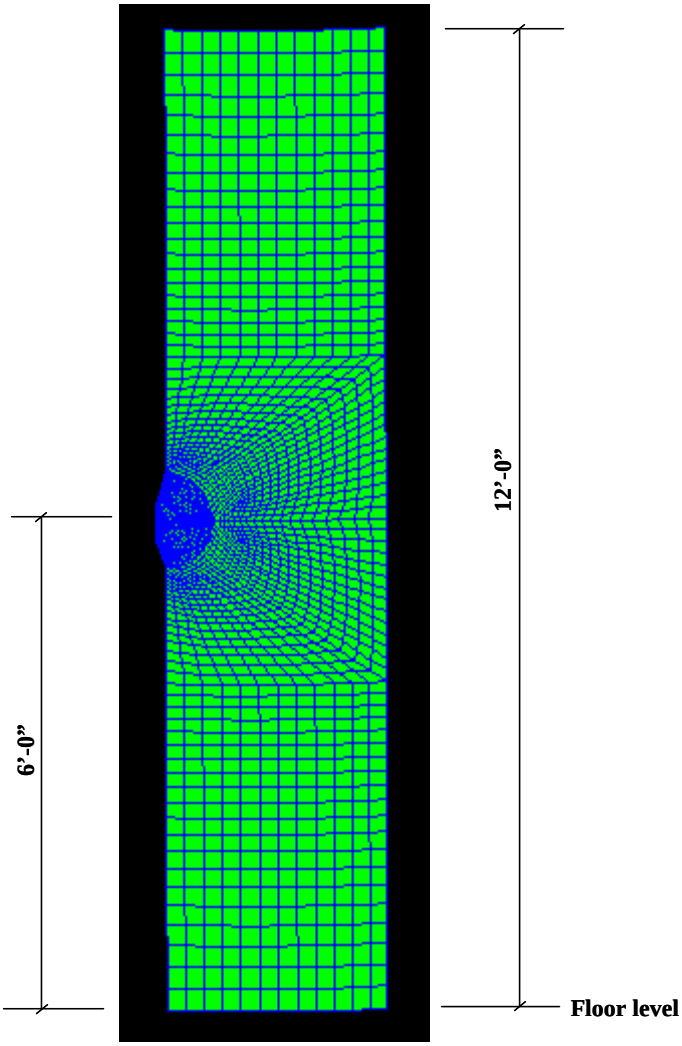

Figure 7.24 – Finite element mesh of 4" gusseted nozzle (overall view)

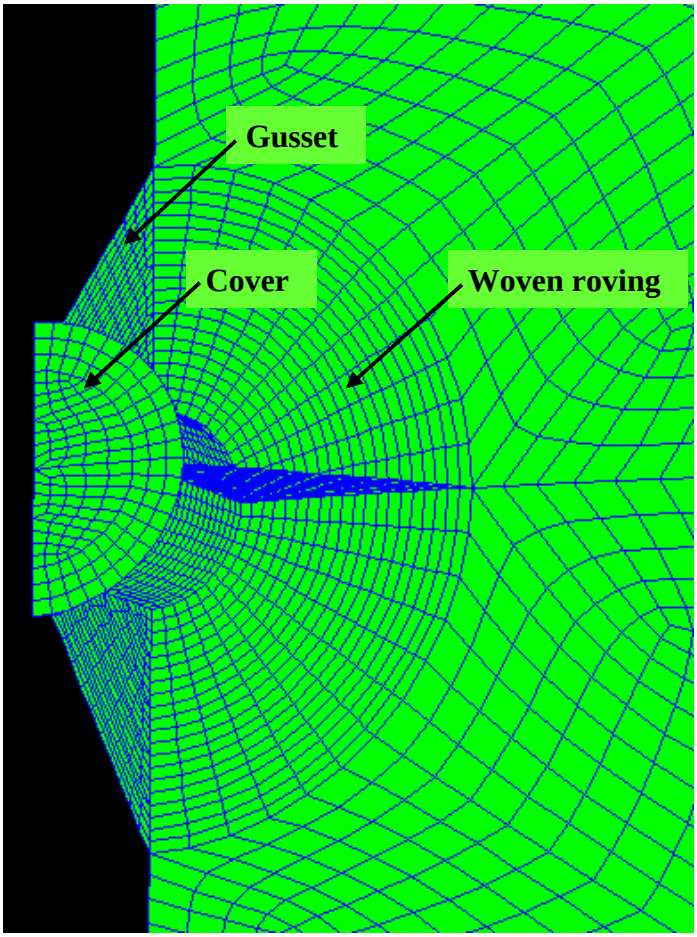

Figure 7.25 – Finite element mesh of 4” gusseted nozzle (detailed view)

7.10 Physical Damage to Original Vessel

The original vessel was loaded to a superposed pressure of 22.0 psi. At this pressure, audible cracking was heard in the vicinity of the 4" gusseted nozzle. Visual inspection revealed that significant cracking had taken place at the connection of the gussets to the vessel body. Photographs of the damage are shown in Figures 7.26 through 7.29. No visual damage was noticed on other portions of the vessel. The test was discontinued due to the damage of the gusseted nozzle.

7.11 Conclusions

Finite element models were developed for the overall vessel and the discontinuity regions. Measured strain gage results were compared to the finite element model predictions. Reasonable agreement was found.

Chapter 8: *Design of Pressure Vessel Modifications*

8.1 Introduction

This chapter addresses the design of the new manway and new 8" diameter nozzle. The design was accomplished with trial and error finite element modeling of the discontinuity region. The Tsai-Wu interaction criterion was modified in the sense that damage values were substituted in place of failure values. The finite element analysis was then conducted with the design goal of reducing the level of critical stress in the region of the discontinuity to the level of critical stress in the vessel wall away from the discontinuity. Knitted fabrics were used in place of the more common woven roving. The resin used for the modifications was Derakane 411-350. This was one of the more flexible resins tested. The installation procedure is described.

8.2 Damage Criterion for Finite Element Models

The objective for the design of the discontinuity regions is to reduce the critical stresses in the area of the discontinuities to the level of stress in the vessel wall. For composites, this is meaningful only in relation to a particular failure criterion (Tsai-Wu, Tsai-Hill, Maximum Stress or Maximum Strain). The Tsai-Wu interaction criterion was chosen for the purposes of checking the critical stresses. As discussed in Chapter 5, the Tsai-Wu interaction criterion predicts failure if the left hand side of the equation exceeds unity. When viewing the results of a finite element analysis in the post processor, a contour plot with the left hand side of the Tsai-Wu criterion as the variable is plotted. When these values exceed unity, failure is predicted. The smaller the values plotted on the contour plot, the lower the level of the critical stresses.

The damage values developed from the acoustic emission testing were substituted for the failure values of the Tsai-Wu failure criteria in Abaqus[8.1]. The development of the damage values is described in Chapters 4 and 5.

Experimental damage values were available for only longitudinal and transverse tension. Experimental values were not available for longitudinal and transverse compression and in-plane shear. For these values, the failure models discussed in Chapter 5 were used to predict a failure value. 40 percent of the predicted failure value was then used as an approximation of when damage would occur. The value of 40 percent was chosen based on observation of when damage generally occurred in the experimental specimens. The interaction parameter F_{xy} was set equal to zero as discussed in Chapter 5.

The vessel wall is constructed with Hetron 922 resin. This resin has similar mechanical properties to Derakane 411-350 (refer to Chapter 3). The design procedure focused on the stresses at the outermost lamina of the vessel wall. This is described in greater detail later in this chapter. Acoustic emission data was not available for specimens constructed with Hetron 922 resin. The acoustic emission results obtained from specimens constructed with Derakane 411-350 were used instead. The calculated damage values are based on Hetron 922 resin.

The values used for the finite element input are as follows:

Damage values based on AE testing (411-350 resin with oriented fibers)

S_{11} + = 46,893 psi

S_{22} + = 7,789 psi

Damage values based on 0.40 * predicted ultimate strength (922 resin with oriented fibers)

S_{11} - = 138,176 psi

S_{22} - = 6,332 psi

S_{12} = 3,120 psi

F_{12} = 0

With these damage values substituted for the failure values in the Tsai-Wu criterion, the resulting contour plots are relevant to damage as opposed to failure.

Hetron 922 and Derakane 411-350 resins have very similar mechanical properties. No acoustic emission testing was performed on coupon specimens made with Hetron 922. Due to the similarity of the mechanical properties, Derakane 411-350 and Hetron 922 are assumed to be interchangeable. Derakane 411-350 was used for the modifications to the vessel. Hetron 922 is the resin used to construct the original vessel wall.

8.3 Selection of New Discontinuity Regions

As described in previous chapters, the original vessel contains several discontinuity regions. These include the top head-to-shell and shell-to-reinforcing ring attachments as well as the 4" diameter gusseted nozzle, the 3" diameter cone nozzles and the 24" diameter manway. Time and expense did not allow for experimental modification and testing of all of the discontinuity regions. It was decided to focus on the nozzles and manway since these are common elements that are relatively easy to install. The 4" gusseted nozzle that had failed at the flange-to-shell connections was removed and an 8" diameter nozzle was installed in its place. A new 24" diameter manway was installed opposite the existing manway. These sizes were chosen because they are structurally significant and readily available.

8.4 Design of New Manway and New 8" Nozzle

8.4.1 Selection of resin

As described in Chapter 4, the more flexible resins (Derakane 8084 and 411-350) showed better performance than the more brittle resins (General ISO, Derakane 470 and Ashland 197) for tensile loading transverse to the fibers. This is generally the initial

failure mode for composites, and therefore it is advantageous to select a resin that can accommodate large strains in this direction. Also, as described in Chapter 4 all resins exhibited similar behavior in longitudinal tension. The 8084 resin was somewhat better than the 411-350 in transverse tension, but the 411-350 was preferred by the person doing the fabrication and was readily available. Therefore, 411-350 was used as the resin for both the new manway and the new 8" diameter nozzle.

8.4.2 Selection of reinforcement

As described in Chapter 4, the woven roving reinforcement that is typically used to reinforce vessels is acoustically "noisy". This is due to the entrapped voids between the fiber bundles. It is also significantly less stiff (approximately 12 %) than the knitted fabrics due to the fact that the fibers are not oriented in an initially straight geometry. Another complication with woven roving is that the designer is limited to only the 0/90 degree orientation. This orientation can be skewed to any angle, but the practicality of cutting the material tends to favor the 0/90 degree orientation. However, if strength and stiffness are desired in one direction only, then 50% of the fabric is oriented in the wrong direction. Knitted fabrics do not have these drawbacks and therefore were chosen as the reinforcing material for the new 8" nozzle and manway.

Four types of knitted fabric were used: uniaxial (0 degree), biaxial (0/90 degree), biaxial (+45/-45 degree) and triaxial (+45/90/-45 degree). The uniaxial fabric is particularly useful when strength and stiffness in primarily one direction are desired. The biaxial fabric is useful when stiffness is desired in two orthogonal directions. The tri-axial fabric is useful when nearly isotropic properties are desired and drapability is an issue (such as in the neck-to-shell connections). The selection of the fabrics and installation are described in greater detail later in this chapter.

8.4.3 Stiffness properties of knitted fabric

The stiffness properties for a lamina with knitted reinforcing fabric and Derakane 411-350 resin are as follows. These values were calculated with Trilam[8.2]:

0-degree unidirectional fabric (24 oz./sq. yard, 50% fiber by weight)

E_{11} = 3,489,421 psi

E_{22} = 1,028,978 psi

ν_{12} = 0.32

G_{12} = 324,454 psi

0/90 degree biaxial knitted fabric (24 oz./sq. yard, 50% fiber by weight)

E_{11} = 1,762,688 psi

E_{22} = 1,762,688 psi

ν_{12} = 0.15

G_{12} = 324,454 psi

+45/-45 degree biaxial knitted fabric (24 oz./sq. yard, 50% fiber by weight)

E_{11} = 968,744 psi

E_{22} = 968,744 psi

ν_{12} = 0.52

G_{12} = 751,750 psi

+45/90/-45 degree triaxial knitted fabric (24 oz./sq. yard, 50% fiber by weight)

E_{11} = 1,072,381 psi

E_{22} = 1,820,180 psi

ν_{12} = 0.26

G_{12} = 593,124 psi

As was the case for the analysis of the original manway, a lamina of random mat is provided for each lamina or reinforcing fabric. The uniaxial fabric and both biaxial fabrics were manufactured with random mat sewn to the back. This made installation less time consuming.

The stiffness properties of the reinforcing fabric combined with the random mat are as follows:

0-degree uniaxial knitted fabric combined with 0.75 oz./sq. ft. random mat, top and bottom

E_{11} = 2,279,497 psi

E_{22} = 1,108,387 psi

ν_{12} = 0.33

G_{12} = 373,969 psi

0/90 degree biaxial knitted fabric combined with 0.75 oz./sq. ft. random mat, top and bottom

E_{11} = 1,705,951 psi

E_{22} = 1,705,951 psi

ν_{12} = 0.21

G_{12} = 373,969 psi

+45/-45 degree biaxial fabric combined with 0.75 oz./sq. ft. random mat, top and bottom

E_{11} = 980,332 psi

E_{22} = 980,332 psi

ν_{12} = 0.52

G_{12} = 755,247 psi

+45/90/-45 degree knitted fabric combined with 0.75 oz./sq. ft. random mat, top and bottom (two laminates)

E_{11} = 1,417,127 psi

E_{22} = 1,417,127 psi

ν_{12} = 0.34

G_{12} = 545,537 psi

8.4.4 Design of reinforcement pattern and quantities

In the manway region the hoop stress is much higher than the axial stress. For the case of a pressure vessel with internal pressure the well known relationships for axial and hoop membrane stress are as follows:

$$\text{Axial Stress} = \frac{P * r}{2 * t}$$

$$\text{Hoop Stress} = \frac{P * r}{t}$$

where:

P = Internal Pressure

r = radius of vessel

t = wall thickness

From these relationships it can be seen that the hoop stress is twice that of the axial stress for the simplified case of internal pressure only. The actual vessel is also subjected to hydrostatic loading. The membrane stress for a vertical cylindrical pressure vessel due to this loading is as follows:

Axial Stress = 0

Hoop Stress at any height of vessel = $\frac{\left[\ \rho * g * \left(H - H'\right)\ \right] * r}{t}$

where:

ρ = density of water

g = acceleration of gravity

H = height of water

H' = height of interest for determining stress

From these relationships it can be seen that the hoop stress will always be more than twice that of the axial stress for a pressure vessel of this type. The fibers in the filament wound portion of the vessel are oriented at an angle of +15/-15 degrees to the horizontal to accommodate these large hoop stresses.

If a finite element analysis is run with no additional reinforcing in the vicinity of the manway, the opening will distort into an oval shape with a greater increase in the hoop direction than in the axial direction (Figure 8.1). This deformation causes localized bending to occur in the vicinity of the manway opening. The vessel shell does not have equal strength in all directions, and it is particularly weak when subjected to tensile

stresses in the axial direction. It is also weak when subjected to compressive stresses in the axial direction.

When a damage analysis of the manway region with no reinforcement is conducted, the areas of critical stress concentration can be clearly seen (Figure 8.2). This contour plot is generated for the outermost lamina of the vessel wall. All finite element analyses discussed were conducted with a superposed pressure of 15.0 psi. This is the design pressure of the original vessel. The scale on the contour plot is set to a maximum of 1.0. As described in Section 8.1, values above 1.0 indicate that critical damage is predicted. Decreasing values of the contour plot correspond to less damage. Critical damage in this case does not correspond to failure, but rather to the onset of damage as determined experimentally with acoustic emission.

An analysis of the original manway with the original woven roving reinforcing pattern as described in Chapter 6 was also conducted. The results of this analysis also indicate areas of increased stress relative to the wall of the vessel away from the discontinuity region (Figure 8.3). As was the case for the analysis with no reinforcing, this contour plot is generated for the outermost lamina of the vessel wall. The critical stresses are reduced greatly from the case with no reinforcing in the discontinuity region, but still are not in the range of the vessel wall away from the discontinuity.

Due to the weakness of the vessel in the axial direction, it would seem that a reasonable approach to reinforcing the manway area would be to provide additional strength in this direction. Also, if the opening were to deform in a more uniform shape (circular as opposed to oval) the localized bending stresses would be reduced. This suggests both more reinforcement in general and more reinforcement in the axial direction.

Finite element analyses were conducted with a trial and error approach. The need for additional reinforcement in general and additional reinforcement in the axial direction led to the final design. As more reinforcing was added to the manway area, the stress concentration appeared to increase near the edges of the reinforcing pad. This was

particularly true above and below the manway. Therefore, additional reinforcement was provided in these areas. This led to the unconventional diamond shape that can be seen in a photograph of the new manway and new 8" nozzle (Figure 8.4). The layup sequences for the new manway are shown in Figures 8.5 through 8.10. A photograph of the new manway taken from the interior of the vessel is shown in Figure 8.11. The layup sequences for the new 8" nozzle are shown in Figures 8.12 through 8.15. A photograph of the new 8" diameter nozzle taken from the interior of the vessel is shown in Figure 8.16. As can be seen in the figures, the reinforcing for both the new manway and new 8" nozzle was diamond shaped. The diamond shape was not continued below the manway due to interference from the hold-down system. Rather, additional reinforcing was added to the inside of the vessel wall in this area.

The finite element meshes for the new manway and new 8" nozzle are shown in Figures 8.17 and 8.18. The deformed shape of the original manway and the installed manway are shown in Figures 8.19 and 8.20 with the displacement magnified 50 times. A damage analysis was run of the installed manway and 8" nozzle. The results for the new manway are shown in Figures 8.21 and 8.22. The results for the new 8" nozzle are shown on Figures 8.23 and 8.24. These analyses show the stresses in the discontinuity regions to be generally the same level of stress as those in the vessel wall (between 0.182 and 0.273 on the damage contour plot). It should be remembered that this is a contour plot for damage as opposed to failure. As described earlier, damage is predicted for values of 1.0 and above on the damage contour plot. Lower values indicate less likelihood of damage.

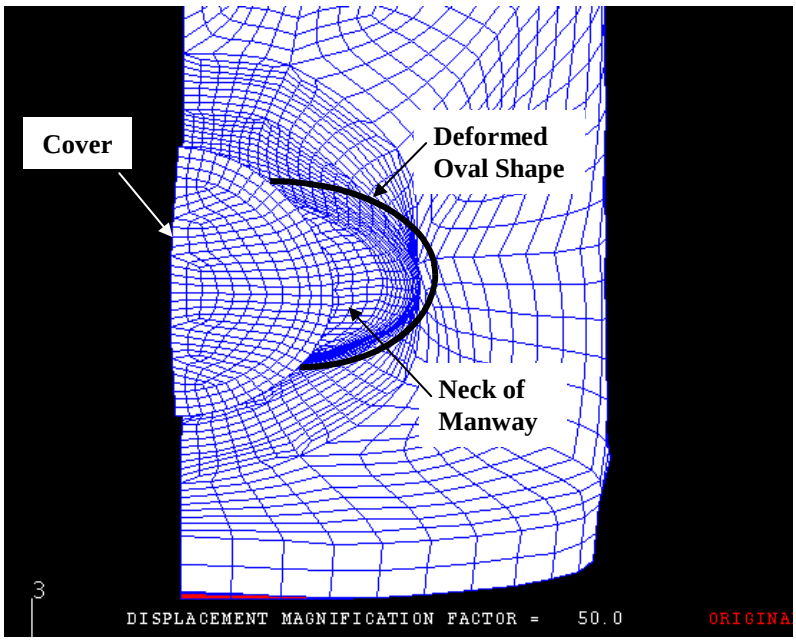

Figure 8.1 – Displaced shape (50 x) of unreinforced manway, 15 psi superposed pressure

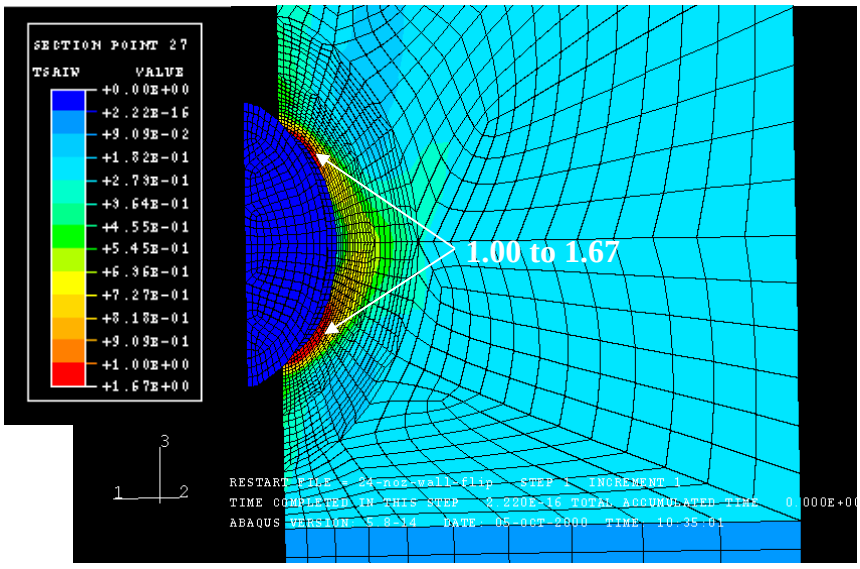

Figure 8.2 – Damage analysis of unreinforced manway, 15 psi superposed pressure

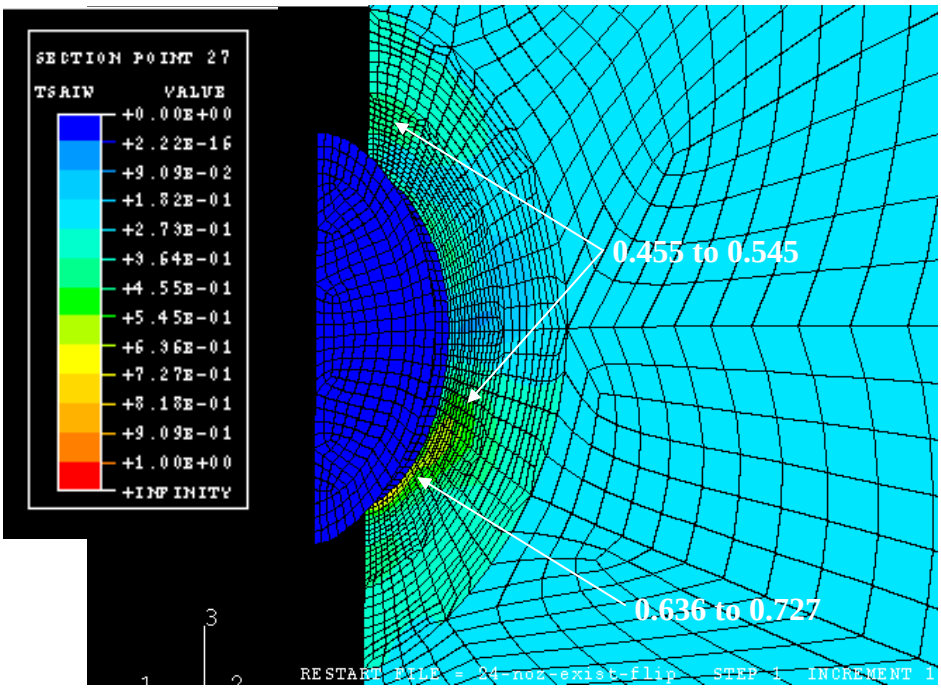

Figure 8.3 – Damage analysis of original manway,
15 psi superposed pressure

Figure 8.4 – Photograph of new manway and new 8”nozzle (exterior of vessel)

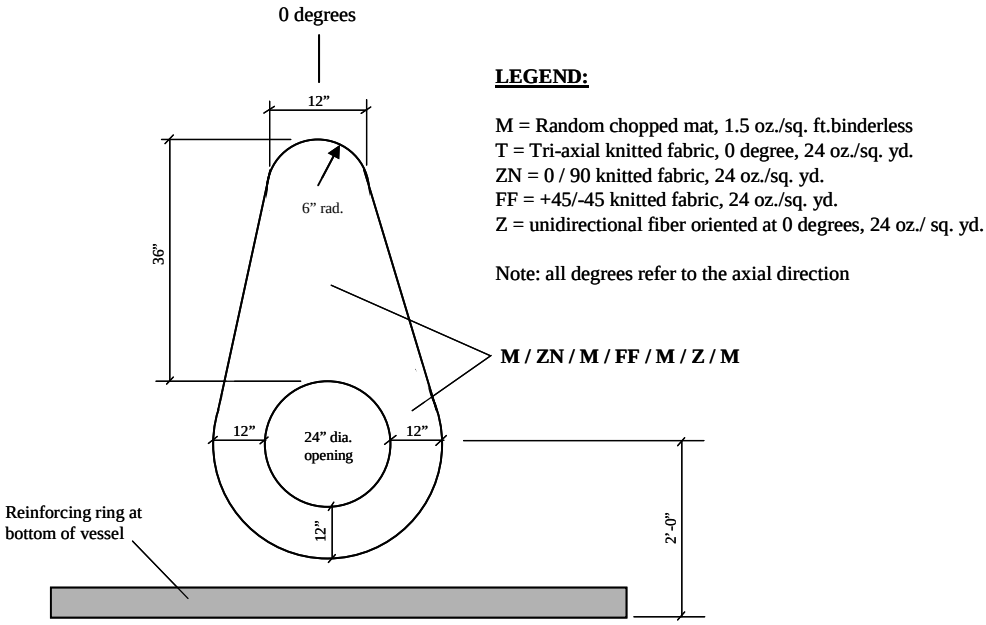

Figure 8.5 – New manway reinforcement – Layer 1 (exterior of vessel)

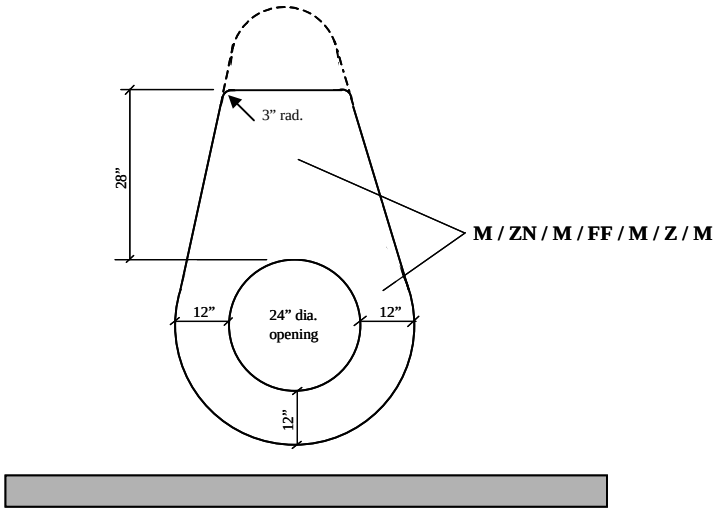

Figure 8.6 – New manway reinforcement – Layer 2 (exterior of vessel)

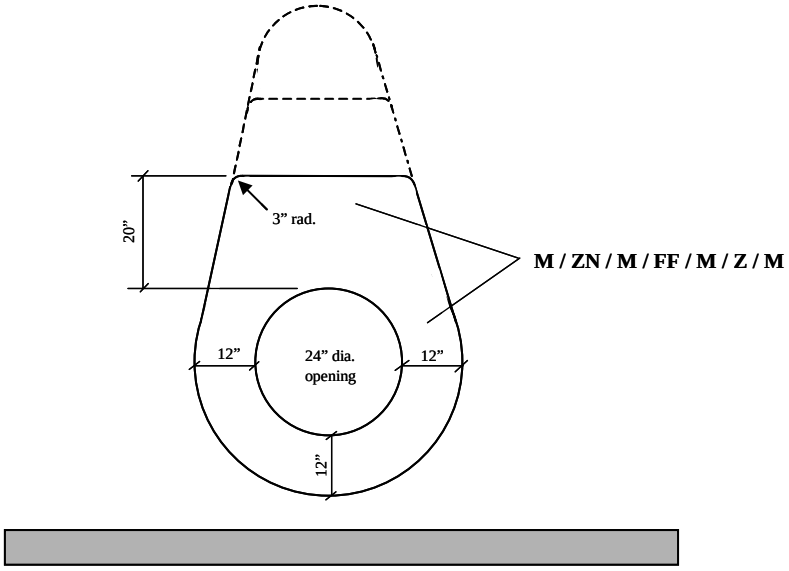

Figure 8.7 – New manway reinforcement - Layer 3 (exterior of vessel)

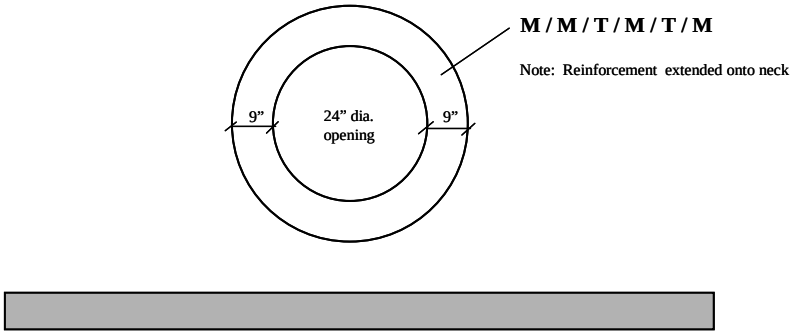

Figure 8.8 – New manway reinforcement - Layer 4 (exterior of vessel)

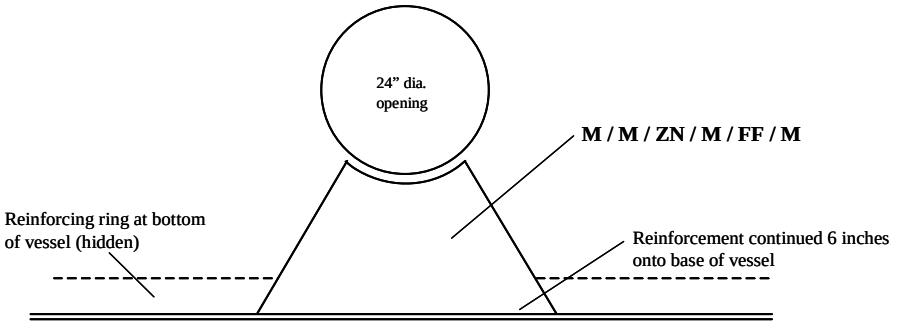

Figure 8.9 – New manway reinforcement – Layer 1 (interior of vessel)

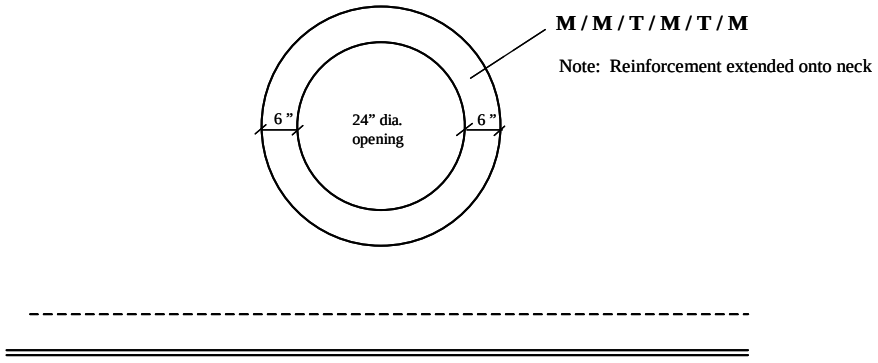

Figure 8.10 – New manway reinforcement - Layer 2 (interior of vessel)

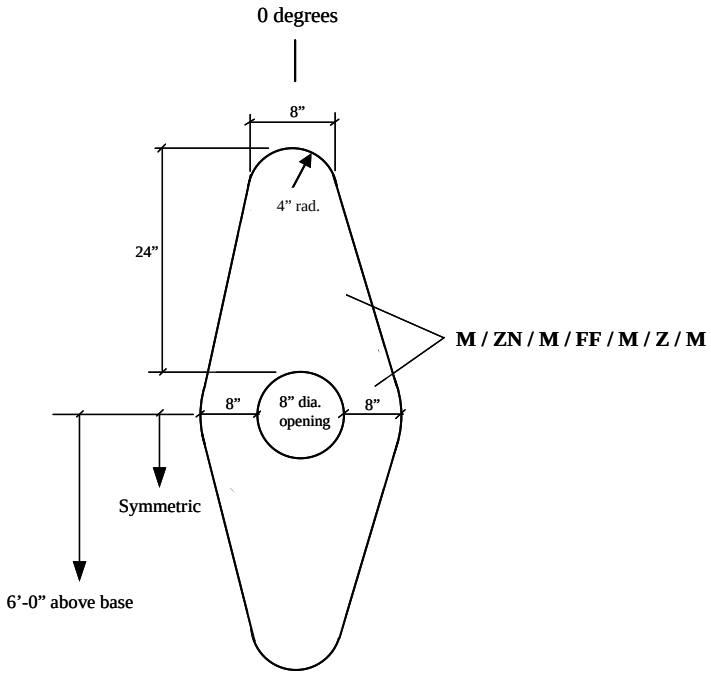

Figure 8.12 – New 8” nozzle reinforcement – Layer 1 (exterior of vessel)

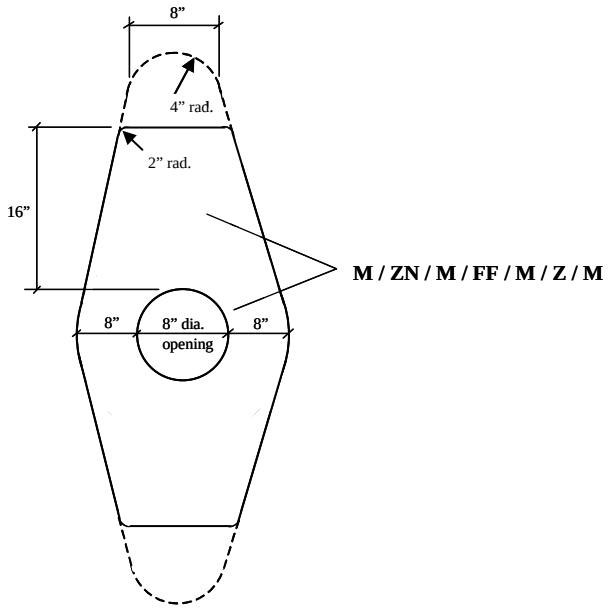

Figure 8.13 – New 8” nozzle reinforcement – Layer 2 (exterior of vessel)

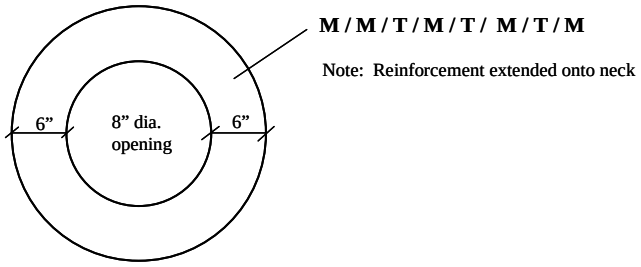

Figure 8.14 – New 8” nozzle reinforcement – Layer 3 (exterior of vessel)

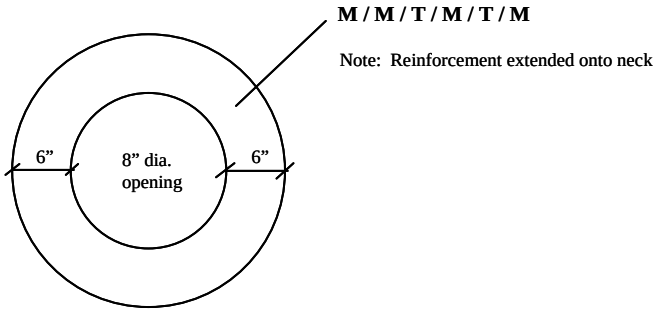

Figure 8.15 – New 8” nozzle reinforcement - Layer 1 (interior of vessel)

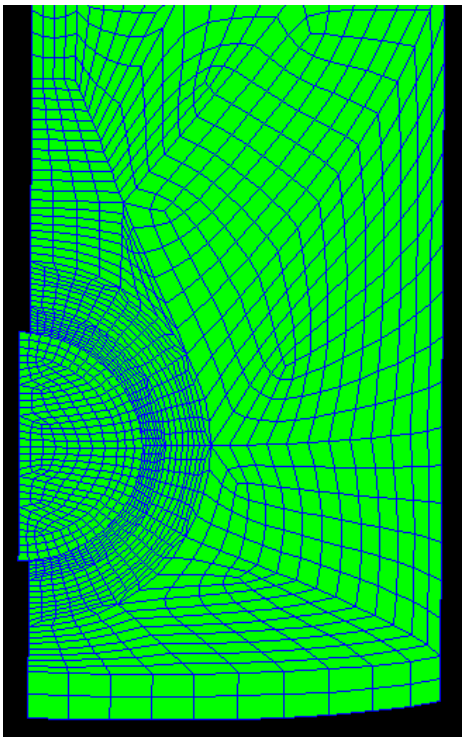

Figure 8.17 – Finite element mesh for new manway

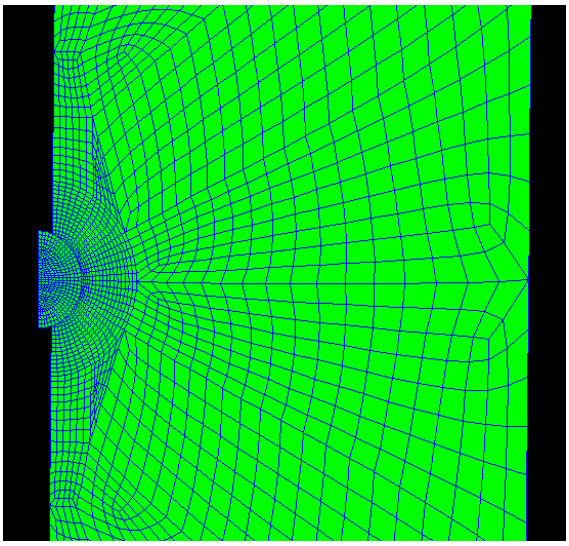

Figure 8.18 – Finite element mesh for new 8” nozzle

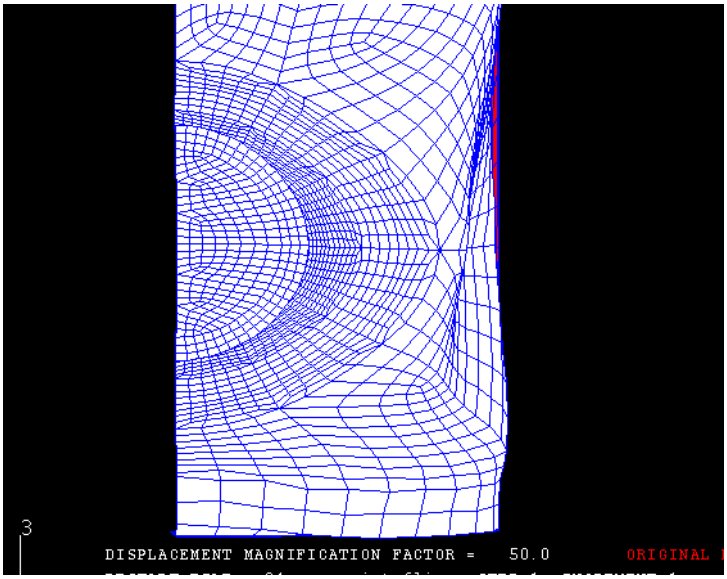

Figure 8.19 – Displaced shape (50 x) of original manway, 15 psi superposed pressure

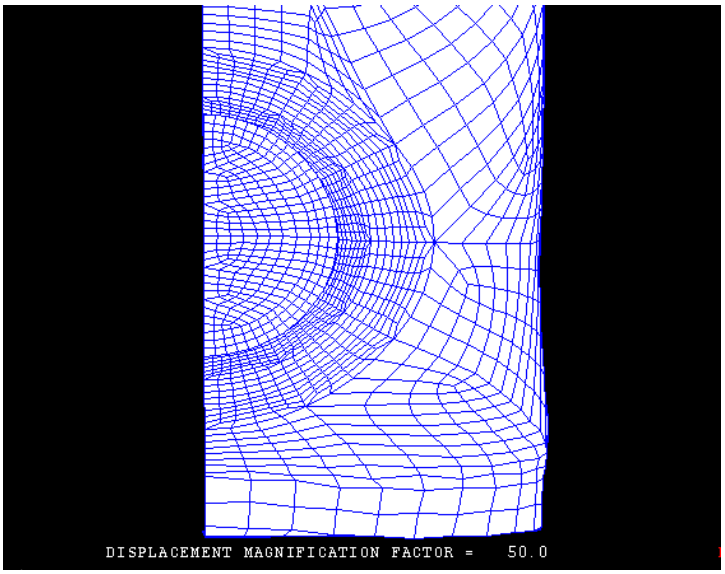

Figure 8.20 – Displaced shape (50 x) of new manway, 15 psi superposed pressure

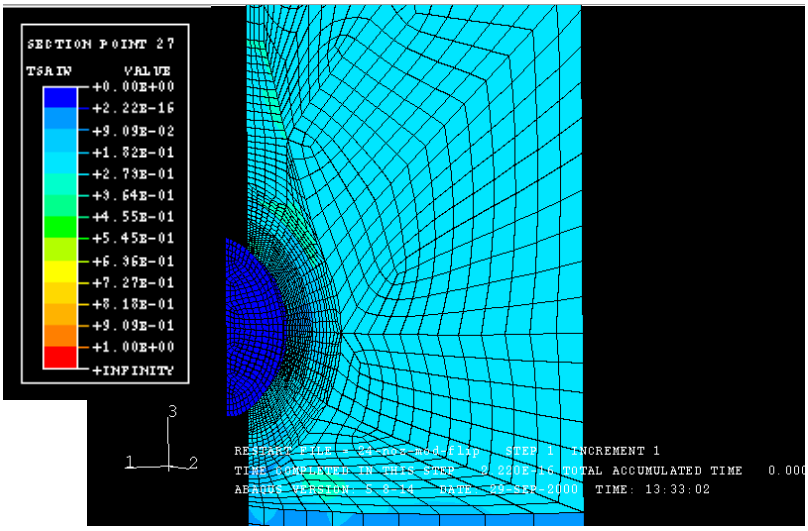

Figure 8.21 – Damage analysis of new manway, 15 psi superposed pressure

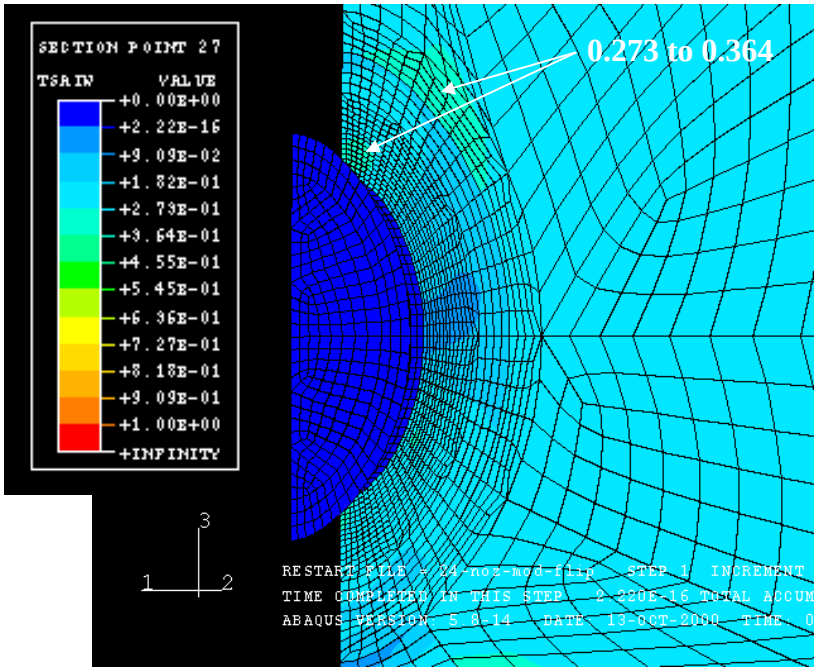

Figure 8.22 – Damage analysis of new manway, 15 psi superposed pressure

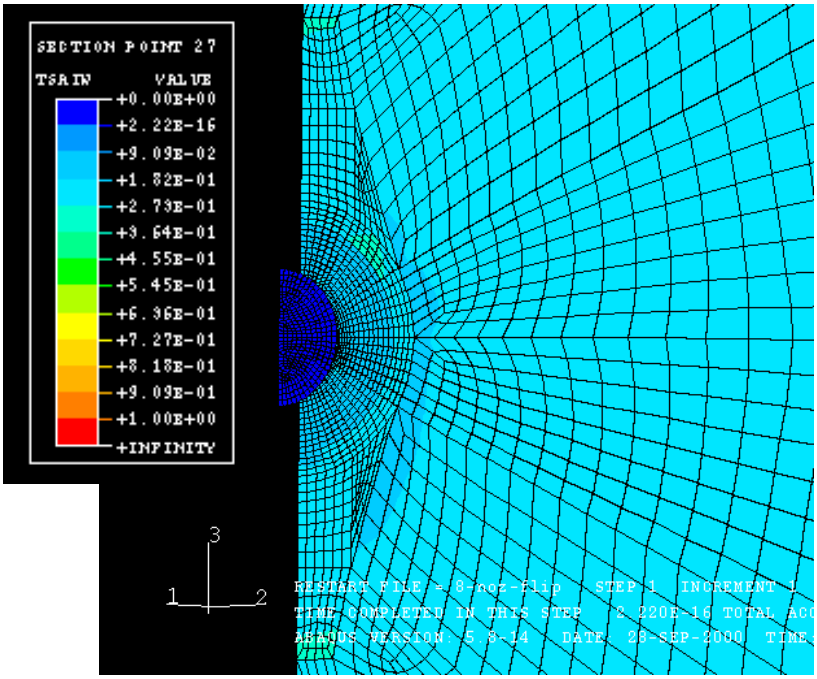

Figure 8.23 – Damage analysis of new 8” nozzle
15 psi superposed pressure

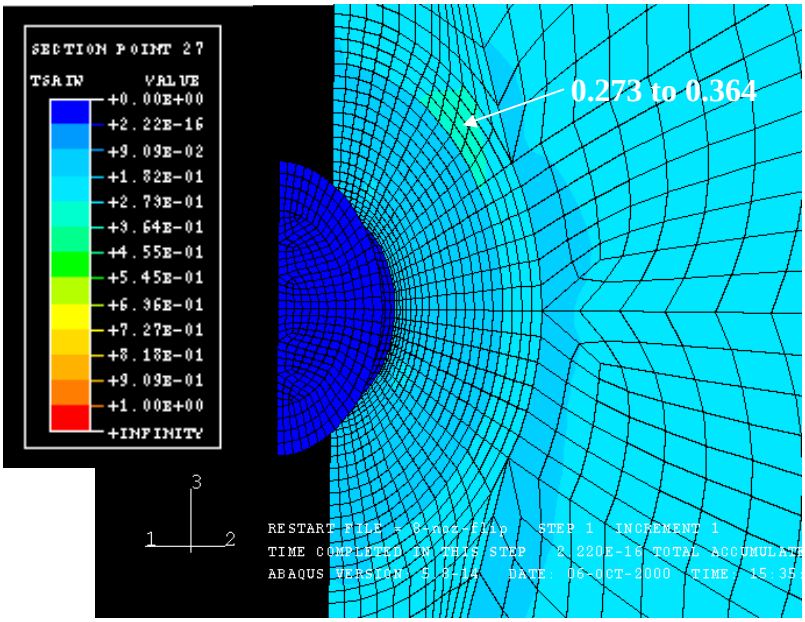

Figure 8.24 – Damage analysis of new 8” nozzle,
15 psi superposed pressure

8.5 Procedure for Installation of New Manway and New 8” Nozzle

The new manway and new 8” nozzle were installed using the following procedure.

1. Mark opening to be cut on vessel and layout reinforcing pattern (Figure 8.25)
2. Cut opening in vessel with hand held saw (Figure 8.26).
3. Grind surface of vessel to remove waxy coating (Figure 8.27 through 8.29).
3. Cut reinforcing fabric to appropriate dimensions (Figure 8.30).
4. Cut random mat reinforcing to appropriate dimensions.
5. Prepare resin by combining with the appropriate amount of catalyst.
6. Apply resin to each lamina of reinforcement and random mat (Figure 8.31). Depending on the area of the reinforcement about 3 laminas of reinforcement, random mat and resin can be applied at one time.
7. Wet-out the combined resin / reinforcement with a metal roller. This is done after all three laminas of reinforcement and three laminas of random mat are combined into a single layer. This is important to remove the entrapped air voids in the resin. Steps six and seven should be done on a clean surface.
8. Apply the resin / reinforcement combination to the wall of the vessel (Figure 8.32). Again, wet-out the resin / reinforcement combination with a metal roller to remove entrapped voids.
9. Allow to exotherm. This generally takes 2 to 3 hours. Once the exotherm has ended, another layer of resin / reinforcement can be applied.
10. Repeat as often as necessary to build-up the desired base thickness (Figure 8.33).
11. Mix resin with chopped fiber to make a putty-like mixture (Figure 8.34). Attach nozzle and manway to vessel with putty.
12. Prepare exterior surface by grinding and applying a coating of resin. Apply desired reinforcement to neck of nozzle and manway (Figures 8.35 and 8.36).

One difficulty that arises during the installation is the critical nature of the timing. It is difficult to accomplish the wet-out of multiple layers of reinforcement prior to the beginning of the exotherm process. If the wet-out takes too long, it becomes increasingly difficult to remove the air voids. Therefore, it is important to use fabric sizes that are easily handled and proceed with the installation as quickly as possible after the catalyst has been added to the resin.

8.6 Simplified Design of New Manway and New 8” Nozzle

After inspection of strain gage data obtained during the pressure test of the modified vessel it was determined that a simpler geometry could be used that would still reduce the critical stresses to an acceptable level near the discontinuity regions. The information from the strain gage data was used to refine the finite element models and the analysis was conducted again with only the circular portion of the reinforcing around the manway and the 8” nozzle. The meshes for this hypothetical case are shown in Figures 8.37 and 8.38. This analysis indicated that additional reinforcing beyond the circular pattern would be required only below the new manway (Figure 8.39). The analysis was then run with additional internal reinforcing below the new manway. This modification served to diminish the stresses below the manway to an acceptable level (Figure 8.40). The displaced shape of this simplified configuration is shown in Figure 8.41. No additional reinforcing beyond the circular pattern was required for the new 8” nozzle (Figure 8.42). These changes affect only the geometry of the reinforcing pattern. The amount, sequence and orientation of the reinforcement remain unchanged. The resin type is also unchanged.

The layup sequences for the simplified new manway reinforcement pattern are shown in Figures 8.43 through 8.48. The layup sequences for the simplified new 8” nozzle design are shown in Figures 8.49 through 8.52.

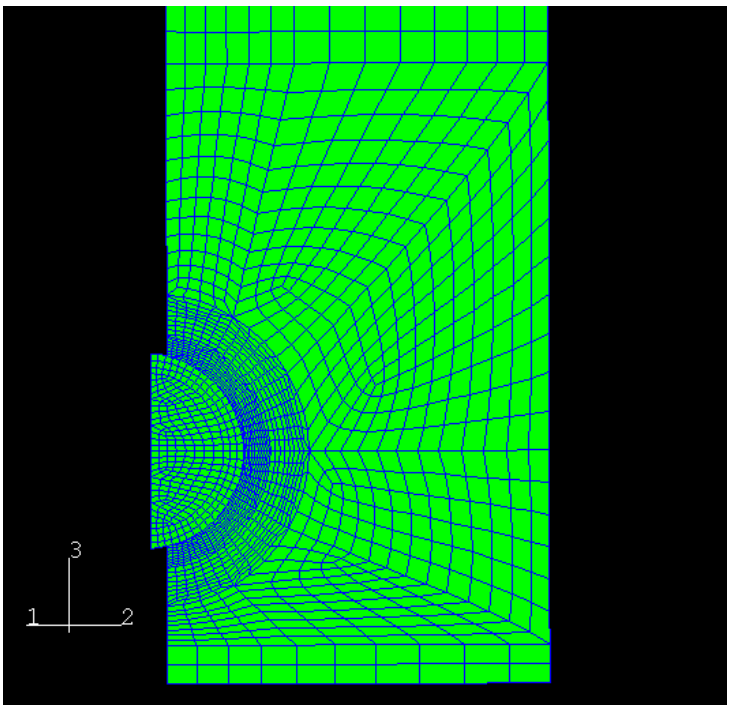

Figure 8.37 – Mesh for simplified manway design

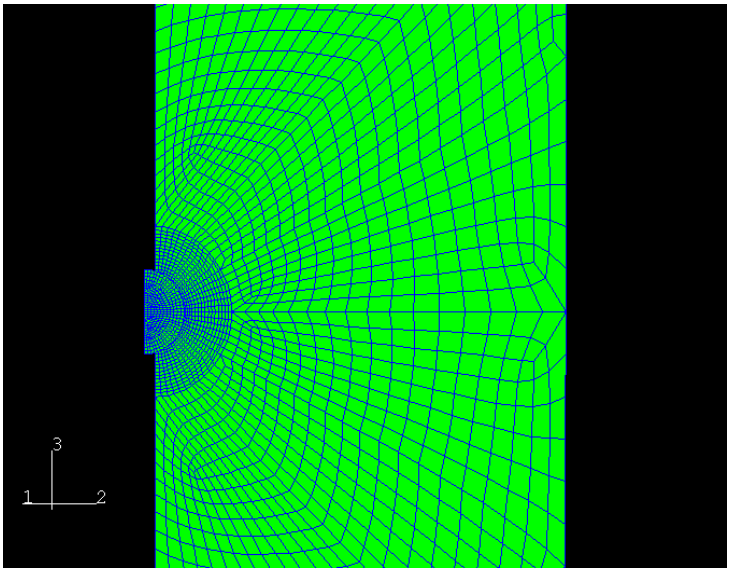

Figure 8.38 – Mesh for simplified 8” nozzle design

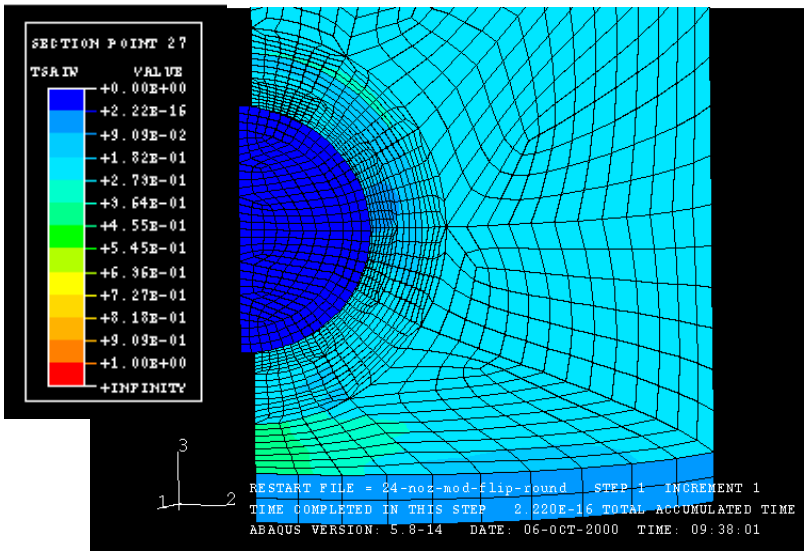

Figure 8.39 – Damage analysis of simplified manway design without bottom reinforcement, 15 psi superposed pressure

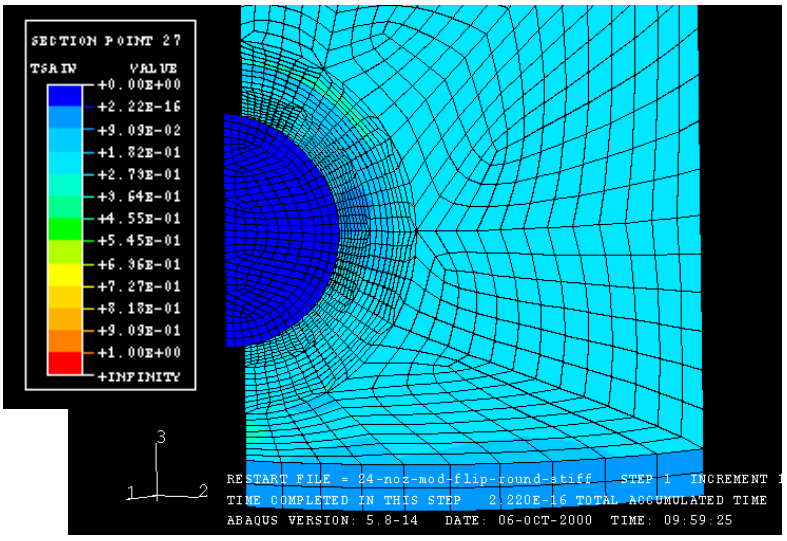

Figure 8.40 – Damage analysis of simplified manway design with bottom reinforcement, 15 psi superposed pressure

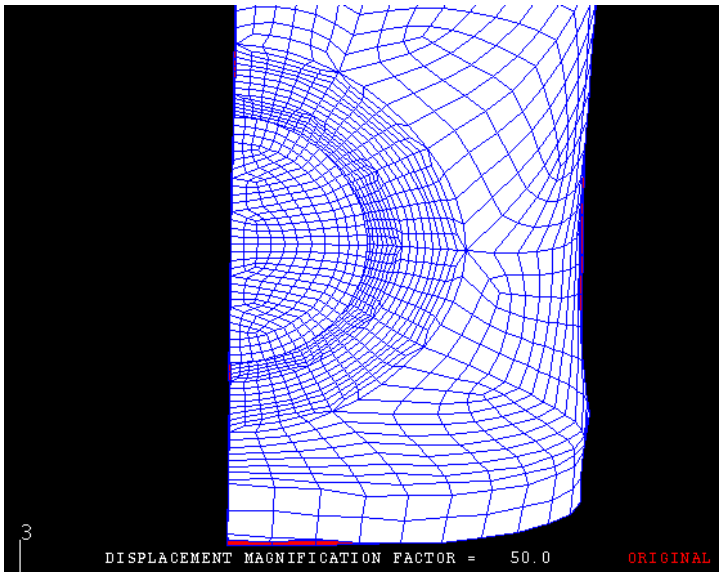

Figure 8.41 – Displaced shape (50 x) of simplified manway design, 15 psi superposed pressure

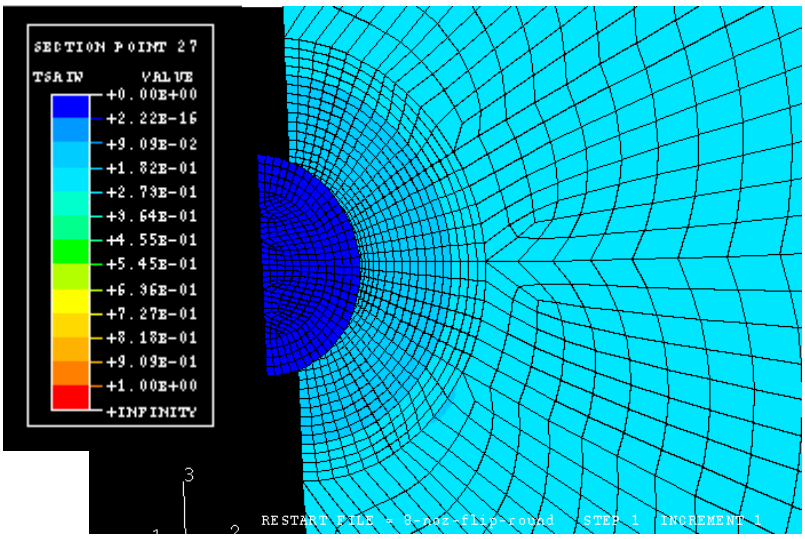

Figure 8.42 – Damage analysis of simplified 8” nozzle design 15 psi superposed pressure

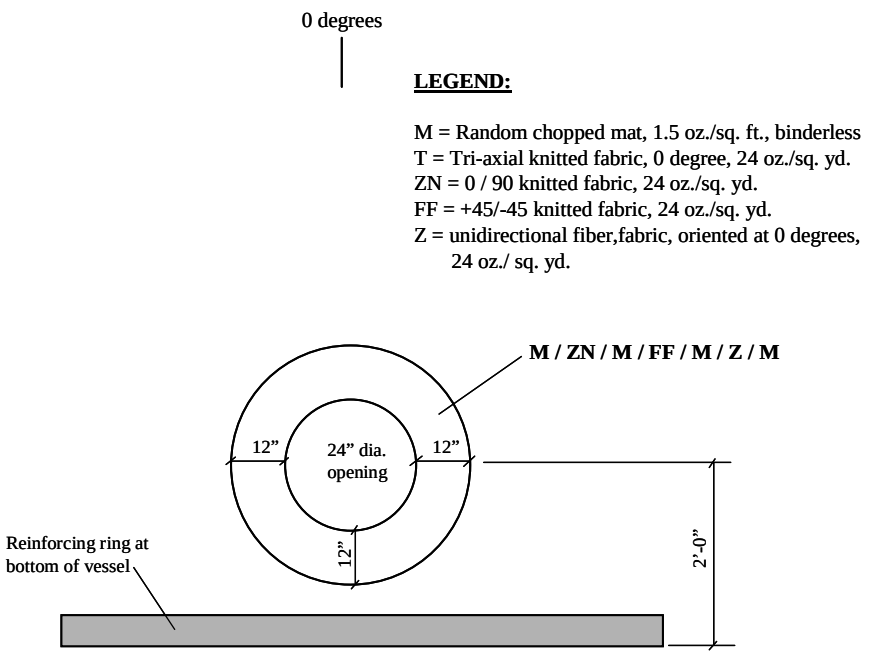

Figure 8.43 – Simplified manway reinforcement – Layer 1 (exterior of vessel)

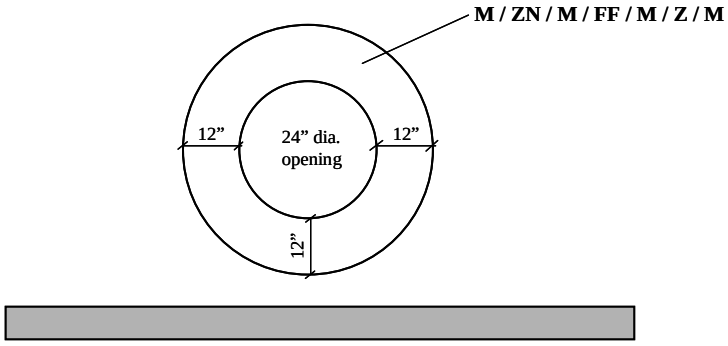

Figure 8.44 – Simplified manway reinforcement – Layer 2 (exterior of vessel)

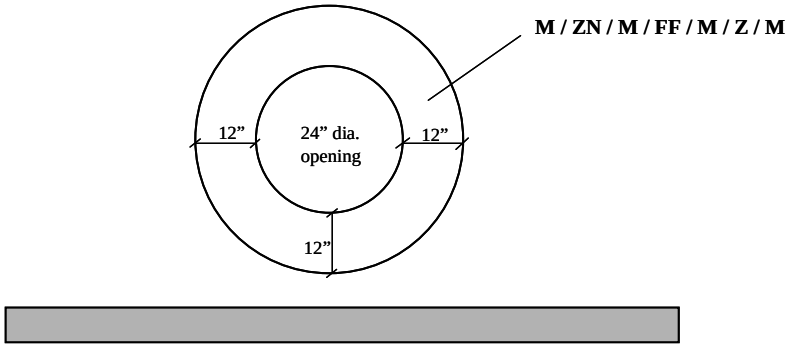

Figure 8.45 – Simplified manway reinforcement - Layer 3 (exterior of vessel)

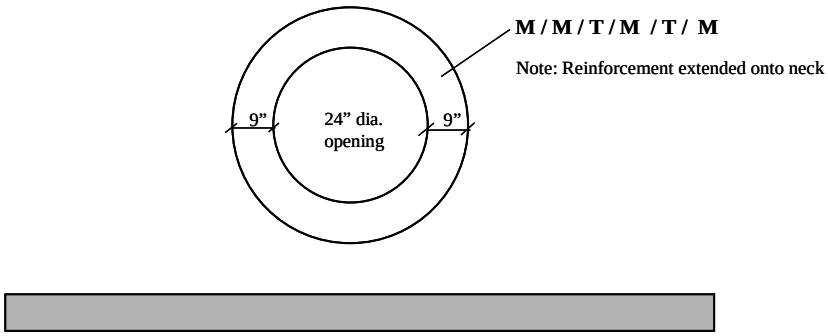

Figure 8.46 – Simplified manway reinforcement – Layer 3 (exterior of vessel)

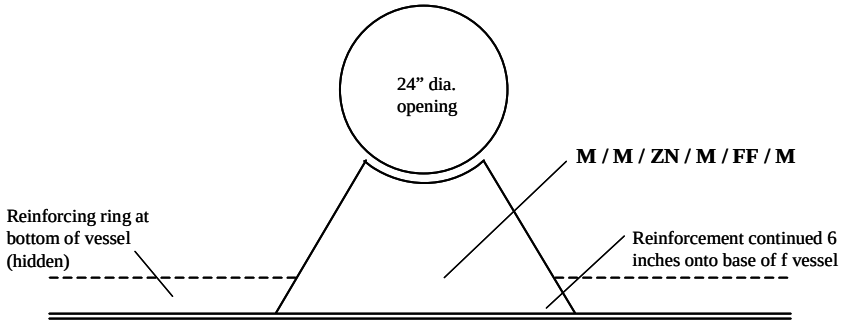

Figure 8.47 – Simplified manway reinforcement – Layer 1 (interior of vessel)

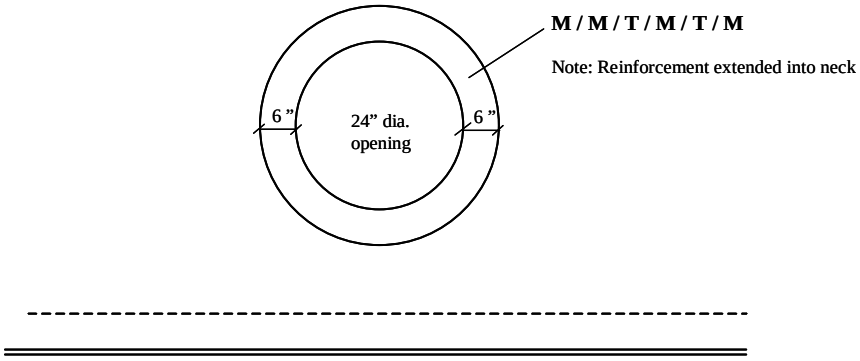

Figure 8.48 – Simplified manway reinforcement - Layer 2 (interior of vessel)

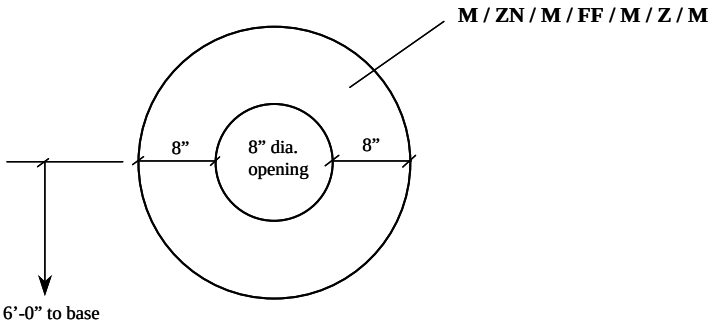

Figure 8.49 – Simplified 8” nozzle reinforcement - Layer 1 (exterior of vessel)

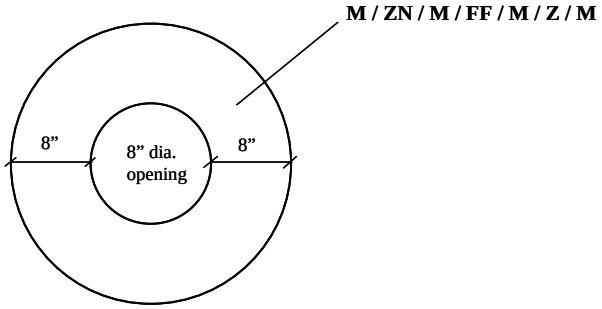

Figure 8.50 – Simplified 8” nozzle reinforcement - Layer 2 (exterior of vessel)

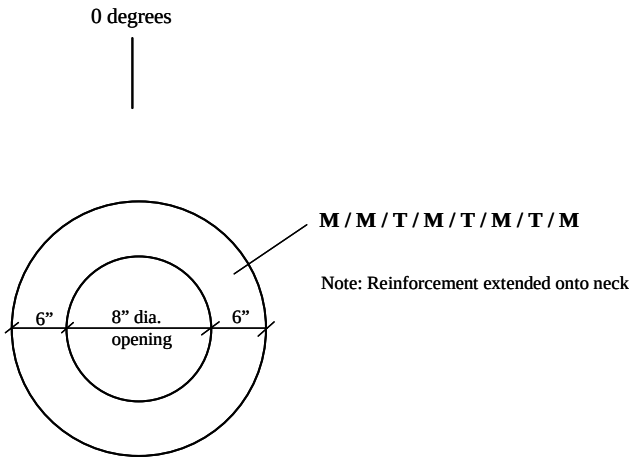

Figure 8.51 – Simplified 6” nozzle reinforcement – Layer 3 (exterior of vessel)

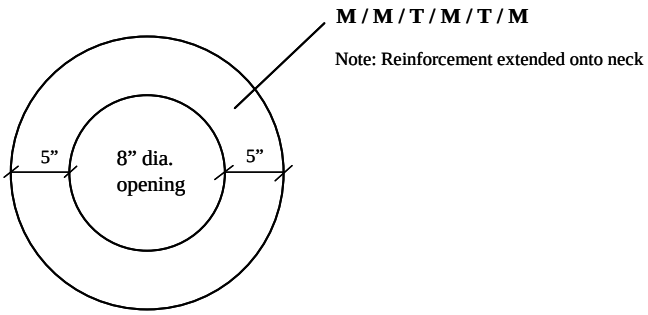

Figure 8.52 – Simplified 8” nozzle reinforcement - Layer 1 (interior of vessel)

8.7 Conclusions

A new manway and 8” nozzle design were implemented. The designs were accomplished with a damage based criterion as opposed to a failure based criterion. This criterion was based on the results of the acoustic emission testing described in Chapter 4. The objective of the design was to reduce the level of critical stresses in the level of the discontinuity region to the level of stresses in the vessel wall away from the discontinuity region. Knitted fabrics and a flexible resin were used.

Chapter 9: *Experimental Verification of Finite Element Models for the Modified Vessel*

In this chapter the measured strain gage results in the vicinity of the new manway and new 8" nozzle are compared to those predicted by the finite element models of these regions. Reasonable agreement was found between the measured and predicted values.

9.1 Comparison of Strain Gage Results with Finite Element Model Results - New Manway

Several strain gages were located in the vicinity of the manway. The strain gage locations are shown in Figure 9.1. The experimental strain results are plotted with the finite element model results for superposed pressure of 15 psi in Figures 9.2 through 9.7. Reasonable agreement was found between the finite element model and the experimental results.

One exception to this is the hoop strains both above and below the manway in the immediate vicinity of the neck. The finite element model over predicts the strains in this area. The strain gage results for the original manway do show a large increase in hoop strain in the immediate vicinity of the neck. Relatively few strain gages were used for the new manway in this area and it is difficult to tell if the problem is with the strain gage or the finite element data.

Another exception is the hoop strains near the base of the vessel. Again it appears that the finite element model over predicts the strains in this area. It is possible the assumptions made regarding the modeling of the hold-down system were inaccurate.

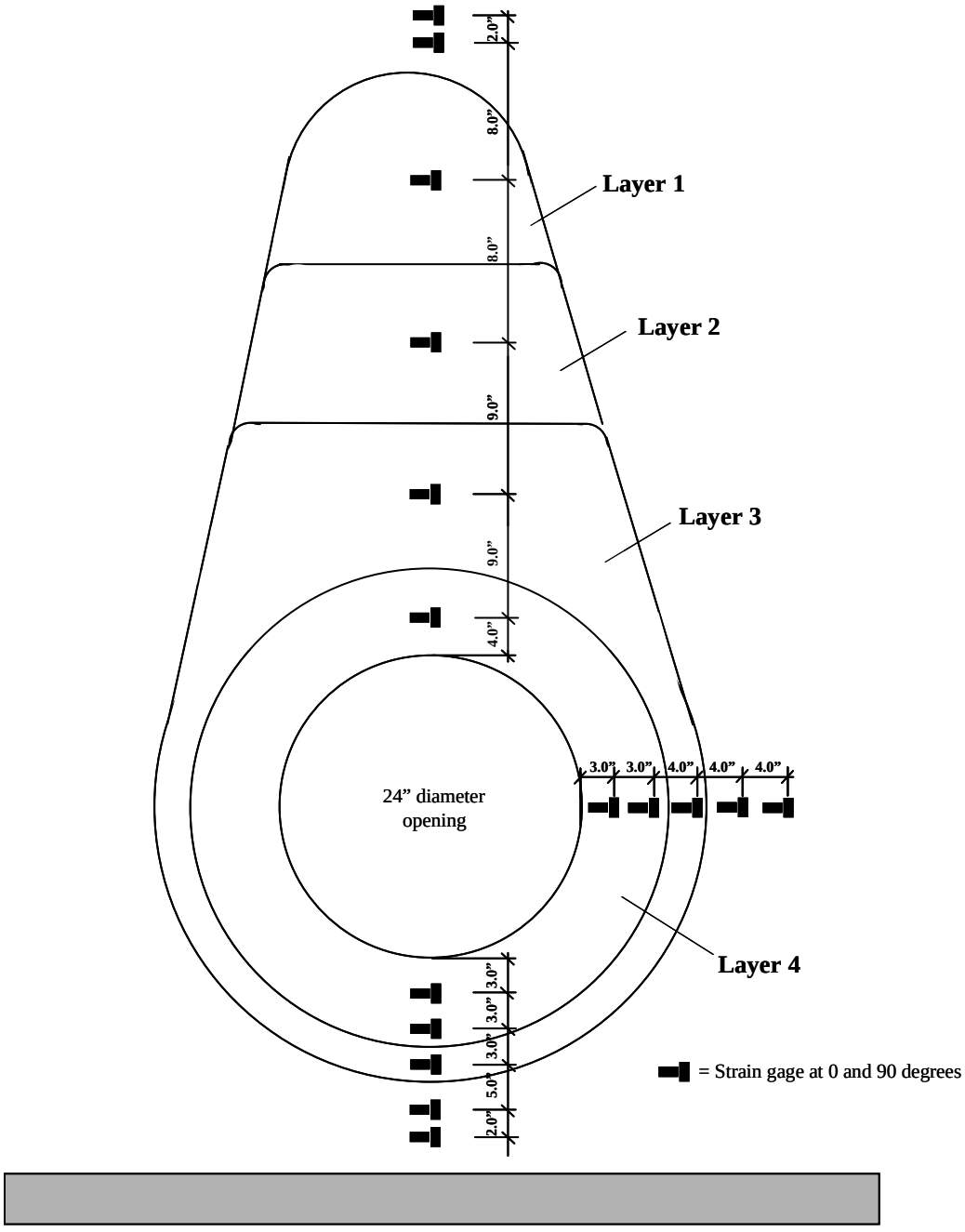

Figure 9.1 – Strain gage locations near new manway

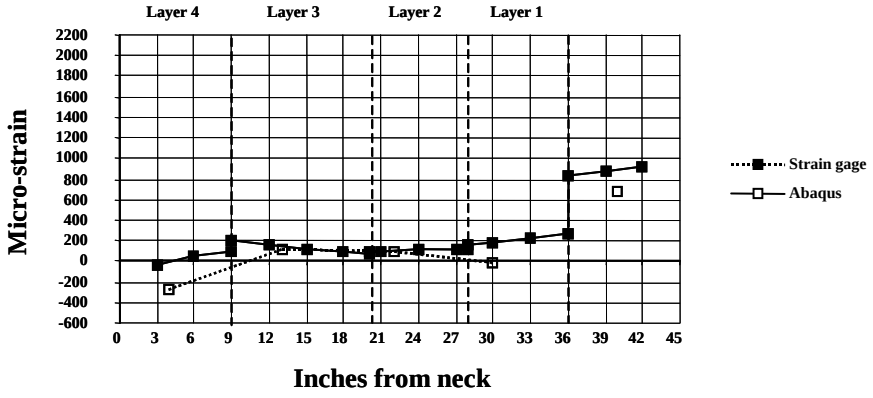

Figure 9.2 – Axial strain above new manway

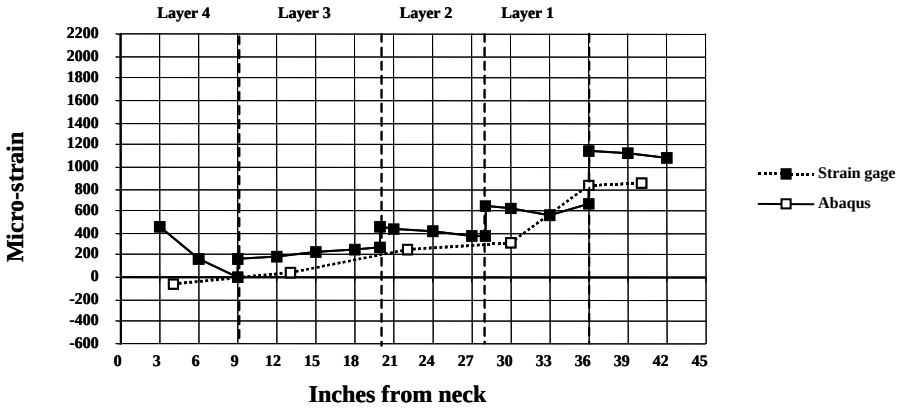

Figure 9.3 – Hoop strain above new manway

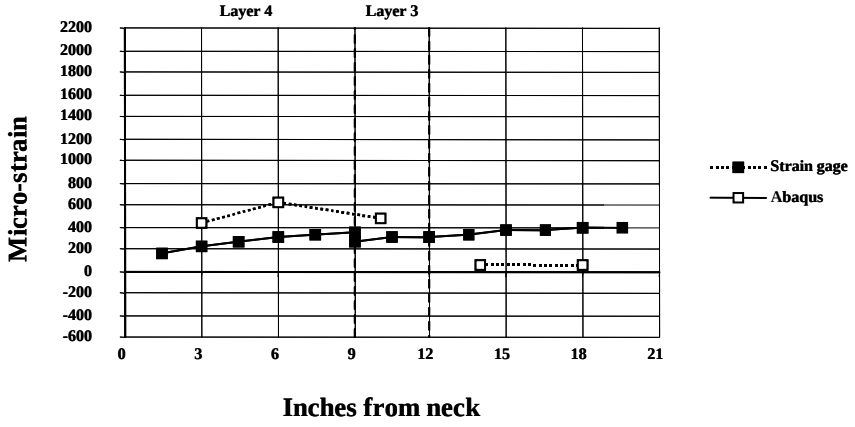

Figure 9.4 – Axial strain to side of new manway

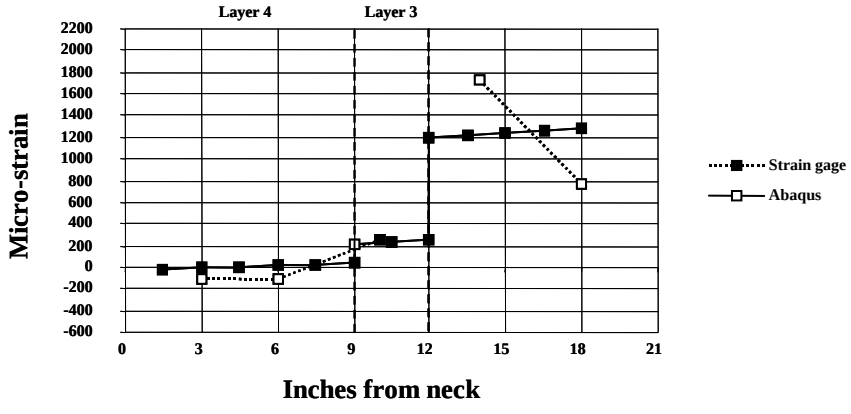

Figure 9.5 – Hoop strain to side of new manway

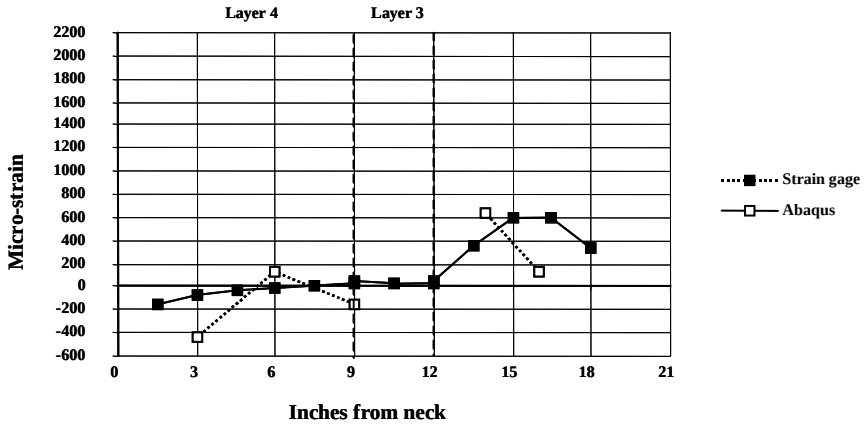

Figure 9.6 – Axial strain below new manway

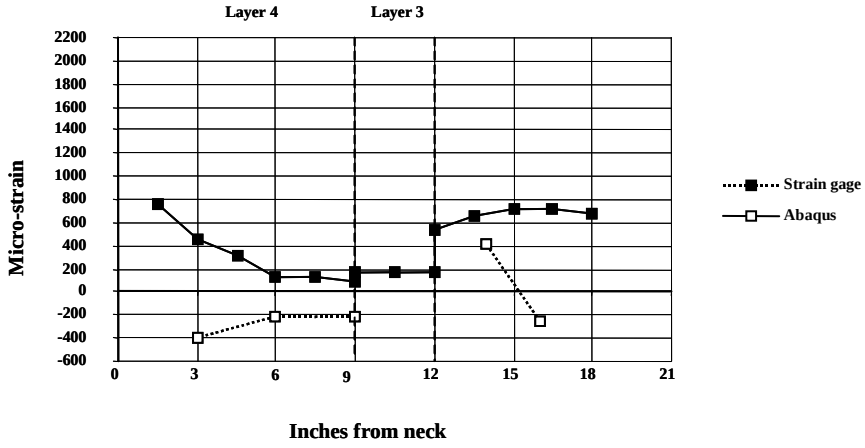

Figure 9.7 – Hoop strain below new manway

9.2 Comparison of Strain Gage Results with Finite Element Model Results - New 8" Nozzle

Several strain gages were located in the vicinity of the new 8" nozzle. Strain gage locations are shown in Figure 9.8. The experimental strain results are plotted with the finite element model results for superposed pressure of 15 psi in Figures 9.9 through 9.12. Reasonable agreement was found between the finite element model and the experimental results.

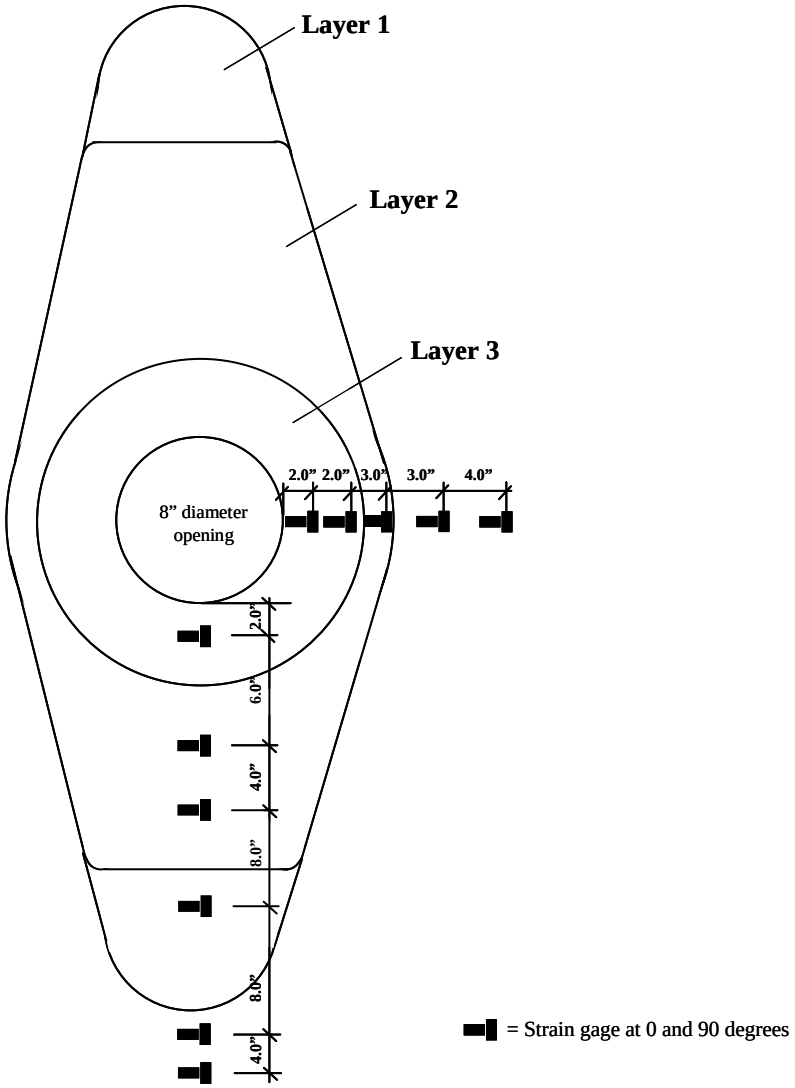

Figure 9.8 – Strain gage locations near new 8” diameter nozzle

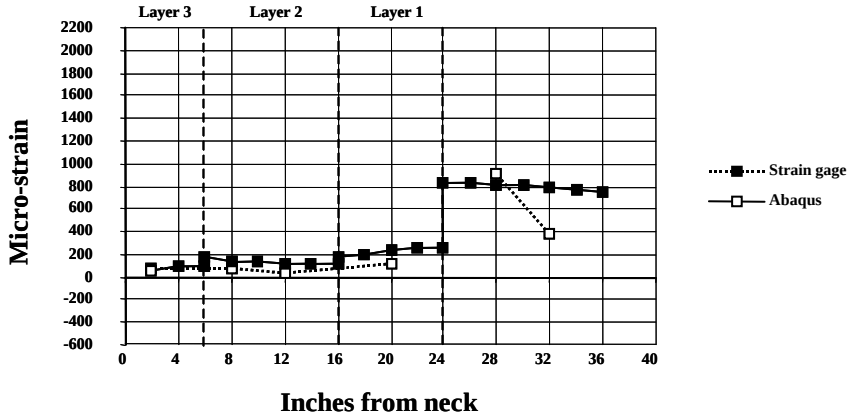

Figure 9.9 – Axial strain below new 8” nozzle

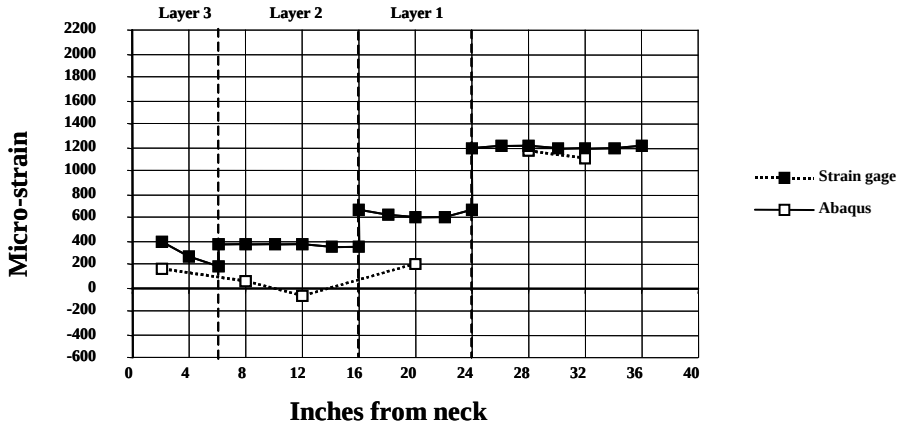

Figure 9.10 – Hoop strain below new 8” nozzle

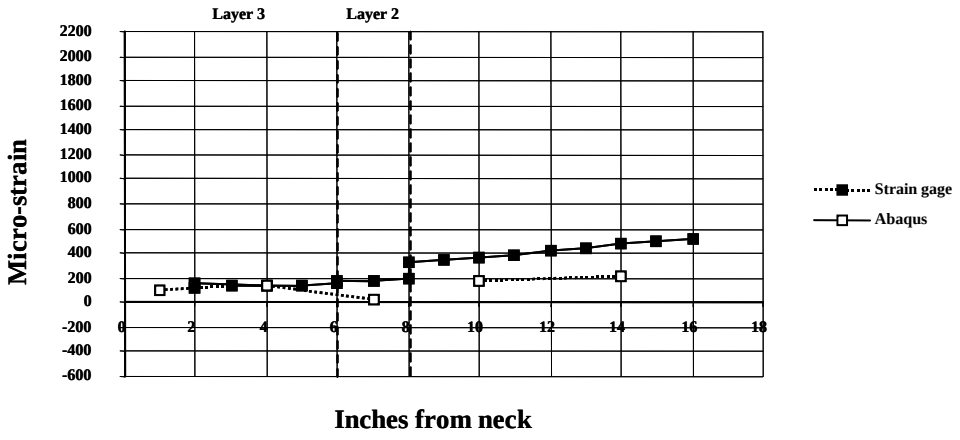

Figure 9.11 – Axial strain to side of new 8” nozzle

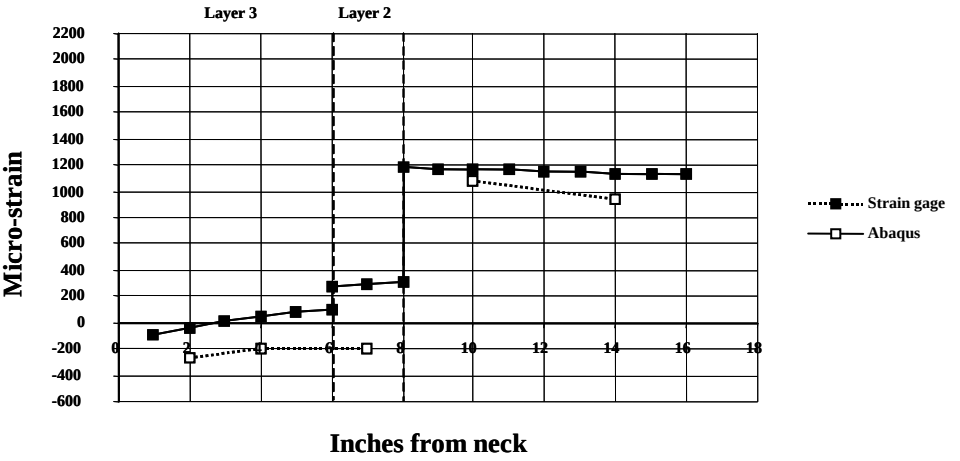

Figure 9.12 – Hoop strain to side of new 8” nozzle

Chapter 10: *Acoustic Emission Results for Original and Modified Vessel*

10.1 Introduction

Acoustic emission testing of the vessel was done in a similar fashion to the coupon testing described in Chapter 3. The vessel was loaded and unloaded several times and significant changes in cumulative signal strength were looked for. The Felicity ratio was also used as an indication of significant damage. The original vessel was monitored with acoustic emission during the filling process. It was also monitored during pressurization on four occasions. The modified vessel was monitored during pressurization on five occasions.

10.2 Acoustic Emission Results of Original Vessel

The locations of the sensors are important for interpretation of the test data. A schematic of the sensor locations on the vessel is shown in Figure 10.1. The arrangement of the sensors provides coverage of the entire vessel. As recommended in the CARP[10.1] procedure additional sensors are placed near nozzles and regions of high local stress. The majority of the sensors were R15I resonant sensors. These sensors are resonant at 150 kHz and have a 40 dB integral preamplifier with a 100-300 kHz band pass filter. These were monitored with the Transportation Instrument. The threshold was 40 dB and the gain was 24 dB.

Three wide band S9208 sensors were monitored with the Mistras 2000 on channels M1, M2 and M6. A fourth sensor (M5) was monitored on the Mistras 2000 for the third pressure test only. This was an R15I resonant sensor. The sensors monitored with the Mistras 2000 are differentiated from the sensors monitored with the Transportation Instrument by the prescript “M” prior to the channel number.

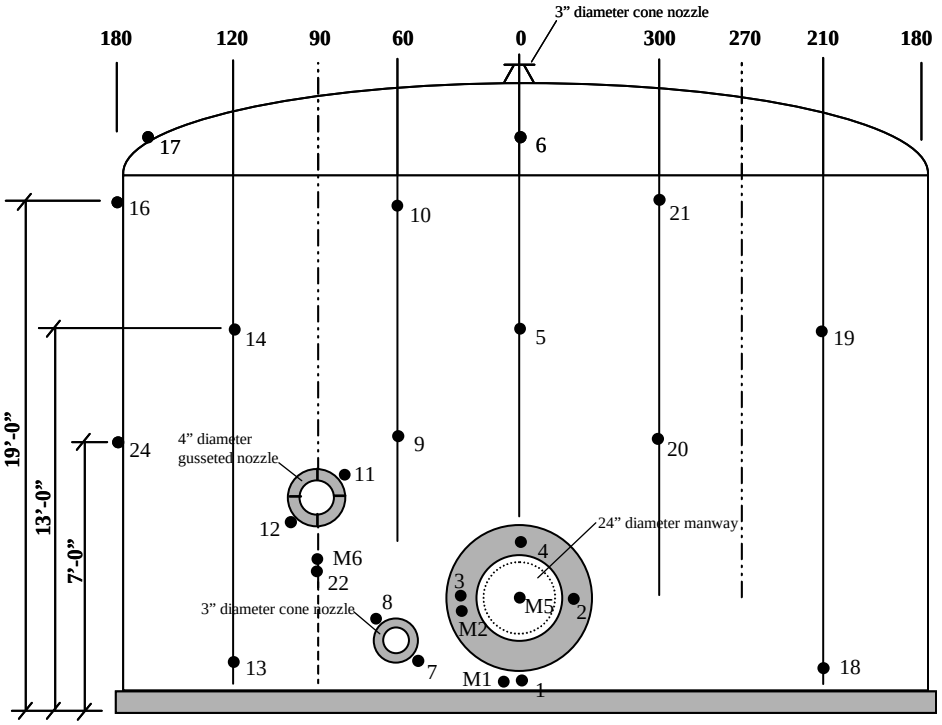

Note: M1, M2 and M6 designate wide band sensors (S9208) monitored with Mistras 2000

M5 designates R15I resonant sensor applied midway through the third pressure test and removed prior to the fourth pressure test. This sensor was monitored with Mistras 2000

All other sensors 150 kHz resonant (R15I) monitored with Transportation Instrument

Figure 10.1 – Acoustic emission sensor locations for original vessel

10.2.1 Hydrostatic test - water to 19.0 feet (June 12, 1998)

The vessel was filled at the inlet nozzle near the bottom of the vessel. The filling of the vessel was continuously monitored from a water height of 2'-0". The cumulative signal strength results from the Transportation Instrument are shown in Figures 10.2 through 10.5. All results shown were generated with VTRNSMON[10.2]. The vessel was very quiet during the entire filling operation. This is unusual during a first filling and suggests a well-made vessel. The maximum cumulative signal strength reached on any channel was 458. This value occurred on Channel 24. Figure 10.5 indicates a large increase in signal strength on this channel during a load hold. The AE events on this channel consisted of 109 hits over a period of 5 seconds. Eleven of these hits had signal strength values of 10 or greater. No additional emission was detected by this channel for the remainder of the test. The examination of this series of events indicates that this is genuine emission. It is significant that it occurs during a load hold and therefore it is not caused by fill noise.

First loadings of vessels are generally noisy. A good deal of non-structural emission is present during a first loading[10.1]. One common cause of non-significant emission is cracking of excess resin. The acoustic emission data collected during this test is not indicative of significant damage and indicates a well-made vessel.

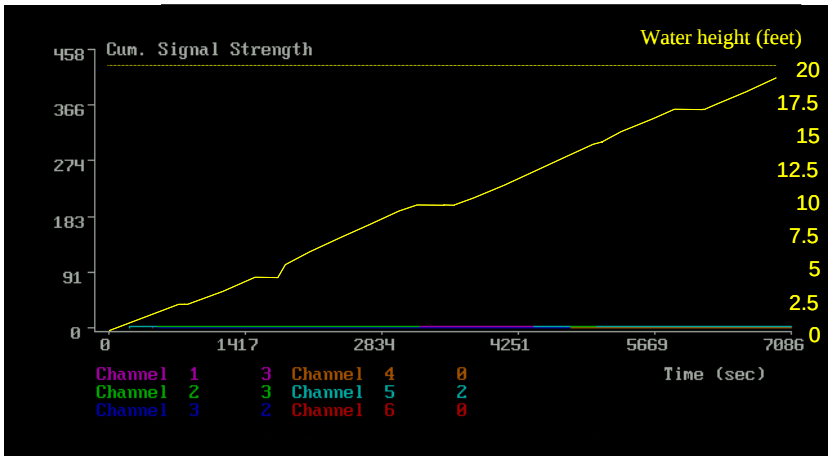

Figure 10.2 – First hydro test – original vessel (Channels 1-6)

Transportation Instrument

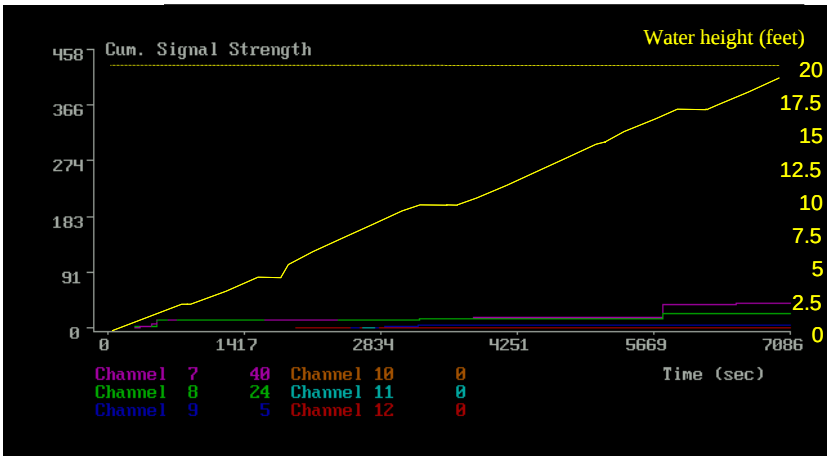

Figure 10.3 – First hydro test – original vessel (Channels 7-12)

Transportation Instrument

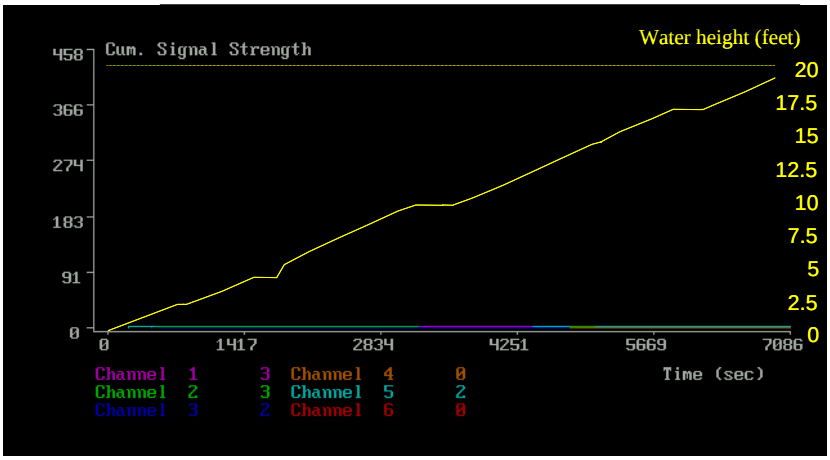

Figure 10.2 – First hydro test – original vessel (Channels 1-6)

Transportation Instrument

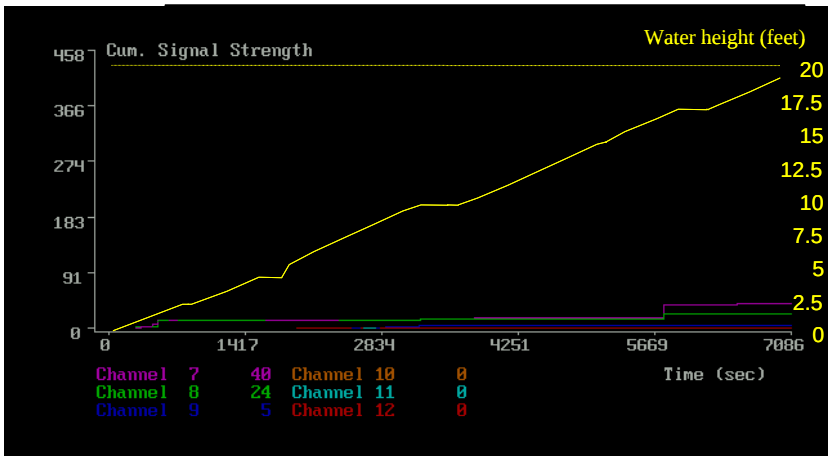

Figure 10.3 – First hydro test – original vessel (Channels 7-12)

Transportation Instrument

10.2.2 First pressure test – 15.1 psi (July 9, 1998)

The maximum superposed pressure reached during the first pressure test was 15.1 psi. This is in the range of the 15.0 psi superposed pressure load for which the vessel was designed. Plots of cumulative signal strength versus time from the Transportation Instrument are shown in Figures 10.6 through 10.9. The maximum cumulative signal strength value reached was 403. This value of cumulative signal strength is quite low. This is particularly true for a first pressurization. This data provides further evidence of a well-made vessel.

Channels 5, 18 and 24 were the most active. An increase in signal strength occurred for these channels during a load increase from 10 to 12.5 psi. Channel 18 was particularly active throughout the test. This channel is located in the vicinity of a hold-down device. It is possible that some minor damage occurred to the vessel in this area during the pressurization. Channel 24 is the same channel that was active during the first filling of the vessel. This channel is located in the vicinity of the 4" gusseted nozzle, though not directly adjacent to it. Channel 5 is above the original manway.

Another significant event was recorded at 13.5 psi. This event was less significant than the one at 12.5 psi. It was recorded by numerous sensors.

A plot of duration versus amplitude is shown in Figure 10.10. This data appears genuine with some overlapping hits[10.3].

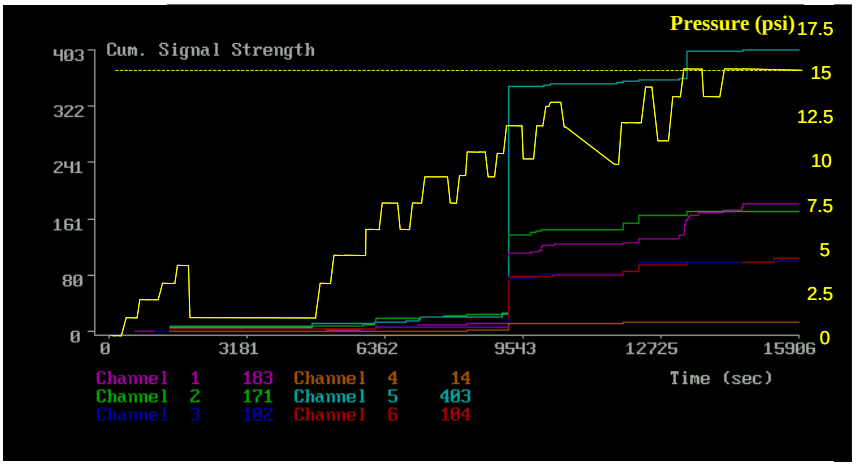

Figure 10.6 – First pressure test – original vessel (Channels 1-6)

Transportation Instrument

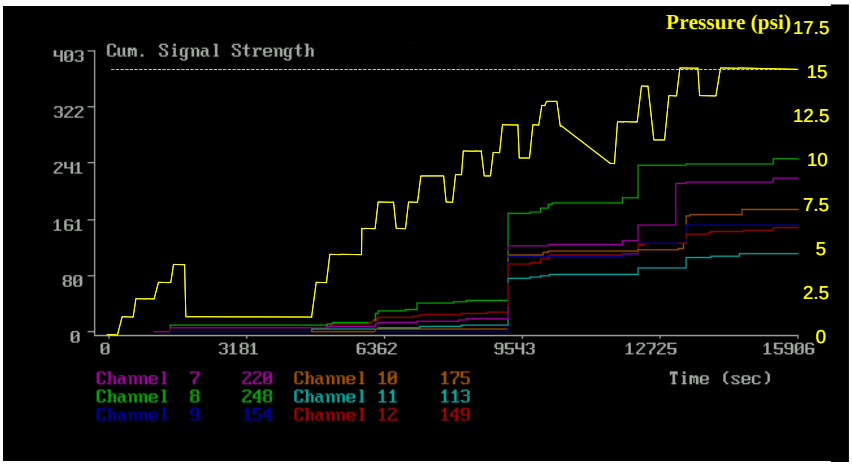

Figure 10.7 – First pressure test – original vessel (Channels 7-12)

Transportation Instrument

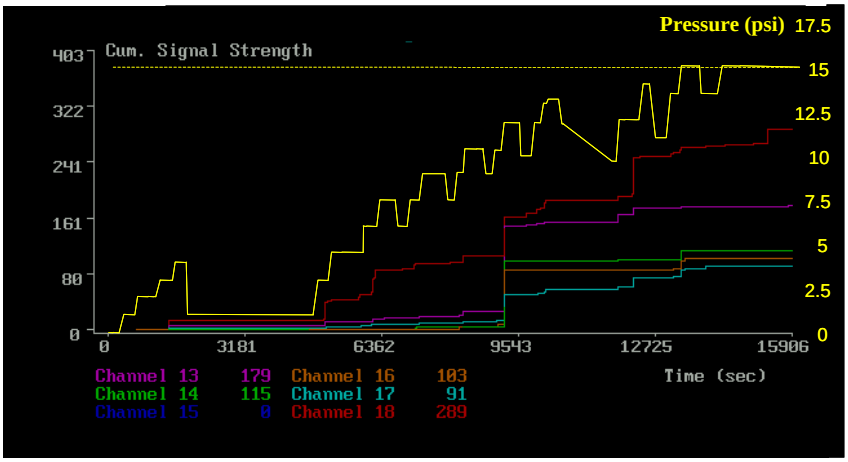

Figure 10.8 – First pressure test – original vessel (Channels 13-18)

Transportation Instrument

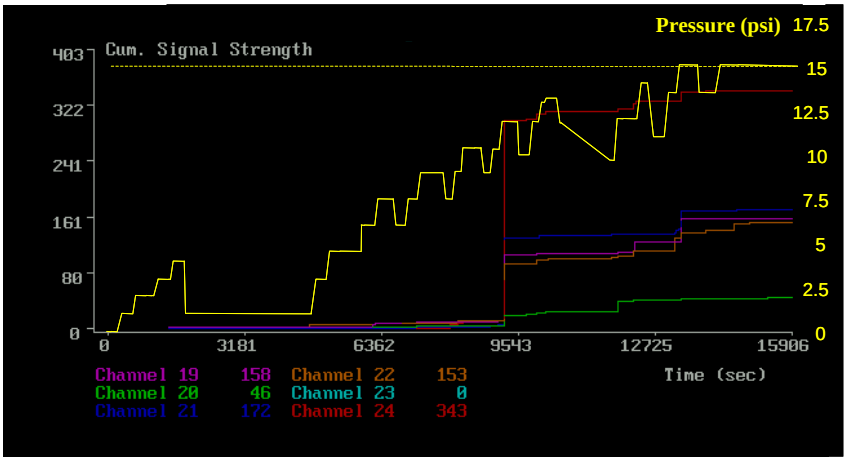

Figure 10.9 – First pressure test – original vessel (Channels 19-24)

Transportation Instrument

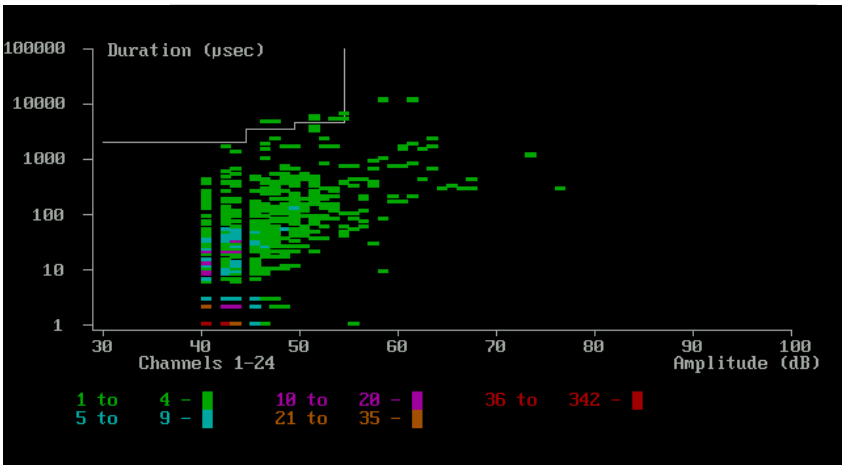

Figure 10.10 – First pressure test – original vessel (Channels 1-24)

Transportation Instrument

10.2.3 Second pressure test - 15.0 psi (July 16, 1998)

A second test is standard for tests conducted according to the CARP procedure[10.1]. Because a second test is permitted if the vessel is not acceptable on the first filling and pressurization most AE tests are conducted after an initial unmonitored fill/ pressurization has been done. Noise on the first loading can be, and often is, non-structural.

Prior to the pressure test, the vessel was drained and refilled. The filling process was monitored continuously with the Transportation Instrument. During the filling process, the hose was disturbed and a good deal of non-genuine acoustic emission was created. This was noted in the test log. The Transportation Instrument data file was filtered to remove this noted source of non-genuine emission. Plots of signal strength versus time for this filling are shown in Figures 10.11 through 10.14. The maximum cumulative signal strength was 538. Channels 11, 22 and 24 were the most active. Channel 18 was also active again. Channel 11 was directly adjacent to the 4" gusseted nozzle. Channel 22 was located approximately 1'-0" below the 4" gusseted nozzle. Channels 18 and 24 were active during the first pressure test and were discussed previously.

A plot of duration versus time for this filling is shown in Figure 10.15. This data again appears to be genuine.

The maximum pressure reached during the second pressure loading was 15.0 psi. Some noise due to the filling procedure was noticed during the test. After inspection of the data, emission that was attributed to fill noise on channel 24 was filtered out. Plots of cumulative signal strength versus time for this loading are shown in Figures 10.16 through 10.19. The maximum cumulative signal strength value for all channels was 4,833. Channels 5 and 12 were the most active. An increase in signal strength occurred for channel 12 during a load increase from 9.0 to 12.0 psi. Channel 12 is directly adjacent to the fill nozzle. Channel 5 is located above the manway.

A plot of duration versus amplitude is shown in Figure 10.20. The emissions appear to be genuine.

The level of defect intensity can be judged with the use of an intensity analysis as described in the CARP recommended practice. This was discussed in the literature review of the CARP recommended practice in Chapter 2. The results of an intensity analysis are shown in Figure 10.21. The results are as follows:

Intensity category “A” (Minor) – none

Intensity category “B” (Intermediate) – channels 5, 8, 18

Intensity category “C” (Follow-up) – channel 24

Intensity category “D” (Major) – none

Channel 12 is not displayed on the intensity analysis. Even though this channel displayed a large increase in signal strength from 9.0 to 12.0 psi this occurred due to essentially only 1 hit. This very large hit had a signal strength of 4191 and duration of 25,085 micro-seconds. The amplitude was 65 dB. A smaller hit with signal strength of 313 occurred 27 micro-seconds later. A third hit with signal strength of 1 occurred 7 micro-seconds after the second hit. For historic index to be determined 19 hits are required. Channel 12 received only 11 hits during the test.

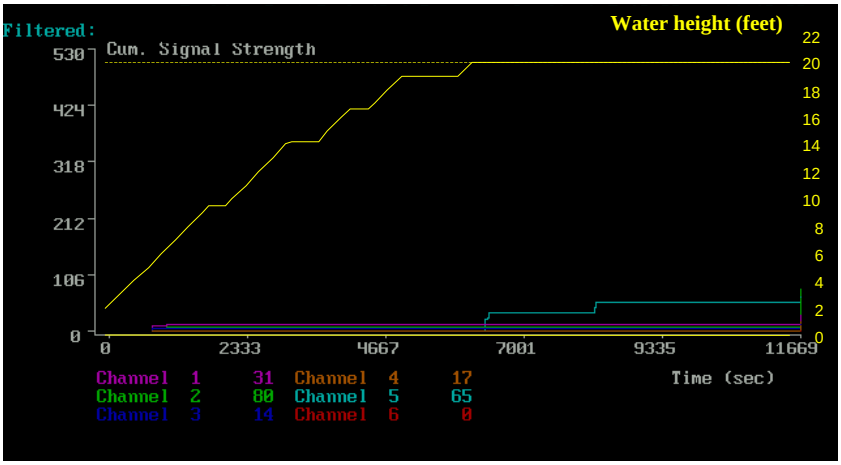

Figure 10.11 – Hydro test prior to second pressure test, original vessel (Channels 1-6)

Transportation Instrument {FILTERED}

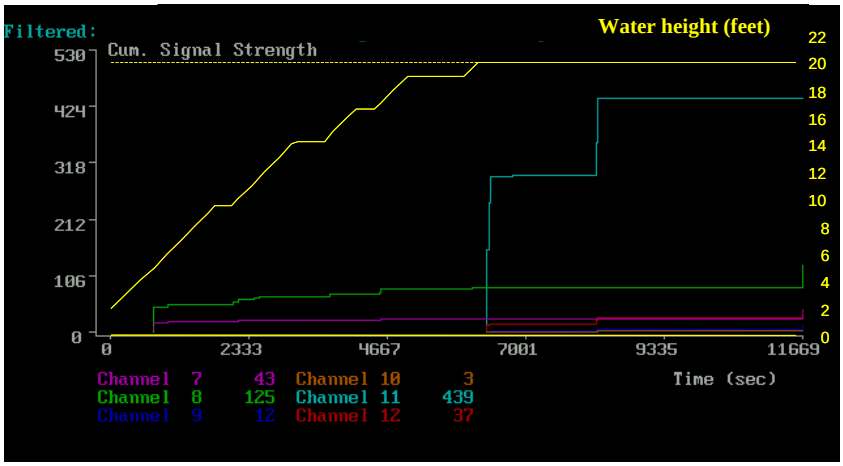

Figure 10.12 – Hydro test prior to second pressure test, original vessel (Channels 7-12)

Transportation Instrument {FILTERED}

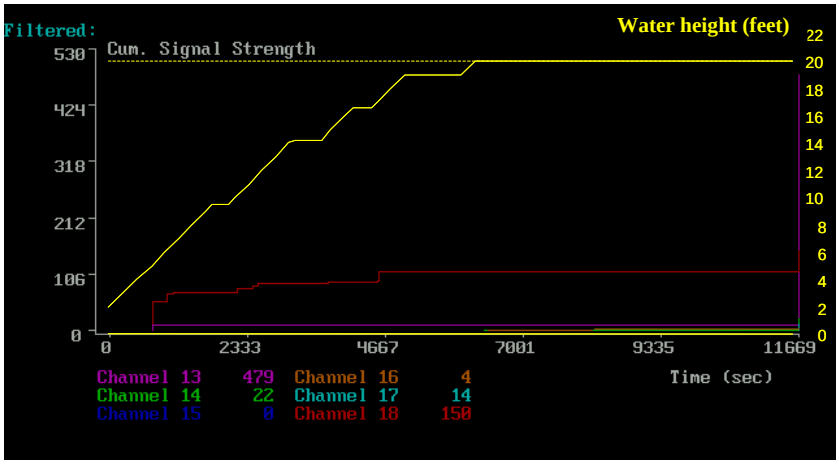

Figure 10.13 – Hydro test prior to second pressure test, original vessel (Channels 13-18)

Transportation Instrument {FILTERED}

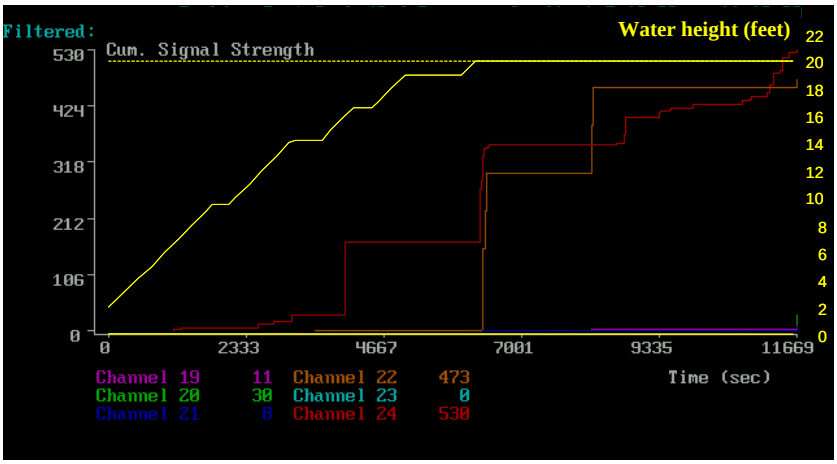

Figure 10.14 – Hydro test prior to second pressure test, original vessel (Channels 19-24)

Transportation Instrument {FILTERED}

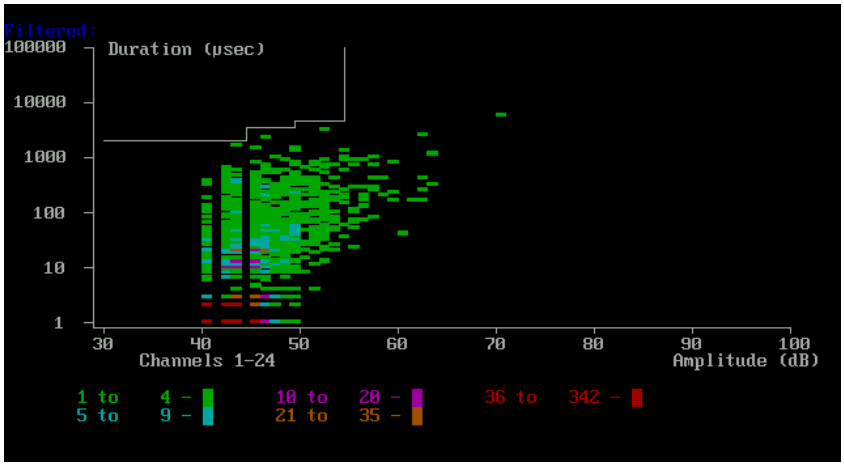

Figure 10.15 – Hydro test prior to second pressure test, original vessel (Channels 1-24)

Transportation Instrument {FILTERED}

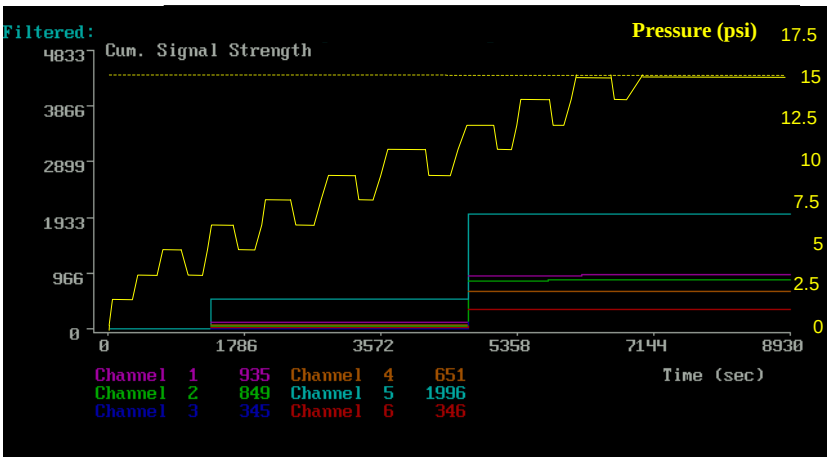

Figure 10.16 – Second pressure test – original vessel (Channels 1-6)

Transportation Instrument {FILTERED}

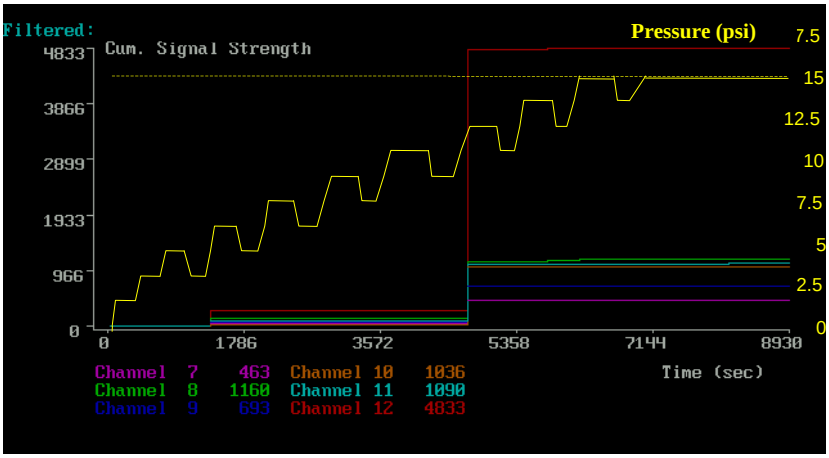

Figure 10.17 – Second pressure test – original vessel (Channels 7-12)

Transportation Instrument {FILTERED}

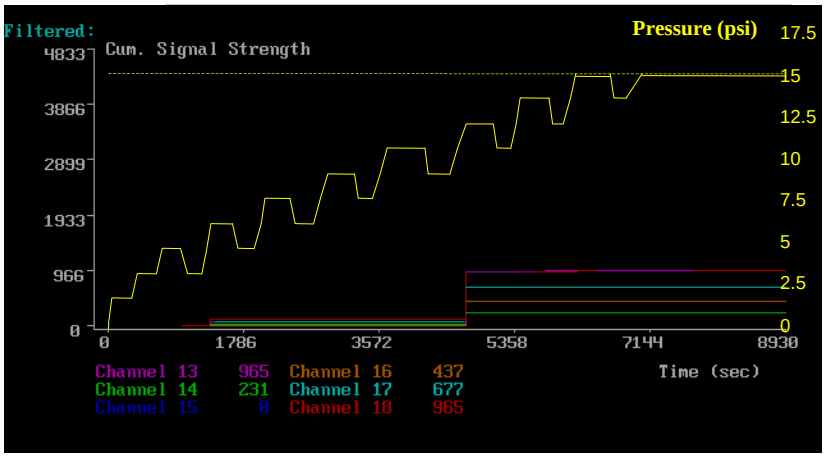

Figure 10.18 – Second pressure test – original vessel (Channels 13-18)

Transportation Instrument {FILTERED}

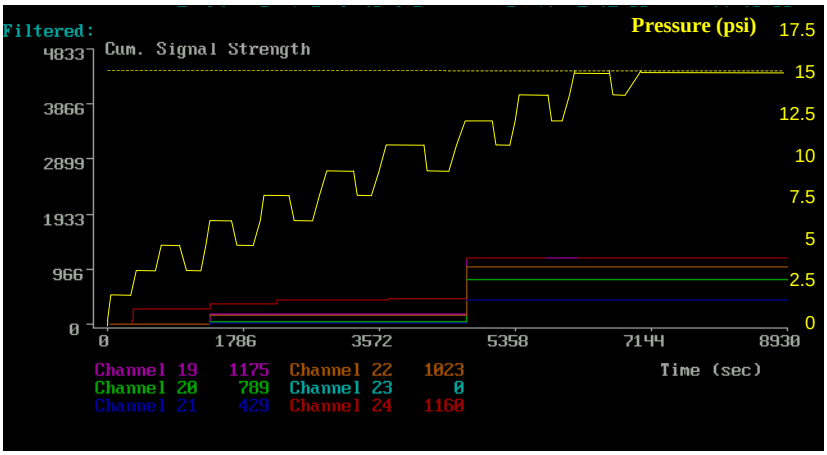

Figure 10.19 – Second pressure test – original vessel (Channels 19-24)

Transportation Instrument {FILTERED}

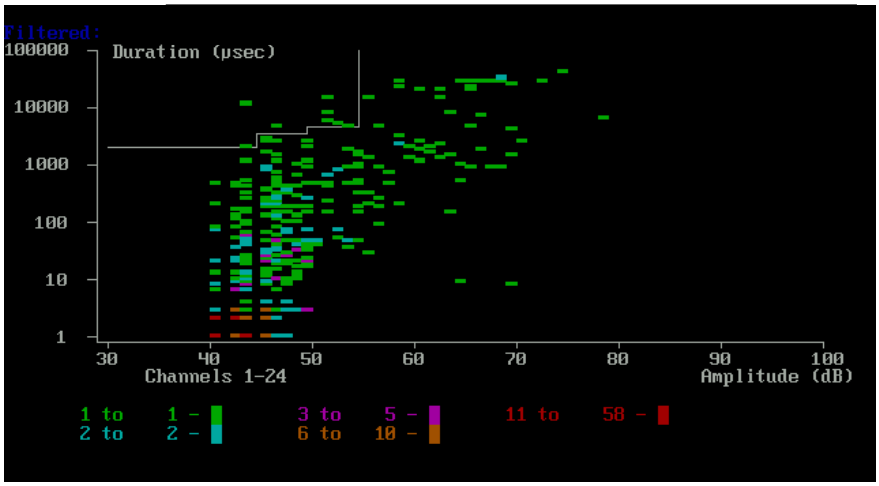

Figure 10.20 – Second Pressure Test – Original Vessel (Channels 1-24) Transportation Instrument {FILTERED}

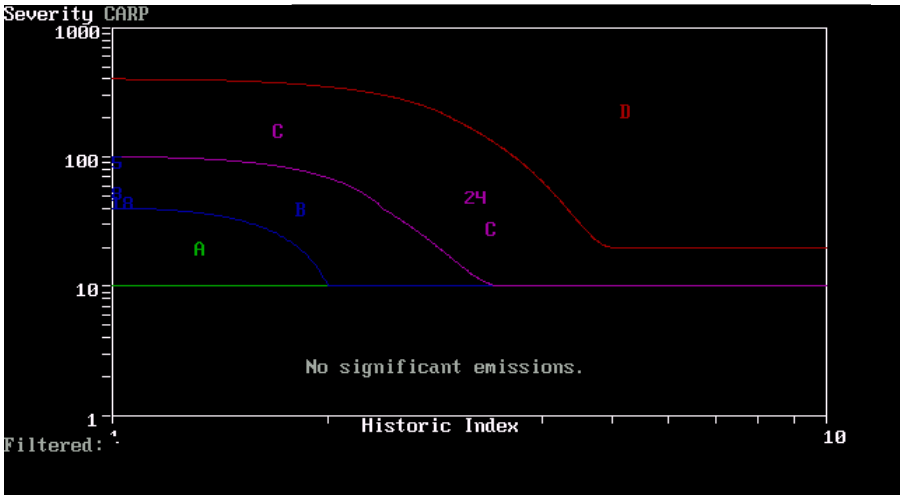

Figure 10.21 – Second Pressure Test – Original Vessel (Channels 1-24) Transportation Instrument {FILTERED}

10.2.4 Third pressure test - 22.0 psi (June 1, 1999)

Approximately one year after the first two pressure tests a third and fourth pressure test were performed. The first two pressure tests were carried out to the design pressure and this was not expected to cause significant damage to the vessel. The maximum pressure reached during the third pressure loading was 22.0 psi.

Significant damage was caused to the 4" gusseted nozzle connections as the pressure was increased from 21.0 to 22.5 psi. The damage was audible and was heard by individuals conducting the test. Visual inspection confirmed the damage. Three photographs of the damage are shown in Chapter 6. One of these is reproduced as Figure 10.22 for convenience.

Plots of cumulative signal strength versus time from the Transportation Instrument are shown in Figures 10.23 through 10.26. Prior to the data shown in these plots, the vessel was loaded to 7.5 psi and unloaded to 0.0 psi. Due to a malfunction with the Transportation Instrument, the acoustic emission data collected during this initial load was lost. Unfortunately, the data from 19.5 to 22.0 psi when the visible cracks developed was also lost. Excluding this information, the maximum cumulative signal strength was 2,644.

Numerous channels showed an increase in signal strength near the end of the first load hold at 12.5 psi. This was particularly true for channels 5, 10, 20, and 24. Channels 5, 10 and 20 are above the manway. Channel 24 was active on the previous loading and was assigned an intensity classification of "C" on that loading. Numerous channels also showed a significant increase in signal strength at the beginning of the load hold at 15.0 psi. Channels 5, 10, 20, and 24 were again the most active.

A significant increase in signal strength was evident in numerous sensors near the end of the load increase from 9.0 to 19.5 psi. The increase in emission began at approximately 17.5 psi.

A plot of duration versus amplitude is shown in Figure 10.27. The emission appears to be genuine.

The results of an intensity analysis for this loading are shown in Figure 10.28. This analysis applies to the data collected with the Transportation Instrument only. The intensity factors assigned to the channels were as follows:

Intensity category “A” – channels 1,2,3,6,7, 12,13

Intensity category “B” – channels 9,14,16,17,18

Intensity category “C” – channels 10, 20, 24

Intensity category “D” – none

This is a first loading in the sense that this is the first time the vessel had been loaded to 22.0 psi. As mentioned previously, vessels are usually not monitored during a first loading and an intensity analysis is therefore not conducted. However, the values shown here do give some indication of the level of damage.

Three channels were recorded on the Mistras 2000. Type S9208 wide band sensors were used for channels M1, M2 and M6. The wide band sensors used are generally less sensitive than the R15I sensors for testing of composites. The wide band sensors can be more sensitive than the R15I sensors in the lower frequency range, however. For these reasons, a quantitative comparison between the data collected with the wide band sensors and that collected with the resonant sensors is not possible. The results can be compared on a qualitative basis only. An R15I sensor was used for channel M5. This channel was added on the manway cover at a load of 19.5 psi due to concern that the manway cover may be in distress. Some of the data from the Mistras was lost, but the important data from 19.5 to 22.0 psi was recorded. This data is shown in Figure 10.29. A very significant increase in signal strength can be seen in Channel M6 during the loading from 21.0 to 22.5 psi. This channel was located 1’-0” below the distressed 4” gusseted nozzle. Smaller increases in signal strength can be seen in channels M2 and M5. Channel M2 was adjacent to the manway and channel M5 was on the manway cover as described earlier.

A plot of duration versus amplitude is shown in Figure 10.30. The emission appears to be genuine.

The results of an intensity analysis for this loading are shown in Figure 10.31. This analysis applies to the data collected with the Mistras 2000.

The very significant damage that occurred to the gusset plates of the 4" gusseted nozzle is indicated with an intensity category of "D" for channel M6. Channel M2 near the manway received a very high intensity category of "C". This channel was in the vicinity of the 4" gusseted nozzle and may have been picking up the damage from the nozzle.

Intensity category "A" – none

Intensity category "B" – channel M5

Intensity category "C" – channel M2

Intensity category "D" – channel M6

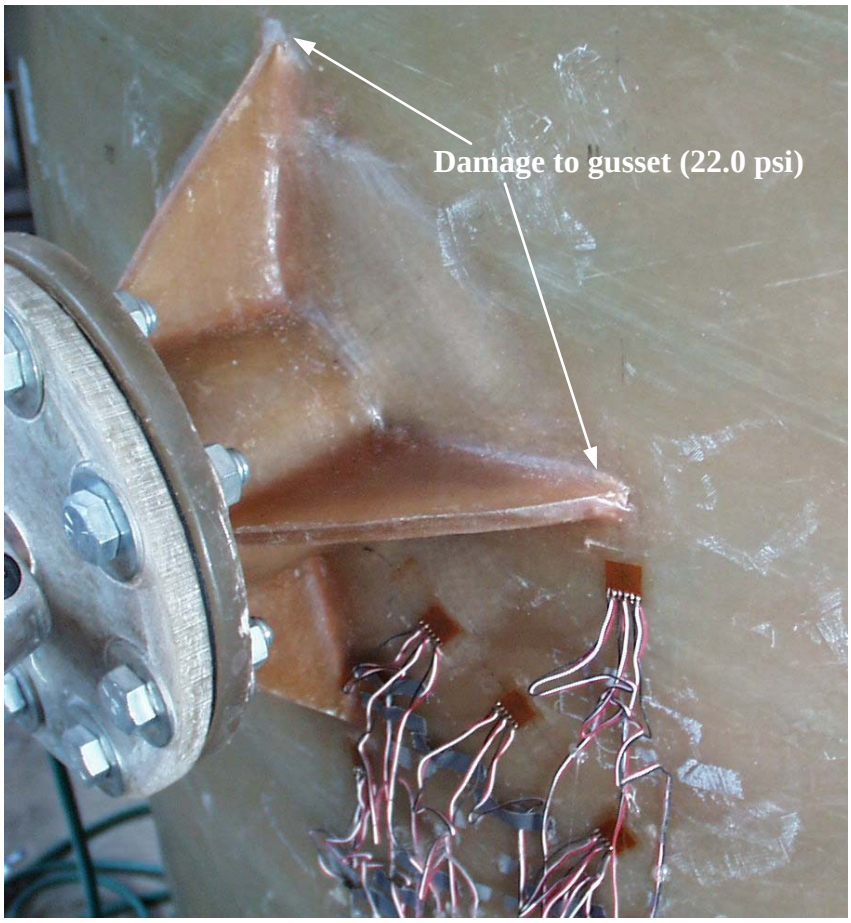

Figure 10.22 – Damage to 4” gusseted nozzle

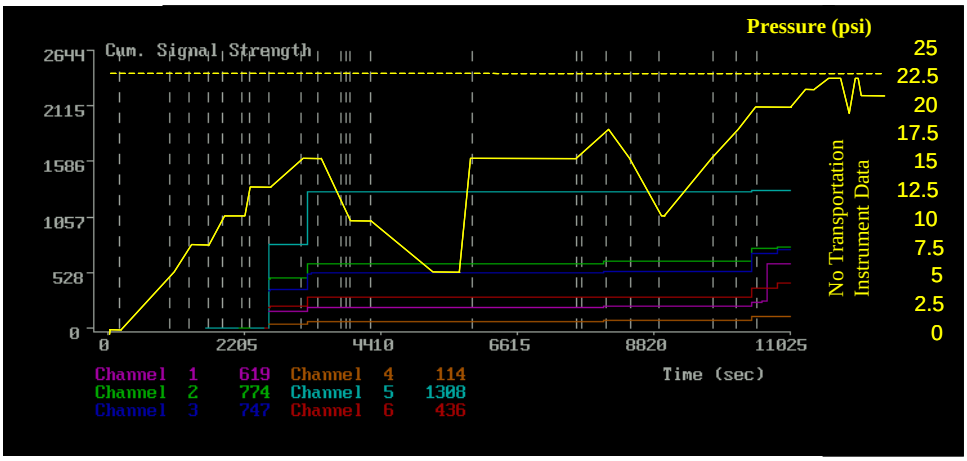

Figure 10.23 – Third pressure test – original vessel (Channels 1-6)

Transportation Instrument

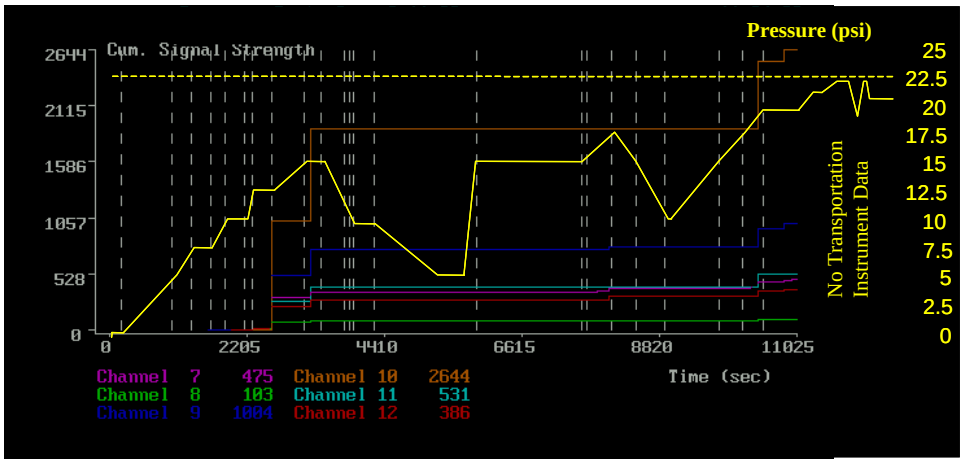

Figure 10.24 – Third pressure test – original vessel (Channels 7-12)

Transportation Instrument

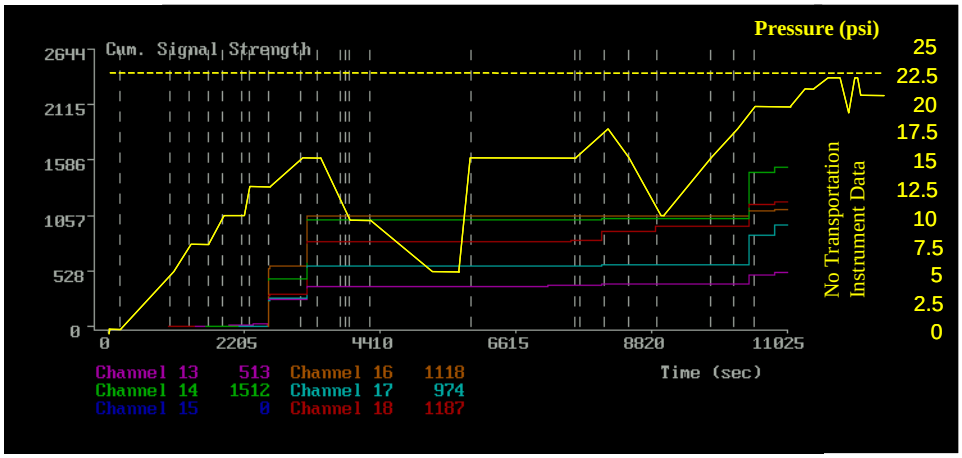

Figure 10.25 – Third pressure test – original vessel (Channels 13-18)

Transportation Instrument

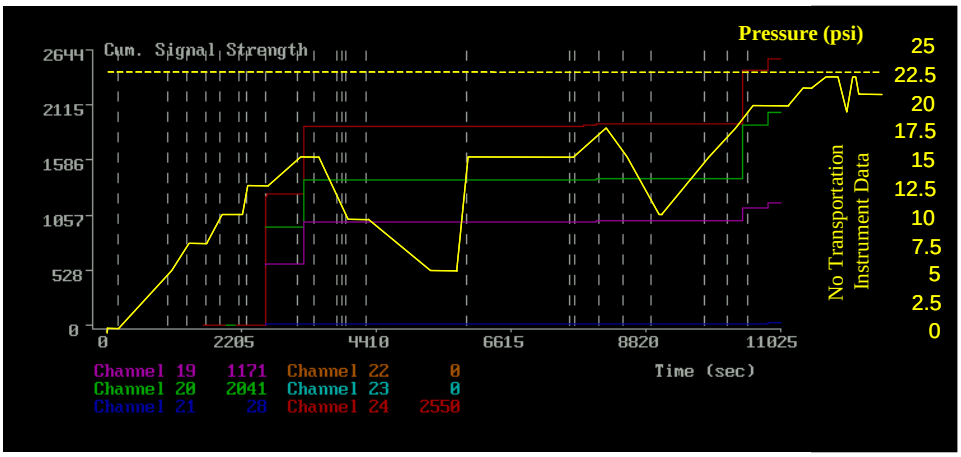

Figure 10.26 – Third pressure test – original vessel (Channels 19-24)

Transportation Instrument

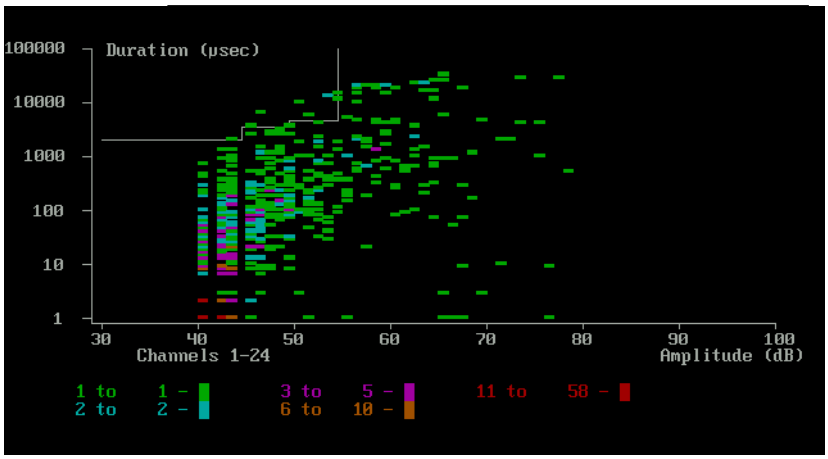

Figure 10.27 – Third pressure test – original vessel (Channels 1-24)

Transportation Instrument

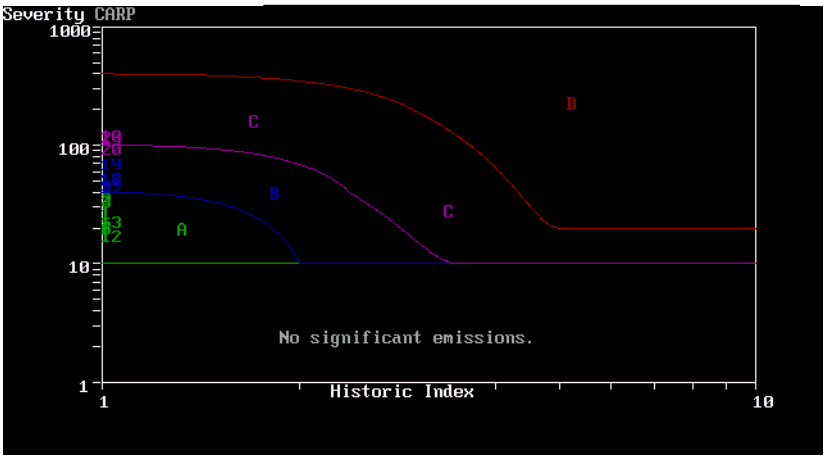

Figure 10.28 – Third pressure test – original vessel (Channels 1-24)

Transportation Instrument

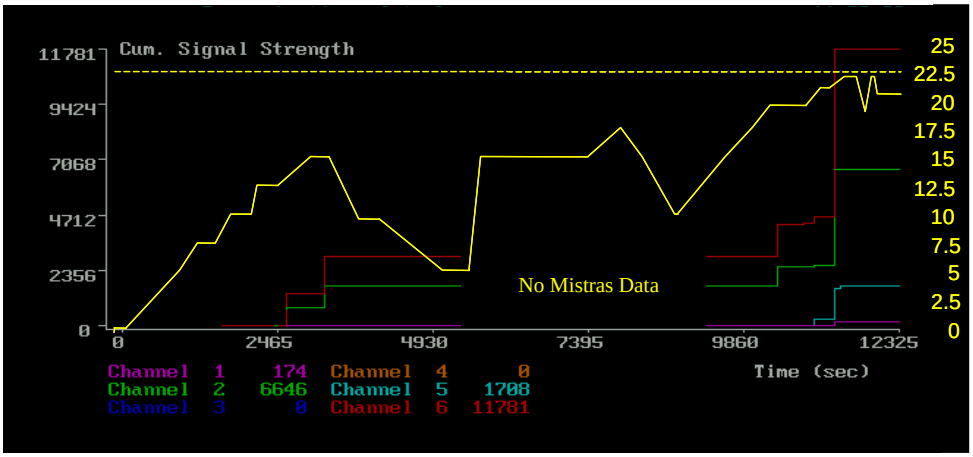

Figure 10.29 – Third pressure test – original vessel (Channels 1-6)

Mistras 2000

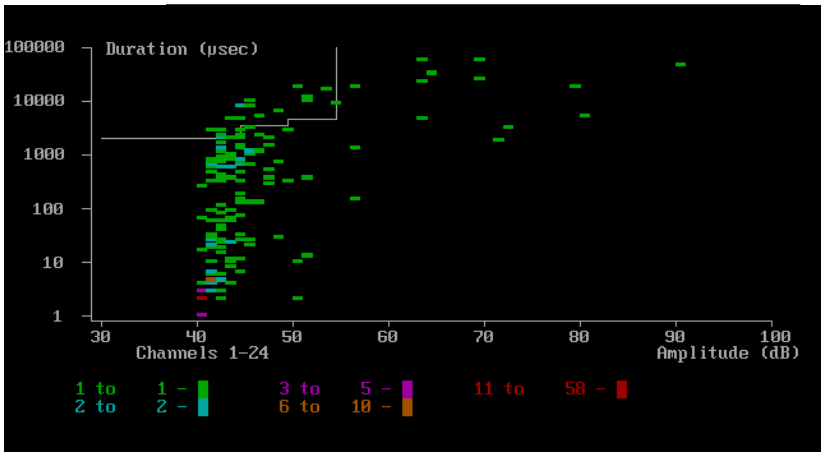

Figure 10.30 – Third pressure test – original vessel (Channels 1-24)

Mistras 2000

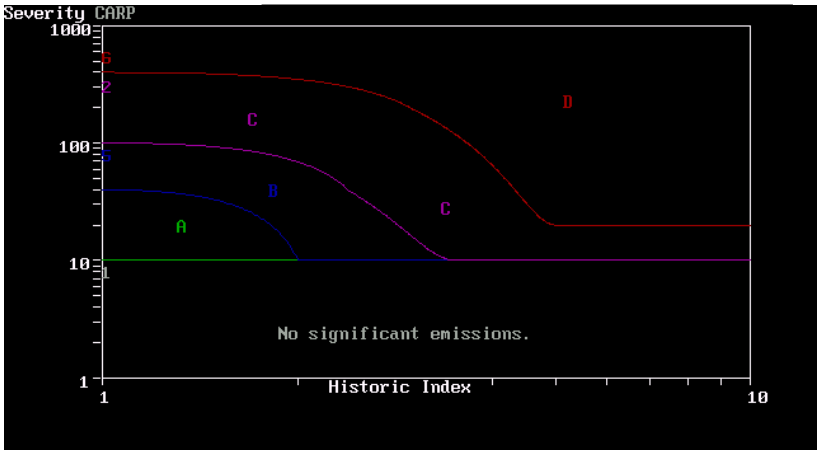

Figure 10.31 – Third pressure test – original vessel (Channels 1-24)

Mistras 2000

10.2.5 Fourth pressure test - 15.0 psi (June 17, 1999)

The maximum pressure reached during the fourth pressure loading was 15.0 psi. Plots of cumulative signal strength versus time from the Transportation Instrument are shown in Figures 10.32 through 10.35. Due to a malfunction with the Transportation Instrument, the acoustic emission data collected from 10.0 to 15.0 psi with this instrument was lost. Excluding this information, the maximum cumulative signal strength was 28. This is to be expected due to the low level of load and the fact that this is a reloading.

Channels M1, M2 and M6 were again recorded on the Mistras 2000. Channel M5 was not used for this reload. This data is shown in Figure 10.36. A very significant jump in signal strength can be seen in Channel M6 at the end of a load hold at 10 psi. This is the channel located 1'-0" below the distressed 4" gusseted nozzle. This increase in signal strength is very significant because it occurred at the end of a load hold. The emission appears to be genuine. This conclusion is based partly on the fact that emission occurs both before and after this large burst.

A plot of duration versus amplitude is shown in Figure 10.37. This data is typical for in-service vessels. Acoustic emission from in-service vessels typically shows a good deal of emission but relatively few high amplitude hits. This is due to the fact that most of the fiber breakage has already occurred.

The results of an intensity analysis for this loading are shown in Figure 10.38. This analysis applies to data collected with the Mistras 2000. As mentioned in Section 10.2.4, data collected with wide band sensors is comparable with that of resonant sensors on a qualitative basis only. The results are as follows:

Intensity category "A" – none

Intensity category "B" – none

Intensity category "C" – none

Intensity category "D" – channel M6

The emission generated here can be used to calculate a Felicity ratio based on the previous loading to 22.0 psi. The calculated Felicity ratio based on superposed pressure is as follows:

$$\text{Felicity ratio} = \frac{10.0 \text{ psi}}{22.0 \text{ psi}} = 0.45$$

This is much less than 1.0 and is indicative of significant damage. The Felicity ratio is described in Chapter 4.

The test was discontinued at 15 psi due to continuing emission recorded on several channels on the Transportation Instrument during the load hold. The very low Felicity ratio and the continuing emission during a load hold were both indications that the vessel was in a good deal of distress. Since it was known that the vessel was damaged, there was fear that further loading might lead to leaking and failure of the vessel.

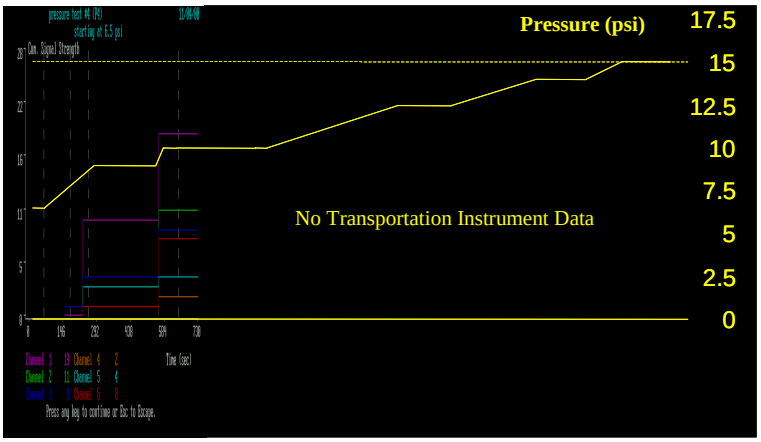

Figure 10.32 – Fourth pressure test – original vessel (Channels 1-6)

Transportation Instrument

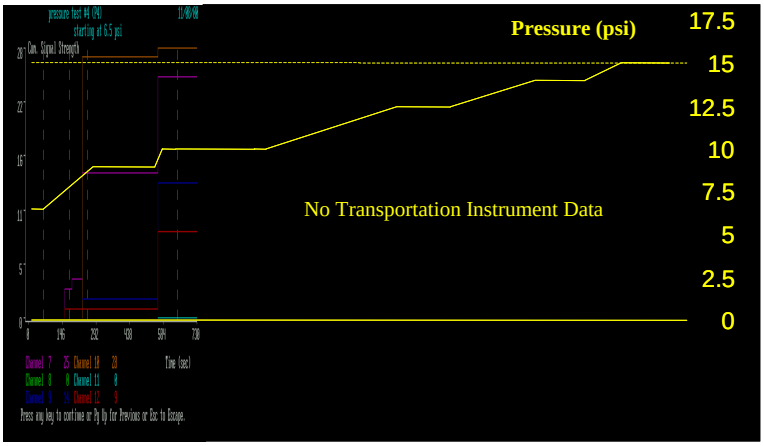

Figure 10.33 – Fourth pressure test – original vessel (Channels 7-12)

Transportation Instrument

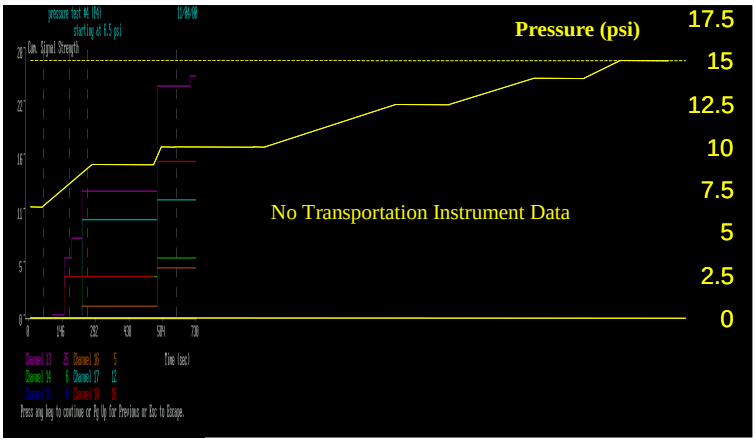

Figure 10.34 – Fourth pressure test – original vessel (Channels 13-18)

Transportation Instrument

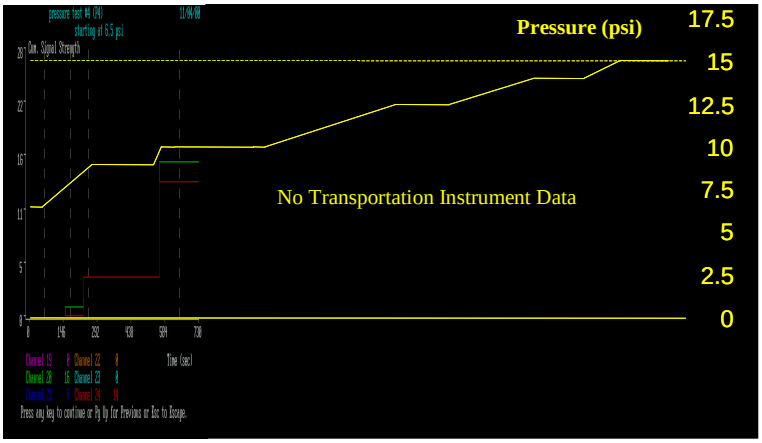

Figure 10.35 – Fourth pressure test – original vessel (Channels 19-24)

Transportation Instrument

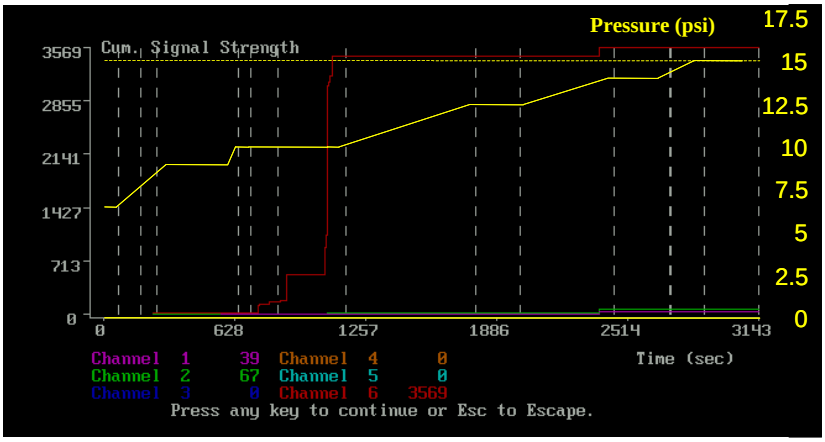

Figure 10.36 – Fourth pressure test – original vessel (Channels 1-6)

Mistras 2000

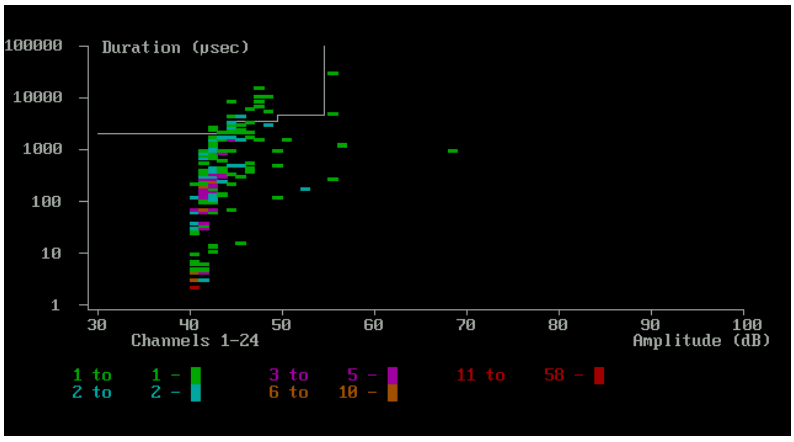

Figure 10.37 – Fourth pressure test – original vessel (Channels 1-6)

Mistras 2000

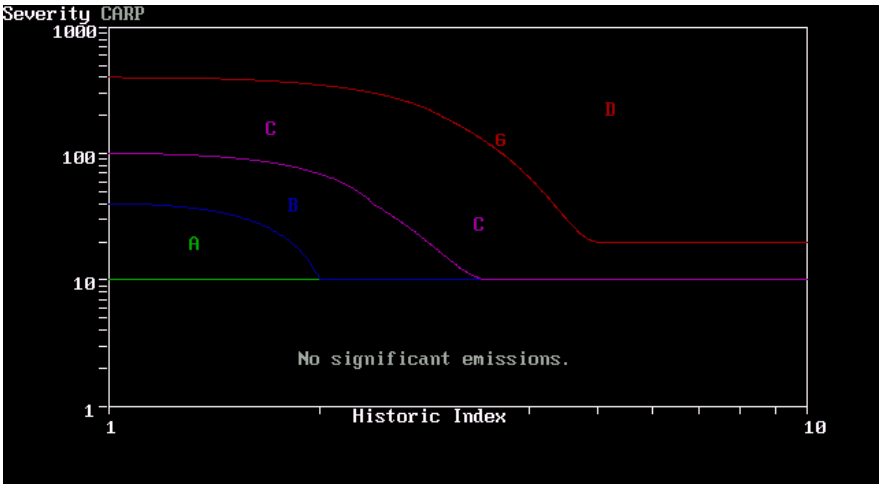

Figure 10.38 – Fourth pressure test – original vessel (Channels 1-6)

Mistras 2000

10.3 Acoustic Emission Results of Modified Vessel

A schematic of the sensor locations for the loading of the modified vessel are shown in Figure 10.39. All sensors were R15I. These were monitored with the Transportation Instrument. No sensors were monitored with the Mistras 2000.

10.3.1 First pressure test - 9.0 psi (August 5, 2000)

The maximum pressure reached during the first pressure loading was 9.0 psi. Plots of cumulative signal strength versus time for this loading are shown in Figures 10.40 through 10.42. This loading was very quiet. The maximum cumulative signal strength was 204.

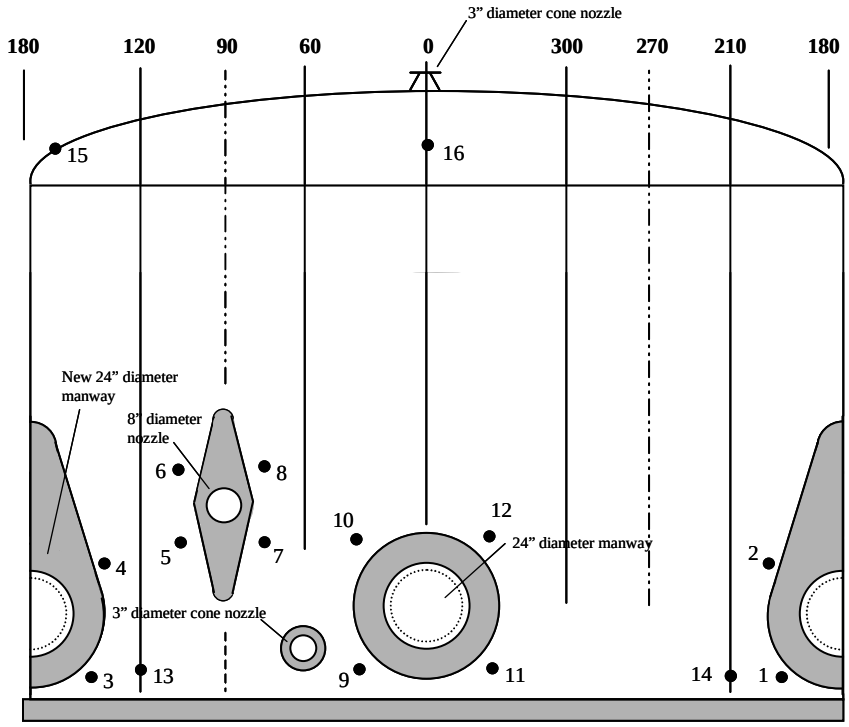

Note: All sensors 150 kHz resonant (R15I) monitored with Transportation Instrument

Figure 10.39 – Acoustic emission sensor locations for modified vessel

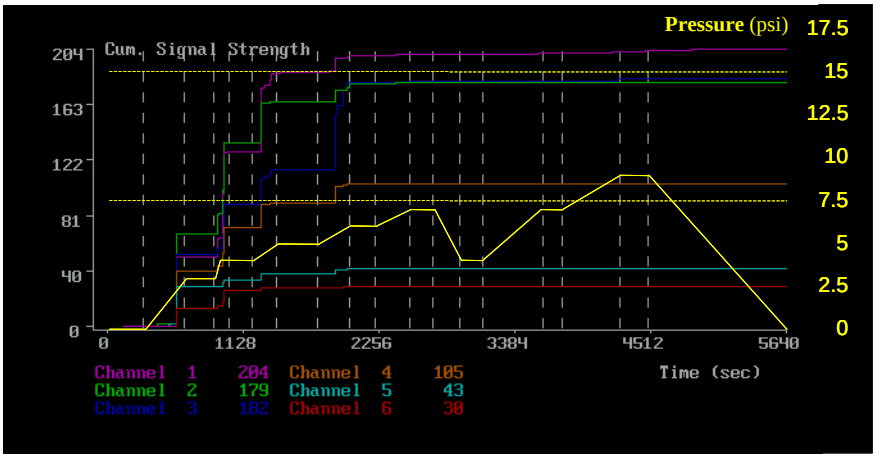

Figure 10.40 –First pressure test – modified vessel (Channels 1-6)

Transportation Instrument

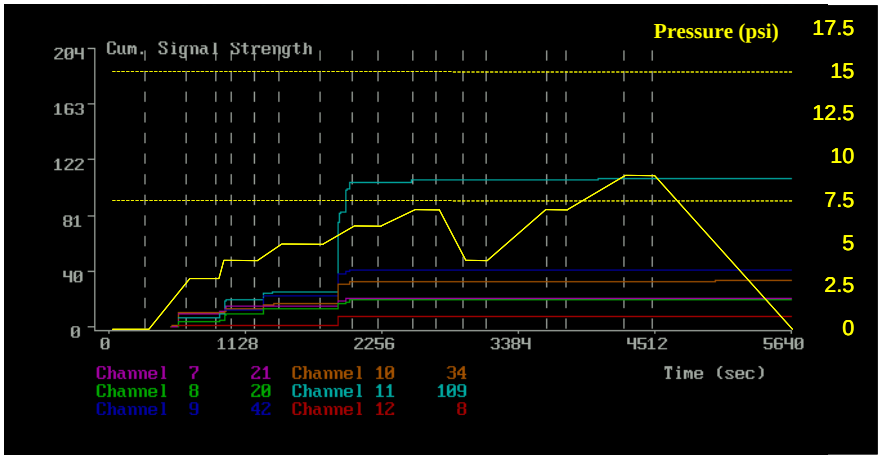

Figure 10.41 – First pressure test – modified vessel (Channels 7-12)

Transportation Instrument

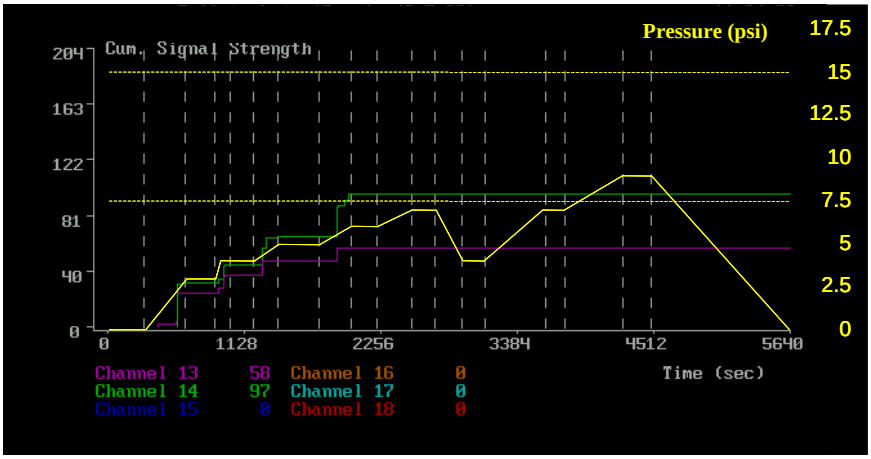

Figure 10.42 – First pressure test – modified vessel (Channels 13-18)

Transportation Instrument

10.3.2 Second pressure test - 23.0 psi (August 8, 2000)

The maximum pressure reached during the second pressure loading was 23.0 psi. A very large increase in cumulative signal strength occurred during a load hold. The load hold was necessary because of the failure of a safety valve at 21.0 psi. After the valve failed, the load dropped to 12.0 psi and the valve was removed. During removal of the valve a good deal of non-genuine acoustic emission was recorded. Therefore, this data was filtered to remove the non-genuine emission.

The filtered data is shown in Figures 10.43 through 10.45. A very large increase in signal strength is apparent on numerous channels at 23.0 psi. A plot of duration versus amplitude for the filtered data file is shown in Figure 10.46.

Individuals present during the test heard audible noise from the vicinity of the vessel at this pressure. This pressure approaches the design pressure for the hold down system. The hold-down system relies on bolted friction connections. It is possible that one of the hold-down connections slipped and that this led to the large amount of emission at 23.0 psi. However, since the tank had been pressurized very close to this level of load previously this seems unlikely. It is more likely that the significant emission was due to cracking of excess resin on the exterior of the vessel. During the installation procedure a good deal of resin dripped down from the new manway area. Most of this was removed with a chisel but some remained. Another possibility is that the interior reinforcing that was continued onto the floor of the vessel pulled away from the intersection of the vessel wall and the vessel floor. After the test was conducted, a visual inspection of the interior of the vessel was made. There was some visual evidence to suggest this happened. The visual evidence consisted of a discolored area approximately 4 inches long in the vessel wall to vessel bottom interface (Figure 10.47).

Prior to the incident at 23.0 psi, channels 14 and 16 had been giving the most emission. Channel 16 was located at the top of the vessel and whatever damage may have been taking place was not visible. Due to fear of failing the vessel or the hold-down system, it was decided to discontinue the test and to reload the vessel at a later date. As

mentioned previously, first loadings of vessels are seldom monitored and the results from a first loading alone are not conclusive.

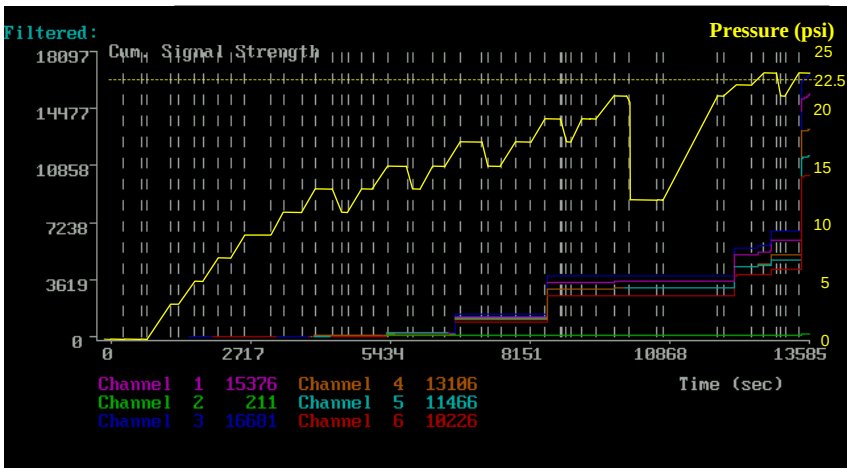

Figure 10.43 – Second pressure test – modified vessel (Channels 1-6)

Transportation Instrument {FILTERED}

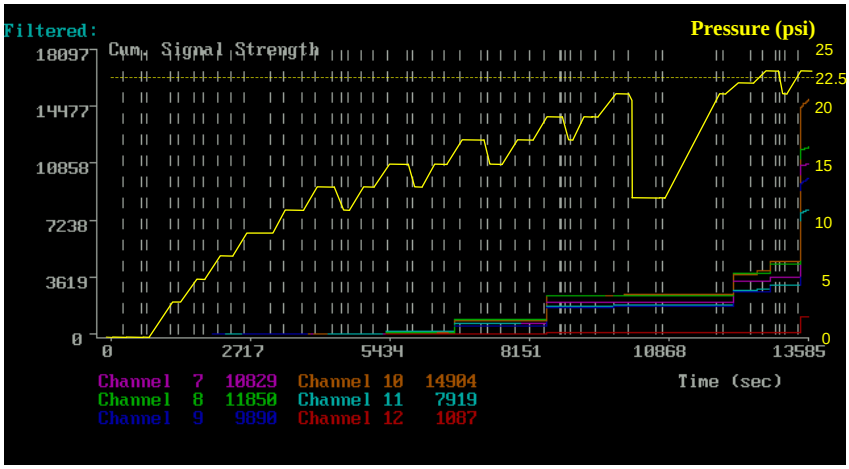

Figure 10.44 – Second pressure test – modified vessel (Channels 7-12)

Transportation Instrument {FILTERED}

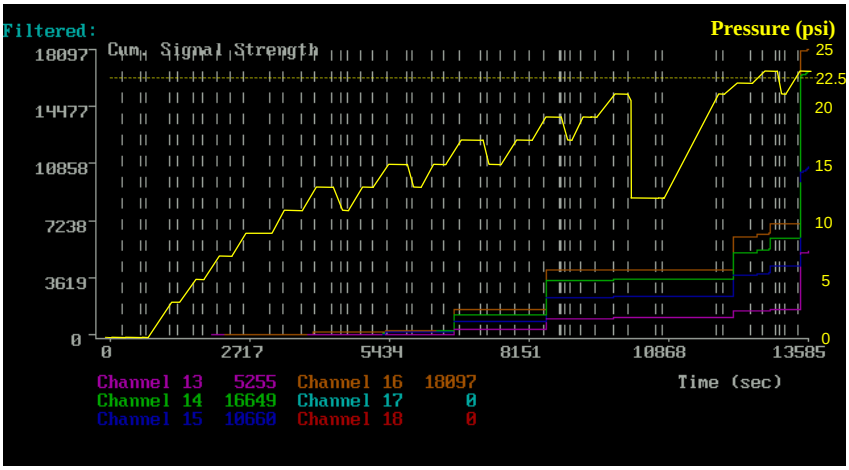

Figure 10.45 – Second pressure test – modified vessel (Channels 13-18)

Transportation Instrument {FILTERED}

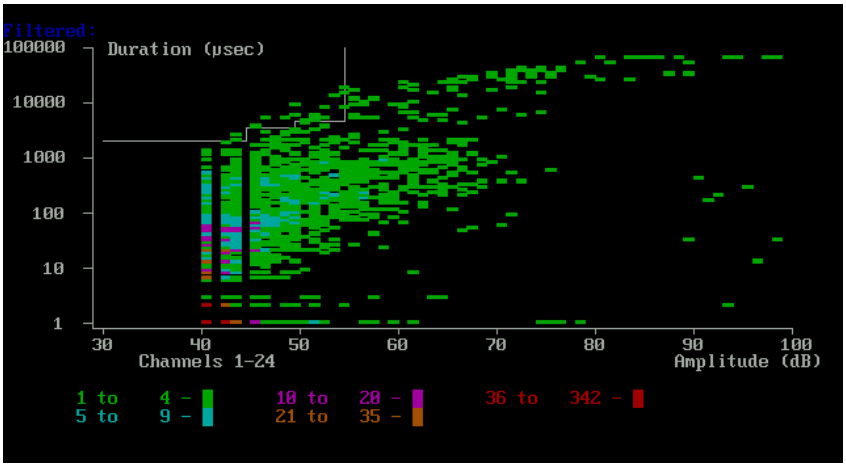

Figure 10.46 – Second pressure test – modified vessel (Channels 1-24)

Transportation Instrument {FILTERED}

Figure 10.47 – Damage to interior reinforcement at intersection of vessel wall and vessel base

10.3.3 Third pressure test - 18.0 psi (August 9, 2000)

The maximum superposed pressure reached during the third pressure loading was 18.0 psi. Plots of cumulative signal strength versus time from the Transportation Instrument are shown in Figures 10.48 through 10.50. The maximum cumulative signal strength was 210. This level of signal strength is very low and indicates that no significant damage was detected during this reloading.

The results of an intensity analysis for this loading are shown in Figure 10.51. The results of the analysis are as follows:

Intensity category “A” – none

Intensity category “B” – none

Intensity category “C” – none

Intensity category “D” – none

The results of this reloading indicate that the new manway and new 8” nozzle worked well. This is based on the lack of significant emission during the reload to 18.0 psi.

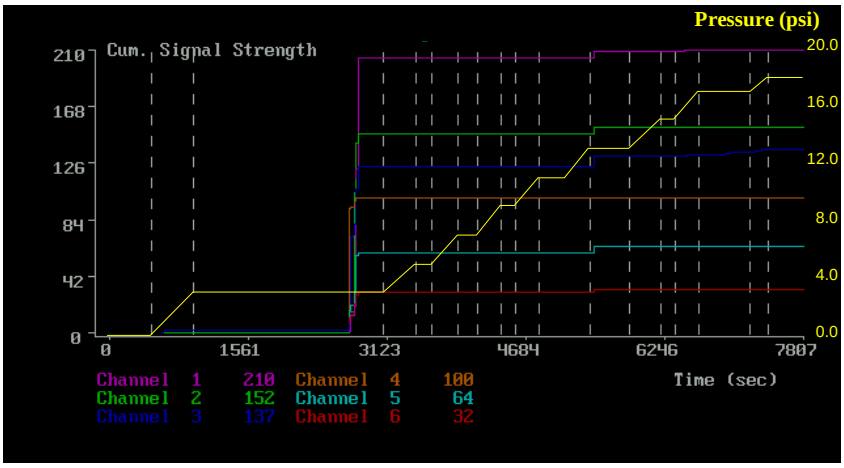

Figure 10.48 – Third pressure test – modified vessel (Channels 1-6)

Transportation Instrument

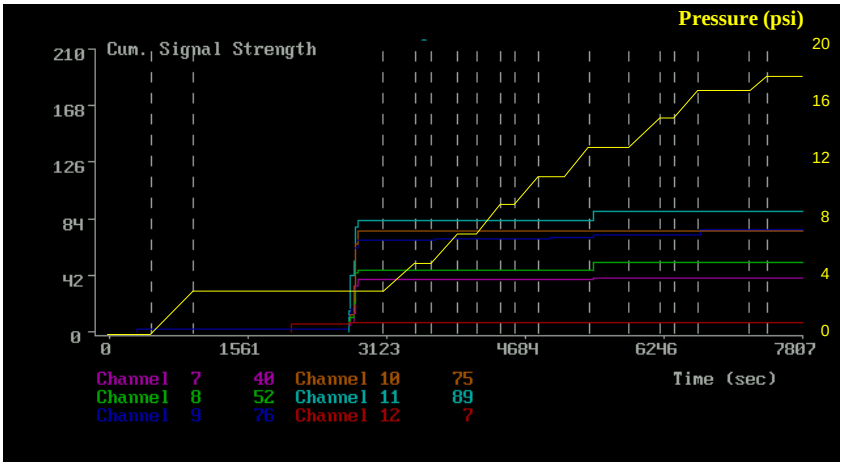

Figure 10.49 – Third pressure test – modified vessel (Channels 7-12)

Transportation Instrument

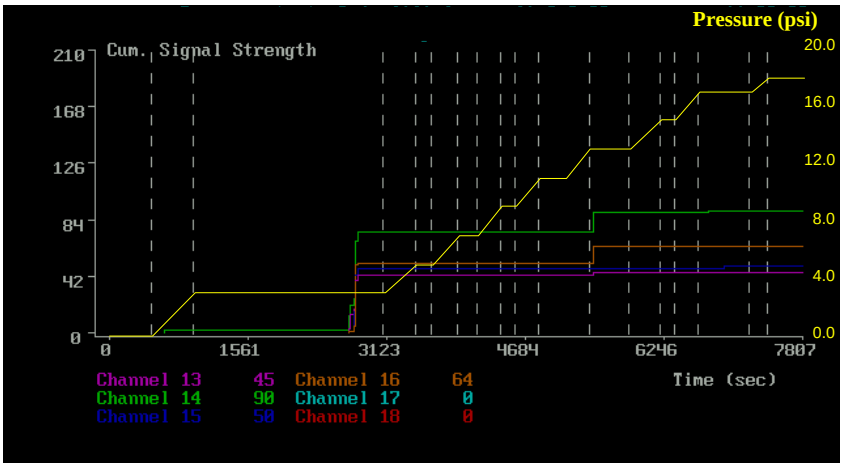

Figure 10. 50 – Third pressure test – modified vessel (Channels 13-18)

Transportation Instrument

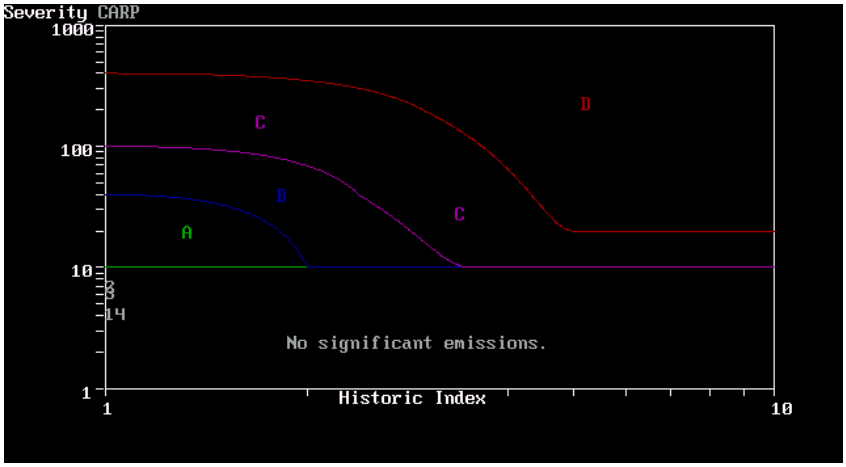

Figure 10.51 – Third pressure test – modified vessel

Transportation Instrument

10.3.4 Fourth pressure test - 22.0 psi (August 14, 2000)

The maximum pressure reached during the fourth pressure test was 22.0 psi. Plots of cumulative signal strength versus time for this loading are shown in Figures 10.52 through 10.54. The maximum cumulative signal strength was 231. This level of signal strength is also very low and indicates that no significant damage was detected during this reloading.

The results of the intensity analysis for this loading are shown in Figure 10.55. The results are as follows:

Intensity category “A” – channel 16

Intensity category “B” – none

Intensity category “C” – none

Intensity category “D” – none

The data recorded during this reloading to 22.0 psi further indicates that the new manway and 8” nozzle are working well. This is based on the lack of a Felicity ratio that is less than 1.0.

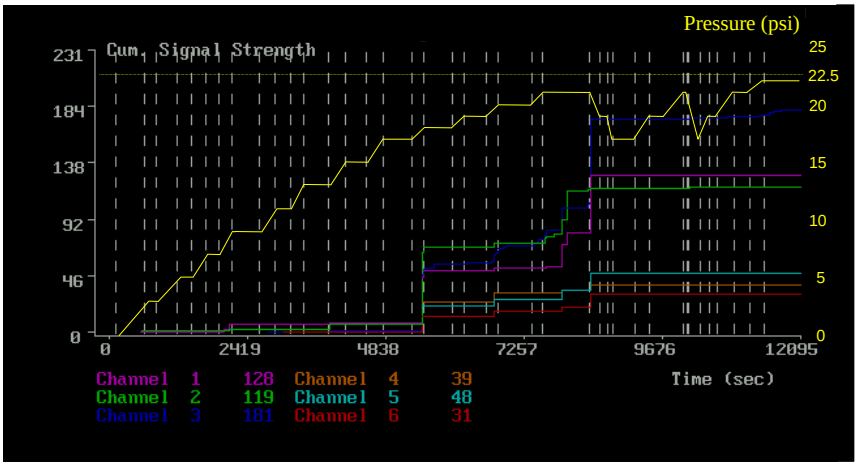

Figure 10.52 – Fourth pressure test – modified vessel (Channels 1-6)

Transportation Instrument

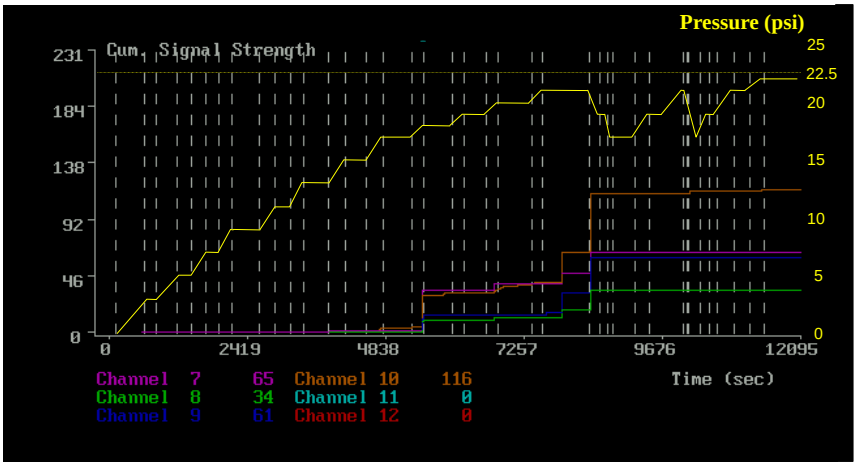

Figure 10.53 – Fourth pressure test – modified vessel (Channels 7-12)

Transportation Instrument

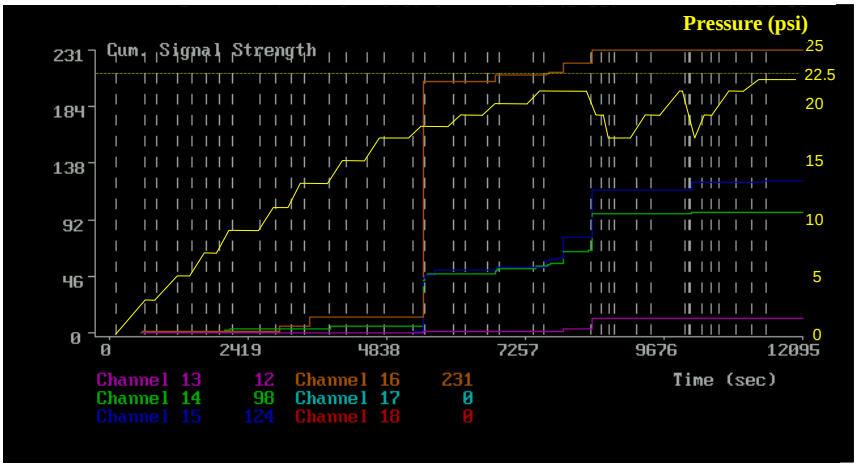

Figure 10.54 – Fourth pressure test – modified vessel (Channels 13-18)

Transportation Instrument

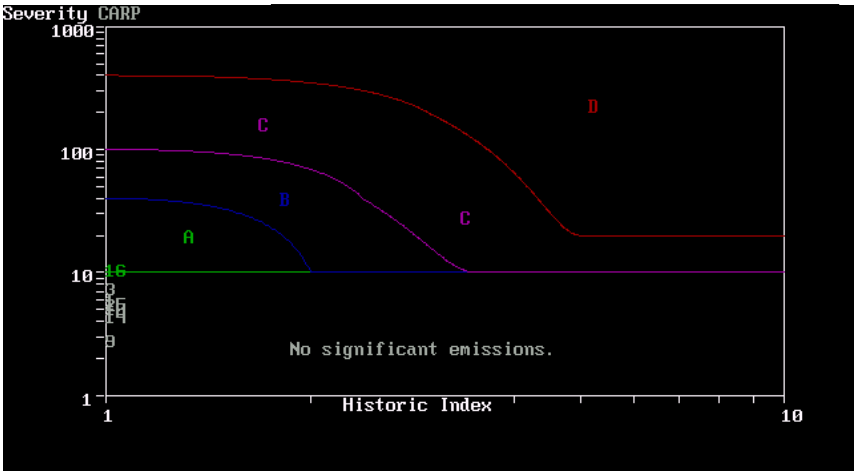

Figure 10.55 – Fourth pressure test – modified vessel

Transportation Instrument

10.3.5 Fifth pressure test - 22.0 psi (August 15, 2000)

The maximum superposed pressure reached during the fifth pressure test was 22.0 psi. Plots of cumulative signal strength versus time for this loading are shown in Figures 10.56 through 10.58. The maximum cumulative signal strength was 30. This level of signal strength is also very low and indicates that no significant damage was detected during this reloading. The conditioning period for this reloading was approximately 20 hours.

The results of the intensity analysis for this loading are shown in Figure 10.59. The results are as follows:

Intensity category “A” – none

Intensity category “B” – none

Intensity category “C” – none

Intensity category “D” – none

This data further verifies that the new manway and 8” nozzle are working well. This is again based on the lack of a Felicity ratio of less than 1.0.

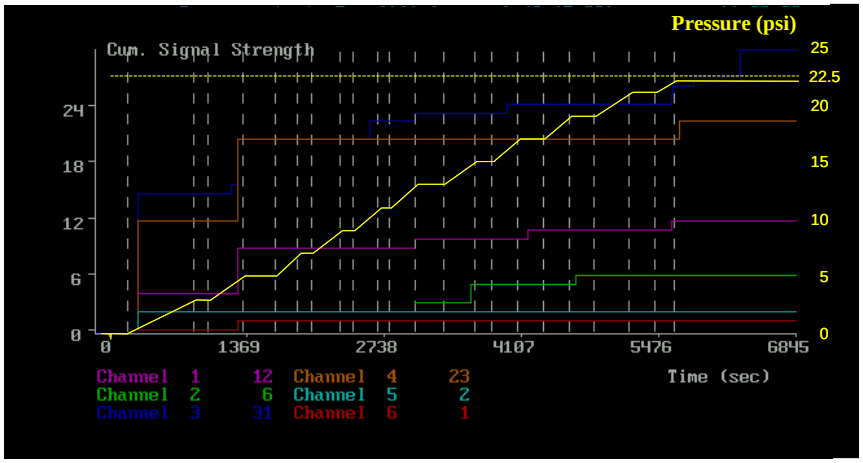

Figure 10.56 – Fifth pressure test – modified vessel (Channels 1-6)

Transportation Instrument

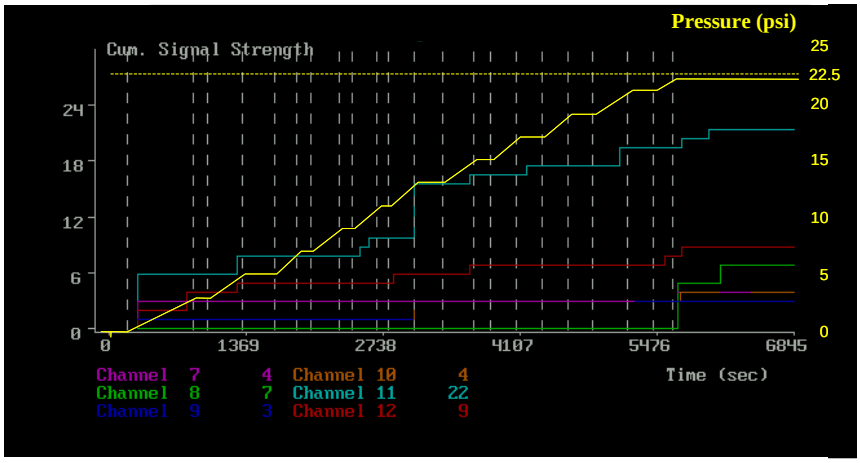

Figure 10.57 – Fifth pressure test – modified vessel (Channels 7-12)

Transportation Instrument

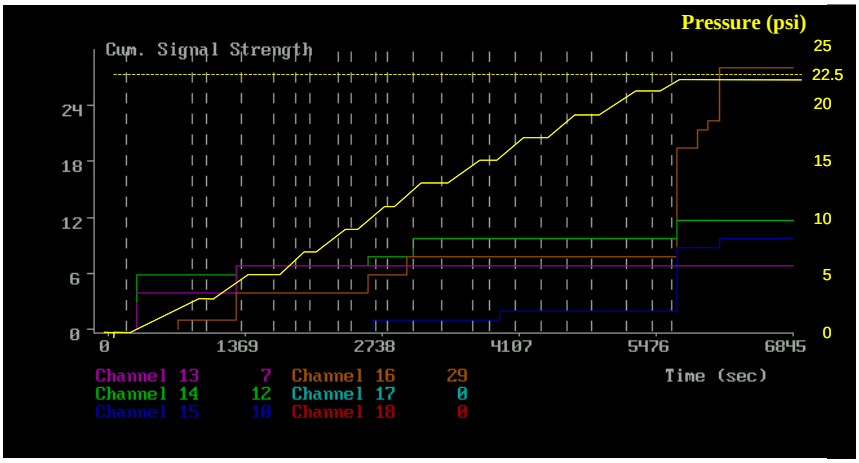

Figure 10.58 – Fifth pressure test – modified vessel (Channels 13-18)

Transportation Instrument

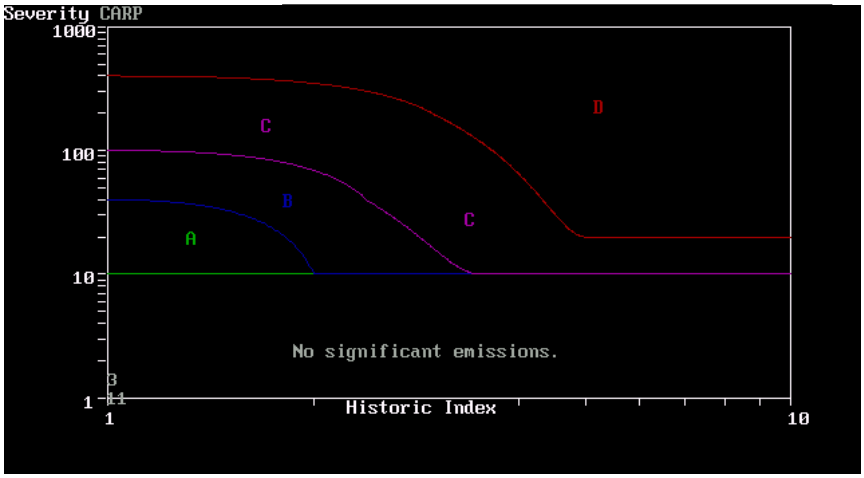

Figure 10.59 – Fifth pressure test – modified vessel

Transportation Instrument

10.4 Summary and Conclusions

Original vessel:

The original vessel was filled with water and loaded to a superposed pressure of 15.0 psi on two occasions. These loadings were essentially inconclusive because the superposed pressure was not severe enough to cause significant damage. Therefore, the vessel was pressurized approximately one year later to a superposed pressure of 22.0 psi. At this level of load, significant damage was done to the 4" gusseted nozzle. Unfortunately, the Transportation Instrument data at this level of load was lost. However, data from the Mistras 2000 was recorded and reflects the damage to the 4" gusseted nozzle at 22.0 psi.

The vessel was unloaded and reloaded to a superposed pressure of 15.0 psi. Much of the data from the Transportation Instrument was again lost. Data from the Mistras 2000 was recorded. The wide band sensor in the vicinity of the damaged nozzle was again acoustically active. The results of an intensity analysis of the Mistras data indicated an intensity factor of "D" for the channel in the vicinity of the gusseted nozzle. This indicates significant damage at a very low level of load. The Felicity ratio for this loading was calculated to be 0.45. This value also indicates very significant damage. The test was discontinued at 15.0 psi to avoid failing the vessel.

Modified vessel:

The modified vessel was loaded first to a superposed pressure of 9.0 psi. This was not sufficient to cause damage. The vessel was then loaded to a superposed pressure of 23.0 psi. At this level of load, audible noise could be heard in the vicinity of the vessel. Large increases in signal strength were recorded at this level of load. Several different sources may have caused this emission. These possible sources include slip of the hold-down system, cracking of excess resin and minor damage to the interior reinforcing at the vessel wall to vessel bottom interface. Slipping of the hold-down system is unlikely since the vessel was previously loaded to approximately the same level of load without slipping. The first loading of vessels is generally not monitored with

acoustic emission due to the inherently noisy nature of first loadings. Determination of acceptability is based on reloads.

The vessel was reloaded on three different occasions. The next reloading was to a superposed pressure of 18.0 psi. This level of load produced very little emission. The following two loadings were to a superposed pressure of 22.0 psi. Again, very little emission was produced. Based on the lack of a Felicity effect and very low intensity categories for all channels, it was concluded that the vessel had not been significantly damaged during the initial loading to 23.0 psi. The new manway and new 8" nozzle worked well as evidenced by the reload data.

Chapter 11: *Summary and Conclusions*

11.1 Summary of Work Conducted

A testing program has been carried out on both large and small scale fiber reinforced polymer specimens.

The small scale testing consisted of 1" by 7" by 3/8" coupons that were loaded in four point bending. Dimensions given are nominal. The loading process was continuously monitored with acoustic emission sensors. Both fiber-architecture and resin type were varied. A loading procedure and AE criteria were developed to determine the onset of damage in the coupon specimens.

The large scale testing consisted of a 7 foot diameter by 21'-6" tall filament wound pressure vessel. The vessel was designed and manufactured by Ershigs, Inc. of Bellingham, Washington. The design pressure for the vessel was 15.0 psi. The vessel was first tested in its original state as delivered from the manufacturer. The 4" gusseted nozzle experienced damage at a superposed pressure of 22.0 psi. Strain gages were used to monitor the vessel during loading. Finite element models of the vessel and the discontinuity regions were developed. These were compared to the strain gage results and reasonable agreement was found.

The results found from the coupon specimens were used to develop an AE based damage criterion. This criterion was substituted for the Tsai-Wu criterion in Abaqus. Numerous trial and error analyses were conducted in Abaqus to develop appropriate layup sequences for the new 24" manway and new 8" nozzle. The primary design objective was to reduce the level of stress in the discontinuity regions to the level of stress away from the discontinuity regions. Knitted fabrics were used in place of the more commonly used woven roving. This was due to the ability to orient the fibers and their quietness when tested with acoustic emission.

Modifications were made to the vessel. These included the removal of the distressed 4" gusseted nozzle and the installation of a new 24" diameter manway and new

8” diameter nozzle. The modified vessel was loaded to a superposed pressure of 23.0 psi. Significant emissions were recorded at this pressure. The vessel was then repeatedly reloaded and no significant emissions were recorded. It was concluded that the vessel modifications were structurally sound.

11.2 Drawbacks of Existing Failure Based Criteria

The present state of practice for designing with composites is broken into two basic camps: the maximum strain criterion and the biaxial stress criterion. Each of these methods has significant shortcomings. These are discussed in detail in Chapter 5 and will be summarized here for convenience.

Maximum strain criterion:

The maximum strain criterion does not account for biaxial stresses. Experimental data for biaxial loading does not match the failure values predicted by maximum strain theory. Shear interaction is also neglected. The shape of the maximum strain criterion in stress space is a skewed parallelogram (Figure 11.1).

Both RTP-1 and Section X have provisions for the use of the maximum strain criterion. These codes generally limit the maximum strain for a laminate to 1,000 micro-strain regardless of fiber orientation. This value was largely based on testing programs similar to that of Isham[11.1] as discussed in Chapter 2. These experimental programs were conducted prior to the development of more flexible resins. As was shown in Chapter 4, more flexible resins can undergo significantly higher strain prior to damage than more conventional resins.

Another problem with this approach is that it does not account for the fiber orientation of the individual laminas. As was shown in Chapter 4, laminas can generally undergo higher strains in the longitudinal direction as opposed to the transverse direction prior to damage. Current practice dictates that the same maximum strain is applied for all constructions regardless of resin type. Therefore the higher the modulus of the lamina

the greater the load it is permitted to carry. This is unfortunate because a higher modulus often is indicative of a brittle resin. Fiber type is also disregarded.

Biaxial stress criterion:

The most general of the biaxial stress criteria is the Tsai-Wu quadratic interaction criterion. This criterion does account for biaxial stresses and shear interaction. Experimental data tends to agree more closely with this criterion. The shape of the Tsai-Wu criterion in stress space is an ellipse (Figure 11.1). The application of this criterion requires destructive testing of laminas to determine the failure stress of laminas with differing fiber orientation. Ideally, a biaxial test and shear test are also conducted. In practice, the biaxial test is often neglected and an interaction parameter is used. For design purposes, the failure envelope developed from the destructive tests is then scaled down to an acceptable stress ratio. The value of the stress ratio in Section X is generally 6.0. One problem with this method is that the nonlinear behavior of the lamina is not considered. The mechanical behavior of 90-degree specimens is highly nonlinear from nearly 50% of the failure load to failure. Plots regarding the mechanical behavior of coupon specimens are given in Section 4.5.

These criteria (along with maximum stress and Tsai-Hill) are plotted in Figure 5.1 of Chapter 5. This plot is reproduced in Figure 11.1 for convenience.

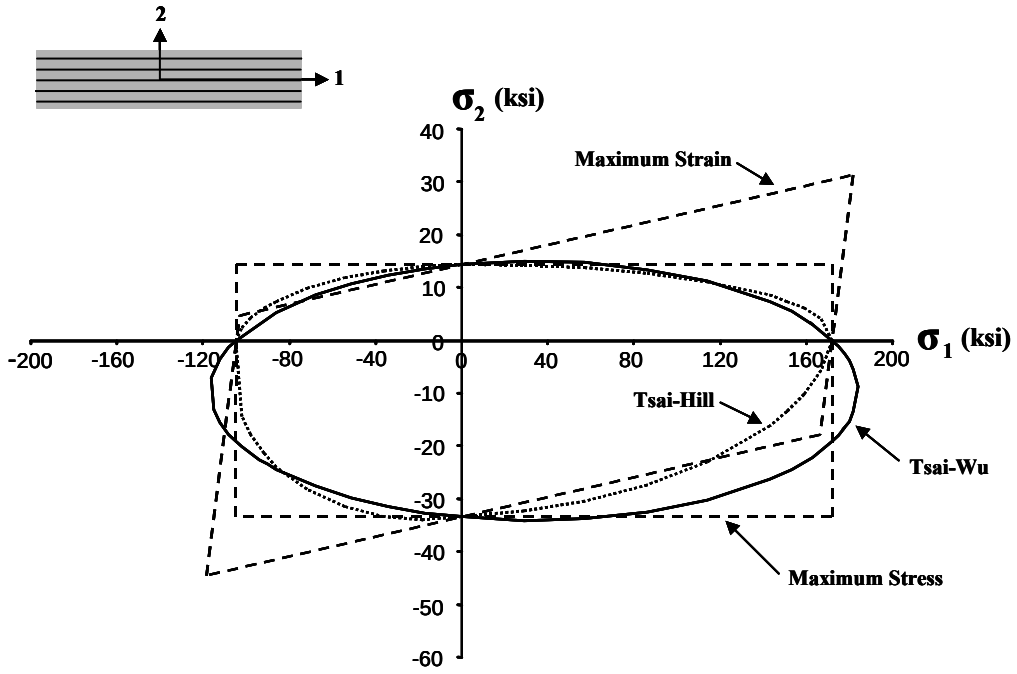

Figure 11.1 - Commonly used 2-D failure criteria

The most significant drawback of both criteria is that they are based on the ultimate failure values of the lamina. Generally, when these criteria are incorporated into a code, a large stress ratio is imposed on failure. In the case of pressure vessels designed by Section X of the ASME code, the required stress ratio is 6.0 (refer to Chapter 2). This is partially due to the poor agreement between the failure criteria and experimental data. However, it is largely due to the fact that laminas experience damage prior to the failure of the entire lamina. The safety factor is an attempt to keep the lamina in the relatively undamaged state in service.

Because the quadratic interaction criterion is based on the ultimate strength of laminas, laminas made with more flexible resins are penalized. For loading perpendicular to the fibers, laminas made with more flexible resins have similar ultimate

strength to laminas made with the more common resins. However, the stress at onset of damage is significantly higher for laminas with more flexible resins.

The failure envelope, damage envelope and typical design envelope are plotted together for specimens constructed with 411 and 197 resin in Figures 11.2 and 11.3. 411 is one of the more flexible resins and 197 is one of the more brittle. The acoustic emission data presented in Chapter 5 was used to determine the 90-degree and 0-degree damage data points. Direct inspection of the acoustic emission data was used as opposed to historic index and a ψ factor. The Tsai-Wu envelope was assumed between these data points. The damage stress in compression was assumed to be equal to that in tension. A value of zero was assumed for the interaction coefficient. A value of zero was assumed for shear stress.

From these plots it is clear that the damage criterion is less conservative than the typical design criterion with a stress ration of 6.0. This is true even for stress applied parallel to the fibers. For stress applied parallel to the fibers, the stress ratio for damage is 2.0 for the specimen with the 411 resin and 2.5 for the specimen with the 197 resin. For stress applied perpendicular to the fibers the differences due to the resins are more noticeable. For stress applied perpendicular to the fibers, the stress ratio based on damage is 2.0 for the specimen with the 411 resin and 4.3 for the specimen with the 197 resin. For stress applied perpendicular to the fibers, the damage criterion approaches the typical design criterion for the specimen with 197 resin.

Not only is the damage criterion less conservative, the shape of the damage envelope is very different for the specimen with the flexible resin when compared to the specimen made with the brittle resin. This is true even though the shape of the failure envelope is very similar for the specimens made with the two different resins.

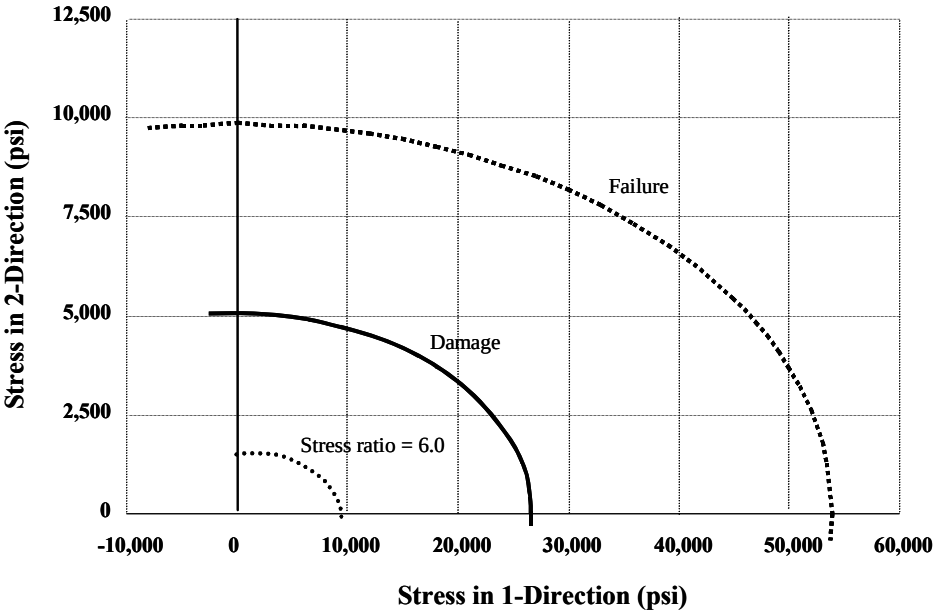

Figure 11.2 – Comparison of stress ratio and damage criterion – 411 resin

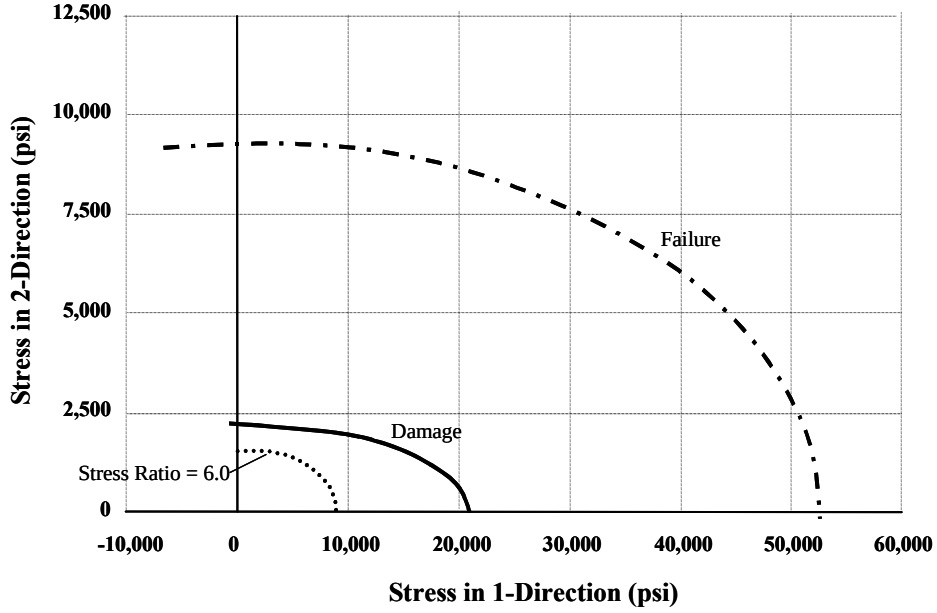

Figure 11.3 – Comparison of stress ratio and damage criterion – 197 resin

11.3 Recommended Acoustic Emission Procedure for Damage Based Criterion

A test method that directly addresses the onset of significant damage (as opposed to ultimate strength) has been developed. The method involves loading and reloading of laminas. The method makes use of the Felicity ratio[11.2] to determine damage. The development of the method is addressed in Chapter 4. A more thorough description of the AE procedure for establishing the design criterion is given here.

Laminas of differing fiber orientations and loading types are required. These are identical to those required by Section X[11.3] of the ASME code.

The loading procedure for determining an acceptable Felicity ratio is of utmost importance. An approximate estimate of the failure load is required. It is not important that the estimate be exact. An error of –20 to +40 percent is acceptable. The loading schedule shown in Figure 11.2 is recommended. Additional load / unload cycles should be used until a Felicity ratio of less than 1.0 is measured. The first load should be to 20% of the estimated failure load. Each subsequent load / unload cycle is increased 5% above the previous cycle. A conditioning period of at least 24 hours is required between each loading.

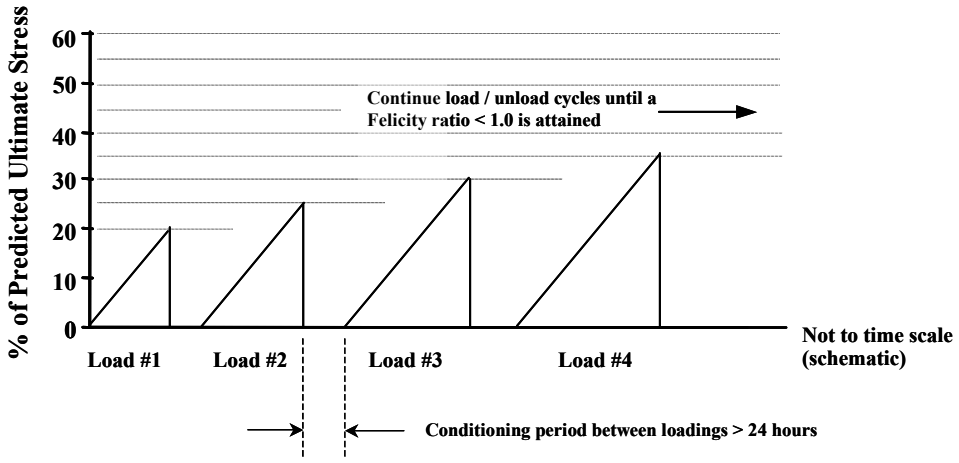

Figure 11.2 Recommended Loading Schedule

Stress should be monitored continuously and load should be applied pseudo-statically. Polymers are strain rate dependent and the loading should not result in a rate of stress increase greater than 10% of the estimated ultimate stress in 10 seconds. Strain can be monitored as well but is not necessary for the procedure. As discussed in Chapter 4, the onset of damage will generally occur in the linear range of mechanical behavior. Loadings should be continued until the Felicity ratio falls below 1.0. The Felicity ratio is defined as follows:

$$\text{Felicity ratio} = \frac{\text{Strain at onset of significant AE}}{\text{Previous strain to which specimen was loaded}}$$

When this loading procedure is followed, a Felicity ratio between 0.90 and 1.00 will normally be obtained. Due to experimental error, a lower Felicity ratio may be obtained. It is recommended that a range of acceptable Felicity ratios of between 0.85 and 1.00 be used. It is important to use only the data from the loading when the Felicity

ratio first drops below 1.0. The damage stress is defined as the stress at the onset of significant AE for the loading when the Felicity ratio first drops below 1.0.

The onset of significant AE must be determined from the cumulative signal strength versus time curve. Time must be correlated to stress. If possible, stress data should be gathered simultaneously with the AE data during a loading and plotted along with cumulative signal strength versus time.

As described in Chapter 4, the onset of significant AE was determined by direct inspection of the data. This type of determination is subject to interpretation and therefore is not appropriate for widespread use. The historic index[11.2] method was found to be less sensitive than direct inspection. Historic index generally lagged the direct inspection method by one load step. One load step approximately corresponded to 10% of the damage strain. However, the historic index is a well established AE parameter and therefore it is recommended that historic index be used to establish the onset of significant AE. It is recommended that the stress at onset of significant AE for any loading number be defined as the stress when the historic index value first becomes greater than 1.4.

The results of several tests were reviewed to compare direct inspection to historic index as a means of determining the onset of damage. This review indicated that a reduction of 20% is a conservative estimate to account for the lack of sensitivity of the historic index. It is recommended that the damage stress as determined by the AE procedure be multiplied by a factor of 0.75 to account for the lack of sensitivity of the historic index and experimental error.

The equation to be modified is the one given in Section RD-1188.5 of Section X[11.3]. The equation is reproduced as Equation 11.1 for convenience.

$$R^2(F_{xx}\sigma_x^2 + 2F_{xy}\sigma_x\sigma_y + F_{yy}\sigma_y^2 + F_{ss}\sigma_s^2) + R\,(F_x\sigma_x + F_y\sigma_y) - 1 = 0 \qquad \text{(Eqn. 11.1)}$$

where:

$F_{xx} = 1/XX_c$

$F_{yy} = 1/YY_c$

$F_{ss} = 1/S^2$

$F_x = 1/X - 1/X_c$

$F_y = 1/Y - 1/Y_c$

$F_{xy} = F_{xy}^* \sqrt{F_{xx} F_{yy}}$, with F_{xy}^* taken to be –1/2

where:

X = ultimate tensile strength of a lamina in the *x* (strong) direction

X_c = ultimate compressive strength of a lamina in the *x* direction

Y = ultimate tensile strength of a lamina in the *y* (weak) direction

Y_c = ultimate compressive strength of a lamina in the *y* direction

S = ultimate shear strength with respect to shear stress in the x-y plane

This criterion has been modified to accept the AE based damage criterion in Equation 11.2. The modified terms have been denoted with bold italic script.

$$(\boldsymbol{F_{xx}}\sigma_{\boldsymbol{x}}^2 + 2\boldsymbol{F_{xy}}\sigma_x\sigma_y + \boldsymbol{F_{yy}}\sigma_y^2 + \boldsymbol{F_{ss}}\sigma_s^2) + (\boldsymbol{F_x}\sigma_x + \boldsymbol{F_y}\sigma_y) \leq 1.0 \qquad \text{(Eqn. 11.2)}$$

where:

$\boldsymbol{F_{xx}} = 1/\boldsymbol{XX_c}$

$\boldsymbol{F_{yy}} = 1/\boldsymbol{YY_c}$

$\boldsymbol{F_{ss}} = 1/\boldsymbol{S^2}$

$\boldsymbol{F_x} = 1/\boldsymbol{X} - 1/\boldsymbol{X_c}$

$\boldsymbol{F_y} = 1/\boldsymbol{Y} - 1/\boldsymbol{Y_c}$

$\boldsymbol{F_{xy}} = \boldsymbol{F_{xy}^*}\sqrt{\boldsymbol{F_{xx}F_{yy}}}$, with $\boldsymbol{F_{xy}^*}$ taken to be –1/2

where:

$\boldsymbol{X}$ = ψ * damage stress of a lamina in the *x* (strong) direction under tensile loading

$\boldsymbol{X_c}$ = ψ * damage stress of a lamina in the *x* direction under compressive loading

$\boldsymbol{Y}$ = ψ * damage stress of a lamina in the *y* (weak) direction under tensile loading

$\boldsymbol{Y_c}$ = ψ * damage stress of a lamina in the *y* direction under tensile loading

$\boldsymbol{S}$ = ψ * damage stress of a lamina with respect to shear stress in the x-y plane

ψ = 0.75

damage stress = the stress at onset of significant AE when the Felicity ratio first drops below 1.0. This definition is valid only

in relation to the loading schedule described in Figure 4.1. Felicity ratios below 0.85 are not acceptable.

stress at onset of significant AE = the stress when the historic index value first becomes greater than 1.4

The ψ term is necessary to account for lack of sensitivity of the historic index and experimental error as described above.

The F_{xy} interaction parameter in equation 11.1 and the $\boldsymbol{F_{xy}}$ interaction parameter in equation 11.2 are discussed in Chapter 5. It is possible that a value of zero would be more appropriate for this parameter[11.4]. However, this is beyond the scope of the work discussed here.

The stress ratio is not applied to the AE based damage criterion.

11.4 Summary of Significant Findings

The following conclusions and recommendations are based on the research reported in this dissertation.

1. Governing design codes and standards for tanks and pressure vessels use design methods based on the following, either singly or in combination:
    a) cyclic loading followed by a destructive test
    b) maximum design stress based on destructive testing of individual laminas
    c) maximum design strain of 0.1%
2. Micromechanics equations based on constituent material properties do not give a reliable indication of lamina strength.
3. Micromechanics equations based on constituent material properties do give a reasonable value of lamina stiffness in the linear range.

4. Governing codes and standards[11.3, 11.5] use either simplified rules or the quadratic interaction criterion for design to 1 b) and 1 c) above.

5. Design factors (factor of safety, stress ratio, etc.) are not consistent between current codes and standards.

6. Design methods 1 b) and 1 c) above discourage the use of flexible resins, which are more expensive, and encourage the use of the stiffer less expensive brittle resins.

7. Prior to initiation of damage, a lamina fabricated with a flexible resin will sustain a higher strain and frequently a higher stress when loaded perpendicular to the fibers.

8. Maximum strains occur as the result of discontinuity and thermal stresses and not in areas of primary stress[11.6]. Cracking will not cause immediate failure, but may result in leakage or degraded fatigue strength.

9. For the reasons listed in 7 and 8 above it is advantageous to use flexible resins for tank and pressure vessel construction.

10. Acoustic emission is a widely used non-destructive method for detecting defects and damage in tanks and pressure vessels. Test methods are detailed in the governing codes and standards[11.2, 11.3, 11.5].

11. Acoustic emission can be used to detect onset of damage in constituent laminas. A recommended experimental procedure is outlined in Section 11.3 of this dissertation.

12. Lamina stress and strain values based on the onset of significant acoustic emission can be used in place of the stress and strain values specified for design under the methods outlined in 1 b) and 1 c).

13. Modifications to an existing vessel have been designed with the acoustic emission based damage criterion. The modifications included the addition of

a manway and an 8 inch diameter nozzle. The vessel was tested and performed well.

14. To account for the lack of sensitivity of the historic index and experimental error, a ψ factor of 0.75 should be applied to the damage results obtained by the acoustic emission procedure. The stress ration should be taken as 1.0.

15. The ψ factor given above may need to be reduced for the internal surface and first structural layup.

11.5 Directions for Future Research

The testing described was conducted on small coupon specimens loaded in four point bending. It is recommended that the damage criterion be applied to specimens similar to those required by Section X of the ASME code. This involves direct tensile, compressive and shear testing of specimens. Acoustic emission caused by grip noise should be addressed. Edge effects are an issue in both ultimate strength and damage testing. The effects of free edges on the data should be considered. Further investigation into the establishment of the ψ term for these types of specimens is desirable.

The biaxial testing was conducted with specimens having fibers at 45 degrees to the applied load. True biaxial tests are desirable to establish further data points. This is frequently accomplished by testing of sealed tube specimens.

Destructive and acoustic emission testing of full scale vessels that are designed according to the damage criterion is desirable. Long term fatigue testing is also desirable.

For all testing it is recommended that the Felicity ratio be used to establish damage. Historic index should be used to determine the onset of significant acoustic emission. A ψ term should be applied to the onset of AE as determined by historic index to account for the lack of sensitivity. Dependent on the outcome of further testing, it may be beneficial to reduce the ψ factor for portions of the vessel.

References

Chapter 1

1.1 Cortez, Enos, Francis and Heck, "Use of Acoustic Emission to Characterize Resin Performance in Laminates," *First International Symposium on Acoustic Emission from Reinforced Composites*, The Society of the Plastics Industry, July 1983.

1.2 American Society of Mechanical Engineers, "Reinforced Thermoset Plastic Corrosion Resistant Equipment," *ASME RTP-1*, 1995 Edition (Revision of ASME RTP-1 – 1992 Edition), with Addendums ASME RTP 1a-1995, ASME RTP-1b-1997, ASME RTP 1c-1998, ASME RTP-1d, 1998 and ASME RTP –1e, 1999.

1.3 ASME Subcommittee on Fiber-Reinforced Plastic Pressure Vessels, "Section X: Fiber-Reinforced Plastic Pressure Vessels", *ASME Boiler and Pressure Vessel Code*, 1998 Edition with 1999 Addenda and 2000 Addenda.

1.4 Gibson, Ronald F., "Principles of Composite Material Mechanics," McGraw Hill, Inc., 1994.

1.5 Isham, A. B., "Design of Fiberglass Reinforced Plastic Chemical Storage Tanks", *The Society of the Plastics Industry, 21st Annual Meeting of the Reinforced Plastics Division*, 1966.

1.6 Garcia, E., "Material Selection, Design and Tooling for Structural Plastics", *American Society of Civil Engineers, Session 46, Atlanta, Georgia*, May 1984.

1.7 Fowler, T. J., Blessing, J. A., Conlisk, P. J., "New Directions in Testing", *Third International Symposium on Acoustic Emission from Composite Materials, AECM-3*, July 1989, Paris, France.

1.8 Fowler, T. J. and Gray, E., "Development of an Acoustic Emission Test for FRP Equipment," *American Society of Civil Engineers Convention and Exposition*, Boston, April 1979.

1.9 The Committee on Acoustic Emission from Reinforced Plastics (CARP), "Recommended Practice for Acoustic Emission Evaluation of Fiber Reinforced Plastic (FRP) Tanks and Pressure Vessels," *a Division of the Technical Council of The American Society for Nondestructive Testing, Inc., Draft I*, October 1999.

1.10 ASTM E 1316-00, "Standard Terminology for Nondestructive Examinations", *American Society of Testing and Materials*, Pennsylvania, USA, 2000.

1.11 ASME Subcommittee on Non-destructive Examination, "Section V: Non-destructive Examination Non-Interfiled", *ASME Boiler and Pressure Vessel Code*, July 1998.

1.12 Osborne, A., "Trilam II," *Osborne Composite Engineering Limited, Laminate Analysis Program, Version 94*, July 1994.

Chapter 2

2.1 Cortez, Enos, Francis and Heck, "Use of Acoustic Emission to Characterize Resin Performance in Laminates," *First International Symposium on Acoustic Emission from Reinforced Composites*, The Society of the Plastics Industry, July 1983.

2.2 Lorenzo, L. and Hahn, H. T., "Static and Fatigue Fracture Monitoring in Unidirectional Composites by Acoustic Emission," *Composite Materials: Fatigue and Fracture*, a symposium sponsored by ASTM committee D-30 on high modulus fibers and their composites, 1986.

2.3 Fowler, T. J. and Gray, E., "Development of an Acoustic Emission Test for FRP Equipment," *American Society of Civil Engineers Convention and Exposition*, Boston, April 1979.

2.4 Isham, A. B., "Design of Fiberglass Reinforced Plastic Chemical Storage Tanks", *The Society of the Plastics Industry, 21st Annual Meeting of the Reinforced Plastics Division*, 1966.

2.5 Garcia, E., "Material Selection, Design and Tooling for Structural Plastics", *American Society of Civil Engineers, Session 46, Atlanta, Georgia*, May 1984.

2.6 Luger, Marvin, "Directional Reinforcements in Composite Material," paper presented at American Society of Civil Engineers convention, Las Vegas, Nevada, 1982.

2.7 ASME Boiler and Pressure Vessel Committee, Subcommittee on Fiber-Reinforced Plastic Pressure Vessels, "Section X: Fiber Reinforced Plastic Pressure Vessels," 1998 Edition with 1999 Addenda and 2000 Addenda.

2.8 American Society of Mechanical Engineers, "Reinforced Thermoset Plastic Corrosion Resistant Equipment, ASME RTP-1," 1995 Edition (Revision of ASME RTP-1 – 1992 Edition), with Addendums ASME RTP 1a-1995, ASME RTP-1b-1997, ASME RTP 1c-1998, ASME RTP-1d, 1998 and ASME RTP –1e, 1999.

2.9 Committee on Acoustic Emission from Reinforced Plastics (CARP) of the Composites Institute, **"**Recommended Practice for Acoustic Emission Testing of Fiberglass Reinforced Plastic Resin Tanks/Vessels," *The Society of the Plastics Industry, Inc.*, 1987.

2.10 The Committee on Acoustic Emission from Reinforced Plastics (CARP), "Recommended Practice for Acoustic Emission Evaluation of Fiber Reinforced Plastic (FRP) Tanks and Pressure Vessels," *a Division of the Technical Council of The American Society for Nondestructive Testing, Inc.*, Draft I, October 1999.

Chapter 3

3.1 Dow Plastics, “Derakane Epoxy Vinyl Ester Resins, Technical Product Information,” March 1996.

3.2 Osborne, A., “Trilam II,” Osborne Composite Engineering Limited, Laminate Analysis Program, Version 94, July 1994.

3.3 Gibson, Ronald F., “Principles of Composite Material Mechanics,” McGraw Hill, Inc., 1994.

3.4 ASTM D2584-94 “Standard Test Method for Ignition Loss of Cured Reinforced Resins,” *American Society of Testing and Materials*, Pennsylvania, USA, 1994.

Chapter 4

4.1 Cortez, Enos, Francis and Heck, “Use of Acoustic Emission to Characterize Resin Performance in Laminates,” *First International Symposium on Acoustic Emission from Reinforced Composites*, The Society of the Plastics Industry, July 1983.

4.2 Barnes, C. A., “Acoustic Emission Signature Analysis”, *Dissertation in progress*, the University of Texas at Austin.

4.3 Fowler, T. J. and Gray, E., “Development of an Acoustic Emission Test for FRP Equipment,” *American Society of Civil Engineers Convention and Exposition*, Boston, April 1979.

4.4 The Committee on Acoustic Emission from Reinforced Plastic (FRP) Tanks and Pressure Vessels**, “**Recommended Practice for Acoustic Emission Evaluation of Fiber Reinforced Plastic (FRP) Tanks and Pressure Vessels”, a Division of the Technical Council of The American Society for Nondestructive Testing, Inc., Draft I, October 1999.

Chapter 5

5.1 Gibson, Ronald F., “Principles of Composite Material Mechanics,” McGraw Hill, Inc., 1994.

5.2 Jenkins, C. F., “Report on Materials of Construction Used in Aircraft and Aircraft Engines,” *Great Britain Aeronautical Research Committee*, 1920.

5.3 Waddoups, M. E., “Advanced Composite Material Mechanics for the Design and Stress Analyst,” *General Dynamics, Fort Worth Division Report FZM-4763*, Fort Worth, Texas, 1967.

5.4 Hill, R., “A Theory of the Yielding and Plastic Flow of Anisotropic Metals,” *Proceedings of the Royal Society of London*, Series A, **193**, pp. 281-297, 1948.

5.5 Azzi, V. D. and Tsai, S. W., “Anisotropic Strength of Composites,” *Proceedings of the Society for Experimental Stress Analysis*, **XXII (2)**, pp. 283-288, 1965.

5.6 Tsai, S. W., “Strength Theories of Filamentary Structures,” *Fundamental Aspects of Fiber Reinforced Plastic Composites*, Chapter 1, pp. 3-11, Wiley Interscience, New York, 1968.

5.7 Tsai, S. W. and Wu, E. M., “A General Theory of Strength for Anisotropic Materials,” *Journal of Composite Materials*, **5**, pp. 58-80, 1971.

5.8 Gol’denblat, I. And Kipnov, V. A., “Strength of Glass Reinforced Plastics in the Complex Stress State,” *Mekhanika Polimerov*, **1**, pp. 70-78, 1965. English translation: *Polymer Mechanics*, **1**, pp. 54-60, 1966.

5.9 Wu, E. M., “Optimal Experimental Measurements of Anisotropic Failure Tensors”, *Journal of Composite Materials*, **6**, pp. 472-489, 1972.

5.10 Tsai, S. W. and Hahn, H. T., *Introduction to Composite Materials*, Technomic Publishing Co., Lancaster, PA, 1980.

5.11 Schapery, R., “Engineering Mechanics of Composite Materials,” class notes, 1998.

5.12 Osborne, A., “Trilam II,” Osborne Composite Engineering Limited, Laminate Analysis Program, Version 94, July 1994.

5.13 Hashin, Z., “Failure Criteria for Unidirectional Fiber Composites,” Journal of Applied Mechanics, **47**, pp. 481-505, 1980.

5.14 Tennyson, R. C., MacDonald, D., and Nanyaro, A. P., “Evaluation of the Tensor Polynomial Failure Criterion for Composite Materials,” *Journal of Composite Materials*, **12**, pp. 63-75, 1978.

Chapter 7

7.1 Osborne, A., “Trilam II,” Osborne Composite Engineering Limited, Laminate Analysis Program, Version 94, July 1994.

7.2 Gibson, Ronald F., “Principles of Composite Material Mechanics,” McGraw Hill, Inc., 1994.

7.3 Halpin, J. C. and Tsai, S. W., “Effects of Environmental Factors on Composite Materials,” AFML-TR-67-423, June 1969.

7.4 Tsai, S. W. and Pagano, N. J., “Invariant Properties of Composite Materials,” *Composite Materials Workshop*, pp. 233-252, Technomic Publishing Co., Lancaster, PA, 1968.

7.5 Hibbitt, Karlsson and Sorensen, Inc., “Abaqus”, Version 5.8, Pawtucket, Rhode Island, 1998.

7.6 The MacNeal-Schwendller Corporation, “MSC/Patran,” Version 8, Los Angeles, CA, 1998.

Chapter 8

8.1 Hibbitt, Karlsson and Sorensen, Inc., “Abaqus”, Version 5.8, Pawtucket, Rhode Island, 1998.

8.2 Osborne, A., “Trilam II,” Osborne Composite Engineering Limited, Laminate Analysis Program, Version 94, July 1994.

Chapter 10

10.1 The Committee on Acoustic Emission from Reinforced Plastic (FRP) Tanks and Pressure Vessels**, “**Recommended Practice for Acoustic Emission Evaluation of Fiber Reinforced Plastic (FRP) Tanks and Pressure Vessels”, a Division of the Technical Council of The American Society for Nondestructive Testing, Inc., Draft I, October 1999.

10.2 MONPAC-PLUS Test Analysis System and Transportation Test Analysis System, “VTRNSMON”, July 1993, Monsanto Company, St. Louis, Missouri.

10.3 Barnes, C. A., “Acoustic Emission Signature Analysis,” *Dissertation in progress*, The University of Texas at Austin.

Chapter 11

11.1 Isham, A. B., “Design of Fiberglass Reinforced Plastic Chemical Storage Tanks”, *The Society of the Plastics Industry, 21st Annual Meeting of the Reinforced Plastics Division*, 1966.

11.2 The Committee on Acoustic Emission from Reinforced Plastic (FRP) Tanks and Pressure Vessels**, “**Recommended Practice for Acoustic Emission Evaluation of Fiber Reinforced Plastic (FRP) Tanks and Pressure Vessels”, a Division of the Technical Council of The American Society for Nondestructive Testing, Inc., Draft I, October 1999.

11.3 Schapery, R., “Engineering Mechanics of Composite Materials,” *Course Notes, Aerospace Engineering 384P*, Spring 1998.

11.4 ASME Boiler and Pressure Vessel Committee, Subcommittee on Fiber-Reinforced Plastic Pressure Vessels, “Section X: Fiber Reinforced Plastic Pressure Vessels,” 1998 Edition with 1999 Addenda and 2000 Addenda.

11.5 American Society of Mechanical Engineers, “Reinforced Thermoset Plastic Corrosion Resistant Equipment, ASME RTP-1,” 1995 Edition (Revision of ASME RTP-1 – 1992 Edition), with Addendums ASME RTP 1a-1995, ASME RTP-1b-1997, ASME RTP 1c-1998, ASME RTP-1d, 1998 and ASME RTP –1e, 1999.

11.6 ASME Boiler and Pressure Vessel Committee, Subcommittee on Fiber-Reinforced Plastic Pressure Vessels, “Section X: Fiber Reinforced Plastic Pressure Vessels, Mandatory Appendix 4,” 1998 Edition with 1999 Addenda and 2000 Addenda.